FINITE ELEMENT METHOD ANALYSIS OF SLABS ON ELASTIC HALF SPACE EXPANSIVE SOIL FOUNDATIONS

A Dissertation

by

RIFAT BULUT

Submitted to the Office of Graduate Studies of
Texas A&M University
in partial fulfillment of the requirements for the degree of

DOCTOR OF PHILOSOPHY

December 2001

Major Subject: Civil Engineering

FINITE ELEMENT METHOD ANALYSIS OF

SLABS ON ELASTIC HALF SPACE

EXPANSIVE SOIL FOUNDATIONS

A Dissertation

by

RIFAT BULUT

Submitted to Texas A&M University
in partial fulfillment of the requirements
for the degree of

DOCTOR OF PHILOSOPHY

Approved as to style and content by:

Robert L. Lytton (Chair of Committee)	Kirk W. Brown (Member)
Dallas N. Little (Member)	Calvin E. Woods (Member)

John M. Niedzwecki
(Head of Department)

December 2001

Major Subject: Civil Engineering

Finite Element Method Analysis of Slabs on
Elastic Half Space Expansive Soil Foundations
(December 2001)

Rifat Bulut
B.S., Middle East Technical University;
M.S., Texas Tech University

Chair of Advisory Committee: Dr. Robert L. Lytton

ABSTRACT

A finite element computer program has been developed to analyze slabs on elastic half space expansive as well as compressible soils. Mindlin orthotropic plate theory is adopted for structural analysis of ribbed or constant thickness slabs. The foundation soil is assumed to be an isotropic, homogeneous, and elastic half space. The behavior of an elastic half space is calculated by dividing the surface of the elastic half space into rectangular regions. These regions are represented by stiffness matrices and they are assembled onto the rectangular plate finite elements.

The shape of the soil surface underneath the slab is described by the differential soil movement (y_m) and edge moisture variation distance (e_m). The mounded soil surface requires an iterative procedure in the computer program for this soil-structure interaction system. The program calculates displacements, moments in x- and y-directions, twisting moments, and shear forces. The comparisons of the results with the Post Tensioning Institute's (PTI) Design and Construction of Post-Tensioned Slabs-on-Ground manual examples show that the PTI analysis is conservative for the center lift case, but is not conservative for the edge lift case.

ACKNOWLEDGMENTS

I am deeply grateful to my advisor Dr. Robert L. Lytton for his constant support, valuable guidance and inspiration during the course of my stay at Texas A&M University. I am fortunate to have had the opportunity of learning from him. I greatly appreciate his advice, encouragement, guidance, and financial support, which made the completion of this dissertation possible.

I would like to thank Dr. Kirk W. Brown, Dr. Dallas N. Little, and Dr. Calvin E. Woods for serving as the advisory committee and Dr. Gerald R. Bratton for serving as the graduate council representative. I would also like to extend my thanks to Dr. J. N. Reddy for his help with the finite element method and its programming techniques.

Finally, I am deeply indebted to all the members of my family for their constant support and encouragement.

TABLE OF CONTENTS

TABLE OF CONTENTS (Cont'd)

LIST OF FIGURES

LIST OF FIGURES (Cont'd)

LIST OF FIGURES (Cont'd)

LIST OF TABLES

CHAPTER I
INTRODUCTION

1.1 The Problem

The soil, which represents a great portion of the earth's surface, is very complicated to deal with in regard to its engineering behavior. The main problem is certainly the variety of its material properties which can make it elastic, plastic, nonhomogeneous, anisotropic, and compressible, expansive or collapsing. It is necessary to understand the properties of the supporting soil and also to describe its behavior mathematically in order to design a foundation properly. A geotechnical engineer dealing with the problematic soils is often faced with the need to calculate displacements of the foundation soil and to analyze the effects of the displacements on the slab.

Foundation design on an expansive soil provides a major challenge to a geotechnical engineer because of the unique properties of these soils; shrink and swell. Expansive soils swell when they absorb moisture from the environment and shrink when they lose moisture to the environment. Moisture movement in expansive soils is thus a major cause for volume change and this moisture movement is a result of unbalanced moisture energy (or soil suction) between the expansive soil and its environment. The moisture distribution does not occur uniformly within the soil underlying the foundation and thus results in differential soil movement. It is this differential movement that results in major distresses in the slab foundations. The climatic condition of a site is a major factor controlling the magnitude of the differential soil movement. The climatic condition of a site will determine the active zone, the possible maximum seasonal changes of soil moisture condition and thus the wet and dry soil suction profiles (Fig. 1.1).

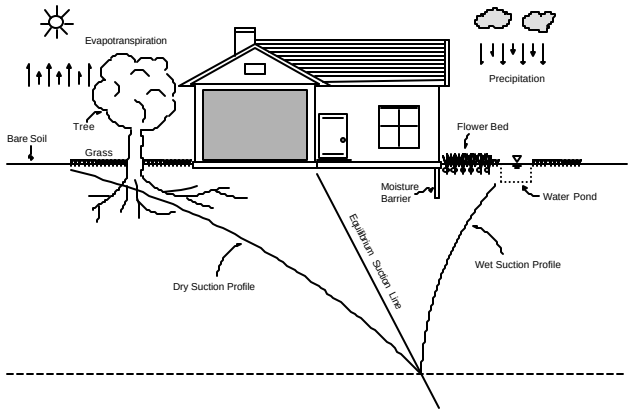

Fig. 1.1. Typical Environmental Effects on a House Foundation.

The style and format of this dissertation follows that of the *Journal of Geotechnical Engineering*, ASCE.

These seasonal changes of soil moisture or soil suction will dictate differential soil movement. Therefore, it is very important for a geotechnical engineer dealing with expansive soil to have knowledge of the soil suction distribution within the soil below a slab foundation.

To determine the vertical soil deformation in excess of the soil's expansion characteristics, the foundation soil needs be properly formulated. There is a spectrum of foundation models ranging from Winkler's type to the semi-infinite, homogeneous and isotropic, elastic continuum. Perhaps the best representation for the most frequently occurring soil materials is the elastic half space, behavior of which is described by Boussinesq's equation (Huang 1993).

Slab foundations have been analyzed using different approaches such as approximate numerical solutions, finite difference methods, and finite element methods. The finite element method incorporating the foundation soil has recently been widely accepted in analyzing the slab foundations because of its versatility and reliability over other methods. Two plate (or slab) theories are commonly used in finite element applications: Kirchoff plate theory and Hencky-Mindlin plate theory.

1.2 Background

Slab foundations on expansive soils have been used in residential homes and lightly loaded commercial buildings for many years. Many of these slabs were constructed as a result of experience and observation rather than rational design based analysis (Wray 1978). A significant number of these slabs were considered to be failures due to the design approaches that were dependent on engineering design principles. In the late 1960s, the Building Research Advisory Board (BRAB) initiated a research study in order to regulate design of the increased number of residential and light commercial building constructed on expansive soils. BRAB established design criteria for residential slab foundations. This study was completed in 1968 and currently known as the BRAB method. The BRAB (1968) method is highly empirical and based entirely on experience gained from observing the performance of slab-on-ground foundations throughout the USA. Four types of slab are selected which are intended to represent all combinations of soil and climatic conditions that are likely to occur. The initial selection of slab type is carried out from a table relating it to soil type, according to the Unified Soil Classification System, the minimum density, plasticity index, unconfined compressive strength, and the climatic rating. However, the influence of climate on the very complex effects of soil volume change is not adequately defined. Moreover, the design involves dividing slabs of irregular shape into overlapping rectangles. The total average dead and live loads are assumed to be uniformly

distributed over the whole slab. This procedure may simplify the calculations but it is unrealistic.

The Post Tensioning Institute (PTI) initiated a research study at Texas A&M University for development of new guidelines for characterization of expansive soils under different climatic conditions and of new finite element structural analysis method for the design of slab foundations. The method published by the Post Tensioning Institute (1980) is based on research conducted by Wray (1978) and the updated version of the method was published in 1996 and is the most recent attempt to improve the rationality of the previous design methods. A slab resting on an elastic continuum is analyzed using a modified form of a finite element program developed by Huang (1974). The selection of the elastic continuum foundation model over the most popular and widely used Winkler (or spring) type models makes the PTI method more realistic.

The more rational improvement in the PTI method is perhaps in the characterization of expansive soils, while taking into account all possible dimatic effects, to predict the volume change of the foundation soil. Recommendations are provided for estimating the edge moisture variation distance, e_m, as a function of the Thorntwaite moisture index, I_m. In addition, a more rational method has been adopted in the determination of vertical soil movement from the computer program VOLFLO based on moisture diffusion and volume change relationship. The variables used in this analysis are the type of clay mineral, percent clay, depth to constant suction, the constant suction value, velocity of moisture flow, and the edge moisture variation distance.

As a result of these research studies, there have been many improvements and developments in slab foundation designs, from empirical to more rational based on engineering principles.

1.3 Objective of Study

The most current design procedure for the slabs on expansive soils is the method by the Post Tensioning Institute (1996). In the PTI design method, the analysis of the plate structure with the finite element method has some shortcomings that are the objectives of this research. For instance, only rectangular slabs can be analyzed with the PTI method. For non-rectangular geometries, the rectangular slabs are overlapped to match the actual geometry. The PTI slab analysis is based on classical plate theory (Kirchhoff plate theory or thin plate theory), but an improved method should allow for thick plates if needed. Stiffening beams in the PTI method are converted to an equivalent slab thickness for calculating the bending moment, shear, and deflection and the method allows for a uniform distributed load all over the slab as well as line loads along the perimeter. However, an improved method needs to allow a slab cross-section that has stiffening beams and different magnitudes of distributed loads at different locations on the slab.

Therefore, the research approach is to develop and conduct a finite element analysis of a slab resting on an expansive soil, which is modeled as an elastic half space, to predict the magnitudes of bending moment, shear, and deflection under applied design loads.

1.4 Outline of Dissertation

Chapter II presents an extensive literature review on topics related to slabs on expansive soil foundations. In order to have a better understanding of the present status of knowledge in this field, the discussion in Chapter II summarizes the design methods that are extensively used in many parts of the world.

Chapter III covers the theoretical background of the soil suction concept, which is a very important parameter for unsaturated expansive soils. The discussion also includes topics on soil suction measurement techniques. Expansive soils are also briefly mentioned in this chapter.

Chapter IV summarizes the major foundation models in the literature. The formulation of the elastic half-space foundation, which is adopted in this research, is presented in detail.

Chapter V is devoted to the presentation of the theory of the plates and the finite element method. Both the Kirchhoff's plate and Mindlin's plate are discussed while only the latter is adopted for the finite element analysis in this research.

Chapter VI describes the finite element computer program developed in this thesis and Chapter VII explains the applications of the computer program with several examples.

Chapter VIII covers a brief summary of design tools for slabs on expansive soils while the study of this research is concluded in Chapter IX.

CHAPTER II
BACKGROUND OF RIBBED SLABS ON EXPANSIVE SOILS

2.1 Introduction

Investigations are continually being undertaken into the development of more rational analysis and design procedures for ribbed slab foundations on expansive soils. Since the problems associated with constructing structures on expansive soil were first recognized, numerous foundation and structural design methods have been proposed to prevent such damages. A stiffened raft foundation may be a solution to those problems because of its relative ease of construction, economy, and satisfactory performance (Lytton and Woodburn 1973). The stiffened raft usually consists of a slab about 10 to 15 cm (about 4 to 6 inches) thick, with regularly spaced edge and cross stiffening beams. These are designed to limit distortion of the superstructure to tolerable levels as the underlying soil undergoes differential movement. The typical damages caused by swelling foundation soil are cracking in building walls, distorted slabs, and misaligned or broken buried utility pipes.

If a foundation is placed on an expansive soil, the geotechnical engineer faces a major challenge because the soil can respond with a change in volume (shrinking/swelling). The expansive soil can respond not only to the structural loading but also to a change of soil moisture condition. The unique property of expansive soil is the change in volume when it absorbs moisture from its environment (swelling) or loses moisture to its environment (shrinking). Lightly loaded structures such as houses, apartments, and pavements have been affected by these reactive heaving soils (mainly smectite type clay) in all over the world (Fig. 2.1).

Fig. 2.1. Distribution of Expansive Soils in the World (after Wray 1978).

To employ the slab analysis procedures, the geotechnical engineer needs to predict the differential soil movement caused by the expansive soils. It is known that the climatic condition of a site is a major factor controlling the magnitude of the differential soil movement. The climatic condition of a site will determine the active zone, the possible maximum seasonal changes of soil moisture condition (wet and dry soil suction profiles, Fig. 2.2). Thus, it is of great importance for a geotechnical engineer dealing with expansive soil to have knowledge of soil suction distribution within the soil. Once the soil suction profile is obtained, the soil volume change induced by these soil suction changes can be estimated.

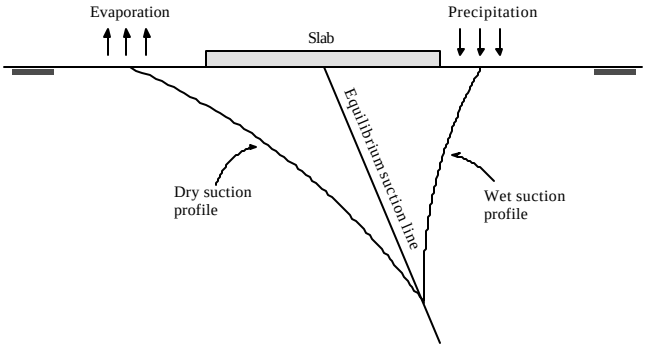

Fig. 2.2. Suction Profiles.

When a lightly-loaded structure such as a slab-on-ground foundation is constructed over expansive soils, the climate conditions at the site has a great influence on the type of distress that the foundation will undergo as a result of distortion of the support provided by the foundation soil. In general, there are two major types of expansive soil distortion modes (Lytton 1972): center-lift and edge-lift (Fig. 2.3). The center-lift case usually occurs when the soil at the perimeter of foundation shrinks. The edge-lift case usually occurs when the soil at the perimeter of foundation swells. Either type of distortion will result in structural damages if the slab is not designed properly. The distortion mechanism should be selected to produce the worst values of

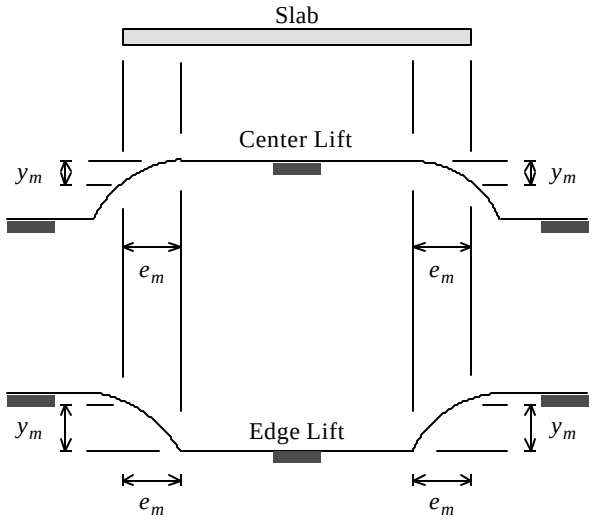

Fig. 2.3. Slab Distortion Modes.

design moment, shear force and deflection (Lytton 1972).

2.1.1 Volume Change Behavior of Expansive Soils

The volume change behavior of expansive soils may not be predicted satisfactorily using traditional soil mechanics theories as well as elastic or plastic theory due to the large magnitudes of volumetric strains involved (Lytton 1996). However, there are many methods that rely on these theories as well as on some laboratory methods such as consolidometer tests or even on moisture content determinations. Lytton (1973) has shown that the volume change of expansive soils can be predicted satisfactorily with the use of soil suction, which has proven to be a stress state variable for unsaturated soils (Fredlund and Rahardjo 1993). This is a more rational approach since suction as a measure of the negative stress in the pore water, which pulls the soil particles together, is dependent on boundary conditions such as vegetation and climate. Suction is a thermodynamic quantity which will retain all the effects of the climate, such as humidity and temperature, within itself and carry them as a stress effect on the soil particles. Lytton (1973) has formulated his volume change theory using the soil suction principle and the influence of the overburden stress, soil fabric, and cracks within the soil mass.

2.1.2 Structural Analysis of Slabs

The early structural analysis procedures to predict bending moments, shear forces, and deflections for the slab-on-ground foundations are simple for the design purposes, but are not based on the actual mechanics of soil-structure interaction principles. In such cases, for example, one-dimensional analysis is adopted and this analysis is carried out in both directions to represent a two-dimensional case. Moreover, for the arbitrary shape slabs, the analysis involves dividing slabs into overlapping rectangles. The dead and live loads are assumed to be uniformly distributed over the whole slab. These analysis procedures may simplify the calculations, but they are not realistic. Later, Lytton (1970) introduced the elastic mathematical models of beams and slabs, which are based on the principles of mechanics, to improve the rationality of the analysis procedures. The effect of representing the two-dimensional problem as a one-dimensional beam-on-ground is also investigated by Lytton (1970), using the finite difference method to solve the two-dimensional plate equation on coupled spring foundation. With the development of high speed computers, the analysis procedures for two and three dimensional complex problems using the finite element method has become a common practice. Wray (1978) analyzed a slab resting on an elastic half-space foundation using the finite element method, which is the most rational analysis proposed to date. The finite element method seems to be a promising structural analysis method because of its versatility of applying it to many complex structures.

2.2 Existing Design Methods

There are more than ten design procedures for the slab-on-ground foundations (Wray 1978). However, among the existing methods the ones by Building Research Advisory Board (1958, 1963, 1968), Lytton (1970, 1971, 1972, 1973), Walsh (1974, 1978), Frazer and Wardle (1975), and Post Tensioning Institute (1996) have been mentioned in the literature quite often. These methods have reasonably rational bases, but all have some shortcomings both in their theory and in their degree of simplification. Consequently, it has been necessary to mention these methods briefly, to evaluate the validity of the basic assumptions and the design variables.

2.2.1 The Building Research Advisory Board (BRAB) Method

The BRAB (1968) method is highly empirical and based entirely on experience gained from observing the performance of slabs-on-ground throughout the USA (Wray 1978). Four types of slab are selected which are intended to represent all combinations of soil and climatic conditions that are likely to occur (PTI 1996). The slab types are:

TYPE I: Unreinforced

TYPE II: Lightly reinforced against shrinkage and temperature cracking

TYPE III: Reinforced and stiffened

TYPE IV: Structural (not directly supported on the ground)

The initial selection of slab type is carried out by relating it to soil type, according to the Unified Soil Classification System, the minimum density, plasticity index or the unconfined compressive strength, and the climatic factor. BRAB produces a map (Fig. 2. 4) showing the distribution of the climatic rating, C_w, for the USA, but there is not enough information how it is being estimated.

Fig. 2.4. Climatic rating, C_w, for the USA (from Wray 1978).

Type I and Type II slabs are usually constructed on stable soils and Type III is recommended for use on expansive soils. The Type IV is used as a suspended floor slab in the areas where the soil bearing capacity is not sufficient. The Type III slab has several assumptions; the design loads of the structure are uniformly distributed over the slab area and the support index, C, which is dependent upon the climatic rating ,C_w, and the soil plasticity index ,PI, is a constant for all slab sizes (Fig. 2.5). The support index is a measure of the proportion of the slab that is being supported by the foundation soil.

The Type III slab design involves dividing slabs of irregular shape into overlapping rectangles with long and short sides of length L and L′, respectively. Among several support conditions the ones similar to the models shown in

Fig. 2.3 are adopted permitting a one-dimensional analysis which is carried out in both directions, L and L′, to represent the two-dimensional case. The design values for maximum moment, M_{max}, shear, V_{max}, and deflection, W_{max}, by applying the above mentioned simplifications and assumptions, are given by

$$M_{\max} = \frac{qL^2L'(1-C)}{8}, \quad V_{\max} = \frac{qLL'(1-C)}{2}, \quad W_{\max} = \frac{qL^4L'(1-C)}{48EI} \tag{2.1}$$

where:
q = uniformly distributed load,
E = elastic modulus of concrete,
I = second moment of inertia of section,
C = support index,
L = slab length, and
L' = slab width.

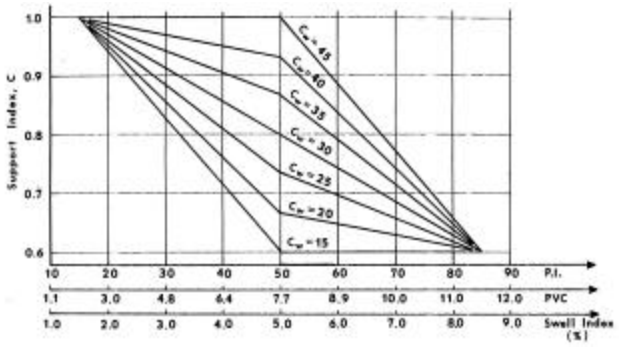

Fig. 2.5. Support Index, C (from Wray 1978).

The relationships given in Fig. 2.5, for determining the support index which is an important parameter in Eq. 2.1, are empirical and they cannot be used for other climatic conditions. The value of C is independent of the slab length. This assumption is not in accordance with observed measurements (Wray 1978).

2.2.2 Lytton's Method

Lytton (1970) improved the rationality of the BRAB procedure by abandoning the concept of an empirical support index and proposing elastic mathematical models of beam and slab on a curved mound. Lytton formulated the foundation soil for center lift (Fig. 2.3) analysis using the Winkler model and for edge lift analysis using the coupled spring model. The design quantities are then calculated directly once the relevant properties influencing the soil-structure interaction have been established. Lytton modified the general beam equation by including the effects of shearing resistance, which was represented by the coupled springs, of the foundation soil. The differential equation, which was put forward to represent a beam on a coupled spring mound, is given by

$$\frac{d^2}{dx^2}\left(EI\frac{d^2w}{dx^2}\right) - \frac{d}{dx}\left(GhB\frac{d}{dx}(w-y)\right) + kB(w-y) = q \tag{2.2}$$

where:
EI = beam flexural stiffness,
w = transverse deflection of the beam,
y = position of mound,
G = effective soil shear modulus,
h = effective depth within which soil shearing resistance is mobilized,
B = effective width within which soil support for the beam is mobilized,
k = effective subgrade modulus, and
q = distributed load on the beam.

A second equation for the case of an isotropic elastic plate, which includes the effects of the soil shearing resistance, on the same foundation type is given by

$$D\nabla^4 w - \nabla\left[Gh\cdot\nabla(w-y)\right] + k(w-y) = p \tag{2.3}$$

where:
D = flexural rigidity of the plate,
p = distributed load on the plate,

$$\nabla = \frac{\partial}{\partial x} + \frac{\partial}{\partial y}, \quad \nabla^4 = \frac{\partial^4}{\partial x^4} + 2\frac{\partial^4}{\partial x^2\partial y^2} + \frac{\partial^4}{\partial y^4}$$ Laplace operators.

The shape of the curved mound was chosen to fit experimentally determined or observed field shapes and was given in the form

$$y = \beta x^m \tag{2.4}$$

where:
m = the mound exponent,
β = a constant,
x = distance along the beam, and
y = distance below the highest point of the mound.

Lytton proposes that the beam equation can be applied to a slab when the slab is assumed to take a cylindrical deflection pattern, however, it is also pointed out that if two dimensional bending becomes the primary mode of distortion, then the assumption of the cylindrical deflection pattern is not valid. This differential equation applies only in the region where the beam is in contact with the soil, and a second equation, in which kB and GhB are put equal to zero, applies from the points not in contact with the soil. An iterative process is required to locate these points. A rigid beam solution was also developed to determine maximum moment and shear envelopes. The main benefit gained from these studies is an appreciation of the relative importance of the different design variables and the rational mathematical models of soil-structure interaction.

Lytton (1972) proposed to use line loads around the perimeter and along the centerline of the slab and a uniformly distributed dead and live load over the whole slab. The maximum moment is then calculated in each direction, assuming both the soil and slab to be rigid, and then reduced by a correction term to account for soil compressibility. In the case of center lift, the equation for the one-dimensional design moment, M_1 in the direction L is given by

$$M_1 = \frac{q_e LL'}{2} + \frac{L^2}{8}\left(2q_e + q_c + q_l L'\right) - c\frac{TL}{8} \tag{2.5}$$

where:
q_e = line load acting on the perimeter,

q_c = line load acting through the center of the building,
q_l = uniformly distributed load from dead and live loads,
T = total load on the rectangle,
c = support index,
and for the edge lift case

$$M_1 = \frac{q_c L L'}{4} + \frac{L^2}{8}\left(2q_e + q_l L'\right) - c\frac{TL}{8} \qquad (2.6)$$

In the case where the one-dimensional design moment obtained from Eqs. 2.5 and 2.6 are adjusted for the two-dimensional plate behavior for the long direction

$$M_L = M_1\left(1.4 - 0.4\frac{L}{L'}\right) \qquad (2.7)$$

and for the short direction

$$M_S = M_1\left[1 + 0.9(1.2 - c)\left(\frac{L}{L'} - c\right)\right] \qquad (2.8)$$

The design values for the shear force and deflection are estimated from

$$V = \frac{4M}{L}, \qquad w = \frac{ML^2}{12EI} \qquad (2.9)$$

where V is the shear force and w is the deflection.

The support index presented by BRAB depends on experience and empirical consideration of observed site conditions, however Lytton proposes a support index, c, by using the rational analysis of the interaction between the expected swelling profile and the slab. The support index can be obtained from

$$c = \frac{m+1}{m+2}\left[\frac{m+1}{m}\frac{1}{ky_m}\frac{T}{A}\right]^{\frac{1}{m+1}} \qquad (2.10)$$

where:
m = mound exponent,
A = slab area,
T = total load acting on the slab,
y_m = maximum differential heave, and
k = Winkler subgrade modulus.

The support index can also be estimated from the nomograph (Lytton 1972) which is given in Fig. 2.6 below. More precise methods of determining the differential soil movement, y_m, based on the thermodynamics of soil moisture and the volume strain theory for swelling soils were developed by Lytton (1973) and they will be presented in detail in coming sections.

2.2.3 Walsh's Method

Walsh (1974) proposed a design method which is essentially a combination of the BRAB (1968) and Lytton (1970) approaches, Walsh's main contribution being an attempt to rationalize the determination of the support index. As in the case of BRAB, simplified design recommendations were given; four slab types were defined, and their selection was based on soil type and expected differential soil movement. The Type III slab was recommended for use in areas where problems could be anticipated because of the presence of expansive soils.

Again the foundation is separated into overlapping rectangles and each rectangle is analyzed in both directions assuming the simplified two-dimensional center and edge heave patterns. Walsh (1974) also assumes the dead and live loading to be uniformly distributed over the whole slab area, but uses the beam on mound equation (Eq. 2.2) proposed by Lytton (1970) to determine the support index.

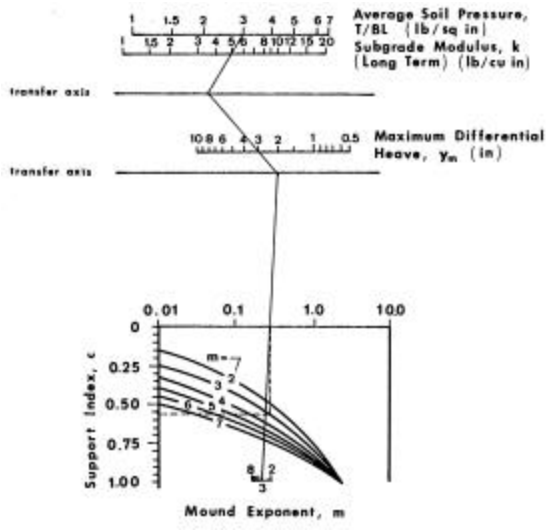

Fig. 2.6. Nomograph for Support Index, c (from Lytton 1972).

The slab is assumed to be flexible and interacts with the mound as shown in Fig. 2.7. Walsh adopts the same type of spring foundation model and differential equations proposed by Lytton (1970). The design values of moment, shear, and stiffness can then be determined from equations identical to those proposed by BRAB (Eq. 2.1).

Walsh (1978) has attempted to modify his earlier method by introducing a procedure for the determination of the stiffness constant, k. The mound is assumed to be consisting of a soft mound with stiffness, k_S, underlain by a hard mound with stiffness, k_H. A laboratory or field procedure is outlined to obtain swell-pressure curves from which k_S can be determined. The beam on mound equation was modified to

$$EI\frac{d^4z}{dx^4} + A^H\frac{d^2\left(z - y_o^H\right)}{dx^2} + B^H\left(z - y_o^H\right) + A^S d^2\frac{\left(z - y_o^S\right)}{dx^2} + B^S\left(z - y_o^S\right) = q \qquad (2.11)$$

where:
A^H, A^S = the $Rk_S b^2$ for the hard and soft mound, respectively,
B^H, B^S = the Rk_S for the hard and soft mound, respectively,
b = the cooperating width which determines the extent of the coupling effect,
R = the width of the foundation affected by the beam, and

y^H_o, y^S_o = the initial mound shape for the hard and soft mounds, respectively.

In the solution of this equation the hard mound was assumed to heave one-eighth, and have a stiffness 30 times that of the soft mound.

2.2.4 Fraser and Wardle Method

A three-dimensional semi-infinite elastic soil foundation has been introduced by Fraser and Wardle (1975) instead of the Winkler and coupled spring foundation models proposed by Lytton (1970) and Walsh (1974). This is a more rational approach than the previous Winkler and coupled spring models. Fraser and Wardle used an existing finite element program (FOCALS) to analyze a plate structure on the three-dimensional elastic solid foundation model. However, they did not produce a general design procedure for the slab-on-ground foundations built on expansive soils.

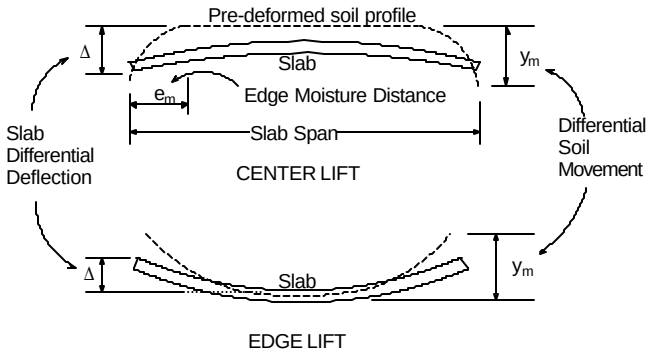

Fig. 2.7. Soil-Structure Interaction Proposed by Walsh (1974).

2.2.5 The Post Tensioning Institute (PTI) Method

The method published by the Post Tensioning Institute is based on research conducted by Wray (1978). PTI published the first edition of "Design and Construction of Post-Tensioned Slabs-on-Ground" in 1980 and the second edition was published in 1996 after some revisions. The PTI method is the most recent attempt to improve the rationality of the previous design methods. The two-dimensional slab resting on an elastic continuum was analyzed, using a modified form of a finite element program developed by Huang (1974). The material properties which are used in the program are Poisson's ratio and Young's modulus for soil and concrete. The input variables were selected as: differential soil movement, edge moisture variation distance (Fig. 2.3), stiffening beam depth, beam spacing, perimeter loading, and slab length. The dead weight of the slab was calculated automatically within the program. The influence of each of the variables on the design values of moment, shear, and deflection was examined and the computer output analyzed to develop equations for a general design procedure.

Recommendations are provided for estimating the edge moisture variation distance, e_m, as a function of the Thorntwaite moisture index, I_m (Fig.2.8). The Thornthwaite index is an indicator of change in moisture in the soil through evapotranspiration or rainfall. A positive Thornthwaite index represents a net surplus of soil moisture while a negative index indicates a net moisture deficit. The Thornthwaite moisture index distribution for the United States is given in Fig. 2.9 below. This moisture index can be applied to any geographical location throughout the world.

In addition, a more rational method has been adopted in the determination of differential swelling soil profile, y_m, which is based on moisture diffusion/volume change relationship. This procedure has been put forward as a computer program known as VOLFLO, which will be described in the next section, and is being used along with the current PTI slab program. The variables used in this analysis are the type of clay mineral, percent clay, depth to constant suction, the constant suction value, velocity of moisture flow and the edge moisture variation distance.

Recommendations are also given for obtaining the values of these variables, for instance, the equilibrium suction value is obtained from the curve given by Russam and Coleman (1961), which relates the constant suction value under a covered area to the Thornthwaite moisture index (Fig. 2.10).

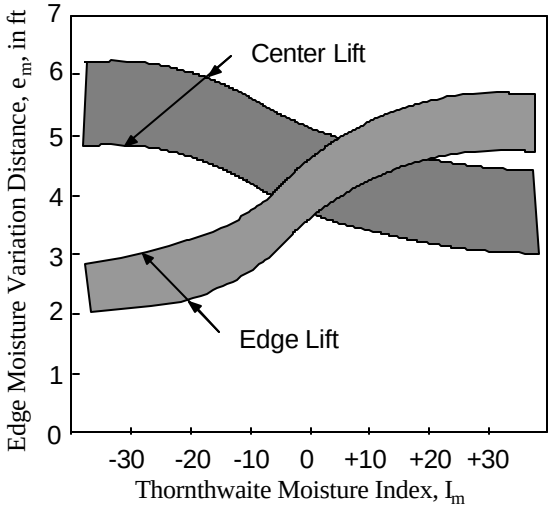

Fig. 2.8.Moisture Variation Distance versus Thornthwaite Index (after PTI 1996).

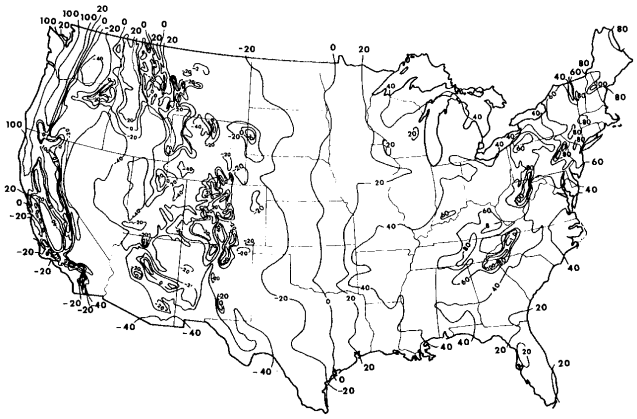

Fig. 2.9. Distribution of the Thornthwaite Index in the US (from Wray 1978).

2.3 Design Parameters y_m and e_m

Design parameters y_m and e_m are two important values that describe the design mound shapes for edge and center lift conditions. These parameters depend on the soil type,

soil moisture diffusion characteristics, and climatic conditions.

2.3.1 The VOLFLO Program

VOLFLO is a computer program which performs volume change and flow calculations for expansive soils. It was developed in the early 1980's at Texas A&M University under the guidance of Prof. Dr. Robert L. Lytton. VOLFLO calculates the soil shrinkage and swelling using soil suction concept. Only the effect of horizontal moisture flow is considered and the effect of vertical moisture movement is neglected. The program calculates volume change and moisture movement rates in expansive soils for five different sets of effects occurring near a foundation system:

1. General case—no effects
2. A vertical barrier to moisture flow at the edge of the foundation
3. A horizontal barrier to moisture flow at the edge of the foundation
4. A tree or flowerbed near the edge of the foundation. Tree roots may or may not extend beneath the foundation
5. Both trees and horizontal barrier. This case is a combination of cases 3 and 4.

The volume change can be calculated for an expansive soil with a depth to constant suction down to 20 feet. The soil may be composed of up to 6 layers within the active zone.

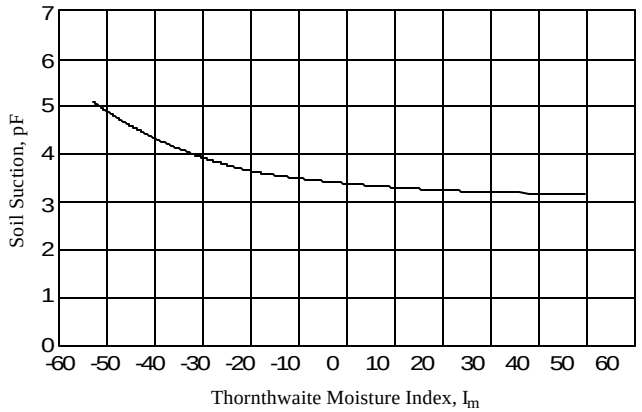

Fig. 2.10. Thornthwaite Index versus Constant Suction (from PTI 1996).

2.3.1.1 Theory of Volume Change and Horizontal Moisture Flow as in VOLFLO

Darcy's law relates the moisture flow in fully saturated soils to a hydraulic gradient through a constant saturated permeability and can be stated as

$$v = k_o \cdot i \tag{2.12}$$

where:
v = velocity of water flow,
k_o = saturated permeability, and
i = hydraulic gradient.

Darcy's equation can be employed for unsaturated soils by assuming that the hydraulic gradient can be represented by a change in suction along two distinct points. For a horizontal moisture flow the equation can be written as (Lytton 1977)

$$v_x = -k\left(\frac{\Delta h}{\Delta x}\right) \tag{2.13}$$

where:
Δh = horizontal change in suction,
Δx = change in horizontal location,
v_x = horizontal velocity of moisture flow, and
k = unsaturated permeability.

For the vertical moisture flow, the total gradient or head consists of the suction head plus elevation head, and therefore Darcy's law for the vertical flow, from which the equilibrium suction profile corresponding to a zero vertical moisture velocity is determined, can be written as

$$v_z = -k\left(\frac{\Delta h}{\Delta z} + 1\right) \tag{2.14}$$

where:
v_z = vertical velocity of moisture flow,
Δz = change in vertical location.

Lytton (1977) used the Gardner's equation, which relates the permeability to suction through some constant soil coefficients, to estimate the differential soil swelling within the active zone using the soil suction envelope values. The general form of the equation is as follows

$$k = \frac{k_o}{1 + a\left|h_t\right|^n} \tag{2.15}$$

where:
k = unsaturated permeability,
h_t = total suction, and
a, n = dimensionless soil property constants.

The change in suction in the vertical direction in an unsaturated soil profile can be estimated if Eq. 2.15 is plugged into Eq. 2.14 as

$$\Delta h = -\Delta z\left[1 + \left(1 + a\left|h\right|^n\right)\frac{v}{k_o}\right] \tag{2.16}$$

Values for the soil property constants a and n, and the in-situ saturated permeability values for the typical expansive soils are given in Table 2.1.

Table 2.1 Typical Field Values of Permeability for Expansive Clay Soils (Lytton 1977).

Soil	a	n	k_o (cm/s)
Yazoo	…	1.0	4.5×10^{-7}
Lackland	…	…	2.7×10^{-6}
Horsham	…	…	2.0×10^{-6}
West Laramie clay shale	10^{-9}	3.0	4.5×10^{-6}
Flagstaff Gully Dam	…	…	2.0×10^{-6}

In the VOLFLO program, for the average expansive soil coefficients as selected from Table 2.1, the modified Gardner's equation (Eq. 2.15) takes the form

$$k = \frac{2\times10^{-6}}{1+10^{-9}\left|h_t\right|^3} \tag{2.17}$$

Velocity of the horizontal moisture flow for the cases 1, 2, and 3, which are mentioned in the previous section, is estimated from the relationship

$$v = v_o\left[\frac{h_{cs}-z}{h_{cs}}\right]^n \tag{2.18}$$

where the variables are depicted in Fig. 2.11 below.

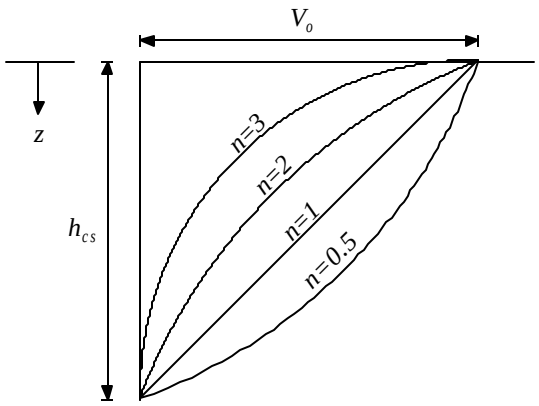

Fig.2.11. Velocity Distribution Factor (after Lytton 1977).

The volume change of expansive soils results from the applied pressure and from changes in suction. A conceptual drawing of pressure and suction versus volume change is shown in Fig. 2.12. For instance, the simultaneous decrease in suction and increase in pressure result in a small change of volume, as given by the path from point A to point C in Fig. 2.12. The suction decreases from point A′ to point B′ while the pressure increases form point B′ to point C′. The volume change process can be viewed as the net result of two processes (Lytton 1994); at constant mechanical pressure or total stress the volume increases along the path from A to B and at constant suction the volume decreases along the path from point B to point C.

For small increments of volume change on the surface described by Fig. 2.12, the volume strain is linearly related to the logarithms of both pressure and absolute value of suction (Lytton 1994). The general relation between the volumetric strain and the pressure, matric and osmotic suction for a swelling soil is given by

$$\frac{\Delta V}{V} = -\gamma_h \log_{10}\left(\frac{h_f}{h_i}\right) - \gamma_s \log_{10}\left(\frac{\sigma_f}{\sigma_i}\right) - \gamma_p \log_{10}\left(\frac{\pi_f}{\pi_i}\right) \tag{2.19}$$

and for a shrinking soil is given by

$$\frac{\Delta V}{V} = -\gamma_h \log_{10}\left(\frac{h_f}{h_i}\right) + \gamma_s \log_{10}\left(\frac{\sigma_f}{\sigma_i}\right) - \gamma_p \log_{10}\left(\frac{\pi_f}{\pi_i}\right) \tag{2.20}$$

where:

h_i, h_f = initial and final matric suction,
σ_i, σ_f = initial and final values of mean principal stress,
π_i, π_f = initial and final osmotic suction,
γ_h = volume change coefficient due to shrinking or swelling,
γ_s = volume change coefficient due to overburden,
γ_p = volume change coefficient due to osmotic effects, and
$\Delta V/V$ = percent volume change in decimal form.

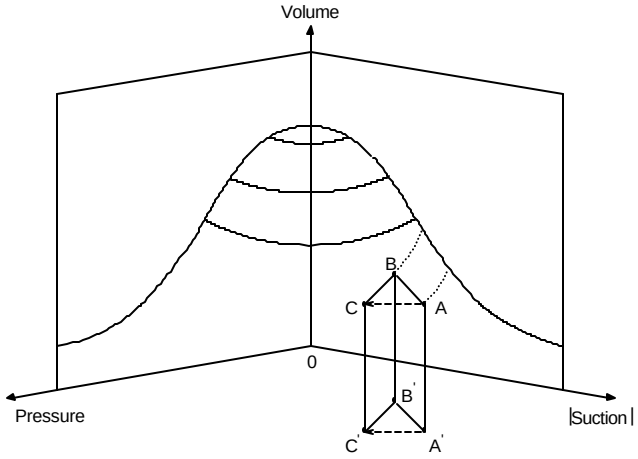

Fig. 2.12. Volume Change with Pressure and Suction for Soils (after Lytton 1994).

The overburden correction coefficient, or the initial mean principal stress, is defined as the pressure at the depth above which no volume change correction is made and can be represented as

$$\sigma_i = h_{co}(\gamma_t) \tag{2.21}$$

where:

h_{co} = depth above which no volume change correction is applied,
γ_t = unit weight of soil.

Similarly, the mean pressure at a depth z can be calculated from the following relationship

$$\sigma_f = z(\gamma_t)(1+2k_o/3) \tag{2.22}$$

where k_o is the lateral earth pressure coefficient. Due to cycling swelling and shrinking of expansive soils, the lateral earth pressure coefficient may vary practically from zero (especially when the soil shrinks) to the passive earth pressure levels (especially when the soil swells). Typical values that have been back-calculated from field observations of swelling and shrinking soils are as follows (Lytton 1994):

k_o = 0.00 when the soil is badly cracked,
k_o = 0.33 when the soil is drying,

k_o = 0.67 when the soil is wetting up, and
k_o = 1.00 when the cracks are closed and the soil is swelling.

The volume change coefficient due to shrinkage and swelling has the following relationship in terms of the percent fine clay content of the foundation soil

$$\gamma_h = [\%\ \text{fine clay (in decimal)}] \times \gamma_{100} \tag{2.23}$$

where γ_{100} is the volume change guide number for different types of active clays, which is given in the parenthesis in Fig. 2.13, which was developed by McKeen (1981) using the pressure plate apparatus and the compressibility—volume change relationship as given by the slope of Fig. 2.12 as

$$\gamma_h = -\frac{\frac{\Delta V}{V}}{\frac{\Delta h}{h}} \tag{2.24}$$

The percent fine clay represents the percent of the portion of the soil which passes the No. 200 sieve which is finer than 2 micron size, in other words

$$\%\ \text{fine clay} = \left[\frac{\%-2\ \text{micron}}{\%-\text{No.}\,200\ \text{sieve}}\right] \tag{2.25}$$

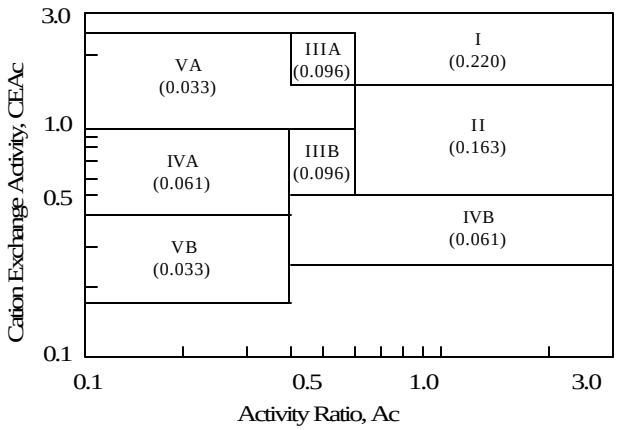

Fig. 2.13. Volume Change Guide Numbers (after McKeen 1981).

The activity ratio, Ac, and the Cation Exchange Activity ratio, CEAc, as given in Fig. 2.13 above, are used to estimate the suction compression index, γ_h, and they are defined as

$$Ac = \frac{PI\ \%}{\left(\%-2\ \text{micron}\right)} \times 100$$
$$\left(\%-\text{No.}\,200\ \text{sieve}\right) \tag{2.26}$$

$$CEAc = \frac{CEC}{\left(\%-2\ \text{micron}\right)} \times 100$$
$$\left(\%-\text{No.}\,200\ \text{sieve}\right)$$

where:
PI = plasticity index,
CEC = Cation Exchange Capacity in milliequivalents per 100 gms of dry soil.

The Cation Exchange Capacity, CEC, can be calculated in a number of ways, one of the practical methods, which was developed by Mojeckwu (1979), is to correlate it to the plasticity limit, PL, or the liquid limit, LL, value of the soil as

$$CEC \cong \left(PL\ \text{in percent}\right)^{1.17}$$
$$CEC \cong \left(LL\ \text{in percent}\right)^{0.912} \tag{2.27}$$

Similar to the derivation of the volume change coefficient for the matric suction, the coefficients for the mean principal stress and osmotic suction changes can be calculated using Fig. 2.12 and Eq. 2.19 (Lytton 1994)

$$\gamma_s = -\frac{\frac{\Delta V}{V}}{\frac{\Delta \sigma}{\sigma}} \quad \text{and} \quad \gamma_p = -\frac{\frac{\Delta V}{V}}{\frac{\Delta p}{p}} \tag{2.28}$$

The compression index for the mean principal stress is also related to the commonly used swelling compression index, C_s by

$$\gamma_s = \frac{C_s}{1+e_o} \tag{2.29}$$

where e_o is the void ratio and C_s is given by the slope depicted in Fig. 2.14.

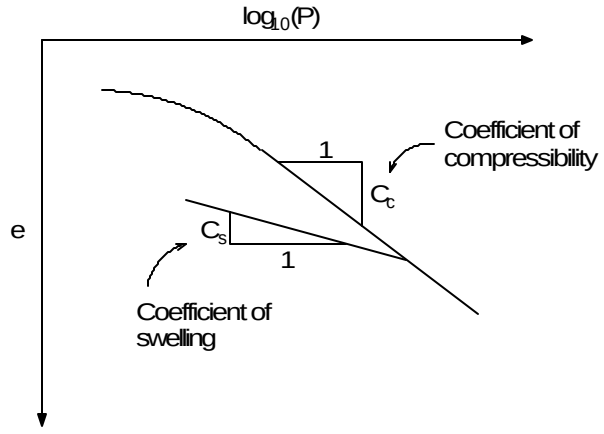

Fig. 2.14. A Typical e-logP Curve.

The compression index, γ_σ, is also related to γ_h by the following equation (Lytton 1994)

$$\gamma_s = \gamma_h \frac{1}{1+\frac{h}{\sigma\left(\frac{\partial h}{\partial \sigma}\right)}} \tag{2.30}$$

where:
θ = volumetric water content,
h = suction, and
$\partial h/\partial\theta$ = slope of the suction versus volumetric water content as shown in Fig. 2.15.

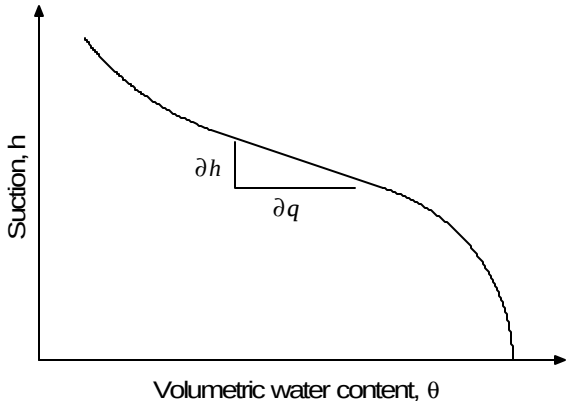

Fig. 2.15. A Typical Soil-Water Characteristic Curve.

The part of Eq. 2.30, which is on the right side of γ_h, is less than 1, so the index γ_s can be taken equal to γ_h for all practical reasons. Then, the vertical volume change at depth z below the edge of the foundation is calculated as

$$\frac{\Delta H}{H} = f\left(\frac{\Delta V}{V}\right) \tag{2.31}$$

where f is a crack fabric factor. The back-calculated values for f are 0.5 when the soil is shrinking and 0.8 when the soil is swelling. Therefore, the total heave or shrinkage at depth z is

$$y_m = \Sigma\left(\frac{\Delta H}{H}\right)_i(\Delta z) \tag{2.32}$$

where Δz is the vertical increment.

2.3.1.2 Naiser's Study of Predicting Vertical Soil Movement

Naiser (1997) improved the current method (i.e., basically the VOLFLO method) of predicting the differential movements for expansive soils. Naiser presents the procedures to calculate suction profiles and to predict soil swelling and shrinking beneath foundations which generate maximum slab distortion modes. The suction profiles are developed using the variables such as depth, time, local surface annual weather and vegetation conditions, the suction compression index, unsaturated permeability, and unsaturated soil diffusivity.

The main contributions of this research are: equations and procedures to calculate the equilibrium suction profile and depth to constant suction for a particular soil profile and location, equations to calculate the horizontal velocity flow of water in unsaturated soils, the methodology to predict differential soil movement shortly after a slab has been constructed and before the soil under the slab has reached an equilibrium moisture content, and procedures to apply differential soil movement theory to soil profiles with multiple layers and moisture effects cases to be used for slab-on-ground design.

The current version of VOLFLO, which is used along with the PTI slab program, is based on the principles described in the previous section and Naiser (1997) has expanded the parameters involved in the current VOLFLO procedure in predicting the volume changes of expansive soils by incorprating the work done by Mitchell (1980) and Gay (1994). Mitchell (1980) developed and applied simple mathematical methods for predicting soil suction profiles. Gay (1994) developed a finite element program (FLODEF) for the transient moisture flow in unsaturated soils and a procedure to estimate the mean volumetric water content for soils dependent upon the location and climatic conditions.

The procedures mentioned above are applied to several moisture effect cases that are common with light commercial and residential structures such as bare soils at the surface, grass at the surface, trees at the surface, and a flowerbed at the surface. Additionally, these procedures include calculating the effects of differential soil movement caused by the introduction of design effects such as vertical and horizontal moisture barriers.

2.3.1.3 Mitchell's Method of Predicting Suction Distribution in a Soil Profile

From the concept that the volume change of an expansive soil is a function of the rate of moisture diffusion, which is due to a suction change gradient, through the soil and as well as the soil type, Mitchell (1980) developed a diffusion equation that governs the soil suction distribution in time and location. The general form of the moisture diffusion equation, which is used to predict the expansive soil movement from a known source of moisture or suction change, is as follows

$$\frac{\partial^2 u}{\partial x^2}+\frac{\partial^2 u}{\partial y^2}+\frac{\partial^2 u}{\partial z^2}+\frac{f(x,y,z,t)}{p}=\frac{1}{\alpha}\frac{\partial u}{\partial t} \tag{2.33}$$

where:
u = soil suction,
x,y,z = cartesian coordinates,
$f(x,y,z,t)$ = moisture inflow rate per unit volume,
t = time,
p = unsaturated permeability, and
α = soil moisture diffusivity.

If the soil moisture diffusivity is assumed as a constant over a small range of soil suction change, the unsaturated permeability can be related the soil moisture diffusivity as follows

$$p = \frac{\alpha\gamma_d}{|S|\gamma_w} \tag{2.34}$$

where:
$|S|$ = absolute value of the slope of the suction versus gravimetric water content curve,
γ_d = dry unit weight of the soil, and

γ_w = unit weight of water.

Mitchell's unsaturated permeability, p, is also related to the saturated permeability, k_o, as given below

$$p = \frac{k_o |h_o|}{0.4343} \tag{2.35}$$

where h_o is a constant suction value of approximately –100 cm for clays. From Eqs. 2.34 and 2.35, the soil moisture diffusivity, α, can be determined easily from three soil properties; unsaturated permeability, dry unit weight, and the slope of suction versus gravimetric water content, which can also easily be established from several soil samples at different suction levels thus different water content levels (Fig.2.16).

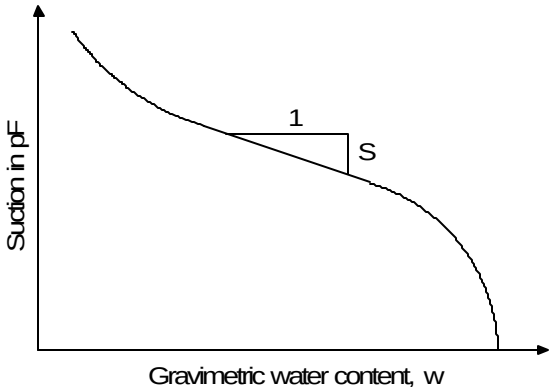

Fig. 2.16. A Typical Suction versus Gravimetric Water Content Curve.

The Mitchell's diffusion coefficient can also be estimated from the suction compression, γ_h, characteristics of the soil and using the slope of the suction versus water content curve, S, which is a negative value, (Lytton 1994) as

$$\alpha = 0.0029 - 0.000162\,(S) - 0.0122\,(\gamma_h) \tag{2.36}$$

and the value of *S* from

$$S = -20.29 + 0.1555(LL\%) - 0.117(PI\%) + 0.0684(\%\text{-}\#200) \tag{2.37}$$

where:

LL = liquid limit in percent,

PI = plasticity index in percent, and

-#200 = percent of the soil passing the #200 sieve.

Mitchell also introduces two test methods that can be employed to estimate the diffusion coefficient; the Soaking Test and the Evaporation Test. Both of the test methods are described in detail by Mitchell (1980). Once the diffusion coefficient of the soil has been measured, the diffusion equation can be solved to obtain the suction distribution within a soil profile by applying the appropriate boundary conditions of the problem. After the suction distribution is obtained, the soil movements induced by these suction changes can be calculated form the volume strain equation.

The suction profiles for time dependent moisture variations in an expansive soil profile can be estimated by solving the diffusion equation (Eq. 2.33) in the *z*-direction, and assuming that the solution is a periodic function of cosine and sine functions, as (Mitchell 1980)

$$h(z,t) = h_c + h_o e^{\left(-z\sqrt{\frac{\pi n}{\alpha}}\right)} \cos\left(2\pi n t - z\sqrt{\frac{n\pi}{\alpha}}\right) \tag{2.38}$$

where:

$h(z,t)$ = suction as a function of depth and time,

h_c = equilibrium suction value expressed in pF,

h_o = amplitude of suction change at the surface,

α = soil diffusion coefficient using Mitchell's unsaturated permeability,

n = number of suction cycles per second, and

t = time in seconds.

To calculate the maximum and minimum suction profiles, Naiser (1997) sets the cosine term in Eq. 2.38 to 1 and arrives at

$$h(z,t) = h_c + h_o e^{\left(-z\sqrt{\frac{\pi n}{\alpha}}\right)} \tag{2.39}$$

Equation 2.39 indicates that the limiting suctions decrease exponentially with depth as a function of the coefficient of diffusion, and therefore the depth to constant suction, z_m, can be obtained by solving Eq. 2.39 for *z* as follows

$$z_m = -\frac{1}{\sqrt{\frac{n\pi}{\alpha}}} \ln\left[\frac{h(z,t) - h_c}{h_o}\right] \tag{2.40}$$

Values of h_c and h_o for clay soils with different levels of Mitchell's unsaturated permeability have been calculated using a trial and error procedure (Lytton 1994). Table 2.2 gives the h_c and h_o values that change with the soil type and Thorntwaite Moisture Index, TMI, for the wet suction profile. Values of *n* are taken as 1 cycle per year for all TMI less than –30.0 and 2 cycles per year for all TMI greater than –30.0. The dry suction profile has a h_c value of 4.5 pF and h_o value of 0.0 pF. Table 2.3 gives the equilibrium suction values, which are dependent on the Mitchell unsaturated permeability and the Thornthwaite Moisture Index, that can be used to estimate suction profiles.

For unsaturated soils, it is known that the permeability is not a constant, but is a variable dependent on total suction. Laliberte and Corey (1967) relates the unsaturated permeability, k, to the total suction, h_t, as follows

$$k = k_o \left(\frac{h_o}{h_t}\right)^n \tag{2.41}$$

where *n* is a positive constant and is close to 1 for clays and 4 for sands. If this equation, for an *n* value of 1, is substituted for the unsaturated permeability in Eq. 2.14, the following equation, which can be employed to the estimate changes in suction in a vertical soil profile, can be obtained

$$\Delta h = -\Delta z\left[1+\frac{v}{k_o}\frac{h}{h_o}\right] \qquad (2.42)$$

where h_o is a constant suction value of approximately –100 cm for clays. This equation takes into account, to some degree, the increased permeability of the soil due to the cracks that are open at high suction levels as compared to the values calculated using Eq. 2.16 (Lytton 1994).

Table 2.2. Values for the Wet Suction Profile (after Lytton 1994).

Thornthwaite Moisture Index	Mitchell unsaturated permeability (cm^2/s)	h_c (pF)	h_o (pF)
-46.4	5×10^{-5}	4.43	0.25
	1×10^{-3}	4.27	0.09
-11.3	5×10^{-5}	3.84	1.84
	1×10^{-3}	2.83	0.83
26.8	5×10^{-5}	3.47	1.47
	1×10^{-3}	2.79	0.79

Table 2.3. Equilibrium Suction Values (after Lytton 1994).

Thornthwaite Moisture Index	Mitchell Unsaturated Permeability (cm^2/s)		
	1×10^{-3}	2.5×10^{-4}	5×10^{-5}
-46.5	4.27	4.32	4.43
-30.0	3.80	3.95	4.29
-21.3	3.42	3.64	4.20
-11.3	2.83	3.10	3.84
26.8	2.79	3.05	3.47

2.3.2 Edge Moisture Variation Distance

Differential expansive soil movement, which is a very important parameter in designing the slab foundations, may take different distortion shapes, but the most important shapes for the design purposes are the ones that generate the maximum values of moment, shear, and deflection. The two critical distortion modes that are used in the slab-on-expansive soil foundation designs are the edge lift and center lift conditions as depicted in Fig. 2.3. The edges of the slab will move up or down in response to the seasonal moisture changes. The distance within which these changes takes place is called the edge moisture variation distance (Lytton 1977). In other words, the edge moisture variation distance is considered to be the distance between the edge of the slab foundation and the point beneath the slab where the suction change is at tolerable value (usually less than 0.2 pF). An empirical relation between the edge moisture variation distance and the Thornthwaite Moisture Index (Fig. 2.8) has been used in the PTI design method. It is also known that the edge moisture variation distance depends on the permeability of the soil (Lytton 1994) and therefore can be obtained by this relation.

Gay (1994) developed a finite element program (named as FLODEF) for the transient moisture flow in unsaturated soils, which uses the unsaturated soil properties such as the soil moisture diffusion and unsaturated permeability. This program has been used extensively by Jayatilaka et al. (1992) in the study of vertical moisture barriers. Lytton (1994) used the results of the program to correlate the edge moisture variation distance with the unsaturated soil properties. Edge lift conditions were simulated by a one year wet spell following a dry suction profile condition. Center lift conditions were simulated by a one year dry spell following a wet suction profile condition. The dry and wet conditions used annual suction variation patterns that were appropriate for each of nine different climatic zones ranging from a TMI of –46.5 to +26.8, a typical range for Texas. The resulting edge moisture variation distances for the center lift cases are depicted in Fig. 2.17.

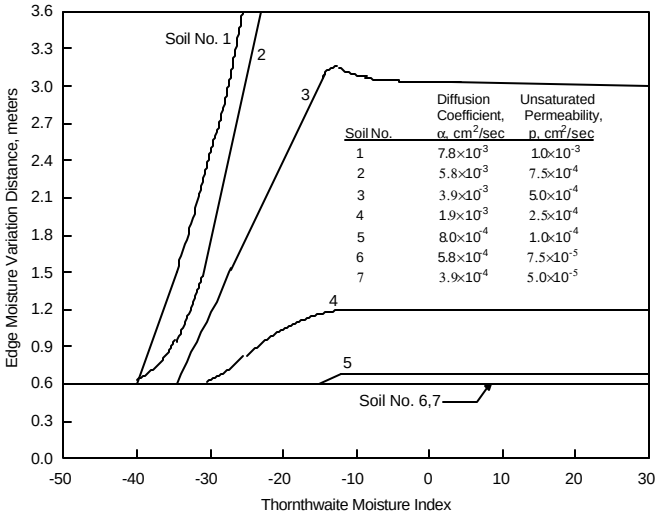

Fig. 2.17. Edge Moisture Variation Distances for Center Lift Case (after Lytton 1994).

Seven different soils were used to calculate the relationship between the edge moisture variation distances and TMI. For the center lift condition (Fig.17), the Soils No. 1, 2, and 3 were selected as pervious and Soils No. 5, 6, and 7 were chosen as practically impervious. Only soils with the properties No. 3 and 4 have edge moisture variation distances in the range used in the current PTI manual (Lytton 1994).

The edge moisture variation distances for the edge lift condition are given in Fig. 2.18. Similar to the center lift case soil types, the Soils No. 5, 6, and 7 are chosen as practically impervious while Soils No. 2, 3, and 4 have edge moisture variation distances in the range used in the current PTI manual, and the Soil No. 1 is more pervious and is outside the range. The edge moisture variation distances of soils with different unsaturated permeabilities different than these seven soil types can be found by interpolation on these two figures.

Simple laboratory tests can be used to determine important properties of expansive soils such as the unsaturated soil permeability and diffusivity, and in return these parameters can be employed to predict a very important parameter, the edge moisture variation distance, for the analysis and design of slab foundations. Lytton (1997) developed a method to determine the edge moisture variation distance for a particular design return period. In developing the method, Lytton makes use of the design return periods that that were used to obtain the edge

moisture variation distances as given in Figs. 2.8, 2.17, and 2.18. The design return period used for Fig. 2.8 is 10 years while for Figs. 2.17 and 2.18 is 50 years. The design periods are usually within these ranges of 10 to 50 years, typically being 20 years with 5% risk (Naiser 1997).

The resulting equation for the edge moisture variation distance is as follows

$$e_{m_r} = e_{m_{10}} + \left(e_{m_{50}} - e_{m_{10}}\right)\left(\frac{z_r - z_{10}}{z_{50} - z_{10}}\right) \tag{2.43}$$

where $e_{m_r}, e_{m_{10}}, \text{and } e_{m_{50}}$ are the edge moisture variation distances for the return period of *r*, 10, and 50 years, respectively. The use of the Gumbel probability density function, which is commonly used to represent the probability of weather events, may be used to establish the risk level that is desired for design service life of the structure. The z_r, z_{10}, and z_{50} values used in Eq. 2.43 are computed from the Gumbel cumulative probability distribution curve as follows

$$z_r = \frac{\boldsymbol{r}}{\left[-\ln\left(1-\frac{1}{r}\right)\right]^{\frac{1}{b}}} \tag{2.44}$$

where both $\boldsymbol{r}$ and $\boldsymbol{b}$ are shape factors and can be assumed as one, and *r* is the desired return period.

Gay (1994) did extensive work in the area of calculating the mean volumetric moisture content for a given soil mass dependent upon the soil's depth of available moisture, d_{am}, and the location's potential evapotranspiration (i.e., the Thornthwaite Moisture Index). The depth of available moisture, d_{am}, is defined as the maximum depth of moisture available for use by transpiring vegetation, which is stored within the soil zone down to the depth to constant suction. Gay developed a set of functional relationships that are used to calculate the mean volumetric moisture content, which are then used to calculate the equilibrium suction value for a particular soil profile and location.

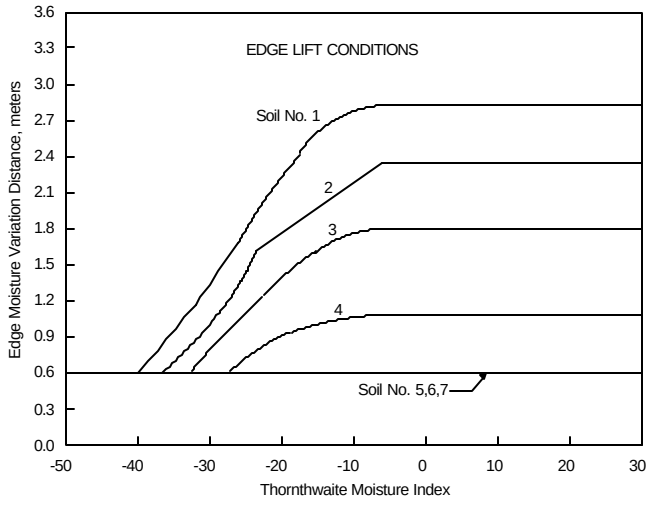

Fig. 2.18. Edge Moisture Variation Distances for Edge Lift Case (after Lytton 1994).

2.4 This Study

The analysis method developed in this study is aimed at improving the rationality of the soil structure interaction models proposed by the earlier researchers. An upper bound solution is obtained by assuming the worst initial mound shape, which is simply defined by two parameters e_m and y_m. The soil is modeled as an elastic half-space. This is more rational than the previous Winkler and coupled-spring models and is represented in the program by surface finite elements. The structure and foundation are represented by conventional rectangular finite elements which enable any raft geometry and load distribution to be dealt with easily.

Once the mound shape has been defined the initial area of contact between it and the raft is readily determined. When the self weight, dead and live loadings are applied, the raft undergoes immediate settlements which is determined by putting the appropriate elastic properties of the soil and the slab into the program. As deflections take place, the contact area normally increases and therefore iterations must be carried out to obtain the equilibrium solution.

CHAPTER III
SOIL SUCTION AND EXPANSIVE SOILS

3.1 Soil Suction Concept

Many techniques have been developed to determine the properties of unsaturated soils. Of these properties, soil suction has proven to be most favorable as it takes into account many of the fundamental concepts associated with the behavior of unsaturated soils (Mitchell and Avalle 1984). Soil suction is one of the most important parameters describing the moisture condition of unsaturated soils.

In general, porous materials have a fundamental ability to attract and retain water. The existence of this fundamental property in soils is described in engineering terms as suction, negative stress in the pore water. In engineering practice, soil suction is composed of two components: matric and osmotic suction. The sum of matric and osmotic suction is called total suction. Matric suction comes from the capillarity, texture, and surface adsorptive forces of the soil. Osmotic suction arises from the dissolved salts contained in the soil water. This relationship can be formed in an equation as follows

$$h_t = h_m + h_p \tag{3.1}$$

where h_t is total suction, h_m is matric suction, and h_p is osmotic suction.

Total suction can be calculated using Kelvin's equation, which is derived from the ideal gas law using the principles of thermodynamics and is given as

$$h_t = \frac{RT}{V}\ln\left(\frac{P}{P_o}\right) \tag{3.2}$$

where:
h_t = total suction,
R = universal gas constant,
T = absolute temperature,
V = molecular volume of water,
P / P_o = relative humidity,
P = partial pressure of pore water vapor, and
P_o = saturation pressure of water vapor over a flat surface of pure water at the same temperature.

The total suction value of a soil sample can be inferred from the relative humidity and suction relationship (i.e., Eq. 3.2) if the relative humidity is evaluated in some way. In a closed system, if the water is pure enough, the partial pressure of the water vapor at equilibrium is equal to the saturated vapor pressure at temperature, T. However, the partial pressure of the water vapor over a partly saturated soil will be less than the saturation vapor pressure of pure water due to the soil matrix structure and the free ions and salts contained in the soil water (Fredlund and Rahardjo 1993). Under isothermal conditions in closed systems the relative humidity may be associated with the water content of the system such as 100 percent relative humidity refers to a fully saturated condition. The relative humidity and the water content relationship in closed environments is the basis behind the working principle of total suction measuring devices such as filter paper methods and psychrometers.

In engineering practice, soil suction has usually been calculated in *pF* units (Schofield 1935) (i.e., suction in $pF = log_{10}(|suction\ in\ cm\ of\ water|)$). However, soil suction is also currently being represented in the *log kPa* unit system (i.e., suction in $log\ kPa = log_{10}(|suction\ in\ kPa|)$). The relationship between these two systems of units is approximately $suction\ in\ log\ kPa = suction\ in\ pF - 1$.

Matric suction can be calculated from pressure plate and pressure membrane devices as the difference between the applied air pressure and water pressure across a porous plate. Matric suction can be formed in a relationship, from equilibrium of pressures across the water meniscus, as follows

$$h_m = -(u_a - u_w) \tag{3.3}$$

where h_m is matric suction, u_a is applied air pressure, and u_w is free water pressure at atmospheric condition.

The osmotic suction of electrolyte solutions, that are usually employed in the calibration of filter papers and psychrometers, can be calculated using the relationship between osmotic coefficients and osmotic suction. Osmotic coefficients are readily available in the literature for many different salt solutions. Table 3.1 gives the osmotic coefficients for several salt solutions.

Osmotic coefficients can also be obtained from the following relationship (Lang 1967) as

$$\phi = -\frac{\rho_w}{\nu m w}\ln\left(\frac{P}{P_o}\right) \tag{3.4}$$

where:
ϕ = osmotic coefficient (dimensionless),
ν = number of ions from one molecule of salt (i.e., ν = 2 for NaCl, KCl, NH_4Cl and ν = 3 for Na_2SO_4, $CaCl_2$, $Na_2S_2O_3$, etc.),
m = molality, moles solute per 1000g solvent,
w = molecular mass of water,
ρ_w = density of water,
P/P_o = relative humidity,
P = partial pressure of pore water vapor, and
P_o = saturation pressure of water vapor over a flat surface of pure water at the same temperature.

The relative humidity term, P/P_o, in Eq. 3.4 is also known as the activity of water, a_w, in physical chemistry of electrolyte solutions. The combination of Eq. 3.2 and Eq. 3.4 gives a useful relationship that can be adopted to calculate osmotic suctions for different salt solutions as

$$h_p = -\nu RTm\phi \tag{3.5}$$

Table 3.2 gives osmotic suctions for several salt solutions using osmotic coefficients from Table 3.1 and Eq. 3.5.

Table 3.1. Osmotic Coefficients for Several Salt Solutions.

Molality (m)	Osmotic Coefficients at 25°C						
	NaCl[a]	KCl[a]	NH_4Cl[a]	Na_2SO_4[b]	$CaCl_2$[c]	$Na_2S_2O_3$[b]	$MgCl_2$[c]
0.0010	0.9880	0.9880	0.9880	0.9608	0.9623	0.9613	0.9627
0.0020	0.9840	0.9840	09840	0.9466	0.9493	0.9475	0.9501
0.0050	0.9760	0.9760	0.9760	0.9212	0.9274	0.9231	0.9292
0.0100	0.9680	0.9670	0.9670	0.8965	0.9076	0.8999	0.9106
0.0200	0.9590	0.9570	0.9570	0.8672	0.8866	0.8729	0.8916
0.0500	0.9440	0.9400	0.9410	0.8229	0.8619	0.8333	0.8708
0.1000	0.9330	0.9270	0.9270	0.7869	0.8516	0.8025	0.8648
0.2000	0.9240	0.9130	0.9130	0.7494	0.8568	0.7719	0.8760
0.3000	0.9210	0.9060	0.9060	0.7262	0.8721	0.7540	0.8963
0.4000	0.9200	0.9020	0.9020	0.7088	0.8915	0.7415	0.9206
0.5000	0.9210	0.9000	0.9000	0.6945	0.9134	0.7320	0.9475
0.6000	0.9230	0.8990	0.8980	0.6824	0.9370	0.7247	0.9765
0.7000	0.9260	0.8980	0.8970	0.6720	0.9621	0.7192	1.0073
0.8000	0.9290	0.8980	0.8970	0.6629	0.9884	0.7151	1.0398
0.9000	0.9320	0.8980	0.8970	0.6550	1.0159	0.7123	1.0738
1.0000	0.9360	0.8980	0.8970	0.6481	1.0444	0.7107	1.1092
1.2000	0.9440	0.9000	0.8980	...	...	...	...
1.4000	0.9530	0.9020	0.9000	...	...	...	...
1.5000	...	...	...	0.6273	1.2004	0.7166	1.3047
1.6000	0.9620	0.9050	0.9020	...	...	...	...
1.8000	0.9730	0.9080	0.9050	...	...	...	...
2.0000	0.9840	0.9120	0.9080	0.6257	1.3754	0.7410	1.5250
2.5000	1.0130	0.9230	0.9170	0.6401	1.5660	0.7793	1.7629

References:
[a]Hamer and Wu 1972
[b]Goldberg 1981
[c]Goldberg and Nuttell 1978

Unsaturated soils consist of three phases: soil solid, water, and air, and the interaction of these phases is very complex. Soil suction, or free energy of soil water, which is a thermodynamic quantity, is the parameter that describes the behavior of unsaturated soils. A brief attempt has been made to describe soil suction, or Gibbs free energy of soil water, from the viewpoint of thermodynamics in Appendix A.

3.2 Soil Suction Measurement

The measurement of soil suction is crucial for applying the theories of the engineering behavior of unsaturated soils. With a reliable soil suction measurement technique, the initial and final soil suction profiles can be obtained from samples taken at convenient depth intervals. The change in suction with seasonal moisture movement is valuable information for many engineering applications.

There are several commonly used soil suction measuring devices in the current geotechnical practice such as filter paper, transistor psychrometer, thermocouple psychrometer, pressure plate and membrane. With the filter paper method, both total and matric suction measurements are possible, but one can only measure total suction with the psychrometers and matric suction with the pressure plates or membranes.

3.2.1 The Filter Paper Method

The filter paper method has long been used in soil science and engineering practice and it has recently been accepted as an adaptable test method for soil suction measurements because of its advantages over other suction measurement devices. The filter paper method is an inexpensive and relatively simple laboratory test method, from which both total and matric suction measurements are possible.

Basically, the filter paper comes to equilibrium with the soil either through vapor (total suction measurement) or liquid (matric suction measurement) flow. At equilibrium, the suction value of the filter paper and the soil will be equal. After equilibrium is established between the filter paper and the soil, the water content of the filter paper disc is measured. Then, by using a filter paper water content versus suction calibration curve developed using osmotic salt solutions, the corresponding suction value is found from the curve.

Table 3.2. Osmotic Suctions of Several Salt Solutions.

Molality (m)	Osmotic Suctions in kPa at 25°C						
	NaCl	KCl	NH_4Cl	Na_2SO_4	$CaCl_2$	$Na_2S_2O_3$	$MgCl_2$
0.001	5	5	5	7	7	7	7
0.002	10	10	10	14	14	14	14
0.005	24	24	24	34	34	34	35
0.010	48	48	48	67	67	67	68
0.020	95	95	95	129	132	130	133
0.050	234	233	233	306	320	310	324
0.100	463	460	460	585	633	597	643
0.200	916	905	905	1115	1274	1148	1303
0.300	1370	1348	1348	1620	1946	1682	2000
0.400	1824	1789	1789	2108	2652	2206	2739
0.500	2283	2231	2231	2582	3396	2722	3523
0.600	2746	2674	2671	3045	4181	3234	4357
0.700	3214	3116	3113	3498	5008	3744	5244
0.800	3685	3562	3558	3944	5880	4254	6186
0.900	4159	4007	4002	4384	6799	4767	7187
1.000	4641	4452	4447	4820	7767	5285	8249
1.200	5616	5354	5343	...	...	...	...
1.400	6615	6261	6247	...	...	...	...
1.500	...	...	...	6998	13391	7994	14554
1.600	7631	7179	7155	...	...	...	...
1.800	8683	8104	8076	...	...	...	...
2.000	9757	9043	9003	9306	20457	11021	22682
2.500	12556	11440	11366	11901	29115	14489	32776

3.2.1.1 Background of the Filter Paper Method

The filter paper method, which was developed in Europe in the 1920s, came to the United States in 1937 with Gardner (1937) started its initial applications in the field of soil science. Since then, the filter paper method has been used and investigated by numerous researchers. Many research scientists have tackled different aspects of the filter paper method. Different types of materials were used, such as filter papers and suction measuring devices, and different experimental techniques to calibrate the filter paper and to measure suction of the soil sample. Therefore, it is very difficult to compare these methods on a one-to-one basis. All the calibration curves established from Gardner (1937) to Swarbrick (1995) appear to have been constructed as a single curve by using different filter papers, a combination of different soil suction measuring devices, and different calibrating testing procedures. However, Houston et al. (1994) developed two different calibration curves; one for total suction and one for matric suction measurements using Fisher quantitative coarse filter papers. For the total suction calibration curve, saturated salt solutions and for the matric suction calibration curve tensiometers and pressure membranes were employed. Houston et al. (1994) reported that the total and matric suction calibration curves were not compatible. This simply implies that two different calibration curves, one for matric and one for total suction, need to be used in soil suction measurements. However, it is believed that the two curves reflect an expected hysteresis between wetting and drying effects and that the appropriate curve for both matric and total suction is the wetting curve

since this matches the process that the filter paper undergoes in the measurement process.

3.2.1.2 Calibration of the Filter Papers

The calibration for the suction wetting curve for filter paper using salt solutions is based upon the thermodynamic relationship between total suction (or osmotic suction) and the relative humidity resulting from a specific concentration of a salt in distilled water. Pressure plate and pressure membrane devices are usually employed in the drying filter paper calibration. The pressure plate apparatus can measure matric suction values up to 150 kPa. However, with the pressure membrane device matric suction values can be extended up to 10,000 kPa.

A wetting curve using sodium chloride solutions and a drying curve using pressure plate and pressure membrane devices were constructed by the author for Schleicher & Schuell No. 589-WH filter papers. The calibration curves are shown in Fig. 3.1. As it is seen from the figure the wetting curve plots below the drying suction curve, as is expected of the hysteresis process.

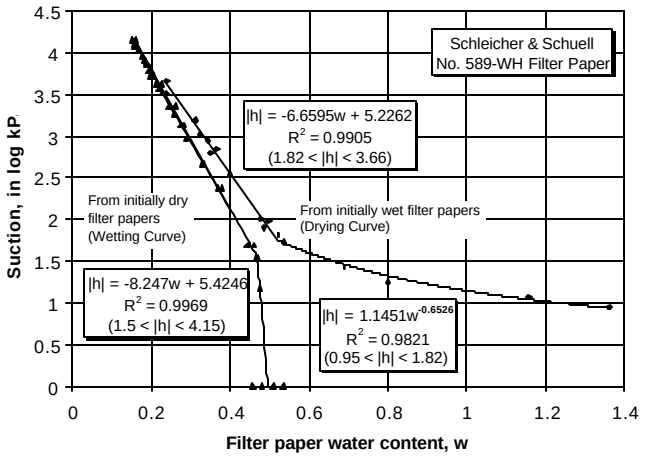

Fig. 3.1. Wetting and Drying Filter Paper Calibration Curves.

3.2.1.3 Soil Total and Matric Suction Measurements with the Filter Paper

Soil total suction measurements are similar to those measurements in the filter paper calibration testing. The same testing procedure can be followed by replacing the salt solution with a soil sample. Soil matric suction measurements are also similar to the total suction measurements except that an intimate contact should be provided between the filter paper and the soil. A suggested testing procedure for soil total and matric suction measurements using filter papers is outlined in Appendix B.

3.2.2 Thermocouple Psychrometers

The thermocouple psychrometer is currently one of the most widely used methods of soil suction determination which can be used either in the field or the laboratory. Spanner (1951) described a method of measuring vapor pressure without the need to place a drop of water on the evaporating junction. The Peltier effect is used to condense a drop of water on the evaporating junction. A typical drawing of a thermocouple psychrometer is depicted in Fig. 3.2.

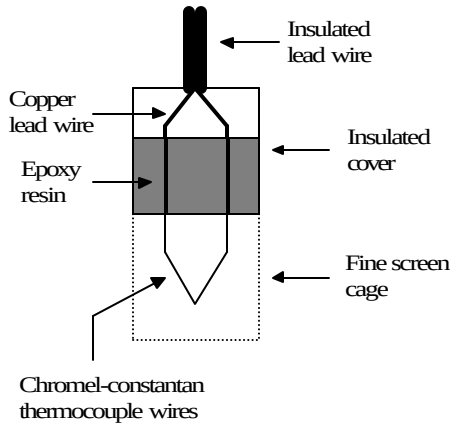

Fig. 3.2. Schematic Drawing of a Thermocouple Psychrometer.

Peltier in 1834 discovered that upon passing a current across a junction of two dissimilar metals, there is an absorption of heat at the junction, causing the temperature to rise or fall, depending on the direction of applied current. If the degree of cooling is sufficient enough to bring the junction below the dew point of the surrounding moisture, the moisture will condense on the junction. Initially, the thermocouple is cooled below the dew point temperature by passing a current through the junction. Once the instrument is cooled, the thermocouple is controlled by the evaporation or condensation of the water on the junction. The temperature of the thermocouple then converges to the dew point where evaporation ceases and the temperature remains constant. The current necessary for the tip to accomplish this and remain at the dew point is related to the relative humidity. A relationship between micro-voltage and soil suction is established by calibration tests as shown in Fig. 3.3.

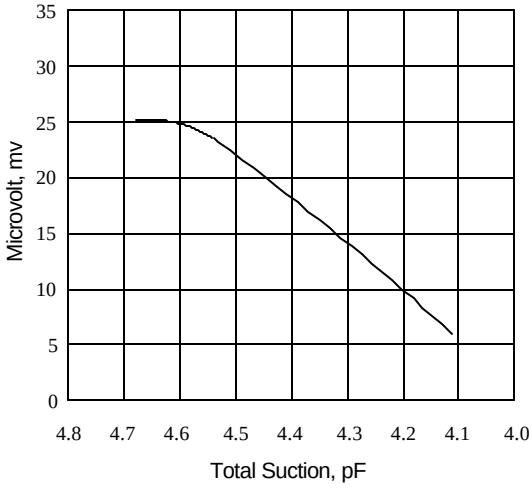

Fig. 3.3. A Typical Thermocouple Psychrometer Calibration Curve.

The thermocouple psychrometers can cover the range of relative humidities from 94% to close to 100%, corresponding to the suction values up to 8,000 kPa.

However, in order to measure suctions to an accuracy of about 10 kPa, the apparatus must be capable of distinguishing dew points to the order of 0.001^{o} C (Spanner 1951). This factor puts a severe limitation on the accuracy of the thermocouple psychrometers. The reliable resolution of the thermocouple psycrometers is in the order of 100 kPa (Lee 1991).

3.2.3 Transistor Psychrometers

With the rapid progress in microchip technology over the last twenty years it has now become possible to use transistors for measuring relative humidity. The transistor psychrometer has been developed in Australia to effectively replace the thermocouple psychrometer for total suction measurement. The transistor psychrometer operates in a thermally insulated bath. The variation of room temperature is controlled to be within $\pm 0.5^{o}$C. The transistor psychrometer is capable of measuring total suction ranging from 100 kPa (about 3 pF) to 10,000 kPa (about 5.5 pF) with an accuracy of about ±10 kPa (±0.01 pF). This accuracy is greater than that required for most engineering applications.

The psychrometer system consists of the following parts: the probes, a thermally insulated bath, and the constant temperature room. For the calibration of the probes and the testing stages, the probes are enclosed in a thermally insulated bath. Standard salt solutions are used for calibrating the probes. A typical drawing of a transistor psychrometer probe is depicted in Fig. 3.4.

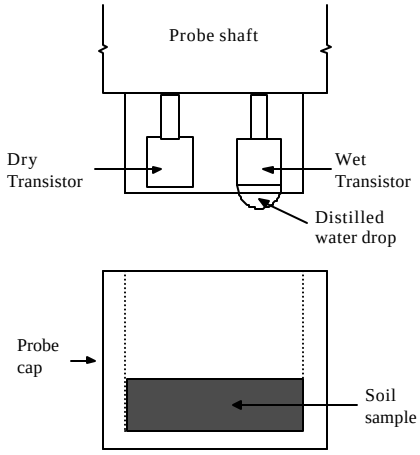

Fig. 3.4. A Schematic Drawing of a Transistor Psychrometer Probe.

There are two transistors, the wet and dry bulb transistors, within each of the probe. The transistors are very sensitive to minor changes in temperature and thus a constant temperature environment is important. The flow of water molecules from the water drop to the saturated filter paper (saturated with the salt solution for the calibration or conditioning) or the surface of a soil specimen produces cooling of the wet transistor relative to the dry transistor. The temperature differences recorded in millivolts (mV) are converted to a total suction for each of the specimens tested.

3.2.4 Pressure Plate and Pressure Membrane

The pressure plate and pressure membrane devices and methods were developed in the soil science field to study the water uptake and retention of soils. The soil water characteristic curve which is obtained by plotting various applied pressures (matric suctions) against the water contents of soil specimens has wide areas of application in geotechnical engineering. The main components of the pressure plate and membrane apparatus are a pressure chamber, a porous ceramic plate or cellulose membrane, and an air compressor. A typical schematic drawing of a pressure plate or pressure membrane apparatus is shown in Fig. 3.5.

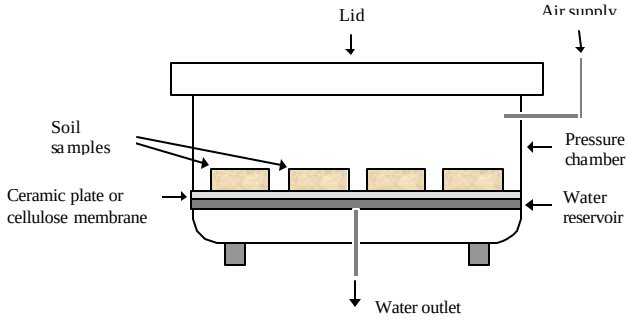

Fig. 3.5. A Schematic Drawing of a Pressure Plate or Pressure Membrane Device.

The main difference between the pressure plate and pressure membrane devices is that the former uses a ceramic porous disk that can be used for pressures up to 150 kPa and the later uses cellulose membranes with which pressures can be extended up to 10,000 kPa. The ceramic disks are rigid enough to carry the soil specimens on them, but a support is provided for the highly flexible membrane.

Prior to each test, the porous plate or the membrane is completely saturated with distilled water and then sealed within the pressure chamber along with the soil specimens which rested on the surface of the plate or membrane (Fig. 3.5). With the influence of the applied air pressure, the moisture inside the soil specimen and the ceramic plate or the membrane is expelled out and collected in a graduated cylinder until a suction equilibrium is reached between the soil specimen and the applied air pressure. At equilibrium, the suction inside the soil specimen equals the applied air pressure. The air pressure is then released and the moisture content of the soil specimen is determined.

3.3 Expansive Soils

Expansive soils cause damages to structures due to soil volume changes induced by changes in soil moisture conditions (soil suction). Swelling or shrinkage does not occur uniformly within the soil mass underlying the structure and thus results in differential soil movements. It is this differential movement that causes major distress in lightweight structures such as houses, warehouses, and pavements. The typical damages caused by the expansive soil are cracking in building walls, distorted foundation slabs, and misaligned or broken utility pipelines. Expansive soil is one of the most costly natural disasters in the U.S., although its destructive impact is not as catastrophic as earthquakes or tornadoes, but it is responsible for $2.2

billion in structural damages each year (Jones and Holtz 1973). The primary problem that arises with expansive soil is its volume change and high swelling pressure as the soil moisture state changes.

Not all soils create problems due to swelling when brought into contact with a water source. Only soils with high swelling potential will cause damage to buildings. The clay minerals are generally classified into three main groups for most engineering purposes as kaolinite, illite, and montmorillonite. Montmorillonites undergo greater volume changes upon changes in suction than do kaolinites and illites. In these soils large magnitudes of volume strains are involved that it is not possible to predict with the classical soil mechanics principles.

3.3.1 Clay Minerals

Clay soils are generally composites of different combinations of several clay minerals, such as kaolinites, illites, and montmorillonites. These clay minerals are tiny crystalline substances with particle sizes ranging from 10^{-6} mm to 1μm, and are generally referred to as colloids. Unlike sands and silts, the grain size distribution of clays has almost no influence on the engineering behavior whereas colloidal properties such as adsorption of water due to large specific surface area of the particles dominate the performance of the clay soils (Grim 1953, Hillel 1980).

Clay minerals are formed by chemical weathering of rock forming minerals (i.e., decomposition of the primary minerals and their recomposition into new ones). Chemically, clay minerals are hydrous alumino-silicates. Typical alumino-silicate clay minerals exist as layered microcrystals, composed of two fundamental structural units: the silicon-oxygen tetrahedron and the aluminum-oxygen or hydroxyl octahedron unit. The units are bonded together into "sheets". Stacking of these sheets, along with different bonding in the crystal lattice, define the different clay minerals. Understanding the structure of clay minerals helps define the micro-scale mechanisms of shrink and swell behavior of expansive soils. For the purpose of distinguishing expanding and nonexpanding clay minerals, it is sufficient to describe the common kaolinite, montmorillonite, and illite minerals in engineering practice.

3.3.1.1 Kaolinite Minerals

Kaolinite consists of alternating layers of silica and alumina sheet (i.e., 1:1 layer). The layers are held together by hydrogen bonding between hydroxyls from the alumina sheet and oxygens from the silica sheet. Such bonding is very strong, preventing water entering into the basic layers and allowing many layers to build up to make large crystals. A typical kaolinite crystal may be 70 to 100 layers thick (Guven 1996). Due to the relatively large particle size and low specific surface area, kaolinite shows much less swelling than most other clay minerals.

3.3.1.2 Illite Minerals

Illite is also a 2:1 type mineral with repeating layers of an alumina sheet in the middle and silica sheet at top and bottom. Illite is very similar to montmorillonite but the layers in illite are bonded together strongly with potassium cations. Such a tight bonding between layers prevents the expansion of the entire lattice and makes illite much less expansive than montmorillonite. The engineering behavior of illite is between kaolinite and montmorillonite.

3.3.1.3 Montmorillonite Minerals

Montmorillonite is made of repeating layers of an alumina sheet (gibbsite) sandwiched by two silica sheets (i.e., 2:1 layer). The bonding between the silica sheets is weak thus water and exchangeable ions can easily enter between the layers, pushing the layers further apart. As a result, the soil volume increases significantly. Because of the extremely small particle sizes and unbalanced charge in the octahedral sheet, mainly due to the isomorphous substitution of aluminum with magnesium or iron in the octahedral sheet, montmorillonite shows a distinctive swelling/shrinking behavior. Upon wetting, montmorillonite clays may swell much more than its dry volume and when dried they tend to shrink and crack (Hillel 1980).

3.3.2 Summary

Microscale mechanisms of shrink/swell behavior of expansive soils, such as clay-water interaction, are only useful for qualitative analysis, since the influence of the different components on volume change is difficult to separate. Also, exact measurements for the type and amount of different clay minerals are practically impossible. Because of all these, the physical and/or mechanical properties of soils that reflect the microscale mechanisms of expansive soils can be described using the concepts of thermodynamics, especially the Gibbs free energy concept (soil suction). Thermodynamics deals with energy and its transformation. The energy associated with the physical and chemical interactions at microscale level within a clay-water system can therefore be transformed into another form of measurable energy using the principles of thermodynamics.

CHAPTER IV
FOUNDATION MODEL

4.1 Introduction

The analysis of the interaction between the slab foundations and the supporting soil foundation is of fundamental importance to geotechnical engineering. Many of the available interaction models are primarily concerned with elastic analysis. The slab and foundation soil interaction has been analyzed with the linear finite element method in this research. The plate is considered to be an assemblage of rectangular finite elements and the behavior of each element is characterized by a stiffness matrix. The element stiffness matrices are assembled into a total structural stiffness matrix by using the conditions of continuity of displacements and equilibrium of nodal forces. Once the plate model has been assembled, it must be connected, in some way, to the supporting soil foundation. This requires the derivation of foundation stiffness coefficients associated with the nodal points corresponding to those in the plate model.

In order to analyze an actual complex foundation problem, often certain assumptions have to be made. The foundation is a very complex medium. However, for the case of an elastic continuum, since it is the response of the foundation within the contact area and not the stresses or displacements inside the foundation soil which are of particular interest. The problem reduces to finding a relatively simple mathematical expression which can describe the response of the foundation within the contact area with a reasonable degree of accuracy. Many researchers have attempted to create a convenient model that properly represents the physical behavior of a real foundation. Thus, a whole spectrum of foundation models is known; at one end is the Winkler model consisting of closely spaced, independent linear springs and at the other extreme is an elastic continuum. There is a large class of foundation materials occurring in practice which can neither be represented by a Winkler type foundation or by an isotropic continuum. To find a physically close and mathematically simple representation of such models for the soil-structure interaction, there are attempts made by Pasternak, Hetenyi, Filonenko-Borodich, and Vlasov which will be described in section 4.2.

In this study, the foundation is assumed to be an isotropic, homogeneous, and elastic half space. The behavior of an elastic half space is calculated by dividing the surface of the elastic half space into rectangular regions. These regions are not proper finite elements in the usual sense, even though their behavior is represented by stiffness matrices and they are assembled in exactly same way as the plate finite elements. Therefore, they may be called rectangular half space elements (Fig. 4.1 below).

4.2 Foundation Models

The Winkler foundation is the simplest and the most widely used model. Most of the finite element computer programs in use today are based on the Winkler (or spring) foundation models. The spring foundation system results in a diagonal matrix that can easily be incorporated into a finite element program. The simplest simulation of a continuous elastic foundation is assumed to be composed of a number of closely spaced, vertical, independent, linear elastic springs providing vertical reaction only. Such a reaction is assumed proportional to the deflection. Thus, the relation between the pressure and the deflection of the foundation surface is

$$p(x,y) = k \cdot w(x,y) \tag{4.1}$$

where:
p = applied vertical stress,
w = vertical deflection, and
k = foundation soil modulus.

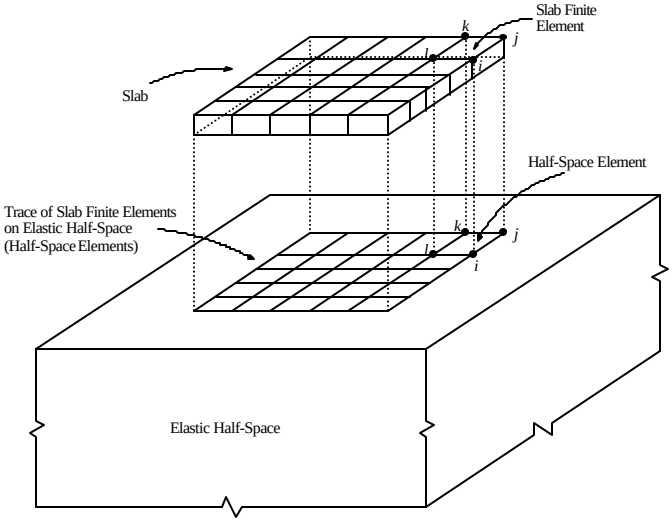

Fig. 4.1. Slab on Elastic Half-Space Foundation.

Equation 4.1 indicates that the vertical force at point (x,y) depends only on the vertical deflection at the same point (x,y) and is independent of the deflections at all other points, so the stiffness matrix of a Winkler foundation is a diagonal matrix with zero coefficients everywhere except on the diagonal, those relating the vertical force to the vertical deflection at the same point. Such a foundation is equivalent to a liquid base as if the foundation soil has no shear strength (Huang 1993). The deformation occurs only immediately under the applied load (Fig. 4.2) and displacements are zero outside the loaded area. It is evident that this type of foundation is not realistic for most real materials.

The equation of equilibrium governing the linear bending of an isotropic plate on a Winkler foundation of subgrade modulus, k, can be written as

$$D\left(\frac{\partial^4 w}{\partial x^4} + 2\frac{\partial^4 w}{\partial x^2 \partial y^2} + \frac{\partial^4 w}{\partial y^4}\right) + kw = q(x,y) \tag{4.2}$$

where, w is the vertical displacement, q is the distributed load, and D is the flexural rigidity of the slab. According to the Winkler's model, the vertical displacement of a slab is constant when it is subjected to a uniformly distributed load, q. Also, the value of the subgrade elastic modulus, k, is not unique, but depends on the geometry of the slab.

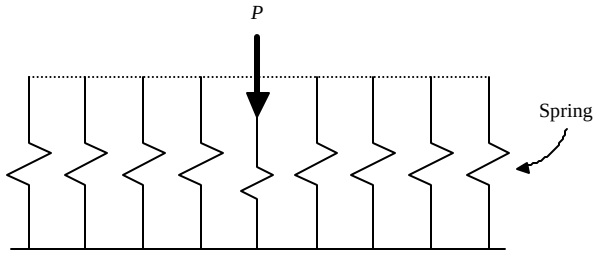

Fig. 4.2. Winkler Foundation Model.

4.2.1 Pasternak Foundation

The extension of the Winkler model by including shear interaction between the spring elements is the Pasternak foundation model. In order to introduce continuity of vertical displacements Pasternak assumes the existence of shear interactions between the spring elements. Pasternak considers a plate consisting of incompressible vertical elements, which deforms only by transverse shear. This plate is located on the top of the springs in order to connect their ends (Fig. 4.3 below). The Pasternak model is governed by the following differential equation

$$p = kw - G\nabla^2 w \tag{4.3}$$

where:

G = shear modulus,

$\nabla^2 = \dfrac{\partial^2}{\partial x^2} + \dfrac{\partial^2}{\partial y^2}$ the Laplacian operator.

The second term on the right hand side of Eq. 4.3 represents the effect of the shear interaction. For an arbitrarily distributed load $p(\xi,\eta)$ over area A, the deflection of the foundation surface of a point $Q(x,y,0)$ is

$$w(x,y) = \frac{1}{2\pi G}\iint_A p(\xi,\eta) K_o(\beta R)\, d\xi\, d\eta \tag{4.4}$$

where:

R = $[(x-\xi)^2 + (y-\eta)^2]^{1/2}$,

β^2 = k/G, and

$K_o(\beta R)$ = modified Bessel function.

The integration is taken over the loaded area.

4.2.2 Hetenyi Foundation

In order to connect the top of the springs of Winkler's foundation model and thus ensure interaction between the spring elements, Hetenyi chose a plate which deforms in bending only (Fig. 4.3 below). The differential equation describing the physical behavior of this system is given as

$$p = kw - D\nabla^4 w \tag{4.5}$$

where:

D = the flexural rigidity of the plate and

$\nabla^4 = \dfrac{\partial^4}{\partial x^4} + 2\dfrac{\partial^4}{\partial x^2 \partial y^2} + \dfrac{\partial^4}{\partial y^4}$ the Laplacian operator.

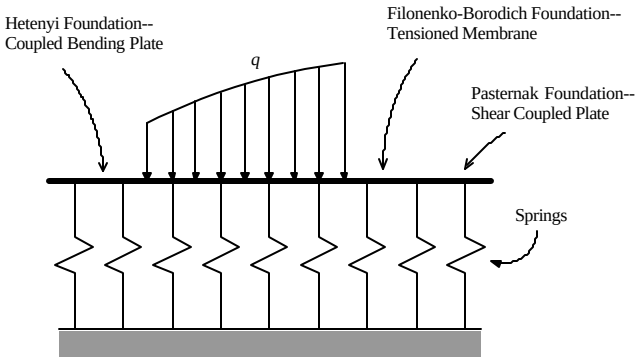

Fig. 4.3. Foundation Models.

4.2.3 Filonenko—Borodich Foundation

A similar approach to both Pasternak and Hetenyi Foundations to achieve the interaction between the spring elements was also used by Filonenko—Borodich. The continuity between the individual spring elements is provided by connecting them to a thin elastic membrane. Filonenko—Borodich proposed to use an elastic membrane subjected to a constant tension field, T, as a connection for the top ends of the Winkler's springs (Fig. 4.3). The differential equation that represents the equilibrium of the proposed system is defined as

$$p = kw - T\nabla^2 w \tag{4.6}$$

where, T is the tension field. The two elastic constants necessary to characterize the soil model are k and T. The models by Pasternak, Hetenyi, and Filonenko—Borodich, also known as two-parameter models, are all equal to the Winkler model if the parameters G, D, and T in Eq. 4.3, Eq. 4.5, and Eq. 4.6, respectively, are taken as zero.

4.2.4 Vlasov Foundation

Vlazov's approach to the formulation of the soil model is based on the application of a variational method. By imposing certain restrictions upon the possible distribution of displacements in an elastic layer, Vlazov was able to obtain a soil response function similar to the ones by Pasternak, Hetenyi, and Filonenko—Borodich. The details of the general variational method of analysis of foundation models can be found in Vlazov and Leontiev (1966).

4.3 Elastic Half Space (or Elastic Continuum) Foundation

The supporting foundation soil for the plate is considered to be an elastic, isotropic, and homogeneous semi-infinite continuum with E_s and ν_s, modulus of elasticity and Poisson's ratio of the soil, respectively. The behavior of the half space, particularly the region located on its surface corresponding to the plate area, actually being the plate trace, is represented by a stiffness matrix. This is achieved by numerical integration, when the singularity occurs, of

Boussineq equation over a small sub-rectangular region of the rectangular finite elements. Generally, a comparison between Winkler and elastic continuum foundations indicates that elastic continuum foundations have a much larger deflection basin (Poulos 2000). In addition, a foundation soil will deform as in Fig. 4.2 under a concentrated load for the Winkler model and as in Fig. 4.4 under the same load for the elastic half space foundation model, the latter is considered to be more realistic (Poulos 2000).

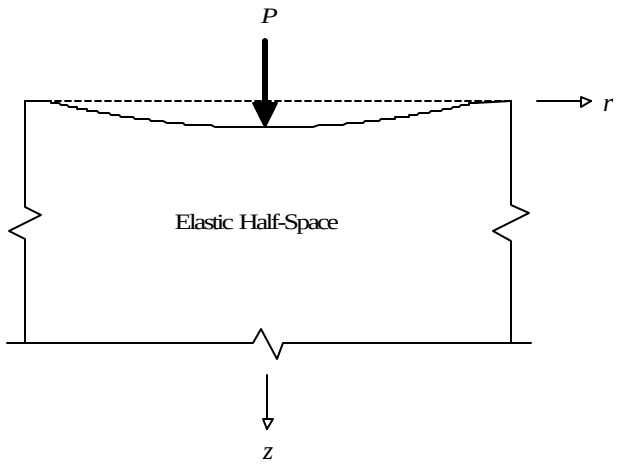

Fig. 4.4. Elastic Half Space Foundation.

A summary of the Boussinesq's solution of the elastic half-space problem is given by Timoshenko and Goodier (1970). In the Boussinesq formulation, the deflection at any point depends not only on the force at that point but also on the forces at all other points, which is a more realistic approach as compared to the Winkler's model. The horizontal displacements produced in the semi-infinite elastic space by the load *P*

$$u = \frac{P(1-2n_s)(1+n_s)}{2pEr}\left[\frac{z}{\sqrt{r^2+z^2}} + \frac{1}{1-2n_s}\frac{r^2 z}{\sqrt{(r^2+z^2)^3}} - 1\right] \quad (4.7)$$

where, *u* is the horizontal displacement, *r* and *z* are defined in Fig. 4.4. At the boundary plane ($z = 0$), see Fig. 4.4, Eq. 4.7 will take the form

$$u = -\frac{P(1-2\nu_s)(1+\nu_s)}{2\pi Er} \quad (4.8)$$

The vertical displacement *w* produced in the elastic half-space by the load *P* is given by

$$w = \frac{P}{2\pi E}\left[\frac{(1+\nu_s)z^2}{\sqrt{(r^2+z^2)^3}} + \frac{2(1-\nu_s^2)}{\sqrt{r^2+z^2}}\right] \quad (4.9)$$

and at the boundary surface ($z = 0$), Eq. 4.9 becomes

$$w = \frac{P(1-\nu_s^2)}{\pi Er} \quad (4.10)$$

This is the form of equation that is frequently referred in foundation engineering applications. However, it is better to rewrite Eq. 4.10 with some notations that are suitable for its modification in the finite element model formulation.

For the elastic half-space continuum model, the force-deflection relationship (as given in Eq. 4.10) can be rewritten as

$$w_{ij} = \frac{1-\nu_s^2}{\pi E_s}\frac{p_j}{r_{ij}} \quad (4.11)$$

where:

w_{ij} = deflection at point *i* due to a force at point *j*,
p_j = force at point *j*,
r_{ij} = distance between points *i* and *j*,
E_s = elastic modulus of the foundation soil, and
ν_s = Poisson's ratio of the foundation soil.

There is no known closed form solution to evaluate Eq. 4.11 for the flexibility coefficients. The only known approximate solutions are the ones by Cheung and Zienkiewicz (1965) and Huang (1993). Cheung and Zienkiewicz (1965) considered the foundation consisting of a series of rectangular pressure areas whose centers coincide with the nodal points of the slab. The flexibility coefficients are obtained by integrating the Boussinesq equation over the rectangular element area for the points at which the Boussinesq equation is not defined.

A similar technique to that of Huang (1993) is adopted in calculating the flexibility coefficients using a five-point Gauss quadrature formula in both *x* and *y* directions (Fig. 4.5 below). The foundation flexibility matrix is determined in two ways: direct and numerical integration. The flexibility matrix coefficients can be obtained directly if the point at which the deflection is sought and the point at which the vertical unit load is applied is different. In other words, if $i \neq j$ (Eq. 4.11), then the coefficients are obtained directly. However, if the point of interest for the deflection and the applied vertical unit load coincide, then Eq. 4.11 becomes singular and thus a numerical integration technique can be employed to overcome the singularity.

For a 4-noded linear rectangular finite element (Fig. 4.5), the flexibility matrix of the foundation soil can be written as

$$\begin{Bmatrix} w_1 \\ w_2 \\ w_3 \\ w_4 \end{Bmatrix} = \begin{bmatrix} f_{11} & f_{12} & f_{13} & f_{14} \\ f_{21} & f_{22} & f_{23} & f_{24} \\ f_{31} & f_{32} & f_{33} & f_{34} \\ f_{41} & f_{42} & f_{43} & f_{44} \end{bmatrix} \begin{Bmatrix} P_1 \\ P_2 \\ P_3 \\ P_4 \end{Bmatrix} \quad (4.12)$$

Equation 4.12 can also be represented in a short form as follows

$$\{w_i\} = [f_{ij}]\{P_j\} \quad (4.13)$$

where:

$$\{w_i\}=\begin{Bmatrix} w_1 \\ w_2 \\ w_3 \\ w_4 \end{Bmatrix},\quad [f_{ij}]=\begin{bmatrix} f_{11} & f_{12} & f_{13} & f_{14} \\ f_{21} & f_{22} & f_{23} & f_{24} \\ f_{31} & f_{32} & f_{33} & f_{34} \\ f_{41} & f_{42} & f_{43} & f_{44} \end{bmatrix},\quad \textit{and}\quad \{P_j\}=\begin{Bmatrix} P_1 \\ P_2 \\ P_3 \\ P_4 \end{Bmatrix}$$

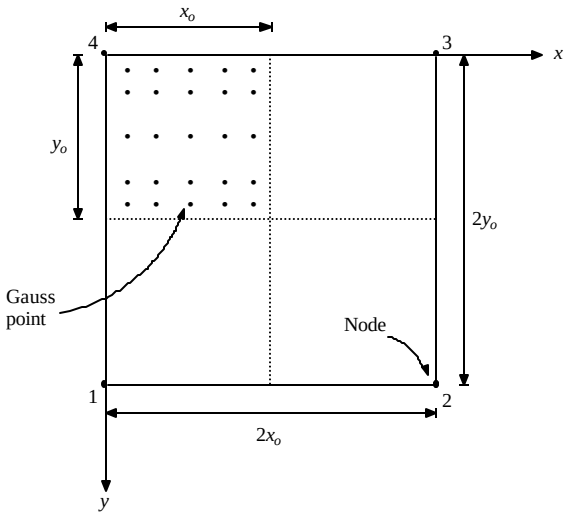

Fig. 4.5. A Typical 4-Node Linear Rectangular Finite Element.

The f_{ij} flexibility coefficients in Eq. 4.13 for the off-diagonal terms can be calculated from

$$f_{ij}=\frac{1-\nu_s^2}{\pi E_s}\frac{1}{r_{ij}} \tag{4.14}$$

However, if $i = j$, then the diagonal coefficients (i.e., f_{11}, f_{22}, f_{33}, and f_{44}) can only effectively be obtained by a numerical integration scheme. In general, the numerical quadrature formula for a two-dimensional domain can be written as

$$\int_{-1}^{+1}\int_{-1}^{+1} F(\xi,\eta)\,d\xi\,d\eta=\sum_{i=1}^{N}\sum_{j=1}^{M} F(\xi_i,\eta_j)W_iW_j \tag{4.15}$$

where:
N, M = number of Gauss (quadrature) points in the ξ and η directions (Fig. 4.6),
(ξ_i, η_j) = Gauss points,
(W_i, W_j) = Gauss weights, and
$F(\xi,\eta)$ = function to be integrated.

Equation 4.11 needs be rewritten so that it can be transformed into a form of Eq. 4.15 as

$$w(x,y)=\left[\frac{1-\nu_s^2}{\pi E_s}\right]\frac{P}{\sqrt{x^2+y^2}} \tag{4.16}$$

The term in the brackets on the right side of Eq. 4.16 is a constant, so only the term in x and y needs to be numerically integrated over a rectangular region described by (x_o,y_o).

$$F(x,y)=\frac{P}{\sqrt{x^2+y^2}} \tag{4.17}$$

The coordinates are transformed as

$$x=\frac{x_o}{2}(1+\xi)\Rightarrow dx=\frac{x_o}{2}d\xi \qquad y=\frac{y_o}{2}(1+\eta)\Rightarrow dy=\frac{y_o}{2}d\eta \tag{4.18}$$

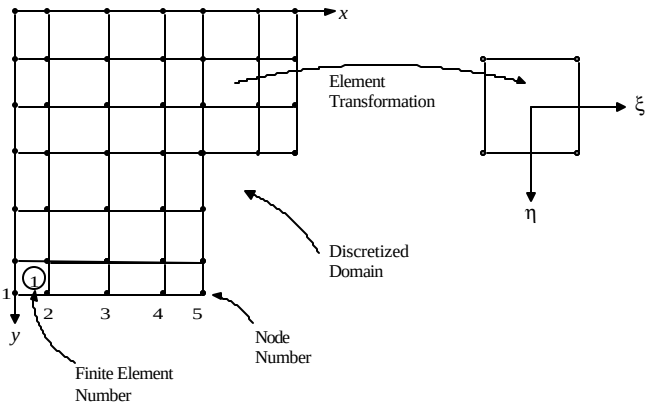

Fig. 4.6. Element Transformation.

In order to obtain the flexibility coefficients from Eq. 4.16, the applied vertical load P is considered as a unit load, and also to make use of the numerical integration, this unit load is distributed over the specified area (x_o,y_o) as a uniform pressure of $1/(x_o \cdot y_o)$. Then, applying the above transformations to Eq. 4.17 results in

$$F(\xi,\eta)=\int_{-1}^{+1}\int_{-1}^{+1}\frac{\dfrac{1}{x_o\cdot y_o}}{\sqrt{\left[\dfrac{x_o}{2}(1+\xi)\right]^2+\left[\dfrac{y_o}{2}(1+\eta)\right]^2}}\frac{x_o\cdot y_o}{4}d\xi\,d\eta \tag{4.19}$$

The Boussinesq equation in (ξ,η) coordinates takes the form

$$w(\xi,\eta)=\frac{(1-\mu_s^2)}{\pi E_s}\int_{-1}^{+1}\int_{-1}^{+1}\frac{\dfrac{1}{x_o\cdot y_o}}{\sqrt{\left[\dfrac{x_o}{2}(1+\xi)\right]^2+\left[\dfrac{y_o}{2}(1+\eta)\right]^2}}\frac{x_o\cdot y_o}{4}d\xi\,d\eta \tag{4.20}$$

Equation 4.20 can further be reduced to

$$w(\xi,\eta)=\frac{(1-\nu_s^2)}{2\pi E_s}\int_{-1}^{+1}\int_{-1}^{+1}\frac{1}{\sqrt{x_o^2(1+\xi)^2+y_o^2(1+\eta)^2}}d\xi\,d\eta \tag{4.21}$$

The flexibility coefficients of a 4—node rectangular element are then calculated directly using Eq. 4.14 and numerically using Eq. 4.21. The stiffness matrix of the foundation soil can be obtained by inverting the flexibility coefficient matrix, [f_{ij}] as

$$[G_{ij}] = [f_{ij}]^{-1} \tag{4.22}$$

where,

$$[G_{ij}] = \begin{bmatrix} g_{11} & g_{12} & g_{13} & g_{14} \\ g_{21} & g_{22} & g_{23} & g_{24} \\ g_{31} & g_{32} & g_{33} & g_{34} \\ g_{41} & g_{42} & g_{43} & g_{44} \end{bmatrix}$$

is the stiffness matrix of the foundation for a 4—node linear rectangular finite element. These stiffness matrices for each rectangular element are added to the corresponding stiffness matrices of the plate structure and then assembled together to result in the final stiffness matrix of the foundation—slab system.

4.3.1 Soil Parameters E_s and ν_s

The effectiveness of a foundation model, in addition to a realistic mathematical model, is also dependent on the accurate determination of the soil properties from either laboratory or field tests. If a soil medium is considered to be a homogeneous isotropic linearly elastic continuum, then load—displacement relationship of every element within the soil mass can be described in terms of the elastic constants of the soil, E_s and ν_s. These are assumed to be intrinsic properties of the soil and therefore independent of the method of testing. However, it is well known that the elastic constants for certain soils are dependent upon a variety of factors as the levels of isotropic and deviatoric stress applied to the specimen, stress history, type and rate of application of load, sample disturbance, moisture state, void ratio, particle size, and structure.

4.3.1.1 Poisson's Ratio ν_s

Poisson's ratio for a soil may be evaluated from the ratio of the radial strain to axial strain from a triaxial compression test. It is found that, in general, the test procedure influences the value of Poisson's ratio and the values determined by triaxial compression tests vary with the magnitude and range of the deviatoric stress (Bishop and Henkel 1962). Some typical values for the Poisson's ratio are given in Table 4.1.

4.3.1.2 Modulus of Elasticity E_s

The modulus of elasticity is often determined from unconfined, triaxial, or oedometric compression tests. Plate loading tests and pressuremeter tests may also be used to determine the in-situ modulus of elasticity of the soil. Some typical values of the modulus of elasticity are shown in Table 4.2.

Table 4.1. Typical Poisson's Ratio Values (after Bowles 1988).

Type of Soil	ν_s
Clay, saturated	0.4—0.5
Clay, unsaturated	0.1—0.3
Sandy clay	0.2—0.3
Silt	0.3—0.35
Sand (dense)	0.2—0.4
gravelly sand	–0.1—1.00
commonly used	0.3—0.4
Rock	0.1—0.4
Loess	0.1—0.3
Concrete	0.15
Ice	0.36

Table 4.2. Range of Values of E_s for Some Soils (after Bowles 1988).

Type of Soil	E_s	
	ksf	Mpa
Very soft clay	50—250	2—15
Soft clay	100—500	5—25
Medium clay	300—1000	15—50
Hard clay	1000—2000	50—100
Sandy clay	500—5000	25—250
Silty sand	150—450	5—20
Loose sand	200—500	10—25
Dense sand	1000—1700	50—81
Loose sand and gravel	1000—3000	50—150
Dense sand and gravel	2000—4000	100—200
Loess	300—1200	15—60
Silt	40—400	2—20

CHAPTER V
PLATE THEORY AND FINITE ELEMENT METHOD

5.1 Introduction

The finite element method may be regarded as a generalization of standard structural analysis procedures, in particular the displacement method of analysis, which permits the evaluation of stresses and strains in a structure. The finite element method is a very powerful method for the solution of differential equations that are in the fields of engineering. In the method, the structural domain is simply divided into regions (finite elements) of appropriate size and shape with all the material properties of the original domain being retained in the individual finite elements. By assuming approximate displacement functions (interpolation functions or shape functions) within an element, it is possible to derive the stiffness matrix of a structure using the principles of energy theorems or virtual work. If conditions of equilibrium are applied at every node of the discretized structure, a set of simultaneous algebraic equations can be formed, and the solution of these equations gives all the nodal displacements. The internal stresses are then obtained using the calculated nodal displacement values. A more complete treatment of the finite element method can be found in numerous books such as Reddy (1993), Zienkiewicz (1971), and Nath (1974).

Considerable research has been done for the development of finite plate elements for the analysis of the bending of plates. Researchers have developed quite a number of elements (i.e., rectangular, triangular, quadrilateral, etc.) with varying number of nodal points along with different types of interpolation functions. The aim of the researcher is to develop an element that has the least number of coefficients and at the same time satisfies the boundary conditions such as continuity of slopes.

In this chapter, the linear finite element models of the classical (or Kirchhoff or thin) and shear deformation (or Mindlin or thick) plate theories for the rectangular elements will be presented. A simple four node-rectangular element is chosen because of the restrictions applied by the foundation model formulation, as it is discussed in Chapter IV. A more complete treatment of the plate theories can be found in numerous books such as Timoshenko and Winowsky-Krieger (1968) and Ugural (1981). Although, the thick plate theory is adopted for this research, the thin plate theory is also explained in order to understand the differences between both theories.

5.2 Plate Material Properties

Before introducing the theory of plates along with their finite element models, it is necessary to describe some definitions and the constitutive equations that are related to the plate formulations. The Mindlin plate employed in this study is composed of linear elastic and orthotropic material. The linear elasticity is governed by Hooke's law, in which the components of stresses are related to the components of strains by elastic coefficients. The static equilibrium of the stresses on an infinitesimal cubic element of dimensions *dx*, *dy*, and *dz* is shown in Fig. 5.1 below. When the material properties are different in different directions, then such materials are called orthotropic.

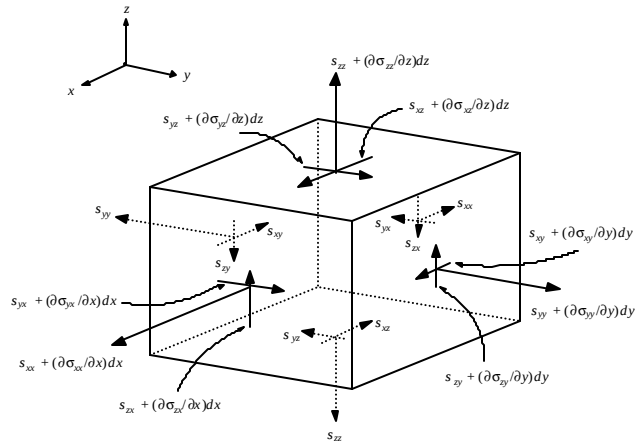

Fig. 5.1. Equilibrium of a Cubic Element Under Applied Stresses.

If there are cases where the elastic properties of the material are not the same in different directions (i.e., if the material is anisotropic), then it is possible to represent different elastic properties in different directions. However, for the present case it is assumed that the material of the plate has three planes of symmetry with respect to its elastic properties. Hooke's law, which relates the stresses to strains for an orthotropic material, can be written as

$$\begin{Bmatrix} \sigma_{xx} \\ \sigma_{yy} \\ \sigma_{zz} \\ \sigma_{yz} \\ \sigma_{xz} \\ \sigma_{xy} \end{Bmatrix} = \begin{bmatrix} C_{11} & C_{12} & C_{13} & 0 & 0 & 0 \\ C_{21} & C_{22} & C_{23} & 0 & 0 & 0 \\ C_{31} & C_{32} & C_{33} & 0 & 0 & 0 \\ 0 & 0 & 0 & C_{44} & 0 & 0 \\ 0 & 0 & 0 & 0 & C_{55} & 0 \\ 0 & 0 & 0 & 0 & 0 & C_{66} \end{bmatrix} \begin{Bmatrix} \varepsilon_{xx} \\ \varepsilon_{yy} \\ \varepsilon_{zz} \\ \varepsilon_{yz} \\ \varepsilon_{xz} \\ \varepsilon_{xy} \end{Bmatrix} \tag{5.1}$$

where C_{ij} are the elastic coefficients. The coefficient matrix C_{ij} is symmetric (Reddy 1999). So, if three orthogonal planes of material symmetry exist, then the number of elastic coefficients is reduced to nine. The inverse of Eq. 5.1, which relates the strain-stress relationship, is given by

$$\begin{Bmatrix} \varepsilon_{xx} \\ \varepsilon_{yy} \\ \varepsilon_{zz} \\ \varepsilon_{yz} \\ \varepsilon_{xz} \\ \varepsilon_{xy} \end{Bmatrix} = \begin{bmatrix} H_{11} & H_{12} & H_{13} & 0 & 0 & 0 \\ H_{21} & H_{22} & H_{23} & 0 & 0 & 0 \\ H_{31} & H_{32} & H_{33} & 0 & 0 & 0 \\ 0 & 0 & 0 & H_{44} & 0 & 0 \\ 0 & 0 & 0 & 0 & H_{55} & 0 \\ 0 & 0 & 0 & 0 & 0 & H_{66} \end{bmatrix} \begin{Bmatrix} \sigma_{xx} \\ \sigma_{yy} \\ \sigma_{zz} \\ \sigma_{yz} \\ \sigma_{xz} \\ \sigma_{xy} \end{Bmatrix} \tag{5.2}$$

where the coefficients H_{ij} are defined as

$$\begin{bmatrix} H_{11} & H_{12} & H_{13} & 0 & 0 & 0 \\ H_{21} & H_{22} & H_{23} & 0 & 0 & 0 \\ H_{31} & H_{32} & H_{33} & 0 & 0 & 0 \\ 0 & 0 & 0 & H_{44} & 0 & 0 \\ 0 & 0 & 0 & 0 & H_{55} & 0 \\ 0 & 0 & 0 & 0 & 0 & H_{66} \end{bmatrix} = \begin{bmatrix} \frac{1}{E_x} & -\frac{n_{yx}}{E_y} & -\frac{n_{zx}}{E_z} & 0 & 0 & 0 \\ -\frac{n_{xy}}{E_x} & \frac{1}{E_y} & -\frac{n_{zy}}{E_z} & 0 & 0 & 0 \\ -\frac{n_{xz}}{E_x} & -\frac{n_{yz}}{E_y} & \frac{1}{E_z} & 0 & 0 & 0 \\ 0 & 0 & 0 & \frac{1}{G_{yz}} & 0 & 0 \\ 0 & 0 & 0 & 0 & \frac{1}{G_{xz}} & 0 \\ 0 & 0 & 0 & 0 & 0 & \frac{1}{G_{xy}} \end{bmatrix}$$

where E_x, E_y, and E_z are Young's moduli in x, y, and z directions respectively, ν_{ij} is Poisson's ratio and defined as the ratio of transverse strain in the jth direction to the axial strain in the ith direction when stress is applied in the ith direction, and G_{xy}, G_{xz}, and G_{yz} are the shear moduli in the x-y, x-z, and y-z planes, respectively. Since the coefficient matrix of Eq. 5.1 and its inverse (Eq. 5.2) are symmetric (Reddy 1993), the following relationships exist between the Young's moduli and Poisson's ratios

$$\frac{\nu_{xy}}{E_x} = \frac{\nu_{yx}}{E_y}, \quad \frac{\nu_{xz}}{E_x} = \frac{\nu_{zx}}{E_z}, \quad \text{and} \quad \frac{\nu_{yz}}{E_y} = \frac{\nu_{zy}}{E_z} \tag{5.3}$$

As it can be seen from Eq. 5.2 and Eq. 5.3, there are only nine independent material coefficients E_x, E_y, E_z, G_{xy}, G_{xz}, G_{yz}, ν_{xy}, ν_{xz}, and ν_{yz} for an orthotropic material. If the material is isotropic, then $E_x = E_y = E_z = E$, $G_{xy} = G_{xz} = G_{yz} = G$, and $\nu_{xy} = \nu_{xz} = \nu_{yz} = \nu$.

5.3 Finite Element Model of Kirchhoff Plate Theory

The displacement linear finite element model of the classical plate theory is presented in this section. The finite element model of the plate is described for a 4-node rectangular element using the virtual work principles. This element is one of the earlier finite element derived for the analysis of bending of thin plates (Zienkiewicz 1971). The element has four nodes and three degrees of freedom at each node thus making a 12 degrees of freedom element. The Kirchhoff plate theory has the following assumptions:

1) the plate is thin and linearly elastic,
2) the plate undergoes small lateral deflections,
3) the transverse normals do not elongate,
4) straight lines perpendicular to the mid-surface before deformation, remain straight after deformation, and
5) the transverse normals rotate such that they remain perpendicular to the mid-surface after deformation.

The assumptions imply that the strain in the z direction is zero (Fig. 5.2 below), that w is independent of z

$$\varepsilon_{zz} = \frac{\partial w}{\partial z} = 0 \tag{5.4}$$

According to Kirchhoff plate theory, the transverse shear strains are zero as well

$$\varepsilon_{xz} = \frac{1}{2}\left(\frac{\partial u}{\partial z} + \frac{\partial w}{\partial x}\right) = 0, \qquad \varepsilon_{yz} = \frac{1}{2}\left(\frac{\partial v}{\partial z} + \frac{\partial w}{\partial y}\right) = 0 \tag{5.5}$$

Integration of the terms in Eq. 5.5 result in the following displacement fields with the assumption that the in-plane stretching of the plate is ignored, resulting in pure bending only.

$$u = -z\frac{\partial w}{\partial x}, \qquad v = -z\frac{\partial w}{\partial y} \tag{5.6}$$

The linear strains in the plate are defined as

$$\varepsilon_{xx} = \frac{\partial u}{\partial x}, \quad \varepsilon_{yy} = \frac{\partial v}{\partial y}, \quad \varepsilon_{xy} = \frac{1}{2}\left(\frac{\partial u}{\partial y} + \frac{\partial v}{\partial x}\right), \quad \varepsilon_{zz} = \varepsilon_{xz} = \varepsilon_{yz} = 0 \tag{5.7}$$

The non-zero strains in terms of the transverse displacement w, using Eq. 5.6 and Eq. 5.7, can be written as

$$\varepsilon_{xx} = -z\frac{\partial^2 w}{\partial x^2}, \quad \varepsilon_{yy} = -z\frac{\partial^2 w}{\partial y^2}, \quad \varepsilon_{xy} = -z\frac{\partial^2 w}{\partial x \partial y} \tag{5.8}$$

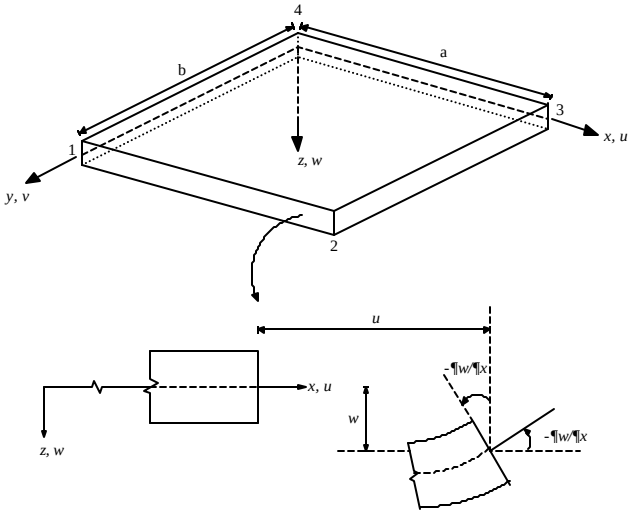

Fig. 5.2. Kirchhoff Assumptions on Deformed Rectangular Plate.

5.3.1 Principle of Virtual Work

This principle relates the forces in equilibrium to the corresponding displacements in a structure. The name of the principle is derived from the fact that a fictitious (virtual) system of forces in equilibrium or of small virtual displacements is applied to the structure and these are related to the actual displacements or actual forces, respectively (Ghali and Neville 1978). The principle of virtual displacements can be stated for a typical element as follows

$$\delta W \equiv \delta W_I - \delta W_E = 0 \tag{5.9}$$

where δW_I is the virtual strain energy stored in the element due to internal stresses and δW_E is the work done by externally applied loads. The internal strain energy can be written as

$$\delta W_I = \int_V \delta\varepsilon_{ij}\sigma_{ij} dV \tag{5.10}$$

and the external work done by a distributed load f on a plate element can be represented as

$$\delta W_E = \int_S f\delta w dx dy \tag{5.11}$$

Then, Eq. 5.9 can be rewritten using the principles of virtual displacements

$$0 = \int_V \left(\delta\varepsilon_{xx}\sigma_{xx} + \delta\varepsilon_{yy}\sigma_{yy} + 2\delta\varepsilon_{xy}\sigma_{xy}\right)dV - \int_S f\delta w dx dy \tag{5.12}$$

If the strains in Eq. 5.8 are substituted in Eq. 5.12 and the variation δ is carried on the w, the following relationship is obtained

$$0 = \int_V \left(-z\frac{\partial^2\delta w}{\partial x^2}\sigma_{xx} - z\frac{\partial^2\delta w}{\partial y^2}\sigma_{yy} - 2z\frac{\partial^2\delta w}{\partial x\partial y}\sigma_{xy}\right)dV - \int_S f\delta w dx dy \tag{5.13}$$

As it was mentioned earlier, the transverse displacement w is a function of x and y only and is independent of z, therefore, it is possible to rewrite the volume integral (Eq. 5.13) as follows

$$0 = \int_S \left\{\left[\int_{-\frac{h}{2}}^{\frac{h}{2}}\sigma_{xx}zdz\right]\left(-\frac{\partial^2\delta w}{\partial x^2}\right) + \left[\int_{-\frac{h}{2}}^{\frac{h}{2}}\sigma_{yy}zdz\right]\left(-\frac{\partial^2\delta w}{\partial y^2}\right) + \left[\int_{-\frac{h}{2}}^{\frac{h}{2}}\sigma_{xy}zdz\right]\left(-2\frac{\partial^2\delta w}{\partial x\partial y}\right)\right\}dxdy$$

$$-\int_S f\delta w dx dy \tag{5.14}$$

where h is the plate thickness and the values in brackets in Eq. 5.14 above are the internal bending moments M_{xx}, M_{yy}, and M_{xy} (Fig. 5.3 below) per unit length along x and y axes and defined as

$$M_{xx} = \int_{-\frac{h}{2}}^{\frac{h}{2}}\sigma_{xx}zdz, \qquad M_{yy} = \int_{-\frac{h}{2}}^{\frac{h}{2}}\sigma_{yy}zdz, \qquad M_{xy} = \int_{-\frac{h}{2}}^{\frac{h}{2}}\sigma_{xy}zdz \tag{5.15}$$

For linear orthotropic slabs with the principal directions of orthotropy coinciding with the x and y axes, the bending moments are related to the derivatives of the transverse deflection w as

$$M_{xx} = -\left(D_x\frac{\partial^2 w}{\partial x^2} + D_1\frac{\partial^2 w}{\partial y^2}\right), \qquad M_{xx} = -\left(D_1\frac{\partial^2 w}{\partial x^2} + D_y\frac{\partial^2 w}{\partial y^2}\right) \tag{5.16}$$

$$M_{xy} = -2D_{xy}\frac{\partial^2 w}{\partial x\partial y}$$

where D_x, D_1, D_y, and D_{xy} are the orthotropic plate rigidities (Timoshenko and Woinowsky-Krieger 1968)

$$D_x = \frac{E_x h^3}{12\left(1-\nu_{xy}\nu_{yx}\right)}, \qquad D_y = \frac{E_y h^3}{12\left(1-\nu_{xy}\nu_{yx}\right)}, \qquad D_{xy} = \frac{G_{xy}h^3}{12} \tag{5.17}$$

$$D_1 = \frac{\nu_{xy}E_y h^3}{12\left(1-\nu_{xy}\nu_{yx}\right)} = \frac{\nu_{yx}E_x h^3}{12\left(1-\nu_{xy}\nu_{yx}\right)}$$

where E_x, E_y, ν_{xy}, ν_{yx}, and G_{xy} are the orthotropic material constants, and h the thickness of the plate.

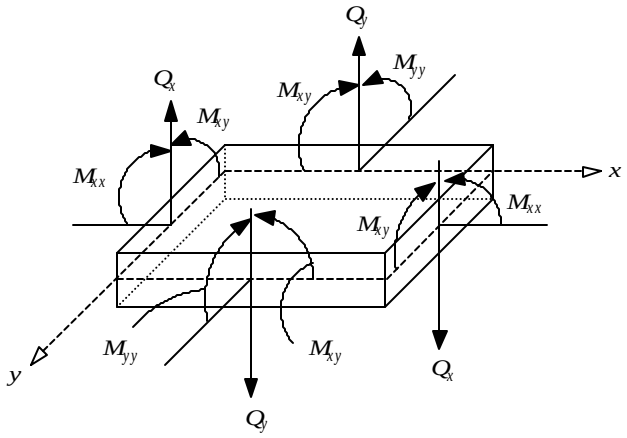

Fig. 5.3. Moment and Shear Force Resultants on a Rectangular Plate Element.

The shear forces as shown in Fig. 5.3 can be calculated from

$$Q_x = \frac{\partial M_{xx}}{\partial x} + \frac{\partial M_{xy}}{\partial y}, \qquad Q_y = \frac{\partial M_{xy}}{\partial x} + \frac{\partial M_{yy}}{\partial y} \tag{5.18}$$

Substituting Eq. 5.16 into Eq. 5.14 results in

$$0 = \int_S \left\{\left(D_x\frac{\partial^2 w}{\partial x^2} + D_1\frac{\partial^2 w}{\partial y^2}\right)\frac{\partial^2\delta w}{\partial x^2} + \left(D_1\frac{\partial^2 w}{\partial x^2} + D_y\frac{\partial^2 w}{\partial y^2}\right)\frac{\partial^2\delta w}{\partial y^2}\right.$$
$$\left. + 4D_{xy}\frac{\partial^2 w}{\partial x\partial y}\frac{\partial^2\delta w}{\partial x\partial y} - \delta w f\right\}dxdy \tag{5.19}$$

Equation 5.16 is also called the weak form of the problem (Reddy 1993). The differential equation governing an orthotropic plate can be obtained from Eq. 5.19 as follows

$$\frac{\partial^2 M_{xx}}{\partial x^2} + 2\frac{\partial^2 M_{xy}}{\partial x\partial y} + \frac{\partial^2 M_{yy}}{\partial y^2} + f = 0 \tag{5.20}$$

where the moments (M_{xx}, M_{yy}, and M_{xy}) were defined above.

5.3.2 Displacement Function for the Finite Element Model

The rectangular bending element shown in Fig. 5.4 below with three degrees of freedom (one deflection and two rotations) at each node, and thus constituting twelve degrees of freedom for the rectangular plate, is selected for this study. The displacement function therefore can be chosen as a polynomial with twelve coefficients. The best arrangement of the coefficients within the polynomial can be written as

$$w = c_1 + c_2x + c_3y + c_4x^2 + c_5xy + c_6y^2 + c_7x^3 + c_8x^2y + c_9xy^2 + c_{10}y^3 + c_{11}x^3y + c_{12}x \tag{5.21}$$

where c_i are the coefficients to be determined.

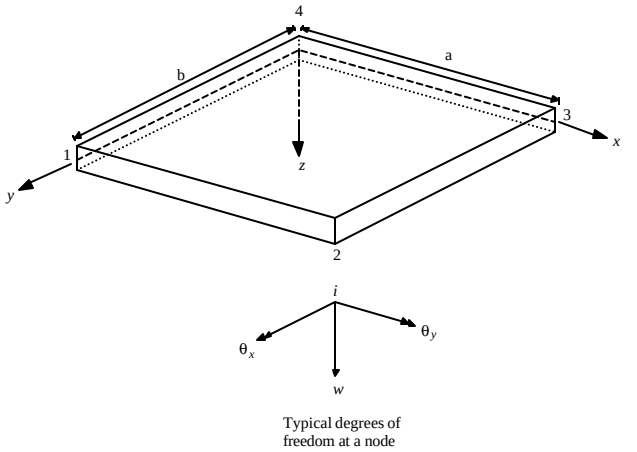

Fig. 5.4. Rectangular Bending Element.

Equation 5.21 can also be written in terms of interpolation functions

$$w(x,y)=\sum_{i=1}^{m}\Delta_i \boldsymbol{f}_i(x,y) \tag{5.22}$$

where Δ_i is the nodal values of the displacement w and its derivatives, and $\phi_i(x,y)$ are the Hermite interpolation functions that are readily available in the finite element books such as the ones by Zienkiewicz (1971) and Reddy (1993). If Eq. 5.22 is substituted for the displacement w and the interpolation functions $\phi_i(x,y)$ for the variation of the displacement δw into Eq. 5.19, the following relationship can be obtained

$$[K]\{\Delta\}=\{f\} \tag{5.23}$$

where $[K]$ is the stiffness matrix, $\{\Delta\}$ is the displacement vector, and $\{f\}$ is the load vector. These matrices are defined as

$$K_{ij}=\int_S\left\{D_x\frac{\partial^2 f_i}{\partial x^2}\frac{\partial^2 f_j}{\partial y^2}+D_1\left[\frac{\partial^2 f_i}{\partial x^2}\frac{\partial^2 f_j}{\partial y^2}+\frac{\partial^2 f_i}{\partial y^2}\frac{\partial^2 f_j}{\partial x^2}\right]+D_y\frac{\partial^2 f_i}{\partial y^2}\frac{\partial^2 f_j}{\partial y^2}\right. \tag{5.24}$$

$$\left.+4D_{xy}\frac{\partial^2 f_i}{\partial x\partial y}\frac{\partial^2 f_j}{\partial x\partial y}\right\}dxdy$$

$$f_i=\int_S f\boldsymbol{f}_i dxdy \tag{5.25}$$

$$\Delta_j=\left(w_i,q_{xi},q_{yi}\right),\qquad (i=1,4) \tag{5.26}$$

After Eq. 5.23 is solved for the displacements at every nodal point of the discretized plate, the bending moments and shear forces can be calculated using Eqs. 5.16 and 5.18, respectively, at the center of each rectangular finite element. The most accurate results of the stresses (bending and shear) for the linear rectangular elements can only be obtained at the center of the elements (Reddy 1993).

5.4 Finite Element Model of Mindlin Plate Theory

This theory is very similar to the Kirchhoff theory except that it allows the transverse shear deformations within the plate. Therefore, this theory is very suitable for analysis of thick plates. The plate finite element model used in this research is based on the Mindlin plate theory. In the formulation of the plate element, the assumptions adopted in the shear deformable plate can be summarized as:

1) the plate is linearly elastic,
2) the plate undergoes small lateral deflections,
3) transverse normals do not elongate,
4) straight lines perpendicular to the midsurface before deformation, remain straight after deformation, and
5) the transverse normals to the midsurface before deformation remain straight but not necessarily normal to the midsurface after deformation.

The last assumption results in a constant state of transverse shear strains through the thickness and zero transverse normal strains (Fig. 5.5 below). The most significant difference between the classical and shear deformation theories is the effect of including transverse shear deformation on the predicted deflections. Therefore, the strains

$$\boldsymbol{e}_{xz}=\frac{1}{2}\left(\frac{\partial u}{\partial z}+\frac{\partial w}{\partial x}\right),\qquad \boldsymbol{e}_{yz}=\frac{1}{2}\left(\frac{\partial v}{\partial z}+\frac{\partial w}{\partial y}\right) \tag{5.27}$$

are not zero. To derive the finite element model for the Mindlin plate, an approach similar to the Kirchhoff plate theory is taken.

5.4.1 Displacement Function

Since the normal before bending does not remain normal after bending, the slopes of the middle surface cannot be used to define u and v displacements, contrary to the Kirchhoff theory. Thus, two new parameters such as rotations of the cross sections ϕ_x and ϕ_y are introduced into the theory. The most important characteristic of the Mindlin theory is that the rotations are no longer partial derivatives of the lateral displacement function w. It is, therefore, only necessary to use the Lagrange approximate functions as will be discussed in the coming sections. Using these rotations, the Mindlin thick plate theory is based on the following displacement functions (Fig. 5.5)

$$u=z\boldsymbol{f}_x,\qquad v=z\boldsymbol{f}_y,\qquad w=w(x,y) \tag{5.28}$$

The bending strains for the thick plate can be written as

$$e_{xx}=\frac{\partial u}{\partial x},\quad e_{yy}=\frac{\partial v}{\partial y},\quad e_{xy}=\frac{1}{2}\left(\frac{\partial u}{\partial y}+\frac{\partial v}{\partial x}\right),\quad e_{xz}=\frac{1}{2}\left(\frac{\partial u}{\partial z}+\frac{\partial w}{\partial x}\right) \tag{5.29}$$

$$e_{yz}=\frac{1}{2}\left(\frac{\partial v}{\partial z}+\frac{\partial w}{\partial y}\right),\quad e_{zz}=0$$

The bending strains can also be represented in another form if Eq. 5.27 is plugged into Eq. 5.28 as

$$e_{xx} = z\frac{\partial f_x}{\partial x}, \quad e_{yy} = z\frac{\partial f_y}{\partial y}, \quad e_{xy} = \frac{z}{2}\left(\frac{\partial f_x}{\partial y} + \frac{\partial f_y}{\partial x}\right) \tag{5.30}$$

$$e_{xz} = \frac{1}{2}\left(f_x + \frac{\partial w}{\partial x}\right), \quad e_{yz} = \frac{1}{2}\left(f_y + \frac{\partial w}{\partial y}\right)$$

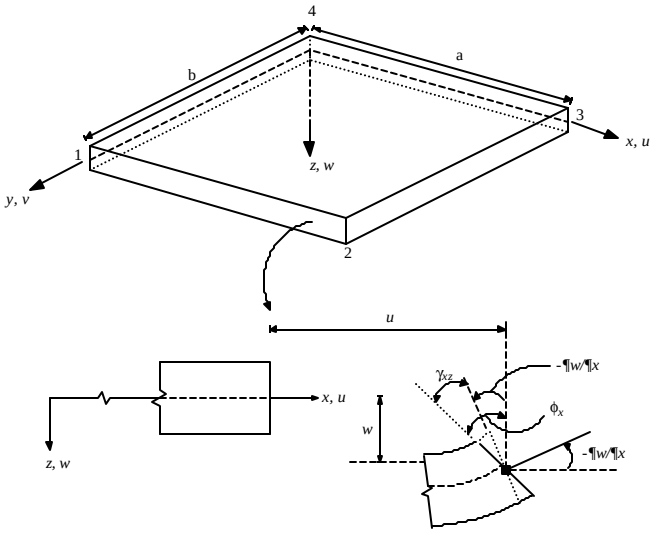

Fig. 5.5. Mindlin Assumptions on Deformed Rectangular Plate.

5.4.2 Application of Virtual Work

The virtual work statements described in Section 5.2.1 can be applied to the thick plate case as

$$0 = \int_V \left(d\varepsilon_{xx}\sigma_{xx} + d\varepsilon_{yy}\sigma_{yy} + 2d\varepsilon_{xy}\sigma_{xy} + 2d\varepsilon_{xz}\sigma_{xz} + 2d\varepsilon_{yz}\sigma_{yz}\right)dV - \int_S dw f dx \tag{5.31}$$

If the linear bending strains in Eq. 5.30 are substituted in Eq. 5.31 and the variation δ is carried on the ϕ_x, ϕ_y, and w, the following relationship can be obtained

$$0 = \int_V \left[z\frac{\partial d\phi_x}{\partial x}\sigma_{xx} + z\frac{\partial d\phi_y}{\partial y}\sigma_{yy} + 2z\left(\frac{\partial d\phi_x}{\partial y} + \frac{\partial d\phi_y}{\partial x}\right)\sigma_{xy} \right.$$
$$\left. + 2\left(d\phi_x + \frac{\partial dw}{\partial x}\right)\sigma_{xz} + 2\left(d\phi_y + \frac{\partial dw}{\partial y}\right)\sigma_{yz} \right] dV - \int_S dw f dx dy \tag{5.32}$$

Equation 5.32 can also be written as

$$0 = \int_S \left\{ \left[\int_{-\frac{h}{2}}^{\frac{h}{2}} \sigma_{xx} z dz\right]\left(\frac{\partial df_x}{\partial x}\right) + \left[\int_{-\frac{h}{2}}^{\frac{h}{2}} \sigma_{yy} z dz\right]\left(\frac{\partial df_y}{\partial y}\right) + \left[\int_{-\frac{h}{2}}^{\frac{h}{2}} \sigma_{xy} z dz\right] 2\left(\frac{\partial df_x}{\partial y} + \frac{\partial df_y}{\partial x}\right) \right.$$
$$\left. + \left[\int_{-\frac{h}{2}}^{\frac{h}{2}} \sigma_{xz} dz\right] 2\left(df_x + \frac{\partial dw}{\partial x}\right) + \left[\int_{-\frac{h}{2}}^{\frac{h}{2}} \sigma_{yz} dz\right] 2\left(df_y + \frac{\partial dw}{\partial y}\right) \right\} dx dy$$
$$- \int_S dw f dx dy \tag{5.33}$$

where h is the plate thickness and the values in the brackets in Eq. 5.33 above are the bending moments and shear stresses (Fig. 5.3) defined as

$$M_{xx} = \int_{-\frac{h}{2}}^{\frac{h}{2}} \sigma_{xx} z dz, \quad M_{yy} = \int_{-\frac{h}{2}}^{\frac{h}{2}} \sigma_{yy} z dz, \quad M_{xy} = \int_{-\frac{h}{2}}^{\frac{h}{2}} \sigma_{xy} z dz$$
$$Q_x = \int_{-\frac{h}{2}}^{\frac{h}{2}} \sigma_{xz} dz, \qquad Q_y = \int_{-\frac{h}{2}}^{\frac{h}{2}} \sigma_{yz} dz \tag{5.34}$$

For linear orthotropic plates with the principal directions of orthotropy coinciding with the x and y axes, the bending moments and the shear stresses are related to the displacements (w, ϕ_x, ϕ_y) as (Reddy 1993)

$$M_{xx} = D_x\frac{\partial f_x}{\partial x} + D_1\frac{\partial f_y}{\partial y}, \quad M_{yy} = D_1\frac{\partial f_x}{\partial x} + D_y\frac{\partial f_y}{\partial y}, \quad M_{xy} = D_{xy}\left(\frac{\partial f_x}{\partial y} + \frac{\partial f_y}{\partial x}\right) \tag{5.35}$$

$$Q_x = C_x\left(f_x + \frac{\partial w}{\partial x}\right), \qquad Q_y = C_y\left(f_y + \frac{\partial w}{\partial y}\right)$$

where C_x and C_y are defined by

$$C_x = \frac{5}{6}G_{xz}h \quad \text{and} \quad C_y = \frac{5}{6}G_{yz}h \tag{5.36}$$

where the (5/6) term is the shear correction coefficient, and G_{xz} and G_{yz} are the shear modulus values in the x-z and y-z planes, respectively. The shear correction coefficient accounts for the difference between the distribution of transverse shear stresses of the Mindlin plate theory and the actual distribution of the stresses. Substitution of Eq. 5.35 into Eq. 5.33 results in

$$0 = \int_S \left\{ \left(D_x\frac{\partial f_x}{\partial x} + D_1\frac{\partial f_y}{\partial y}\right)\frac{\partial df_x}{\partial x} + \left(D_1\frac{\partial f_x}{\partial x} + D_y\frac{\partial f_y}{\partial y}\right)\frac{\partial df_y}{\partial y} \right.$$
$$+ D_{xy}\left(\frac{\partial f_x}{\partial y} + \frac{\partial f_y}{\partial x}\right)\left(\frac{\partial df_x}{\partial y} + \frac{\partial df_y}{\partial x}\right) + C_x\left(f_x + \frac{\partial w}{\partial x}\right)\left(df_x + \frac{\partial dw}{\partial x}\right)$$
$$\left. + C_y\left(f_y + \frac{\partial w}{\partial y}\right)\left(df_y + \frac{\partial dw}{\partial y}\right) - dwf \right\} dS \tag{5.37}$$

Equation 5.33 can be partitioned according to the three displacements (w, ϕ_x, ϕ_y) into three weak form (Reddy 1993) equations as

$$0 = \int_S \left(Q_x\frac{\partial dw}{\partial x} + Q_y\frac{\partial dw}{\partial y} - f dw \right) dS \qquad \langle a \rangle$$

$$0 = \int_S \left(M_x\frac{\partial d\phi_x}{\partial x} + M_{xy}\frac{\partial d\phi_x}{\partial y} + Q_x d\phi_x \right) dS \qquad \langle b \rangle \tag{5.38}$$

$$0 = \int_S \left(M_{xy}\frac{\partial d\phi_y}{\partial x} + M_y\frac{\partial d\phi_y}{\partial y} + Q_y d\phi_y \right) dS \qquad \langle c \rangle$$

The governing differential equations of the thick plate theory can be obtained from (a), (b), and (c) of Eq. 5.38 as

$$\frac{\partial Q_x}{\partial x}+\frac{\partial Q_y}{\partial y}-f=0 \qquad \langle 1\rangle$$

$$\frac{\partial M_{xx}}{\partial x}+\frac{\partial M_{xy}}{\partial y}+Q_x=0 \qquad \langle 2\rangle \tag{5.39}$$

$$\frac{\partial M_{xy}}{\partial x}+\frac{\partial M_{y}}{\partial y}+Q_y=0 \qquad \langle 3\rangle$$

and the combination of the terms (1), (2), and (3) of Eq. 5.39 results in the same governing differential equation as for the thin plate theory (Eq. 5.20)

$$\frac{\partial^2 M_{xx}}{\partial x^2}+2\frac{\partial^2 M_{xy}}{\partial x\partial y}+\frac{\partial^2 M_{yy}}{\partial y^2}+f=0 \tag{5.40}$$

5.4.3 Interpolation Functions for the Finite Element Model

In the finite element model of the thick plates, the first-order displacements (w, ϕ_x, ϕ_y) are involved, not their derivatives. Therefore, the Lagrange interpolation functions can be adopted for this plate. For a linear four-node rectangular element, the interpolation function is in the form

$$\psi(x,y)=c_1+c_2x+c_3y+c_4xy \tag{5.41}$$

where c_i the coefficients to be determined. The interpolation functions in terms of the natural coordinates ($\xi\eta$) are

$$\psi_1=\frac{1}{4}(1-\xi)(1-\eta), \qquad \psi_2=\frac{1}{4}(1+\xi)(1-\eta)$$
$$\tag{5.42}$$
$$\psi_3=\frac{1}{4}(1+\xi)(1+\eta), \qquad \psi_4=\frac{1}{4}(1-\xi)(1+\eta)$$

where the properties of each interpolation function are shown in Fig. 5.6 below.

This element is very effective for the analysis of thick plates. However, when analyzing thin plates, researchers have shown that the element stiffness matrix becomes too stiff (Reddy 1993). For this reason, it is recommended to use reduced order schemes to integrate the equations involving the transverse shear terms.

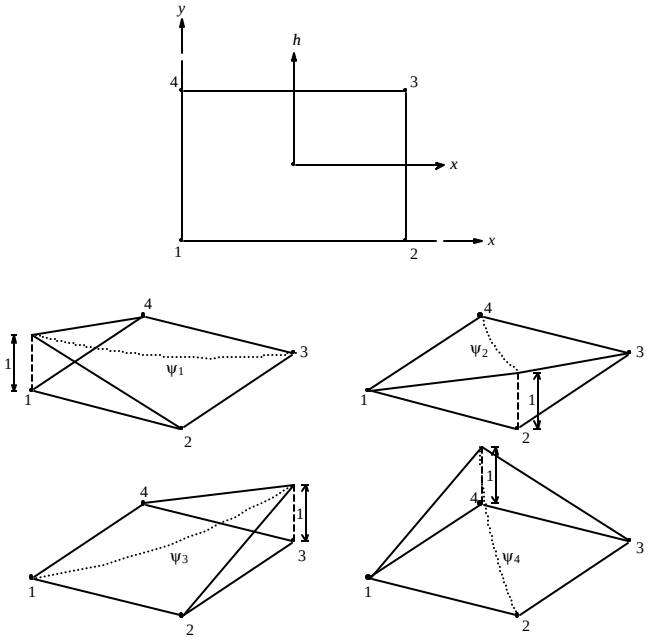

Fig. 5.6. Interpolation Functions for 4-Node Linear Rectangular Element.

The displacement function can be written as

$$w=\sum_{j=1}^{m}w_j\psi_j, \quad \theta_x=\sum_{j=1}^{m}\theta_j^x\psi_j, \quad \theta_y=\sum_{j=1}^{m}\theta_j^y\psi_j \tag{5.43}$$

where ψ_j are the Lagrange interpolation functions, which can be found in the finite element books, and the displacements (w, ϕ_x, ϕ_y) are defined in Fig. 5.4. In general, the approximation functions for the w and (ϕ_x, ϕ_y) are polynomials of different degree. However, the same function can be adopted for both the displacement and the rotations by employing reduced integration for the evaluation of stiffness coefficients associated with the transverse shear strains (Reddy 1993). If Eq. 5.43 is substituted for the displacements (w, ϕ_x, ϕ_y) and the approximation functions ψ_j for the variation of the displacements (δw, $\delta\phi_x$, $\delta\phi_y$) into Eq. 5.37, the following relationship can be obtained

$$\begin{bmatrix}\begin{bmatrix}K^{11}\\K^{21}\\K^{31}\end{bmatrix}&\begin{bmatrix}K^{12}\\K^{22}\\K^{32}\end{bmatrix}&\begin{bmatrix}K^{13}\\K^{23}\\K^{33}\end{bmatrix}\end{bmatrix}\begin{Bmatrix}\{w\}\\\{\theta^x\}\\\{\theta^y\}\end{Bmatrix}=\begin{Bmatrix}\{P^1\}\\\{P^2\}\\\{P^3\}\end{Bmatrix} \tag{5.44}$$

where $[K^{ij}]$ are the sub stiffness matrices, $\{w, \theta^x, \theta^y\}^T$ is the displacement vector, and $\{P^i\}$ is the load vector and they are defined as

$$K_{ij}^{11} = \int_S \left(C_x \frac{\partial \psi_i}{\partial x} \frac{\partial \psi_j}{\partial x} + C_y \frac{\partial \psi_i}{\partial y} \frac{\partial \psi_j}{\partial y} \right) dS$$

$$K_{ij}^{12} = \int_S C_x \frac{\partial \psi_i}{\partial x} \psi_j dS, \qquad K_{ij}^{13} = \int_S C_y \frac{\partial \psi_i}{\partial y} \psi_j dS$$

$$K_{ij}^{22} = \int_S \left(D_x \frac{\partial \psi_i}{\partial x} \frac{\partial \psi_j}{\partial x} + D_{xy} \frac{\partial \psi_i}{\partial y} \frac{\partial \psi_j}{\partial y} + C_x \psi_i \psi_j \right) dS \tag{5.45}$$

$$K_{ij}^{23} = \int_S \left(D_1 \frac{\partial \psi_i}{\partial x} \frac{\partial \psi_j}{\partial y} + D_{xy} \frac{\partial \psi_i}{\partial y} \frac{\partial \psi_j}{\partial x} \right) dS$$

$$K_{ij}^{33} = \int_S \left(D_{xy} \frac{\partial \psi_i}{\partial x} \frac{\partial \psi_j}{\partial x} + D_x \frac{\partial \psi_i}{\partial y} \frac{\partial \psi_j}{\partial y} + C_y \psi_i \psi_j \right) dS$$

and the force

$$P_i^1 = \int_S f \psi_i dS \tag{5.46}$$

For the four-node linear rectangular element with the three degrees of freedom (w_i, ϕ_{xi}, ϕ_{yi}) at each node, the size of the element stiffness matrix is 12×12. After Eq. 5.44 is solved for the displacements at every nodal point, the bending moments and shear forces are calculated at the center of each element using Eq. 5.35.

The Mindlin theory is adopted in this research for the analysis of plates using the finite element method. For the thick plates, the transverse shear deformations may be significant, and in such cases it is better to use the Mindlin plate. Actually, the Mindlin plate can be used for both thick and thin plates. If the plate is thin, then the use of reduced integration scheme will overcome the problem of the coefficients of the stiffness matrix being too stiff (Reddy 1993).

$$y = y_m \left(\frac{e_m - x}{e_m} \right)^m \tag{6.1}$$

where x is the distance measured inward from the edge of the slab (Fig. 6.1). The mound exponent may be set by the user in the program. The mound exponent that was used in the PTI design method was 3 and was based upon the study of the shape of natural soil surfaces, gilgai (Spotts 1976; Wray 1989) and analytical transient predictions of the soil surface profiles (Wray 1978; Jayatilaka 1999; Gay 1994).

These values of y are the differential movements the soil would have in the absence of the weight of the slab which, because of its flexural rigidity, will suppress the higher spots of the differential movement (Fig. 6.1). The problem of soil-slab interaction is solved by superimposing flexible slab on the unloaded differential soil profile.

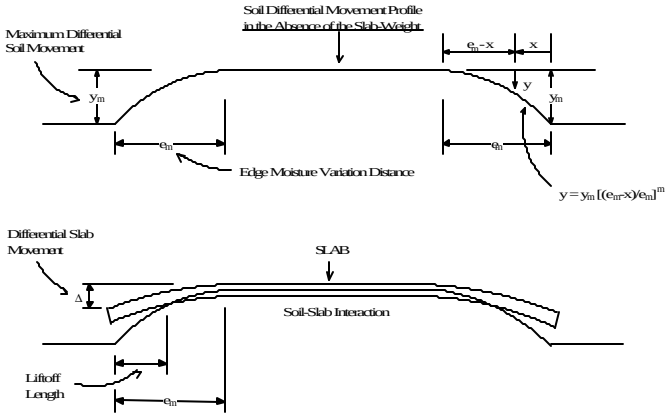

Fig. 6.1. Soil-Slab Interaction Resulting in Differential Slab Movement.

Gaps occur between the slab and the soil at some points when the slab interacts with these mound shapes. The code has an iterative scheme to check for the contact points. Figure 6.2 shows the general flow diagram of the RSLAB^N finite element computer program.

CHAPTER VI
DESCRIPTION OF COMPUTER PROGRAM

6.1 Introduction

The theoretical development of the finite element method formulation of the elastic shear deformable plate theory and the Boussinesq foundation model were implemented into a linear finite element computer code named RSLAB^N. This computer program was developed in FORTRAN 77. The program is in modular format; in other words, it consists of a number of subroutines, each of which performs a particular task within the main body of the program. There are practically no limitations on the number of elements to be handled by the program; however, a fixed number of elements and nodes need to be assigned by adjusting the dimension statements within the program.

The theoretical background of the finite element method, the elastic shear deformable plate theory, and the elastic continuum foundation model have been described in detail in the previous chapters (i.e., Chapter IV and V). This chapter, thus, concentrates only on the FORTRAN programming layout and structure of the program.

6.2 General Description

RSLAB^N finite element method computer code can be used to analyze ribbed slabs or slabs of constant thickness on expansive as well as compressible soils. A transient analysis is not considered and hence time dependency is not a factor in this program. The program employs the small-displacement theory and can consider orthotropic plate behavior so that two different Young's modulus values can be assigned to the reinforced concrete slab in two perpendicular directions. The foundation soil is modeled using the Boussinesq elastic continuum formulation. The Boussinesq equation for surface deflection is used for determining the stiffness matrix of the foundation soil. This is different than the more commonly known Winkler (or spring) model where the springs behave independent of each other while in an elastic continuum model there is interaction of neighboring soil elements.

The code accepts the vertical differential soil movements, y_m, over the range of edge moisture variation distance, e_m, as input data to represent the distortion modes for expansive soils in calculating the displacements and the stresses within the slab. As it has been mentioned in the previous chapters, there are mainly two types of critical foundation soil distortion modes due to the soil swelling and shrinking. These modes of distortion create soil surfaces of mound shapes; edge lift and center lift cases. The shape of the mounded soil surface varies according to an exponential curve which describes the differential movement of the soil. The differential movement is zero at a distance of e_m from the edge of the slab and increases to the full value of y_m at the edge of the slab. The equation of the mounded surface is

6.2.1 Slab Geometry

Before running the program, it is necessary to sketch a plan view of the slab, divide the slab into rectangular finite elements of various sizes, and number the nodes and elements. The program can handle any slab geometry composed of rectangular finite elements. The nodal points and the elements as well can automatically be generated along a straight line provided that the nodal and element numbering system is in a systematic and sequential order. In the program, the slab geometry is defined by the global x- and y-coordinates of each nodal point. The use of rectangular elements limits the size of elements to be employed. If small elements are used in some portion of the slab, the adjoining elements will be of the same width.

In the slab, it is most efficient if the nodes are numbered consecutively from bottom left to the right along the x-axis, starting from lower left corner, and then moving to the right until all nodes in the slab are numbered. The

same numbering system can be followed for the elements. This numbering system will allow the automatic generation of the nodes and elements along a straight line, the systematic numbering of element connectivity information. The input data information, including the numbering system, is explained with an example in Appendix C.

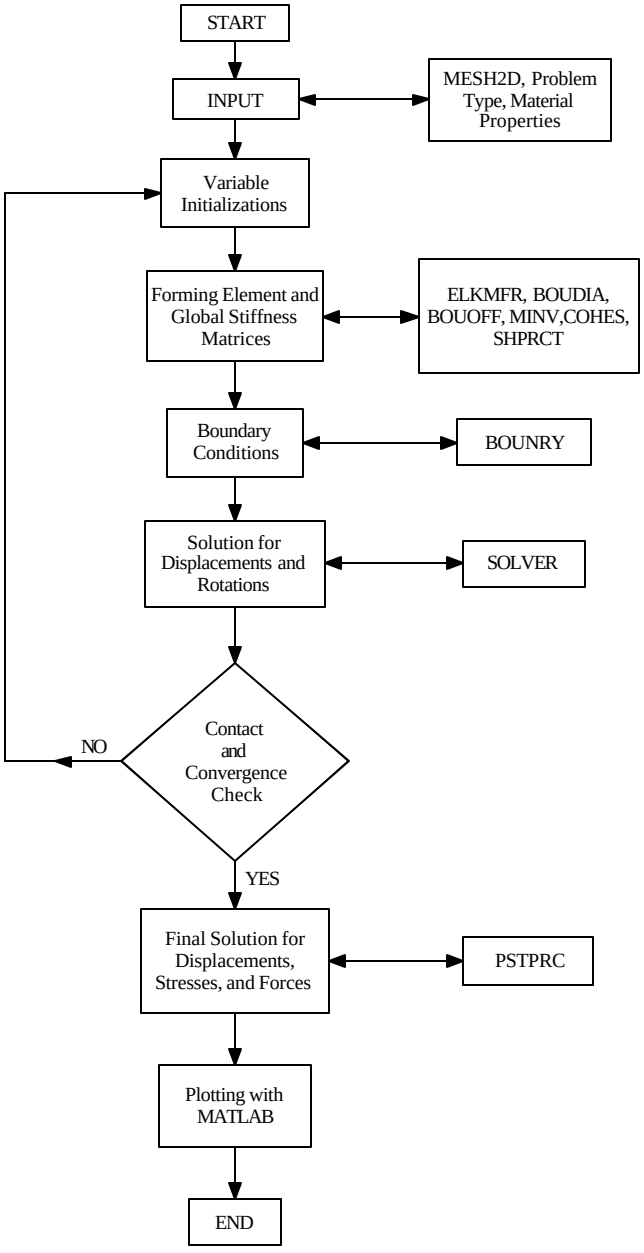

Fig. 6.2. Flow Diagram of RSLAB^N Finite Element Computer Program.

6.2.2 Beams

Stiffening beams can be generated both in x- and y-directions. Within the program, beams are created by increasing the depth of the slab along the corresponding beam locations. The width of beams needs to match the width of finite elements along the beam direction (see Fig. 6.3). There are no any restrictions for the spacing of beams, they can be arranged with any spacing. The beam depths can also vary from one beam to another.

6.2.3 Loading

The program can handle several different loading conditions. It only considers uniformly distributed loads, hence it does not accept point loads. However, point loads can be considered as uniformly distributed loads on small finite element.

A uniformly distributed load can be applied all over the slab. Any line load can be considered as a distributed load applied on small elements along a line in the same direction. The code can also automatically calculate the weight of the slab and apply it as a distributed load on the slab.

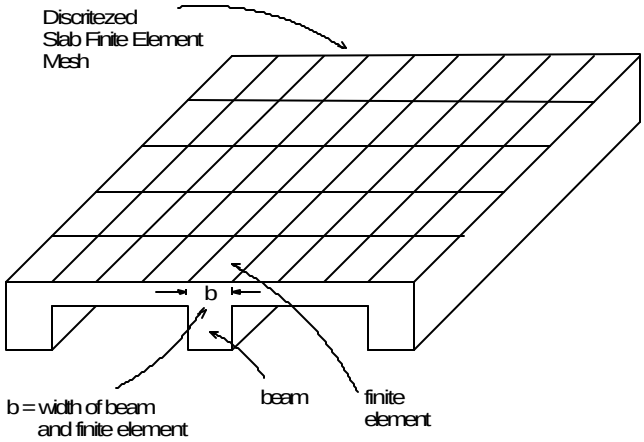

Fig. 6.3. Beam and Finite Element Dimension Compatibility.

6.2.4 Evaluation of Contact

The program has an iterative scheme for checking the contact points between the slab and the pre-deformed mound shapes for the center and edge lift conditions. When gaps are developed at some points, the stiffness coefficients of the soil at those locations are set to zero. The program goes through a number of iterations and checks for contact points between two successive iterations. If the number of contact points between the previous and the current iteration are the same, then the program has converged. It usually takes several iterations to converge to the real solution. These types of problems are considered as non-linear in the geotechnical engineering discipline due to the partial contact conditions and the iteration schemes involved. The program also permits incremental loading in the edge lift condition when a convergence problem is encountered. In this case, the unit weight of reinforced concrete is multiplied by an integer number greater than one, and the program reduces the unit weight to its real value while going through the iterations for the convergence of the slab contact points.

6.2.5 The Output

The code calculates the displacements at each nodal point and the general forces (i.e., stresses, moments, and forces) at middle of each element. These values are printed out with their corresponding global x- and y-coordinates. A small MATLAB program was also developed to represent the numerical values obtained from the program into three-dimensional plots. The graphical plots help to interpret the overall structural behavior of slab foundations.

6.3 General Outline of the Program

In general, a finite element computer program consists of three basic parts: preprocessor, processor, and postprocessor. A basic flow chart of the computer program is given in Fig. 6.4 and each subroutine is described in the coming sections.

In the preprocessor part of the program, the input data of the problem are read in. This includes the geometry (i.e., finite element coordinates and dimensions), the data of the problem (i.e., material properties for the slab as well as for the foundation soil, loading conditions), and indicators for various options (i.e., swelling, shrinking, and compressible soil profile options).

In the processor part, all steps in the finite element method, as discussed in Chapter V, are performed. These include the generation of the element matrices using numerical integration, assembly of element equations, imposition of the boundary conditions, and the solution of the simultaneous algebraic equations for the nodal values of the displacements and rotations.

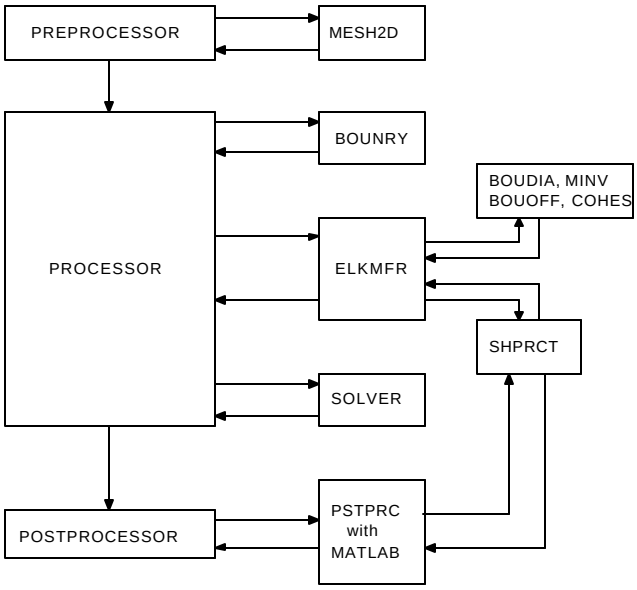

Fig. 6.4. Flow Chart of the Computer Program RSLAB^N.

In the postprocessor part of the program, the solution for the moments and stresses are computed at the middle of each element. For this part, the MATLAB option is also introduced to have a three-dimensional color plot of the displacements, bending and twisting moments, and shear forces.

6.3.1 The Program Subroutines

The subroutines (Fig. 6.3) used in the main program have the following functions:

MESH2D: This subroutine is for generating the finite element mesh (i.e., the global coordinates of the nodal points and the connectivity array for general domains with four-noded rectangular elements), element load information, and coordinate information of the stiffening beams.

BOUNRY: This is to impose the specified displacement type boundary conditions.

ELKMFR: This subroutine is for computing element matrices and vectors. The element calculations are based on linear rectangular elements with an isoparametric formulation. The element matrices assembly is also performed here. This subroutine calls in the SHPRCT, BOUDIA, BOUOFF, MINV, and COHES subroutines.

SHPRCT: This subroutine evaluates the interpolation functions and their derivatives with respect to global coordinates for Lagrange linear rectangular finite elements using the isoparametric formulation.

BOUDIA: This subroutine determines the flexibility matrix coefficients of the diagonal element for the Boussinesq foundation model.

BOUOFF: This subroutine determines the flexibility matrix coefficients of the off-diagonal element for the Boussinesq foundation model.

MINV: This subroutine forms the stiffness matrix for the Boussinesq foundation by inverting the flexibility matrix as obtained from the BOUDIA and BOUOFF subroutines.

COHES: This subroutine is for calculating the downdrag pressure on the stiffening beams caused by the cohesive shear strength of the soil.

SOLVER: This subroutine solves a banded, symmetric system of algebraic equations using the Gauss elimination method.

PSTPRC: This subroutine computes the stresses, moments, and shear forces at the middle of each element. MATLAB is a commercially available software package in the field of science and engineering. It manipulates matrices and has very powerful features of plotting functions and matrices. MATLAB can be adopted to plot nice color plots of displacements and stresses as calculated from the subroutine PSTPRC. A small MATLAB program was written to have the transition of the displacements and stresses from numeric values into MATLAB plots.

CHAPTER VII
APPLICATIONS OF THE COMPUTER PROGRAM

7.1 Introduction

The RSLAB^N finite element computer program is compared in this chapter using several example problems from the PTI manual. The results of these problems are compared with the solutions in the PTI manual. There are no available computer codes, to the author's knowledge, that the results from the RSLAB^N can be compared on a one-to-one basis. The only comparison can be made with the results from the PTI slab analysis and the opinions of some key researchers and engineers who have very extensive experience with slabs on expansive soil foundation systems. From that perspective, the RSLAB^N finite element computer code is a unique analysis program for the ribbed slabs resting on expansive soils.

7.2 Verification of the Computer Program

The linear elastic analysis verification of the program mainly consists of solving 3 example problems contained in the PTI slab manual and then comparing the results with the PTI results. Details of the example problems can be found in the PTI slab manual. These example problems are: (1) a residential slab on expansive soil constructed in a dry climate, (2) a residential slab on expansive soil constructed in a wet climate, and (3) a residential slab constructed on a compressible soil.

7. 2. 1 Example One

A residential slab constructed on expansive soil is analyzed for the displacements and stresses using the finite element program developed in this study. This slab is constructed in a dry climate, where the Thorntwaite Moisture Index is –16, in which the center lift condition generally controls the flexural design (Lytton and Meyer 1971). However, the slab is being analyzed for both center and edge lift conditions. The input parameters used for the program are briefly summarized in Table 7.1 and the slab geometry is depicted in Fig. 7.1. The slab is discretized into 246 rectangular finite elements with 282 nodal points. The slab plan geometry for example three is shown in Fig. 7.2.

7.2.1.1 Example One Center Lift Analysis

The residential slab example is analyzed with the case of stiffening beams, as the beam locations are shown in Fig. 7.1, and with the case of constant thickness. The constant thickness slab is obtained by converting the ribbed slab into an equivalent thickness slab that has the same cross-sectional moment of inertia as with the stiffening beam slab. These two analyses help to explain the distribution of the stresses within a constant thickness slab and as well as a slab with the cross stiffening beams both in x- and y-directions. The comparison of the displacements, moments in x-direction, twisting moments, and shears in the x-direction

Table 7.1. Input Parameters for the Example Problems.

Case	Example 1 Swelling, Shrinking	Example 2 Swelling, Shrinking	Example 3 Compressible Soil
Geometry	Fig. 7.1	Fig. 7.1	Fig. 7.2
e_m—center lift	5.5 ft.	4.5 ft	--
e_m—edge lift	2.5 ft.	5.5 ft	--
y_m—center lift	3.608 in.	0.9 in.	--
y_m—edge lift	0.752 in.	0.706 in.	--
Perimeter Load	1040 lb/ft	1040 lb/ft	840 lb/ft
Live Load	40 psf	40 psf	--
Beam Depth	24 in. (x and y dir.)	24 in. (x and y dir.)	24 in. (x and y dir.)
Beam Width	10 in. (x and y dir.)	12 in. (x and y dir.)	10 in. (x and y dir.)
Slab Thickness	4 in.	4 in.	4 in.
E_c	2.16E8 psf	2.16E8 psf	2.16E8 psf
ν_c	0.25	0.25	0.25
E_s	1.44E5 psf	1.44E5 psf	1.44E5 psf
ν_s	0.4	0.4	0.4
γ_c	150 pcf	150 pcf	150 pcf

Note: E_c: Elastic moduli of the reinforced concrete slab,
ν_c: Poisson's ratio of the reinforced concrete slab,
E_s: Elastic moduli of the foundation soil,
ν_s: Poisson's ratio of the foundation soil, and
γ_c: Unit weight of the reinforced concrete.

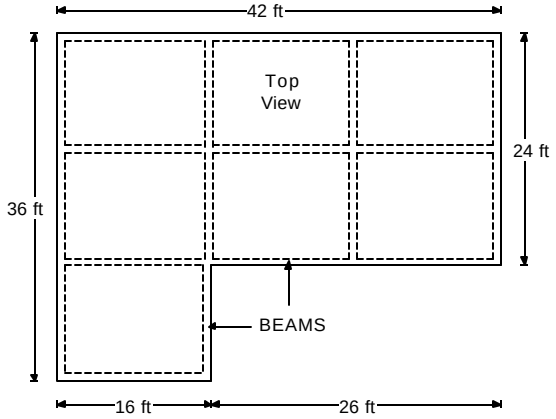

Fig. 7.1. Example One and Example Two Slab Geometry.

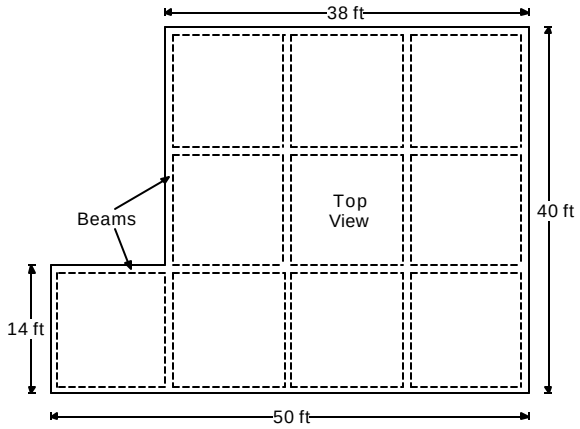

Fig. 7.2. Example Three Slab Geometry.

are depicted in Fig. 7.3, Fig. 7.4, Fig. 7.5, and Fig. 7.6, respectively. The complete set of plots for the displacements, moments, and shear forces for both ribbed and constant thickness slabs are given in Appendix D.

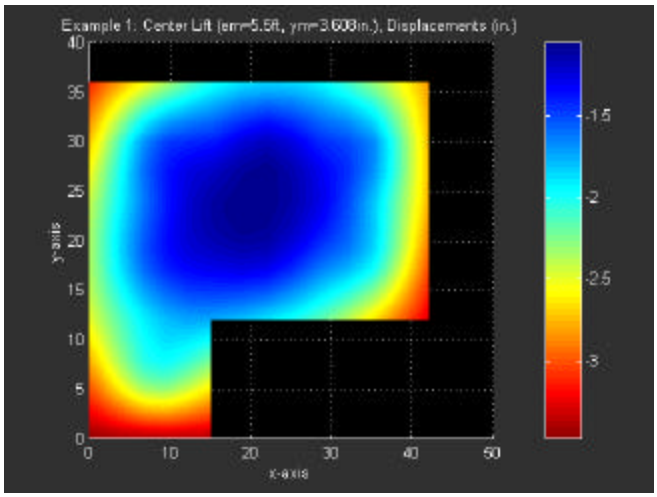

a. Ribbed Slab

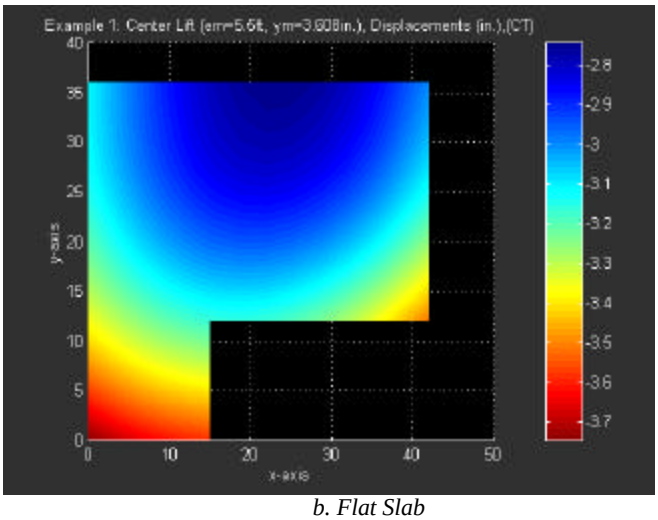

b. Flat Slab

Fig. 7.3. Example One Center Lift Case, Displacements.

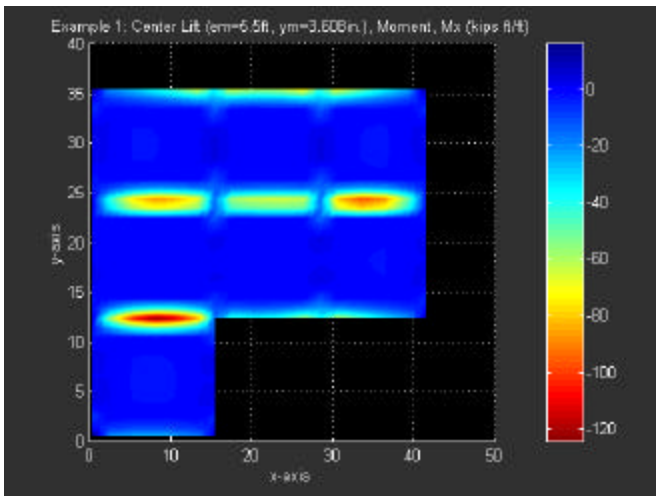

a. Ribbed Slab

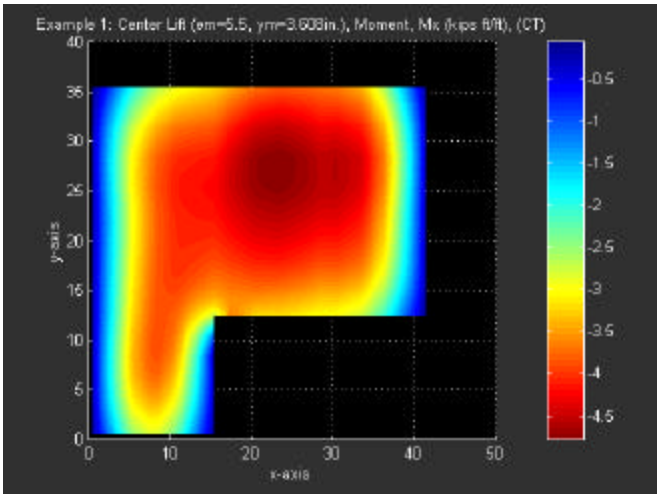

b. Flat Slab

Fig. 7.4. Example One Center Lift Case, Moment in x-direction.

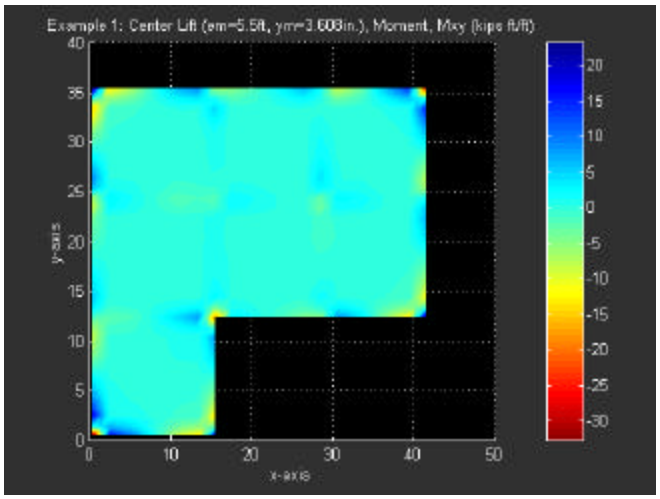

a. Ribbed Slab

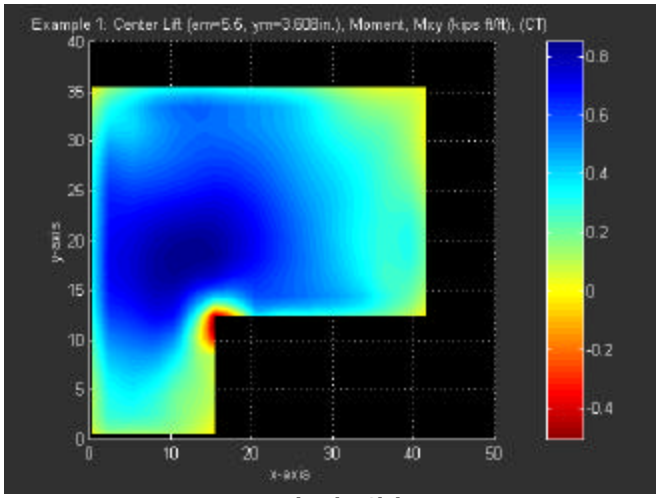

b. Flat Slab

Fig. 7.5. Example One Center Lift Case, Twisting Moment.

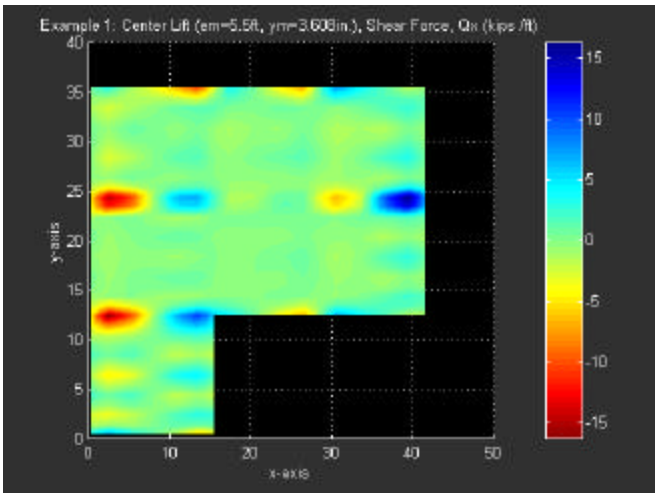

a. Ribbed Slab

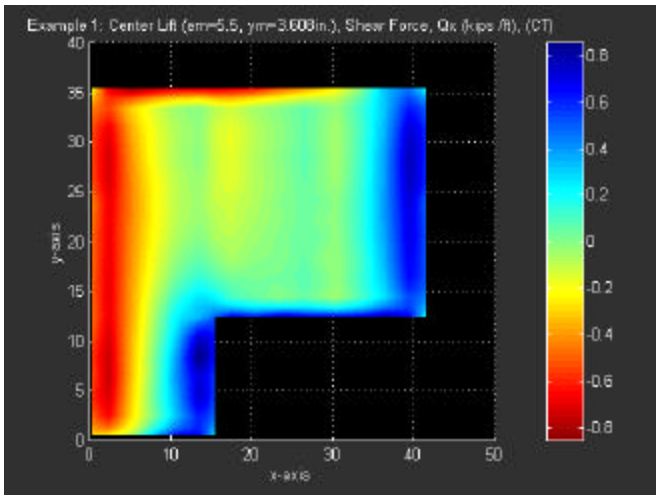

b. Flat Slab

Fig. 7.6. Example One Center Lift Case, Shear in x-direction.

The comparison of results from the program and the PTI manual for Example 1 are depicted in Table 7.2. As it is seen from Table 7.2, values for the maximum average moments and shear forces from the ribbed slab analysis are comparable with the PTI results. However, the results from the constant thickness analysis are lower than the ones from both the ribbed and PTI slab analysis. The differential deflection values obtained from the program for both the ribbed and constant thickness slabs are higher than the differential deflections from the PTI example. But, the program results in more conservative the Δ/L ratios. The Δ/L ratios for the RSLAB^N analyses were found by determining the largest departure, Δ, from the straight line joining the high point to the low point. The length of the line was taken as L.

Table 7.2. Comparison of Deflections and Stresses from Example No. 1, Center Lift Case.

	Constant Thickness Slab (RSLAB^N Analysis)	Ribbed Slab (RSLAB^N Analysis)	Example No. 1 PTI Manual (Design)	
Moment, M_x (kips ft/ft)	4.79	11.52	11.509	
Moment, M_y (kips ft/ft)	5.17	9.83	12.18	
Shear Force, Q_x (kips/ft)	0.93	1.85	2.105	
Shear Force, Q_y (kips/ft)	1.03	1.74	1.965	
Differential Deflection, δ (in.) (Δ/L)	1.01 (1/2008)	2.43 (1/701)	x-direct. 0.72 (1/400)	y-direct. 0.757 (1/665)

Note: L indicates the distance between maximum and minimum deflections.

The maximum average moment quantities shown in Table 7.2 for the ribbed slab are determined by adding the products of the moments in each plate element and dividing the sum by the width of the slab. The same process is followed to determine the maximum average shear forces. The RSLAB^N finite element computer program will enable to demonstrate the soil-structure interaction behavior of the whole slab, which is simply not possible with the PTI method in which the overlapping method of rectangular slabs misses to show the critical stress points within the slab. As it is seen from Fig. 7.4, with the capability of handling the ribbed slab analysis, the program can calculate the moment concentrations within the beams and can predict their locations. Structural engineers now will be able to design the beams for these high values of moments developed within the beams. Twisting moments can als o be calculated with the program. PTI method does not calculate these moments. Figure 7.5 shows that twisting moments can reach very high values, which need special attention for design purposes.

7.2.1.2 Example One Edge Lift Analysis

The constant thickness slab is obtained by converting the ribbed slab into an equivalent thickness slab that has the same cross-sectional moment of inertia as with the stiffening beam slab. The comparison of the displacements, moments in x-direction, twisting moments, and shears in the x-direction are depicted in Fig. 7.7, Fig. 7.8, Fig. 7.9, and Fig. 7.10, respectively. The complete set of plots for the displacements, moments, and shear forces for both ribbed and constant thickness slabs are given in Appendix D.

The comparison of results from the program and the PTI manual for Example 1 are presented in Table 7.3 for the edge lift analysis case. As it is seen from Table 7.3, values for the moments from the constant thickness slab analysis are comparable with the PTI results. However, the results from the ribbed slab analysis are much higher than the ones from both the constant thickness and PTI slab analysis. The program results in higher shear force values for both constant thickness and ribbed slab analysis than the PTI values. The differential deflection values obtained from the program for both the ribbed and constant thickness slabs are higher than the differential deflections from the PTI example. But, the program results in conservative Δ/L ratios.

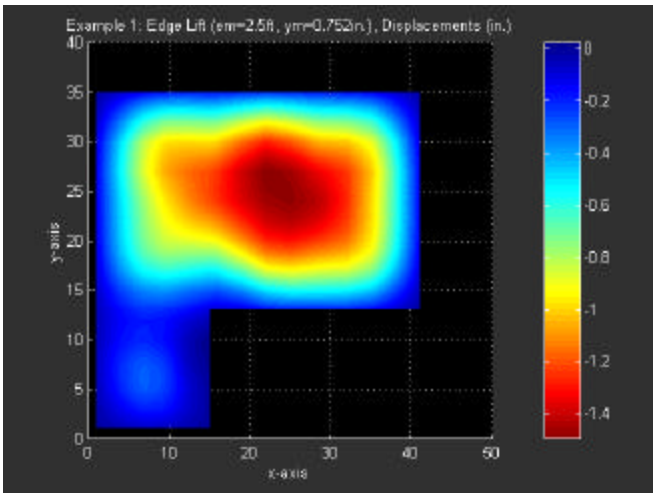

a. Ribbed Slab

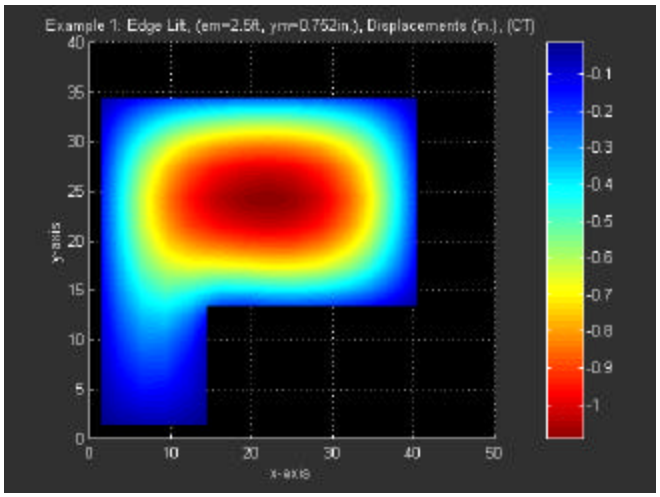

b. Flat Slab

Fig. 7.7. Example One Edge Lift Case, Displacements.

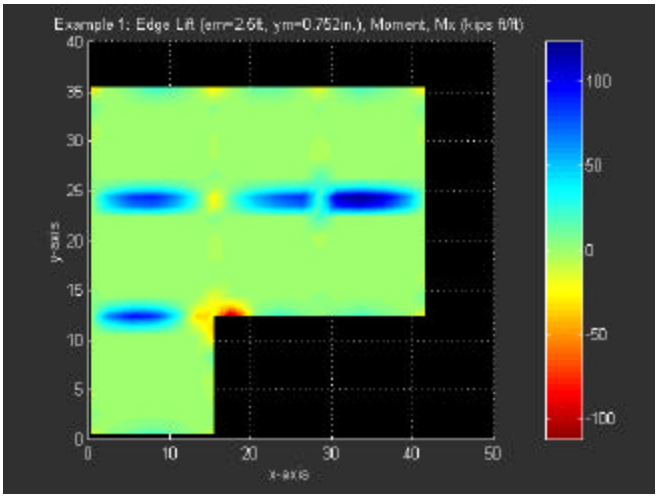

a. Ribbed Slab

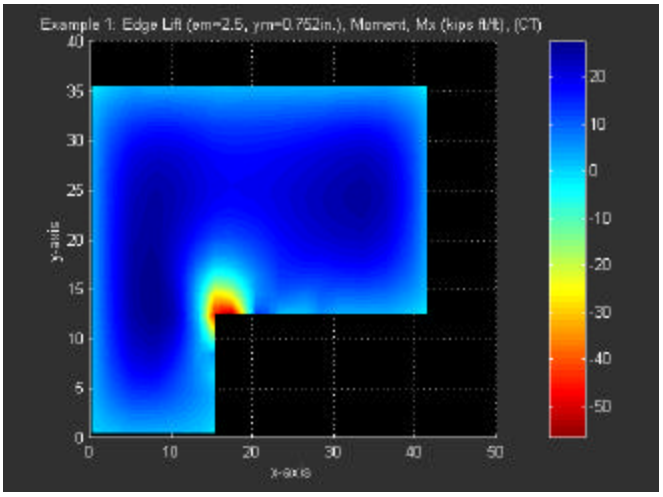

b. Flat Slab

Fig. 7.8. Example One Edge Lift Case, Moment in x-direction.

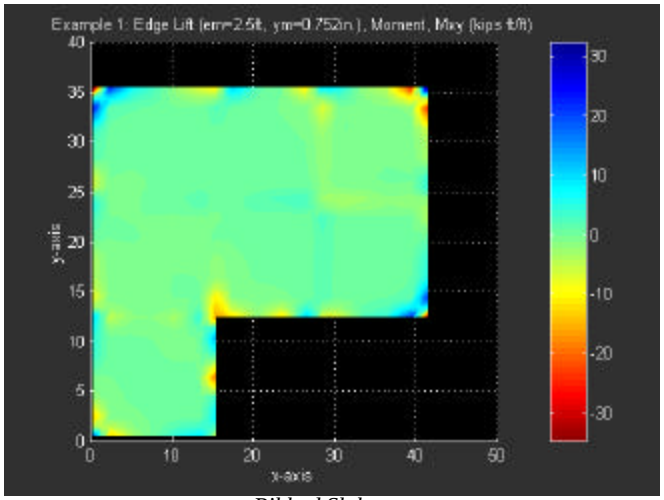

a. Ribbed Slab

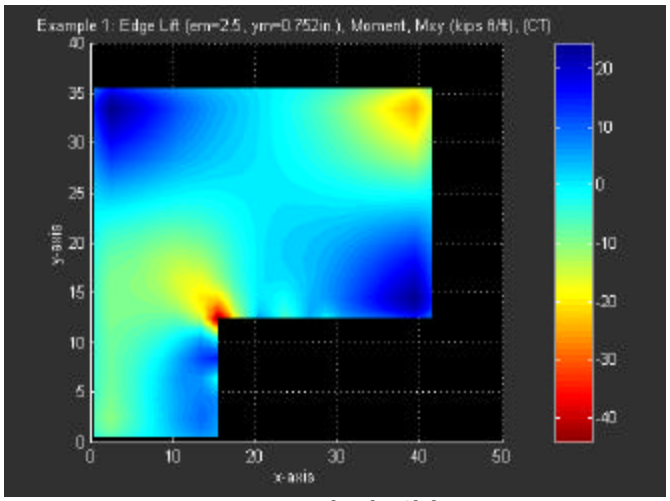

b. Flat Slab

Fig. 7.9. Example One Edge Lift Case, Twisting Moment.

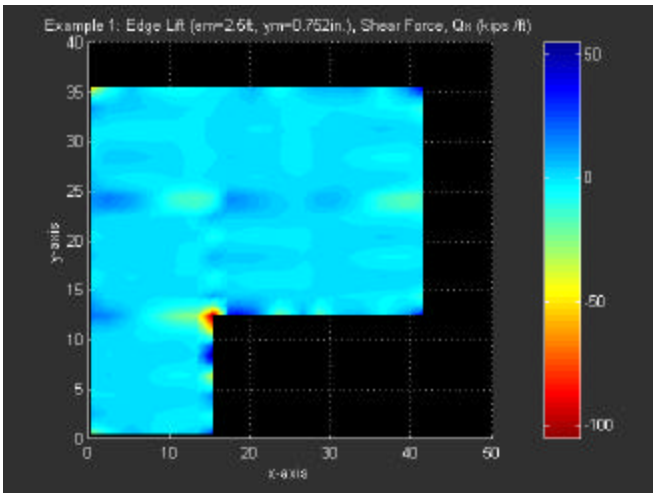

a. Ribbed Slab

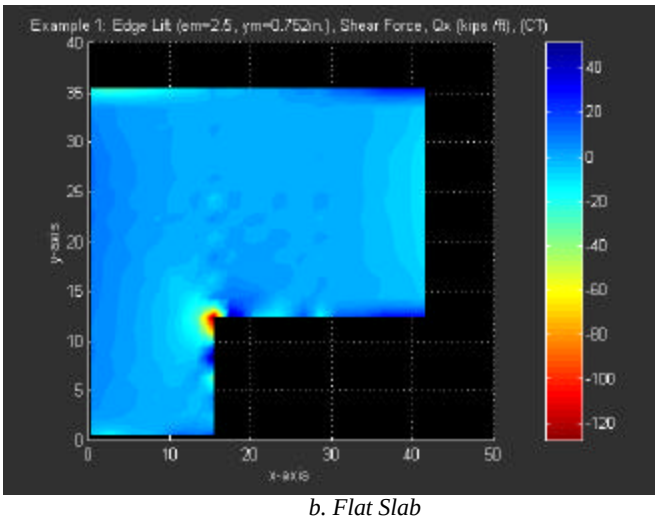

b. Flat Slab

Fig. 7.10. Example One Edge Lift Case, Shear in x-Direction.

The RSLAB^N computer program adopts the thick plate (Mindlin plate) theory. As slab thickness increases shear forces can become critical, and the program predicts that (Fig. 7.10) these forces can reach very high values at the reentrant corner of the slab.

Table 7.3. Comparison of Deflections and Stresses from Example No. 1, Edge Lift Case.

	Constant Thickness Slab (RSLAB^N Analysis)	Ribbed Slab (RSLAB^N Analysis)	Example No. 1 PTI Manual (Design)	
Moment, M_x (kips ft/ft)	2.38	8.73	2.66	
Moment, M_y (kips ft/ft)	2.29	11.10	3.01	
Shear Force, Q_x (kips/ft)	5.71	4.66	1.752	
Shear Force, Q_y (kips/ft)	3.10	4.37	1.681	
Differential Deflection, δ (in.) (Δ/L)	1.09 (1/1366)	1.46 (1/1723)	x-direct. 0.231 (1/2182)	y-direct. 0.219 (1/1315)

Note: L indicates the distance between maximum and minimum deflections.

7.2.2 Example Two

Example two is very similar to Example one, the only differences (see Table 7.1) being in e_m, y_m, and beam width values. These parameters are among the most important variables for the slab analysis as their effects can be compared with the Example one results using Tables 7.4 and 7.5. This slab is also discretized into 246 rectangular finite elements with 282 nodal points. The complete set of plots for the displacements, moments, and shear forces for both ribbed and constant thickness slabs as obtained from the program are given in Appendix E.

Table 7.4 summarizes the analysis results from the program for the center lift case. The program results in comparable solutions for both constant thickness and ribbed slabs. The PTI design values are conservative as its results compared with the values obtained from the program. Due to the same slab geometry shape as with Example one slab, the soil-structure interaction behaviors for both examples are very alike. However, as a result of changes in the parameters e_m and y_m, and the difference in beam widths (see Table 7.1), there are differences in stress concentration values. The whole spectrum of the differences can be seen from the plots in Appendix D and Appendix E.

Table 7.5 gives the results obtained from the program for the case of edge lift analysis. The program results in lower solutions of the moments for the constant thickness slab and higher solutions of the moments for the ribbed slab as compared to the PTI results. The program results in higher shear force values from both constant thickness and ribbed slab analysis than the PTI solutions for the shears.

Example one and Example two edge lift analysis cases indicate that the shear forces obtained by the program are higher than the shear forces obtained from PTI analysis.

Table 7.4. Comparison of Deflections and Stresses from Example No. 2, Center Lift Case.

	Constant Thickness Slab (RSLAB^N Analysis)	Ribbed Slab (RSLAB^N Analysis)	Example No. 2 PTI Manual (Design)	
Moment, M_x (kips ft/ft)	6.50	6.4	7.09	
Moment, M_y (kips ft/ft)	6.30	5.95	7.39	
Shear Force, Q_x (kips/ft)	1.15	1.00	1.40	
Shear Force, Q_y (kips/ft)	1.14	0.61	1.53	
Differential Deflection, δ (in.) (Δ/L)	1.195 (1/1794)	1.465 (1/860)	x-direct. 0.454 (1/634)	y-direct. 0.757 (1/1056)

Note: L indicates the distance between maximum and minimum deflections.

7.2.3 Example Three

The RSLAB^N computer program can also be employed for soil-structure interactions involving compressible soils with full contact conditions between the slab and the underlying foundation soil. The program is used to analyze an example problem contained in the PTI manual. The geometric shape of the slab is depicted in Fig. 7.2 and the variables used in the program are summarized in Table 7.1. The slab is discretized into 540 rectangular finite elements with 592 nodal points. The complete set of plots for the

displacements, moments, and shear forces for both ribbed and constant thickness slabs as obtained from the program are given in Appendix F.

Table 7.6 summarizes the results obtained from the program for the case of compressible soil with full contact condition. The program predicts slightly higher moment values than the PTI moment results. The program results in a higher shear force value in y-direction for the constant thickness slab, while all other values are lower than the PTI solutions.

Table 7.5. Comparison of Deflections and Stresses from Example No. 2, Edge Lift Case.

	Constant Thickness Slab (RSLAB^N Analysis)	Ribbed Slab (RSLAB^N Analysis)	Example No. 2 PTI Manual (Design)	
Moment, M_x (kips ft/ft)	2.36	8.40	4.72	
Moment, M_y (kips ft/ft)	4.00	10.76	6.09	
Shear Force, Q_x (kips/ft)	4.75	5.58	1.906	
Shear Force, Q_y (kips/ft)	4.87	4.26	1.828	
Differential Deflection, δ (in.) (Δ/L)	1.09 (1/1366)	1.46 (1/1723)	x-direct. 0.330 (1/872)	y-direct. 0.307 (1/1641)

Note: L indicates the distance between maximum and minimum deflections.

Table 7.6. Comparison of Deflections and Stresses from Example No. 3, Compressible Soil.

	Constant Thickness Slab (RSLAB^N Analysis)	Ribbed Slab (RSLAB^N Analysis)	Example No. 3 PTI Manual (Design)	
Moment, M_x (kips ft/ft)	5.50	4.13	3.19	
Moment, M_y (kips ft/ft)	4.70	4.03	3.42	
Shear Force, Q_x (kips/ft)	0.97	0.50	0.849	
Shear Force, Q_y (kips/ft)	2.7	0.58	0.831	
Differential Deflection, δ (in.) (Δ/L)	0.88 (1/1869)	1.561 (1/881)	x-direct. 0.124 (1/3677)	y-direct. 0.124 (1/3870)

Note: L indicates the distance between maximum and minimum deflections.

CHAPTER VIII
SUMMARY,
DESIGN TOOLS FOR SLABS ON EXPANSIVE SOILS

8.1 Introduction

In this chapter, basic design aids for slabs on expansive soils are summarized. These aids are based on some new developments (Lytton 2001) in predicting the parameters for volume change behavior of expansive soils and the finite element computer program developed in this research study. The development and application of the program have been described in detail in previous chapters. As it has been explained earlier, the main input data, regarding the expansive soil behavior, to the program are the vertical soil movement, y_m, and edge moisture variation distance, e_m. It is mainly for this reason that practical, easy-to-use design tools are needed for geotechnical practitioners to predict these variables accurately.

The geotechnical engineer should have the basic knowledge of unsaturated expansive soils, their mineralogical information and distribution, climatic information of that particular location, and the effects of site conditions as trees, flower beds and ponds in order to calculate the y_m and e_m parameters. The geotechnical engineer usually provides these parameters to the structural engineer who designs the slab for the possible two worst soil support patterns; center lift and edge lift. The structural engineer should be able to use such a slab analysis program as developed in this study for these soil support conditions to predict the differential displacements, moments, and shear forces for the design of the slab structure.

8.2 Soil Movement

The amount of swelling or shrinking that a soil profile will undergo depends on the thickness of the layer, type of clay mineral present, the surcharge pressure, and the severity of climatic change. The expression relating the volumetric change (Eqs. 2.19 and 2.20) in a soil sample due to changes in suction and mean principal stress is widely used to calculate the vertical differential soil movement, y_m. The design values of y_m for the edge lift and center lift conditions can be estimated either by the computer program VOLFLO-2 or, in the absence of the computer program, by the soil movement tables generated for the cases of lawn irrigation, flower bed, and tree drying (Lytton 2001).

8.2.1 VOLFLO-2

The computer program VOLFLO-2 is based on the work by Naiser (1997) and was briefly described in Chapter II. This program can be used to calculate the y_m values for both transient and equilibrium conditions. For instance, for the given suction values the suction profiles and amount of differential movements at any given month of the year can be calculated for a given number of climatic cycles per year as depicted in Fig. 8.1. The program can also consider the effect of vertical moisture barriers and the distance between the edge of the slab and a tree (Fig. 8.1) to estimate the vertical differential soil movements.

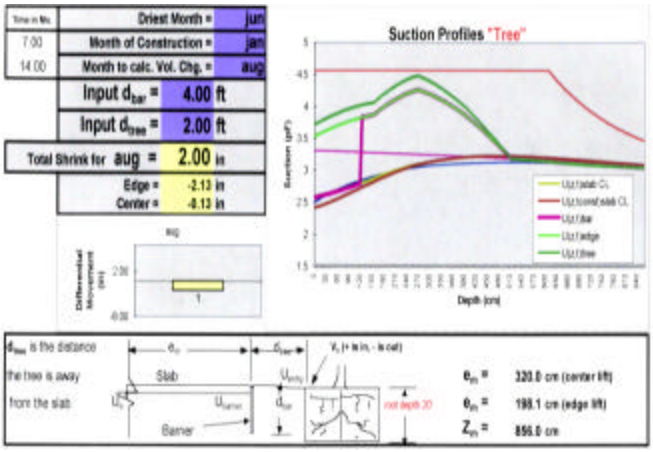

Fig. 8.1. A typical Output from VOLFLO-2 (from Lytton 2001).

8.2.2 Soil Movement Tables

Lytton (2001) provided some guide numbers to estimate differential soil movements y_m in the form of tables for different vegetation and soil surface conditions. The guide numbers can be used in the following equation as

$$y_m = g_i \times (\text{Guide Number from Table 8.1}) \qquad (8.1)$$

where g_i is the volume change coefficient.

The guide numbers for the cases of lawn irrigation, flower bed, tree drying case with and without vertical moisture barriers are presented in tables in Appendix H.

Table 8.1. Soil Movement Guide Numbers for Slab Design (Lytton 2001).

Measured Suction pF at Depth, z_m, m	y_m Guide Numbers						
	Controlling Surface Suction, pF						
	2.5	**2.7**	**3.0**	**3.5**	**4.0**	**4.2**	**4.5**
2.7	+3.2	0	-4.1	-13.6	-25.7	-31.3	-40.0
3.0	+9.6	+5.1	0	-7.5	-18.2	-23.1	-31.3
3.3	+17.7	+12.1	+5.1	-2.6	-11.5	-15.8	-23.1
3.6	+27.1	+20.7	+12.1	+1.6	-5.7	-9.4	-15.8
3.9	+38.1	+30.8	+20.7	+7.3	-1.3	-4.1	-9.4
4.2	+50.4	+42.1	+30.8	+14.8	+3.2	0	-4.1
4.5	+63.6	+54.7	+42.1	+23.9	+9.6	+5.1	0

8.3 Estimating Volume Change Coefficient

Covar (2001) presented a method for the estimation of the volume change coefficient, γ_h, using Atterberg limits, particle size classification, and the coefficient of linear extensibility (COLE) values. The COLE test represents the fractional change in a clod sample resulting from changes in moisture content. Covar (2001) produced a series of charts using a 6500 sample subset of 130,000 samples of the Natural Resources Conservation Services data base. Figure

8.2 depicts the distribution of these soil samples on the Casagrande's Plasticity Index versus Liquid Limit chart.

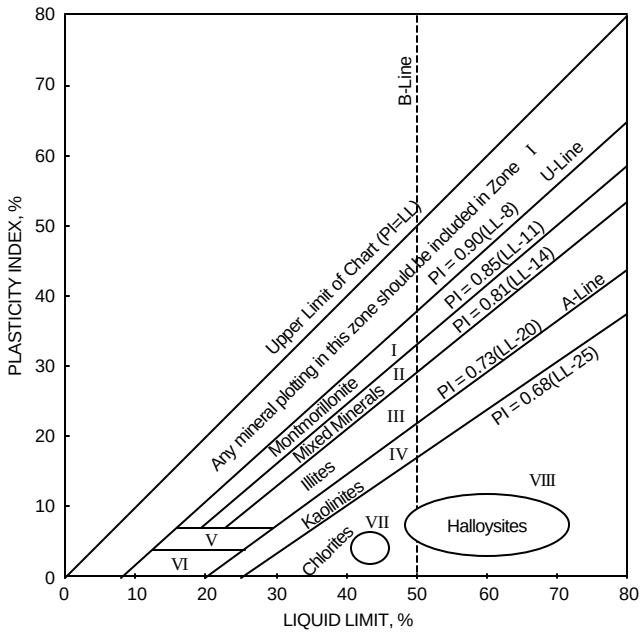

Fig. 8.2. Expansive Soils Zones (from Lytton 2001).

The classification of soil samples, as shown in Fig. 8.2, results in eight different data groups, each representing a group with some mineralogical similarity. The volume change guide number values were obtained for each data group. The volume change coefficient, γ_h, is then obtained as follows

$$\gamma_h = [\text{Percent Fine Clay}] \times [\text{Volume Change Guide Number}] \quad (8.2)$$

The volume change guide numbers for the first data group (Fig. 8.2) are depicted in Fig. 8.3 and for the other zones they are presented in Appendix I.

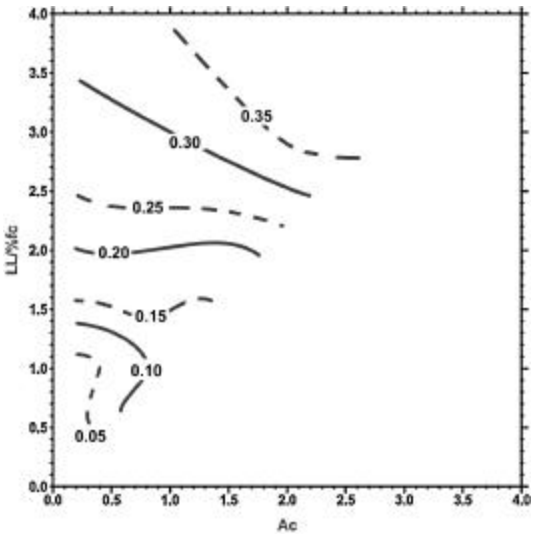

Fig. 8.3. Soil Volume Change Guide Numbers for Data Group 1 (from Covar 2001).

8.4 Edge Moisture Variation Distance (e_m)

The edge moisture variation distance depends on the diffusion coefficient (α_d) of the unsaturated soil. The unsaturated diffusion coefficient is also a function of suction, permeabilty, and the cracks in the soil. Dry soils have a lower diffusion coefficient, and thus smaller edge moisture variation distance. Similarly, wet soils have a higher coefficient, and larger edge moisture variation distance. The basic lab tests, namely the liquid limit, plastic limit, plasticity index, percentage of soil passing No. 200 sieve, and percentage of soil of total sample finer than 2 microns are needed to estimate the edge moisture variation distance. The edge moisture variation distances for both center lift and edge lift cases can be estimated from Fig. 8.4.

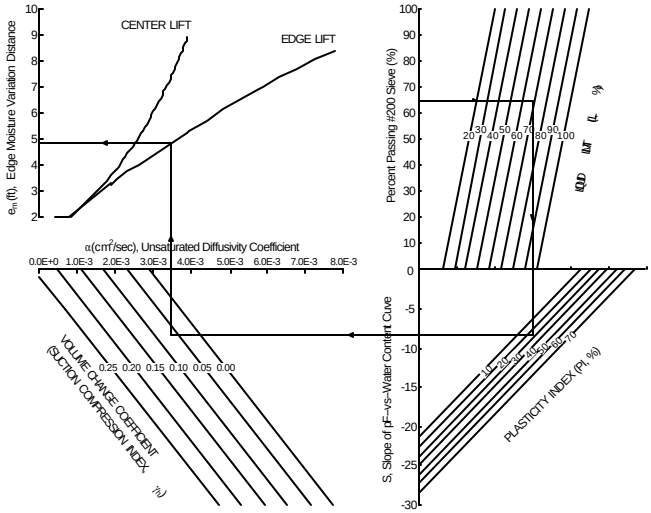

Fig. 8.4. Estimating Edge Moisture Variation Distance (from Lytton 2001).

This edge moisture variation distance can be reduced to a smaller distance with the use of vertical moisture barriers. Lytton (2001) developed charts to estimate the effects of vertical moisture barriers on the edge moisture variation distances and provided the following figures (Fig. 8.5, Fig. 8.6, and Fig. 8.7) for variable depths of cracks from the ground surface to a distance of T.

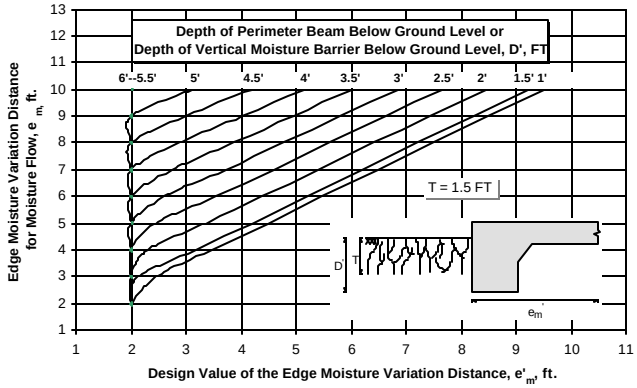

Fig. 8.5. Edge Moisture Variation Distances for T=1.5 ft. (from Lytton 2001).

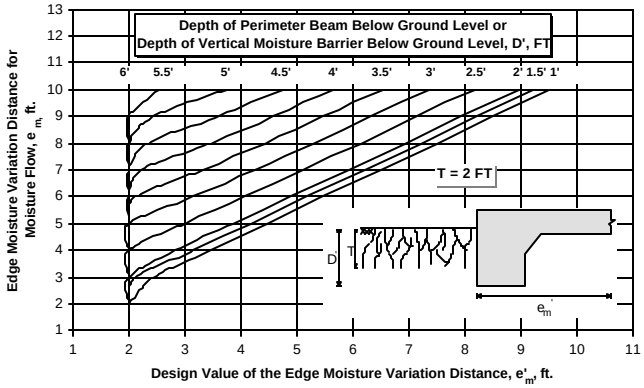

Fig. 8.6. Edge Moisture Variation Distances for T=2.0 ft. (from Lytton 2001).

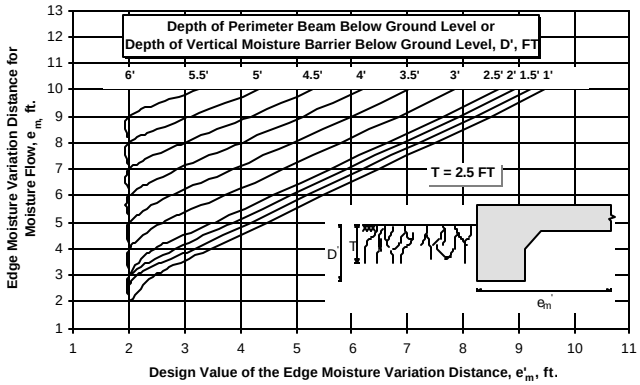

Fig. 8.7. Edge Moisture Variation Distances for T=2.5 ft. (from Lytton 2001).

8.5 Structural Analysis of Slab on Expansive Soil

Using the edge moisture variation distance, e_m, and differential soil movement, y_m, the structural engineer can analyze the slab for displacements, moments, and shear forces and in turn use these results for design of the slab. As explained in the above sections, the geotechnical engineer can provide the two important parameters (i.e., e_m and y_m) using basic unsaturated soil mechanics principles and basic laboratory test results.

The RSLAB^N finite element computer program can effectively be employed for analyses of slabs constructed on expansive soils. This program can calculate displacements, moments, shear forces based on a realistic soil-structure interaction model.

CHAPTER IX
CONCLUSIONS AND RECOMMENDATIONS

9.1 Conclusions

An analytical study was undertaken in this thesis to develop an improved analysis method for calculating the performance of slabs on expansive soils. A Finite element method formulation of slabs on elastic continuum foundations was developed to analyze this complex soil-structure system. The shear deformable plate theory was formulated for use with the finite element method and the programming was done in FORTRAN. The program was written such that it can accommodate the need of current practice for slab designs on problematic expansive soils. The program RSLAB^N developed in this study is improved in several significant ways over the program that was used to develop the PTI slab design method.

To more correctly model the soil-structure interaction, the program can accommodate any practical geometric shapes, stiffening beams, and variable loading conditions. In addition, the calculation of twisting moments is possible with this program. The program can also model the anisotropic properties of the reinforced concrete slab in two perpendicular directions, mainly x- and y-directions. The material properties for the reinforced concrete slab are Young's modulus and Poisson's ratio for the isotropic analysis and Young's modulus in both x- and y-directions, Poisson's ratio, and shear modulus values for the anisotropic analysis.

The foundation soil was modeled as an elastic half-space using the Boussinesq formulation. The foundation model was incorporated into the program as surface finite elements. Currently, due to the nature of the Boussinesq equation, it is only practical to use rectangular finite elements. The elastic continuum model is much more realistic than the Winkler model because the continuum model has the ability of expressing the effects of elements on each other; this is not possible for the Winkler model in which the springs behave independently of each other. The material properties for the Boussinesq foundation model are elastic soil modulus and Poisson's ratio. These parameters are more representative of the soil than the spring constant value for the Winkler model, which depends on the size and shape of the foundation.

The RSLAB^N program was compared with the example problems in the PTI manual. The analysis was done for a flat slab and a ribbed slab having the same cross sectional moment of inertia and the results were compared with the results in the PTI manual. The following specific conclusions can be made from the results of the program for the center lift analysis (Table 7.2 and Table 7.4) based on two example problems:

1. The program results in lower values of average maximum moments and shears for both constant thickness and ribbed slab as compared to the same stresses in the PTI manual.
2. The differential deflections between the high and low points of the slab as calculated from the program for both flat and ribbed slab cases were higher than the deflections from the PTI analysis, but the curvatures were smaller, resulting in conservative Δ/L values.
3. More importantly, with the program it is now possible to examine the overall behavior of the slab and to locate the stress concentrations for the purpose of design. This was not entirely possible with the overlapping process of the PTI method, which was missing the stress concentration values and their locations. The analysis emphasizes that the reentrant corners are the critical locations for stress concentrations. It is also seen that the stiffening beams are carrying most of the stresses.
4. With the program it is now possible to analyze and design for the twisting moments, which are seen to be critical at the corners.

Similarly, the following specific conclusions can be made from the results of the program for the edge lift analysis (Table 7.3 and Table 7.5) based on two example problems contained in the PTI manual:

1. The program results in higher values of average moments and shears for both constant thickness and ribbed slab analysis, except the moments in x- and y-directions in the case of constant thickness slab, as compared to the same stresses in the PTI manual.
2. The differential deflections calculated from the program for both constant thickness and ribbed slab cases were higher than the deflections from the PTI method, while resulting in conservative Δ/L values.

These conclusions were made from analyzing only two example problems from the PTI manual; therefore, it is very difficult to generalize these conclusions for all slab types and different input variables.

The third example problem from the PTI manual is based on a compressible soil case, in which full contact condition is assumed for the analysis. The analysis was done for constant thickness slab and ribbed slab having the same cross-sectional moment of inertia and the results were compared with the results in the PTI manual. The following specific conclusions can be made from the results of the

program for the analysis (Table 7.6) based on comparison with the example problem from the PTI manual:

1. The program results in slightly higher values of average moments for both constant thickness and ribbed slab as compared to the same stresses in the PTI manual. However, smaller maximum average shear force values are obtained in both constant thickness and ribbed slab analysis. However, there is a very high peak value of shear force in the constant thickness slab analysis.
2. The differential deflections calculated from the program for both constant thickness and ribbed slab cases were higher than the deflections from the PTI analysis, but the curvatures were smaller, resulting in conservative Δ/L values.

9.2 Recommendations for Future Enhancement of the Program

The RSLAB^N finite element computer program developed in this thesis can further be improved with additional work undertaken in the following research areas:

1. The number of degrees of freedom per node need to be increased from 3 to 5 in order to accommodate the analysis for the post-tensioning effects as a result of normal in plane stresses. With 5-degrees of freedom, which will make it a non-linear analysis, it is possible to have the effects of large displacements, which is usually a case in slabs on expansive soils.
2. For use in forensic investigations, the program should be capable of representing cracks in the slab. This can be done simply by altering the modulus of the plate element perpendicular to the direction of the crack.
3. Currently, the program uses only rectangular finite elements. This is mainly because of the singularity problem in the Boussinesq equation. This could be overcome by a numerical integration scheme that is only applicable to rectangular finite elements. A similar integration scheme can be developed for various finite elements as triangles, quadrilaterals, etc.
4. Cross-anisotropic soil properties can be incorporated into the elastic half-space foundation soil model.
5. 3-Dimensional versions of VOLFLO-2 or FLODEF can be developed and can be coupled with the RSLAB^N program to represent more realistic deformation patterns beneath the slab.
6. The current program can be modified to handle various e_m and y_m values at various locations within the slab.
7. For possible pavement applications, the program needs to be equipped with coupled transient heat and moisture flow analysis to handle curling and warping as well as loss of support.

REFERENCES

ASTM D 5298 (1993). "Standard Test Method for Measurement of Soil Potential (Suction) Using Filter Paper," *1993 Annual Book of ASTM Standards*, Philadephia, PA.

Bishop, A. W. and Henkel, D. J. (1962). *The Measurement of Soil Properties in the Triaxial Test*, 2nd Edition, Edward Arnold, London, England.

Bowles, J. E. (1988). *Foundation Analysis and Design*, 4th Edition, McGraw-Hill Book Company, New York, NY.

Building Research Advisory Board (1959). "National Research Council—Design Criteria for Residential Slabs-on-Ground," *U.S. National Academy of Sciences Publication 657*, Washington, DC.

Building Research Advisory Board (1962). "National Research Council—Design Criteria for Residential Slabs-on-Ground," *U.S. National Academy of Sciences Publication 1077*, Washington, DC.

Building Research Advisory Board (1968). "National Research Council Criteria for Selection and Design of Residential Slabs-on-Ground," *U. S. National Academy of Sciences Publication 1571*, Washington, DC.

Cheung, Y. K. and Zienkiewicz, O. C. (1965). "Plates and Tanks on Elastic Foundations-An Application of Finite Element Method," *International Journal of Solids and Structures*, Vol. 1, pp. 451-461.

Covar, A. P. (2001). "Estimating Soil Swelling Behavior Using Soil Classification Properties," *Proceedings, The Geotechnical Engineering Division of the American Society of Civil Engineers*, The Annual ASCE Convention, Houston, TX.

Edlefsen, N. E. and Anderson, A. B. C. (1943). "Thermodynamics of Soil Moisture," *Hilgardia*, Vol. 15, pp.31-298.

Frazer, B. E. and Wardle, L. J. (1975). "The Analysis of Stiffened Raft Foundations on Expansive Soil," *Symposium on Recent Developments of the Analysis of Soil Behavior and Their Application to Geotechnical Structures*, University of New South Wales, Kensington, New South Wales, Australia.

Fredlund, D. G. and Rahardjo, H. (1993). *Soil Mechanics for Unsaturated Soils*, John Wiley, New York, NY.

Gardner, R. (1937). "A Method of Measuring the Capillary Tension of Soil Moisture Over a Wide Moisture Range," *Soil Science*, Vol. 43, No. 4, pp. 277-283.

Gay, D. A. (1994). "Development of a Predictive Model for Pavement Roughness on Expansive Clay," Ph.D. Dissertation, Department of Civil Engineering, Texas A&M University, College Station, TX.

Ghali, A. and Neville, A. M. (1978). *Structural Analysis: A Unified Classical and Matrix Approach*, Chapman and Hall, New York, NY.

Goldberg, R. N. (1981). "Evaluated Activity and Osmotic Coefficients for Aqueous Solutions: Thirty-six Uni-Bivalent Electrolytes," *Journal of Physics and Chemistry Reference Data*, Vol. 10, No. 3, pp. 671-764.

Goldberg, R. N. and Nuttall, R. L. (1978). "Evaluated Activity and Osmotic Coefficients for Aqueous Solutions: The Alkaline Earth Metal Halides," *Journal of Physics and Chemistry Reference Data*, Vol. 7, No. 1, pp. 263-310.

Grim, R. E. (1953). *Clay Mineralogy*, McGraw-Hill Book Company, New York, NY.

Guven, N. (1996). "Clay Mineralogy," Class Notes for GCH 5308, Texas Tech University, Lubbock, TX.

Hamer, W. J. and Wu, Y.-C. (1972). "Osmotic Coefficients and Mean Activity Coefficients of Uni-Univalent Electrolytes in Water at 25°C," *Journal of Physics and Chemistry Reference Data*, Vol. 1, No. 4, pp. 1047-1099.

Hetenyi, M. (1946). *Beams on Elastic Foundations*, The University of Michigan Press, Ann Arbor, MI.

Hillel, D. (1980). *Fundamentals of Soil Physics*, Academic Press, San Diego, CA.

Houston, S. L., Houston, W. N., and Wagner, A. M. (1994). "Laboratory Filter Paper Measurements," *Geotechnical Testing Journal*,Vol. 17, No. 2, pp. 185-194.

Huang, Y. H. (1974). "Finite Element Analysis of Slabs on Elastic Solids," *Transportation Engineering Journal*, ASCE, Vol. 100, No. TE2, pp. 403-410.

Huang Y. H. (1993). *Pavement Analysis and Design*, Prentice-Hall, Inc, Englewood Cliffs, NJ.

Jayatilaka, R. (1999). "A Model to Predict Expansive Clay Roughness in Pavements with Vertical Moisture Barriers," Ph.D. Dissertation, Department of Civil Engineering, Texas A&M University, College Station, TX.

Jayatilaka, R., Gay, D. A., Lytton, R. L., and Wray, W. K. (1992). "Effectiveness of Controlling Pavement Roughness Due to Expansive Clays with Vertical Moisture Barriers," *Research Report No. 1165-2F*, Texas Transportation Institute, College Station, TX.

Jones, D. E. and Holtz, W. G. (1973). "Expansive Soils – The Hidden Disaster," *Civil Engineering – ASCE*, Vol. 43, No. 8, pp. 49-51.

Laliberte, G. E. and Corey, A. T. (1967). "Hydraulic Properties of Disturbed and Undisturbed Soils," *ASTM, STP, No. 417*.

Lang, A. R. G. (1967). "Osmotic Coefficients and Water Potentials of Sodium Chloride Solutions from 0 to 40°C," *Australian Journal of Chemistry*, Vol. 20, pp.2017-2023.

Lee, H. C. (1991). "An Evaluation of Instruments to Measure Soil Moisture Condition," M.S. Thesis, Department of Civil Engineering, Texas Tech University, Lubbock, TX.

Lytton, R. L (1969). "Theory of Moisture Movement in Expansive Clays," *Research Report No. 118-1*, Center for Highway Research, University of Texas at Austin, TX.

Lytton, R. L. (1970). "Design Criteria for Residential Slabs and Grillage Rafts on Reactive Clay," *Report for the Australian Commonwealth Scientific and Industrial Research Organization, Division of Applied Mechanics*, Melbourne, Australia.

Lytton, R. L. (1972). "Design Methods for Concrete Mats on Unstable Soils," *3rd Inter-American Conference on Materials Technology*, Rio de Janiero, Brazil.

Lytton, R. L. (1973). "Stiffened Mat Design Considering Viscoelasticity, Geometry, and Site Conditions," *Proceedings 3rd International Conference on Expansive Soils, Vol. 2, Israel Society of Soil Mechanics and Foundation Engineering*, Haifa, Israel.

Lytton, R. L. (1977). "Foundations in Expansive Soils." *Numerical Methods for Geotechnical Engineering*, Desai, C. S. and Christian, J. T. eds., McGraw-Hill Book Company, New York, NY.

Lytton, R. L. (1994). "Prediction of Movement in Expansive Clays," *Geotechnical Special Publication No. 40*, Yeung, A. T. and Felio, G. Y., eds., Vol. 2, ASCE, New York, NY.

Lytton, R. L. (1995). "Foundations and Pavements on Unsaturated Soils." *Proceedings of the First International Conference on Unsaturated Soils*, Paris, France, E. E. Alonso and P. Delage, eds., Vol. 3., A. A. Balkema Publishers, Rotterdam, The Netherlands.

Lytton, R. L. (1996). "Foundations on Expansive Soils," Class Notes for CVEN 646, Texas A&M University, College Station, TX.

Lytton, R. L. (2001). "Methods to Aid Structural and Geotechnical Engineers in Designing Slab-on-Grade." Presented at the Foundation Performance Association Meeting, Houston, TX.

Lytton, R. L. and Meyer, K. T. (1971). "Stiffened Mats on Expansive Clay," *Journal of the Soil Mechanics and Foundations Division*, ASCE, Vol. 97, No. SM7, Proc. Paper 8265, pp. 999-1019.

Lytton, R. L. and Woodburn, J. A. (1973). "Design and Performance of Mat Foundations on Expansive Clay," *Proceedings 3rd International Conference on Expansive Soils, Vol. 1, Israel Society of Soil Mechanics and Foundation Engineering*, Haifa, Israel.

McKeen, R. G. (1977). "Characterizing Expansive Soils for Design," Presented at the Joint Meeting of the Texas, New Mexico, and Mexico Section of the ASCE, Albuquerque, NM.

McKeen, R. G. (1981). "Design of Airport Pavements on Expansive Soils," U.S. Department of Transportation, Federal Aviation Administration, Washington, DC.

Meyer, K. T. and Lytton, R. L. (1966). "Foundation Design in Swelling Clays," Presented at the Texas Section, American Society of Civil Engineers meeting in Austin, TX.

Mitchell, P. W. (1980). "The Structural Analysis of Footings on Expansive Soil," Kenneth W. G. Smith & Associates, *Research Report No. 1*, Webb & Son, Adelaide, Australia.

Mitchell, P. W. and Avalle, D. L. (1984). "A Technique to Predict Expansive Soil Movements," *Proceedings, 5th International Conference on Expansive Soils*, Adelaide, Australia.

Mojeckwu, E. C. (1979). "A Simplified Method for Identifying the Predominant Clay Mineral in Soil," M.S. Thesis, Department of Civil Engineering, Texas Tech University, Lubbock, TX.

Naiser, D. D. (1997). "Procedures to Predict Vertical Differential Soil Movement for Expansive Soils," M.S. Thesis, Department of Civil Engineering, Texas A&M University, College Station, TX.

Nath, B. (1974). *Fundamentals of Finite Elements for Engineers*, The Humanities Press, Inc., New York, NY.

Post Tensioning Institute (1996). *Design and Constructionof Post Tensioned Slabs-on-Ground*, 2nd Edition, Post Tensioning Institute, Phoenix, AZ.

Poulos, D. (2000). "Foundation Settlement Analysis —Practice versus Research," Presented at the 8th Spencer J. Buchanan Lecture, Texas A&M University, College Station, TX.

Reddy, J. N. (1993). *An Introduction to the Finite Element Method*, Mc-Graw-Hill Book Company, New York, NY.

Reddy, J. N. (1999). *Theory and Analysis of Elastic Plates*, Taylor & Francis, Philadelphia, PA.

Russam, K. and Coleman, J. D. (1961). "The Effect of Climatic Factors on Subgrade Moisture Conditions," *Geotechnique*, Vol. 3, No. 1, pp. 22-28.

Schofield, R. K. (1935). "The pF of the Water in Soil," *Transactions, 3rd International Congress of Soil Science*, Vol. 2, pp. 37-48.

Spanner, D. C. (1951). "The Peltier Effect and Its Use in the Measurement of Suction Pressure," *Journal of Experimental Botany*, Vol. 2, No. 5, pp. 145-168.

Sposito, G. (1981). *The Thermodynamics of Soil Solutions*, Oxford University Press, New York, NY.

Spotts, J. W. (1974). "The Role of Water in Gilgai Formation," Ph.D. Dissertation, Department of Civil Engineering, Texas A&M University, College Station, TX.

Swarbrick, G. E. (1995). "Measurement of Soil Suction Using the Filter Paper Method," *1st International Conference on Unsaturated Soils*, eds.: E. E. Alonso and P. Delage, Vol. 2, Paris, France.

Thornthwaite, C. W. (1948). "An Approach Toward a Rational Classification of Climate," *Geographical Review*, Vol. 38, No. 1, pp. 55-94.

Timoshenko, S. P. and Goodier, J. N. (1970). *Theory of Elasticity*, 3rd Edition, McGraw-Hill Book Company, New York, NY.

Timoshenko, S. P. and Woinowsky-Krieger, S. (1968). *Theory of Plates and Shells*, 2nd Edition, McGraw-Hill Book Company, New York, NY.

Ugural, A. C. (1981). *Stresses in Plates and Shells*, McGraw-Hill Book Company, New York, NY.

Vlasov, V. Z. and Leont'ev, N. N. (1966). *Beams, Plates, and Shells on Elastic Foundation*, (Translated from Russian), Israel Program for Scientific Translations, Jerusalem, Israel.

VOLFLO (1986). "Volume Change and Flow Calculations in Expansive Soils," *User's Manual*, Kirby T. Meyers and Associates, Post Tensioning Institute, Phoenix, AZ.

Walsh, P. F. (1974). "The Design of Residential Slabs-on-Ground," *CSRIO Australian Division Building Research Technology*, Vol. 5, pp. 1-15.

Walsh, P. F. (1978). "The Analysis of Stiffened Rafts on Expansive Clays," CSIRO Division of Building Research, *Technical Paper No. 23*, Melbourne, Australia.

Wray, W. K. (1978). "Development of a Design Procedure for Residential and Light Commercial Slabs-on-Ground Constructed over Expansive Soils," Ph.D. Dissertation, Department of Civil Engineering, Texas A&M University, College Station, TX.

Wray, W. K. (1989). "Mitigation of Damage to Structures Supported on Expansive Soils," *National Science Foundation Report*, Washington, DC.

Zienkiewicz, O. C. (1971). *The Finite Element Method in Engineering Science*, 2nd Edition, McGraw-Hill Book Company, London, England.

APPENDIX A
THERMODYNAMIC VIEWPOINT OF THE SOIL SUCTION CONCEPT

A.1 Introduction

The soil, water, and air mixture is a dynamic and, chemically, a very complex system whose composition reflects the many reactions that can proceed simultaneously between the soil solid, water, and air. The net result of these reactions may be considered as complex chemical interactions affected by changes, mainly, in the amount of water and air, and energy from the environment. It is to this very complicated system that chemical thermodynamics must be applied (Sposito 1981).

Study of thermodynamics of water in soil has been performed since the 1900's in the field of soil science. Schofield (1935) proposed the concept of pF, the logarithm of the specific Gibbs free energy, and established the energy concept of water in soil. From the point of view of thermodynamics, a soil is an assembly of solid, liquid, and gaseous, and gravitational and energy fields. These characteristics define the thermodynamic soil system. If chemical reactions are not of principal concern and if the chemical composition of each phase in the soil need not be known in detail, then the stresses in the pore water can be described by relatively simple thermodynamic relationships (Edlefsen and Anderson 1943). From this perspective, it is assumed that the three components of the soil system do not react chemically and do not segregate at any time, and thus the soil is a homogeneous mixture. This point of view is taken normally in soil physics.

A.2 Free Energy of Soil Water

Since thermodynamics deals with energy and its transformation, the most useful thermodynamic function, as far as the soil moisture is concerned, is free energy (Edlefsen and Anderson 1943). The free energy of soil moisture depends on the adsorptive force field that surrounds a soil particle, the hydrostatic pressure on the soil moisture, the dissolved material present, and the temperature. The free energy of soil moisture will decrease with the presence of a force field that surrounds clay soils and with the presence of dissolved salts in the soil water.

The free energy change of a system can be described simply by a body of free water in contact with an unsaturated soil and water flows from a body of free water (whose absolute specific free energy is f_1) into an unsaturated soil (whose absolute specific free energy is f_2). It is customary to use free, pure water under a pressure of 1 atmosphere as the zero point or datum for the free energy of soil moisture. The absolute free energy f_2 of the unsaturated soil moisture is less than that of free, pure water. Therefore, the free energy Δf of soil moisture in all unsaturated soils is negative with respect to the commonly accepted datum. The absolute free energy of the moisture in a comparatively dry soil is less than the absolute free energy of that in a wet soil. The free energy of the moisture is therefore always more negative in a drier soil than in a wetter soil. If two phases of a system are in equilibrium with each other and are at the same temperature and under the same pressure, then both phases must posses the same absolute specific free energy. T typical units of the free energy are in gm-cm/gm or simply cm and pF.

The energy status of water in soil with respect to that of free and pure water has been expressed with the use of Gibb's free energy concept as defined by Edlefsen and Anderson (1943) by

$$f = -e + Pv - Ts = h - Ts \tag{A1}$$

where e is the internal energy of the system, P is the pressure, v is the specific volume, T is the absolute temperature, s is the entropy, and h is the heat content (enthalpy).

The term entropy, s, which is used to describe and deal with energy changes associated primarily with the transformations of heat into other forms of energy in the field of thermodynamics, is an important parameter in the free energy description of soil moisture and is given by the following relationship

$$\Delta s = s_B - s_A = \int_A^B \frac{1}{T} dq \tag{A2}$$

where A and B describes the two different states of the system. However, the free energy concept combines all the criteria and characteristics of entropy in the study of the thermodynamics of soil moisture.

If Eq. A1 is differentiated the following relationship is obtained

$$df = -de + vdP + Pdv - sdT - Tds \tag{A3}$$

If the total work done by the system is represented by

$$dw = de + Tds = Pdv + dw_m \tag{A4}$$

where dw_m is the mechanical work. Then, Eq. A3 becomes

$$df = -sdT + vdP - dw_m \tag{A5}$$

For isothermal conditions ($T = 0$)

$$df = vdP - dw_m \tag{A6}$$

and for constant pressure,

$$df = - dw_m \tag{A7}$$

which indicates that the decrease in the free energy of a system is equal to the work done by the system, excluding the work done during expansion against constant pressure (Edlefsen and Anderson 1943). As soil becomes more unsaturated, the work done on the soil to remove the pore water causes the free energy to decrease. Therefore, the free energy of the pore water will be less than zero, if the free energy of the pore water is taken as the zero reference level.

If the mechanical work is taken as zero, then Eq. A6 becomes

$$\Delta f = \int_{P_1}^{P_2} v dP = f_{P_2} - f_{P_1} \tag{A8}$$

For gases (where $Pv = RT$),

$$\Delta f = \int_{P_1}^{P_2} \frac{RT}{P} dP = RT \ln \frac{P_2}{P_1} \tag{A9}$$

Equation A9 can be used to determine the free energy of the soil water relative to that of free and pure water by comparing the vapor pressure of water in equilibrium with the soil to pure water.

$$\Delta f = \int_{p_o}^{P} \frac{RT}{P} dP = RT \ln \frac{P}{P_o} \tag{A10}$$

where P is the vapor pressure of soil water, P_o is the vapor pressure of free and pure water, and P/P_o is the relative vapor pressure (or relative humidity) above the soil water surface.

The separate effects of a number of variables including temperature, pressure, concentration of solutes in pore water, and water content on the partial free energy of soil water can be investigated. However, the measurement of P/P_o provides direct results accounting for the effects of all the variables involved (Edlefsen and Anderson 1943). When expressed with reference to a unit volume of water, Eq. A10 assumes the units of pressure

$$h_t = \frac{RT}{V_w} \ln \frac{P}{P_o} \tag{A11}$$

where h_t is the total suction (cm or pF) and V_w is the molar volume of water (m^3/kmol).

APPENDIX B
SOIL SUCTION MEASUREMENT WITH THE FILTER PAPER METHOD

B.1 Calibration for the Suction Wetting Curve

The calibration for the suction wetting curve for filter paper using salt solutions is based upon the thermodynamic relationship between total suction (or osmotic suction) and the relative humidity resulting from a specific concentration of a salt in distilled water. The thermodynamic relationship between total suction and relative humidity is given in Eq. 3.2 of Chapter 3. In this study, NaCl was selected as an osmotic suction source for the filter paper calibration. Salt concentrations from 0 (distilled water) to 2.7 molality were prepared and filter papers were simply placed above salt solutions (in a non-contact manner) in sealed containers. The calibration test configuration adopted for this research is shown in Fig. B1.

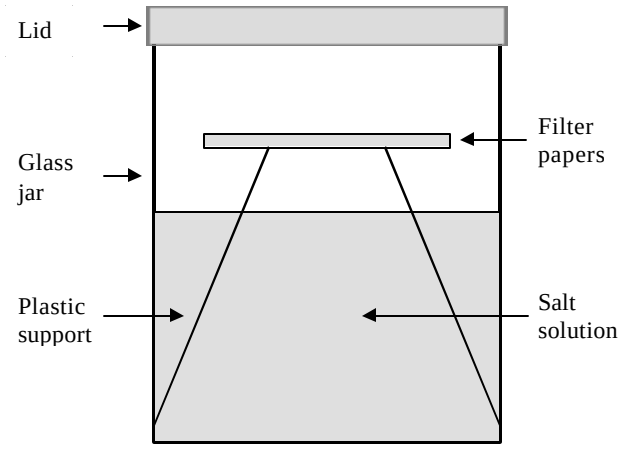

Fig. B1. Total Suction Calibration Test Configuration.

The filter paper and salt solution setups in the sealed containers were put in a constant temperature environment for equilibrium. Temperature fluctuations were kept as low as possible during a two week equilibration period. A water bath was employed for this purpose, in which temperature fluctuations did not exceed $\pm$ 0.1^{o}C.

Before commencing the filter paper calibration experiments and the soil suction measurements, all the items related to filter paper testing were cleaned carefully. Latex gloves and tweezers were used to handle the materials in nearly all steps of the experiment. The filter papers and aluminum cans for water content measurements were never touched with bare hands because oily hands may cause the filter papers to absorb more water. In addition, it is suggested that the filter paper water content measurements are performed by two persons in order to reduce the time during which the filter papers are exposed to the laboratory atmosphere and, thus, the amount of moisture lost or gained during measurements is kept to a minimum.

B.1.1 Experimental Procedure for Wetting Curve Calibration

The procedure that was adopted for the experiment is as follows:

1. NaCl solutions were prepared from 0 (i.e., distilled water) to 2.7 molality (i.e., the number of moles of NaCl in mass in 1000 ml of distilled water).
2. A 250 ml glass jar was filled with approximately 150 ml of a solution of known molality of NaCl. Then, a small plastic cup was inserted into the glass jar to function as a support for filter papers. Two filter papers were put on the plastic cup one on top of the other. The glass jar lid was sealed tightly with plastic tapes to ensure air tightness. The configuration of the setup is depicted in Fig. B1.
3. Step 2 was repeated for each different NaCl concentration.

The glass jars were inserted into large plastic containers and the containers were sealed with water proof tape. Then, the containers were put into sealed plastic bags for extra protection. After that, the containers were inserted into the water bath for an equilibration period. After two weeks of equilibrating time, the procedure for the filter paper water content measurements was as follows:

1. Before taking the plastic containers from the water bath, all aluminum cans were weighed to the nearest 0.0001 g accuracy and recorded on a filter paper water content measurement data sheet, similar to the one provided in ASTM D 5298.
2. After that, all measurements were carried out by two persons. For instance, while one person was opening the sealed glass jar, the other person was transferring the filter paper, using tweezers, into the aluminum can very quickly (i.e., in a few seconds, usually less than 5 seconds). The lid was placed on each aluminum can immediately.
3. Then, the weights of each can with filter papers inside were very quickly measured to the nearest 0.0001 g.
4. Steps 2 and 3 were followed for every glass jar. Then, all the cans were put into the oven with the lids half-open to allow evaporation. All filter papers were kept at 105 $\pm$ 5^{o}C temperature for 24 hours inside the oven. This is the standard test method for soil water content measurements. However, it is only necessary to keep the filter paper in the oven for at least 10 hours.
5. Before taking measurements, the cans were closed with their lids and allowed to equilibrate in the oven for about 5 minutes. Then, a can was removed from the oven and put on an aluminum block for about 20 seconds to cool down; the aluminum block acted as a heat sink and expedited the cooling of the can. This is to eliminate temperature fluctuations and air currents in the enclosed weighing scale. After that, the can with dry filter paper inside was weighed to the nearest 0.0001 g very quickly. The dry filter paper was taken out of the can and the cooled can was also weighed very quickly.
6. Step 5 was repeated for every can.

B.1.2 Wetting Calibration Curve

A wetting curve was constructed from the filter paper test results by following the procedure described above. The curve obtained for Schleicher & Schuell No. 589-WH filter papers using sodium chloride salt solutions is depicted in Fig. B2. Figure B2 clearly shows the sensitivity of total suction to very small changes in filter paper water content values when the relative humidity approaches 100%, as expected from the nature of Kelvin's equation (i.e., total suction is equal to zero when relative humidity is 100 percent, fully saturated condition). From the figure, it is seen that total suction decreases dramatically when relative humidity approaches 100 percent.

B.2 Calibration for the Suction Drying Curve

Pressure plate and pressure membrane devices were employed in the drying filter paper calibration. A schematic drawing of a pressure plate or pressure membrane apparatus is depicted in Fig. B3. For the drying suction calibration of the filter paper, a contact path is provided between the filter paper and the measuring device so as to eliminate the osmotic suction component of total suction. In other words, if transfer of the soil water is allowed only through fluid flow, dissolved salts will move with the soil water, and the measuring device will not detect the osmotic suction component.

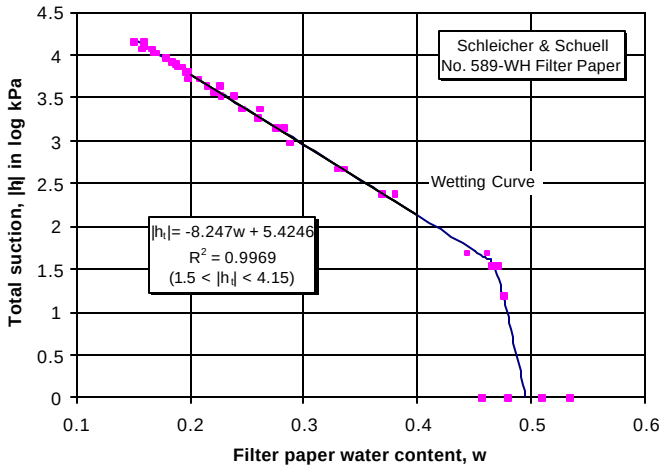

Fig. B2. Filter Paper Wetting Calibration Curve.

Pressure plate and pressure membrane devices operate by imposing a suction value (i.e., applied air pressure minus water pressure at atmospheric condition) on a given specimen which can be a soil or filter paper. The filter paper is put into the suction measuring device in a manner that ensures good contact with the porous plate or cellulose membrane. In this process, the main concern is to make sure that an intimate contact is provided between the water inside the filter paper and the water inside the porous disk so that transfer of the water is allowed only through continuous water films. To investigate the degree of contact between the filter paper and porous disk, the testing procedure and setup as depicted in Fig. B3 were undertaken in this study. Three different soils (i.e., a fine clay, sandy silt, and pure sand) were used in the calibration process of filter papers in order to investigate the role of soils in establishing a good contact between the filter paper and porous disk.

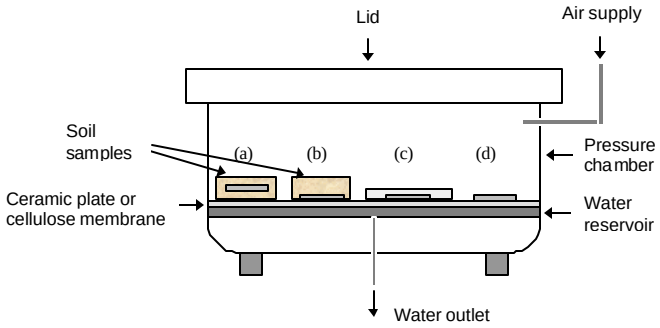

(a) One filter paper between two larger size protective filter papers embedded into the soil sample.
(b) One filter paper makes contact with the porous plate or membrane and covered on top with a larger size protective filter paper in the soil sample.
(c) One filter paper makes contact with the porous plate or membrane and covered on top with two larger size protective filter papers.
(d) One filter paper on the porous plate or membrane.

Fig. B3. Schematic Drawing of a Pressure Plate Device.

B.2.1 Experimental Procedure for Drying Curve Calibration

The procedure that was adopted for the experiment is as follows:

1. Prior to each test, the porous disk or membrane and the soils were saturated with distilled water at least one day in advance, so that all the pores were fully saturated with water.
2. The testing configuration as in Fig. B3 was established using one of the soils (i.e., fine clay or sandy silt or pure sand). Figure B3 explains how the filter papers, soil, and protective papers were arranged in the experiment. The soil specimens with the filter papers were placed on the saturated disks and the level of distilled water on the plate was raised enough to cover all of the filter papers. All of the air bubbles were eliminated during placement of the filter paper, soil, and protective paper arrangement on the ceramic disk by carefully pressing the bubbles out to the edges of each.
3. After the pressure chamber was tightened, with the influence of the applied air pressure the water inside the soil specimen and filter papers were forced out through the porous plate or membrane and collected in a graduated cylinder until a suction equilibrium between the soil and filter papers and the applied air pressure was established.

An equilibration period between 3 and 5 days is commonly suggested for matric suction measurements using pressure plates and membranes (ASTM D 5298; Houston et al. 1994; Lee 1991). The equilibrating periods used for this study varied between 3, 5, and 7 days depending on the testing set up. For instance, when filter papers were embedded in the soil, equilibrating periods were 7 days for the fine clay and 5 days for the sandy silt set up, but the equilibrating period was 3 days when filter papers embedded in the pure sand or when only filter papers were used. However, all the three soils were also tested with filter

papers inside in the same pressure chamber to check the differences between the filter paper water contents. To obtain the filter paper water contents, the same procedure described in the Wetting Curve Calibration Procedure was followed.

B.2.2 Drying Calibration Curve

A drying curve was established from the filter paper test results by following the procedure described above. The curve obtained for Schleicher & Schuell No. 589-WH filter papers using both pressure plate and pressure membrane devices is depicted in Fig. B4. Each data point on Fig. B4 is an average of at least three tests and each test data is an average of at least four filter papers. The standard errors for the straight line and curved portions of the drying curve are 0.135 and 0.116 log kPa units, respectively. The standard error for the straight line portion of the wetting curve is 0.044 log kPa. With the pressure membrane the highest matric suction obtained was 4,570 kPa and suctions below 150 kPa were obtained using the pressure plate apparatus. The corresponding wetting calibration curve is also shown in Fig. B4. It plots below the drying suction curve, as is expected of the hysteresis process.

Very high filter paper water contents were obtained when all the three soils were used as in the set up (a) as shown in Fig. B3. However, the filter paper water contents were all comparable as obtained from the set ups (b), (c), and (d) as in Fig. B3. The results from (b) were slightly wetter than (c) and the results from (d) were slightly drier than (c). In obtaining the calibration curve, the filter papers from the set up arrangements (b), (c), and (d) were used.

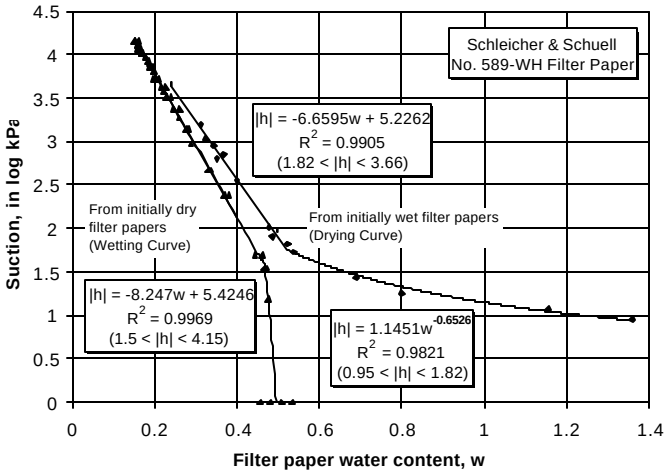

Fig. B4. Drying and Wetting Calibration Curves.

B.3 Soil Total Suction Measurements

Glass jars that are between 250 to 500 ml volume size are readily available in the market and can be easily adopted for suction measurements. Glass jars, especially, with 3.5 to 4 inch (8.89 to 10.16 cm) diameter can contain the 3 inch (7.62 cm) diameter Shelby tube samples very nicely. A testing procedure for total suction measurements using filter papers can be outlined as follows:

B.3.1 Experimental Procedure

1. At least 75 percent by volume of a glass jar is filled up with the soil; the smaller the empty space remaining in the glass jar, the smaller the time period that the filter paper and the soil system requires to come to equilibrium.
2. A ring type support, which has a diameter smaller than filter paper diameter and about 1 to 2 cm in height, is put on top of the soil to provide a non-contact system between the filter paper and the soil. Care must be taken when selecting the support material; materials that can corrode should be avoided, plastic or glass type materials are much better for this job.
3. Two filter papers one on top of the other are inserted on the ring using tweezers. The filter papers should not touch the soil, the inside wall of the jar, and underneath the lid in any way.
4. Then, the glass jar lid is sealed very tightly with plastic tape.
5. Steps 1, 2, 3, and 4 are repeated for every soil sample.
6. After that, the glass jars are put into the ice-chests in a controlled temperature room for equilibrium.

Researchers suggest a minimum equilibrating period of one week (ASTM D5298; Houston et al. 1994; Lee 1991). After the equilibration time, the procedure for the filter paper water content measurements can be as follows:

1. Before removing the glass jar containers from the temperature room, all aluminum cans that are used for moisture content measurements are weighed to the nearest 0.0001 g accuracy and recorded.
2. After that, all measurements are carried out by two persons. For example, while one person is opening the sealed glass jar, the other is putting the filter paper into the aluminum can very quickly (i.e., in a few seconds) using tweezers.
3. Then, the weights of each can with wet filter paper inside are taken very quickly.
4. Steps 2 and 3 are followed for every glass jar. Then, all cans are put into the oven with the lids half-open to allow evaporation. All filter papers are kept at 105 ± 5^{o}C temperature inside the oven for at least 10 hours.
5. Before taking measurements on the dried filter papers, the cans are closed with their lids and allowed to equilibrate for about 5 minutes. Then, a can is removed from the oven and put on an aluminum block (i.e., heat sinker) for about 20 seconds to cool down; the aluminum block functions as a heat sink and expedites the cooling of the can. After that, the can with the dry filter paper inside is weighed very quickly. The dry filter paper is taken from the can and the cooled can is weighed again in a few seconds.
6. Step 5 is repeated for every can.

After obtaining all of the filter paper water contents an appropriate calibration curve, such as the one in Fig. B4, is employed to get total suction values of the soil samples.

B.4 Soil Matric Suction Measurements

Soil matric suction measurements are similar to the total suction measurements except instead of inserting filter papers in a non-contact manner with the soil for total suction testing, a good intimate contact should be provided between

the filter paper and the soil for matric suction measurements. Both matric and total suction measurements can be performed on the same soil sample in a glass jar as shown in Fig. B5. A testing procedure for matric suction measurements using filter papers can be outlined as follows:

B.4.1 Experimental Procedure

1. A filter paper is sandwiched between two larger size protective filter papers. The filter papers used in suction measurements are 5.5 cm in diameter, so either a filter paper is cut to a smaller diameter and sandwiched between two 5.5 cm papers or bigger diameter (bigger than 5.5 cm) filter papers are used as protectives.
2. Then, these sandwiched filter papers are inserted into the soil sample in a very good contact manner (i.e., as in Fig. B5). An intimate contact between the filter paper and the soil is very important.
3. After that, the soil sample with embedded filter papers is put into the glass jar container. The glass container is sealed up very tightly with plastic tape.
4. Steps 1, 2, and 3 are repeated for every soil sample.
5. The prepared containers are put into ice-chests in a controlled temperature room for equilibrium.

Researchers suggest an equilibration period of 3 to 5 days for matric suction testing (ASTM D 5298; Houston et al. 1994; Lee 1991). However, if both matric and total suction measurements are performed on the same sample in the glass jar, then the final equilibrating time will be at least 7 days of total suction equilibrating period. The procedure for the filter paper water content measurements at the end of the equilibration is exactly same as the one outlined for the total suction water content measurements. After obtaining all the filter paper water contents the appropriate calibration curve may be employed to get the matric suction values of the soil samples.

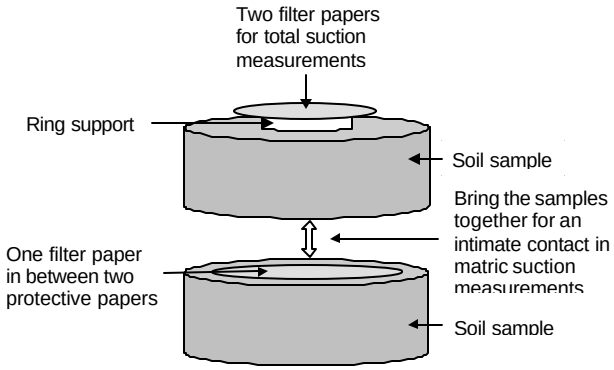

Fig. B5. Total and Matric Suction Measurements.

APPENDIX C
PROGRAM RSLAB^N INPUT DATA FORMAT

C.1 Input Data

All the variables described below, except TITLE, are in accordance with the FORTRAN language integer and real number specifications. In other words, all the variables starting with I, J, K, L, M, and N are integer numbers and all others are real numbers. The input data to the program can be outlined as follows:

- Data Card 1:
  TITLE
- Data Card 2:
  KASE, NORTP, NPRINT, NEM, NNM
- Data Card 3: SKIP the card if KASE ≠ 1.
  MAXIT, MULT
- Data Card 4: SKIP the card if KASE ≠ 2.
  MAXIT
- Data Card 5:
  MATLAB
  (If MATLAB = 0, go to the card # 7)
- Data Card 6: If MATLAB ≠ 0.
  NCOLN, NROWN
  MATNNX(I) (I=1, NCOLN)
  MATNNY(I) (I=1, NROWN)
  MATENX(I) (I=1, NCOLE)
  MATENY(I) (I=1, NROWE)
- Data Card 7:
  DO I=1, K1
  M, GLXY(M,1), GLXY(M,2)
  ENDDO
- Data Card 8:
  DO I=1, K2
  N, (NOD(N,I), I=1,NPE)
  ENDDO
- Data Card 9:
  NBEAMS
- Data Card 10: SKIP the card if NBEAMS = 0.
  DO I=1, NBEAMS
  MFIRST, MLAST, INCR, THK
  ENDDO
- Data Card 11:
  NLOADS
- Data Card 12: SKIP the card if NLOADS = 0.
  DO I=1, NLOADS
  LFIRST, LLAST, LINC, PLODS
  ENDDO
- Data Card 13:
  NTEL
- Data Card 14: SKIP the card if NTEL = 0.
  DO I=1, NTEL
  NT, UPRES(NT)
  ENDDO
- Data Card 15: SKIP the card if KASE ≠ 1.
  MDISP
  MLINE(I) (I=1, MDISP)
  VEXP(I) (I=1, MDISP)
  DO I=1, MLINE(I)
  MFIRST, MLAST, MINC
  ENDDO
  NINLDS
  (If NINLDS = 0, go to the Card # 16)
  DO I=1, NINLDS
  L, VIDS(L)
  ENDDO
- Data Card 16: SKIP the card if KASE ≠ 2.
  NDISP
  NLINE(I) (I=1, NDISP)
  VSHR(I) (I=1, NDISP)
  DO I=1, NLINE(I)
  NFIRST, NLAST, NINC
  ENDDO
  MINLDS
  (If MINLDS = 0, go to the Card # 17)
  DO I=1, MINLDS
  K, VIDS(K)
  ENDDO
- Data Card 17: SKIP the card if NORTP ≠ 1.
  E1, E2, ANU12, G12, G13, G23
- Data Card 18: SKIP the card if NORTP = 1.
  E, ANU
- Data Card 19:
  YMS, PRS
- Data Card 20:
  KCOHES
- Data Card 21: SKIP the card if KCOHES = 0.
  COHESN
- Data Card 22:
  UWRC, DSLOAD, STHIK

The input variables to the program, as explained above in a systematic order, have the following meanings:

TITLE: Title of the problem being solved (maximum 80 characters).

KASE: An indicator for the type of the problem being analyzed. KASE = 0 – Compressible soil, KASE = 1 – Swelling soil (Edge Lift Case), and KASE = 2 – Shrinking soil (Center Lift Case).

NORTP: An indicator for the orthotropic plate analyzes option. NORTP = 1 – Orthotropic plate analysis and NORTP ≠ 1 – Isotropic plate analysis.

NPRINT: An indicator for printing certain output. NPRINT = 0 – Not to print the element matrices and vectors, first element dimension, soil element flexibility and stiffness matrices, total element stiffness matrix, global matrices,

boundary condition information, number of integration points. NPRINT = 1 – Not to print the information in the NPRINT = 0 case except the soil element flexibility and stiffness matrices and total element stiffness matrix. The NPRINT = 0 or 1 will, however, print the basic solution output such as the element coordinates, material properties, displacement and stress results.

NEM: Number of the elements in the mesh.

NNM: Number of nodes in the mesh.

MAXIT: Maximum number of iterations allowed for the convergence in both KASE = 1 and 2.

MULT: A multiplication factor to increase the density of reinforced concrete at the beginning of the iterations to establish a smooth convergence for KASE = 1 problems. The increased density will reduce to its real value at the end of convergence. If a zero value is assigned to MULT (i.e., MULT = 0), then this option will be skipped.

MATLAB: This is an indicator to obtain such output files that are suitable for postprocessing using the commercially available MATLAB software. To assign a zero value to MATLAB will eliminate this option.

NCOLN: Number of columns of nodes in the finite element mesh (see Fig. C1).

NROWN: Number of rows of nodes in the finite element mesh.

MATNNX(I) (I=1, NCOLN): The array which stores the nodal numbers along a row in the x-direction.

MATNNY(I) (I=1, NROWN): The array which stores the nodal numbers along a column in the y-direction.

NCOLE = NCOLN – 1

NROWE = NROWN – 1

MATENX(I) (I=1, NCOLE): The array which stores the element numbers along a row in the x-direction.

MATENY(I) (I=1, NROWE): The array which stores the element numbers along a column in the y-direction.

GLXY(M,1): The global x-coordinate of the node M.

GLXY(M,2): The global y-coordinate of the node M. If the distances between the nodes along a straight line are equal and the nodes are consecutively numbered in an increasing order, then the coordinates of the middle nodes can automatically be generated just by entering the coordinates for the first and the last node on that line.

NOD(N,I) (I=1,NPE): The element connectivity for the Nth element. NPE is the number of nodes per element, which is always 4 (NPE = 4) in this program. The element connectivity information should be provided in a counter-clockwise direction starting from the lower left corner node for each element. It is suggested that the nodes and elements on a mesh be numbered as shown in Fig. C1. If the elements are consecutively numbered in an increasing order on a straight line, then the element connectivity arrays of the middle elements can automatically be generated just by entering the element connectivity information for the first and the last element on that line.

NBEAMS: Number of stiffening beams both in x- and y-directions on different uniformly numbered elements. In other words, although only one beam lies on the elements 1, 5, 9, 13, 23, 33, and 43 (Fig. C1), it is considered as two beams for the input data so that a systematic creation of the inter-elements can be achived. For instance, for the beam mentioned above, the increment between the elements 1, 5, 9, and 13 is the same which is 4, and the increment between the elements 13, 23, 33, and 43 is the same which is 10. Therefore, when assigned such a beam it is necessary to input the first element number, the last element number, and the increment between the elements. Then, one should provide the following information for the mentioned beam as follows:

1, 13, 4
13, 43, 10

on two different lines.

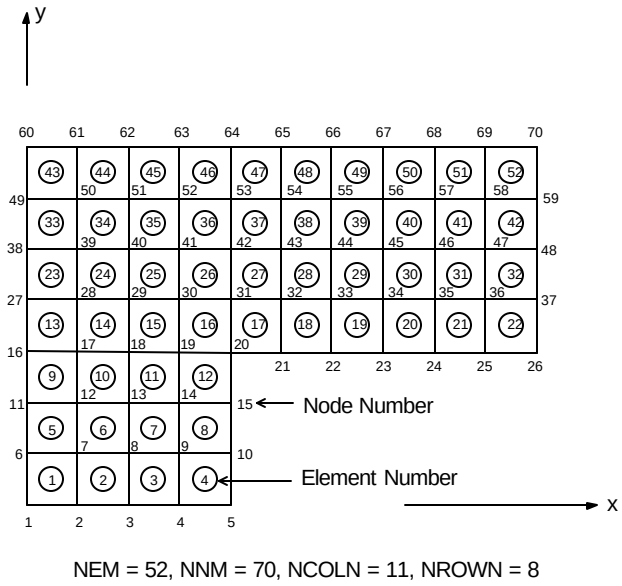

Fig. C1 A Typical Finite Element Mesh.

MFIRST: The first element number for the beam information.

MLAST: The last element number for the beam information.

INCR: The increment between the elements on the same line.

THK: Thickness of the beam (without considering the thickness of the slab).

NLOADS: Number of uniformly distributed pressures both in x- and y-directions on different uniformly numbered elements lie on a straight line (line-elements). The numbering system of the elements on which the pressures are applied is exactly the same as in the case for the beams as described in NBEAMS section above.

LFIRST: The first element number on which the pressure is applied.

LLAST: The last element number on which the pressure is applied.

LINC: The increment between the elements on the same line.

PLODS: The amount of the pressure being applied.

NTEL: The total number of individual pressures being applied on different individual elements.

UPRES(NT): The amount of pressure being applied on element number NT.

MDISP: Number of different displacements (y_m values from VOLFLO) for the edge lift case (KASE = 1).

MLINE(I) (I=1, MDISP): Number of lines, which connect the nodal points, having the same displacement values and the same increment values. For instance, the line that connects the nodal points 1, 6, 11, 16, 27, 38, 49, and 60 (Fig. C1) is considered to be two lines of having different increments. This part has the same logic of automatic creation of the nodal points or element numbers as mentioned under sections NBEAMS and NLOADS. For the line mentioned above, the increment between the nodal points 1, 6, 11, and 16 is the same and is 5, and the increment between the points 16, 27, 38, and 49 is the same and is 11. Therefore, when such a line is assigned it is only necessary to input the first nodal number, the last nodal number, and the increment between the points. Then, one should provide the following information for the line as follows:

1, 16, 5
16, 49, 11

VEXP(I) (I=1, MDISP): The vertical displacement value, which is a positive number, corresponding to the Ith line created in section MLINE.

MFIRST: The first nodal point corresponding to the Ith line of section MLINE.

MLAST: The last nodal point corresponding to the Ith line of section MLINE.

MINC: The increment between two consecutive nodal points corresponding to the Ith line of section MLINE.

NINLDS: Total number of nodal points considered for individual displacement locations (nodal points). This is to input displacements, as obtained from VOLFLO, at some particular nodal points within e_m (edge moisture variation distance) distance.

VIDS(I): The vertical displacement value (KASE = 1) at Ith node. It is a positive number.

NDISP: Number of different displacements (y_m values from VOLFLO) for the center lift case (KASE = 2).

NLINE(I) (I=1, NDISP): Number of lines, which connect the nodal points, having the same displacement values and the same increment values. For instance, the line that connects the nodal points 1, 6, 11, 16, 27, 38, 49, and 60 (Fig. C1) is considered to be two lines of having different increments. This part has the same logic of automatic creation of the nodal displacement values of section MLINE. For the line mentioned above, the increment between the nodal points 1, 6, 11, and 16 is the same and is 5, and the increment between the points 16, 27, 38, and 49 is the same and is 11. Therefore, when such a line is assigned it is only necessary to input the first nodal number, the last nodal number, and the increment between the points. Then, one should provide the following information for the line as follows:

1, 16, 5
16, 49, 11

VSHR(I) (I=1, NDISP): The vertical displacement value, which is a positive number, corresponding to the Ith line created in section NLINE.

NFIRST: The first nodal point corresponding to the Ith line of section NLINE.

NLAST: The last nodal point corresponding to the Ith line of section NLINE.

NINC: The increment between two consecutive nodal points corresponding to the Ith line of section NLINE.

MINLDS: Total number of nodal points considered for individual displacement locations (nodal points). This is to input displacements, as obtained from VOLFLO, at some particular nodal points within e_m (edge moisture variation distance) distance.

VIDS(I): The vertical displacement value (KASE = 2) at Ith node. It is a positive number.

E1: Young's moduli of the reinforced concrete slab in the global x-direction (orthotropic plate analysis).

E2: Young's moduli of the reinforced concrete slab in the global y-direction (orthotropic plate analysis).

ANU12: Poisson's ratio for the reinforced concrete in the x-y plane (orthotropic plate analysis).

G12: Shear modulus for the reinforced concrete slab in x-y plane (orthotropic plate analysis).

G13: Shear modulus for the reinforced concrete slab in x-z plane (orthotropic plate analysis).

G23: Shear modulus for the reinforced concrete slab in y-z plane (orthotropic plate analysis).

E: Elastic modulus for the isotropic reinforced concrete slab.

ANU: Poisson's ratio for the isotropic reinforced concrete slab.

YMS: Elastic modulus for the foundation soil.

PRS: Poisson's ratio for the foundation soil.

KCOHES: An indicator for computing the downdrag force applied on the faces of the stiffening beams by the cohesive soil. KCOHES ≠ 0 indicates the option for considering the pressure applied on the beams by the soil.

COHES: Cohesive shear strength of the soil.

UWRC: Unit weight of the reinforced concrete slab.

DSLOAD: Uniformly distributed load all over the slab.

STHIK: Thickness of the slab.

C.2 Input File

An example problem, Center Lift Case.

```
    TITLE
 2, 0, 0, 52, 70              KASE, NORTP, NPRINT, NEM, NNM
10                                    MAXIT
1                                     MATLAB
11, 8                               NCOLN, NROWN
16,17,18,19,20,21,22,23,24,25,26      MATNNX(I) (I=1, NCOLN)
1,6,11,16,27,38,49,60                 MATNNY(I) (I=1, NROWN)
13,14,15,16,17,18,19,20,21,22         MATENX(I) (I=1, NCOLE)
1,5,9,13,23,33,43                     MATENY(I) (I=1, NROWE)
1,   0.0,   0.0                 M, GLXY(M,1), GLXY(M,2)
5,   4.0,   0.0
6,   0.0,  1.0
10, 4.0,  1.0
11, 0.0,  2.0
15, 4.0,  2.0
16, 0.0,  3.0
26,  10.0,  3.0
27,    0.0,  4.0
37,  10.0,  4.0
38,    0.0,  5.0
48,  10.0,  5.0
49,    0.0,  6.0
59,  10.0,  6.0
60,   0.0,   7.0
70,  10.0,  7.0
1,    1,   2,   7,   6            N, (NOD(N,I), I=1,4)
```

```
4,    4,   5, 10,   9
5,    6,   7, 12, 11
8,    9, 10, 15, 14
9,   11, 12, 17, 16
12, 14, 15, 20, 19
13, 16, 17, 28, 27
22, 25, 26, 37, 36
23, 27, 28, 39, 38
32, 36, 37, 48, 47
33, 38, 39, 50, 49
42, 47, 48, 59, 58
43, 49, 50, 61, 60
52, 58, 59, 70, 69
7                                   NBEAMS
1,    4,    1,  0.5                 MFIRST, MLAST, INCR, THK
16, 22,   1, 0.5
43, 52,   1, 0.5
1,    9,   4, 0.5
13, 33, 10, 0.5
4,   12,   4, 0.5
32, 42, 10, 0.5
7                                   NLOADS
1,    4,    1,  100.0               LFIRST, LLAST, LINC, PLOADS
16, 22,   1,  100.0
43, 52,   1,  100.0
1,    9,   4,  100.0
13, 33, 10,  100.0
4,   12,   4,  100.0
32, 42, 10,  100.0
4                                   NTEL
6,   50.0                           NT, UPRES(NT)
34, 75.0
41, 85.0
27, 100.0
2                                   NDISP
7    3                              NLINE(I) (I=1,NDISP)
0.15   0.10                        VSHR(I)  (I=1,NDISP)
1,    5,  1                         NFIRST, NLAST, NINC
20, 16,  1
60, 70,  1
1,   16,  5
27, 49, 11
10, 15,  5
37, 59, 11
7,   17,  5
28, 50, 11
51, 58,  1
1                                   MINLDS
30,  0.12                           K, VIDS(K)
2.16E8,  0.25                       E, ANU
1.44E5,  0.40                       YMS, PRS
0                                   KCOHES
150.0,  25.0,  0.20                 UWRC, DSLOAD, STHIK
```

APPENDIX D
EXAMPLE ONE DISPLACEMENT AND STRESS PLOTS

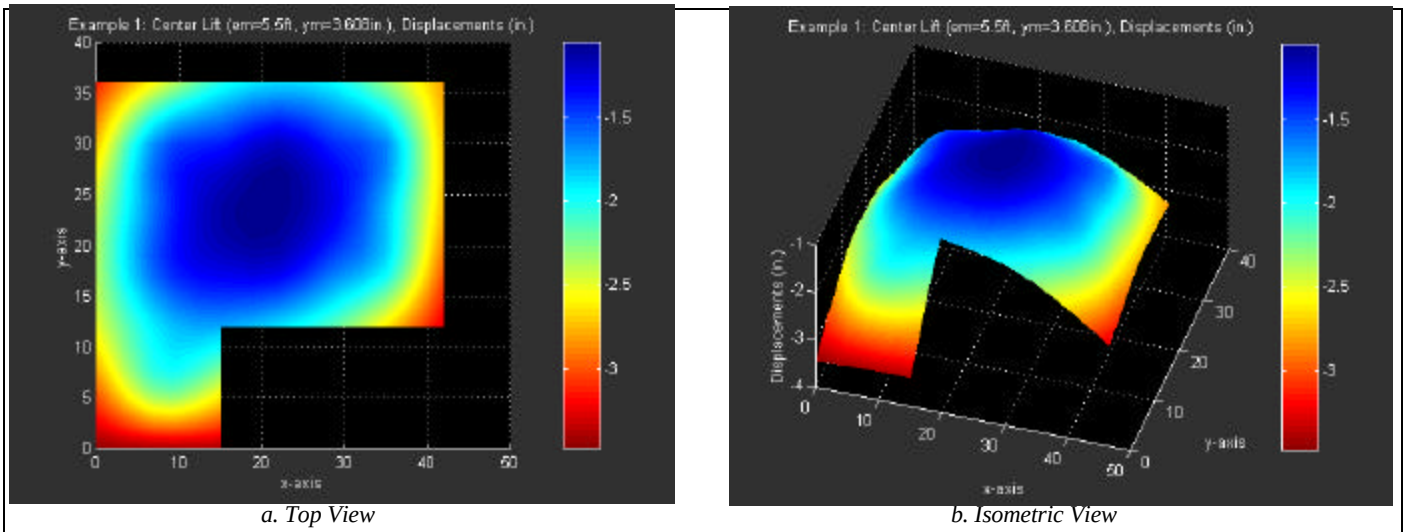

a. Top View *b. Isometric View*

Fig. D1. Example One Center Lift Case, Ribbed Slab, Displacements.

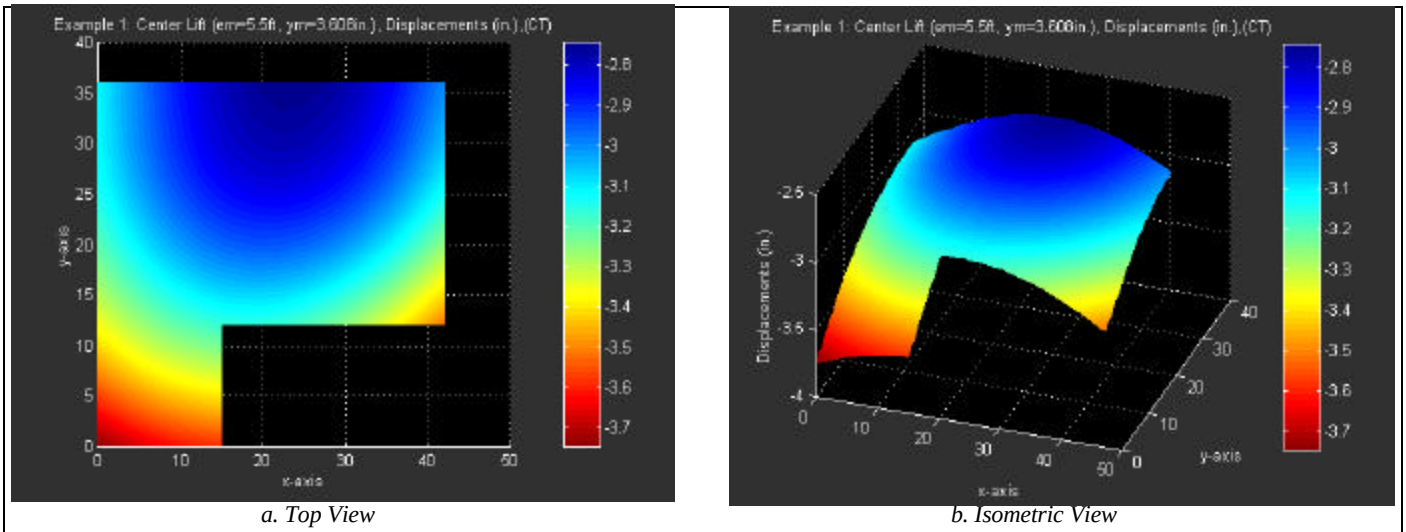

a. Top View *b. Isometric View*

Fig. D2. Example One Center Lift Case, Flat Slab, Displacements.

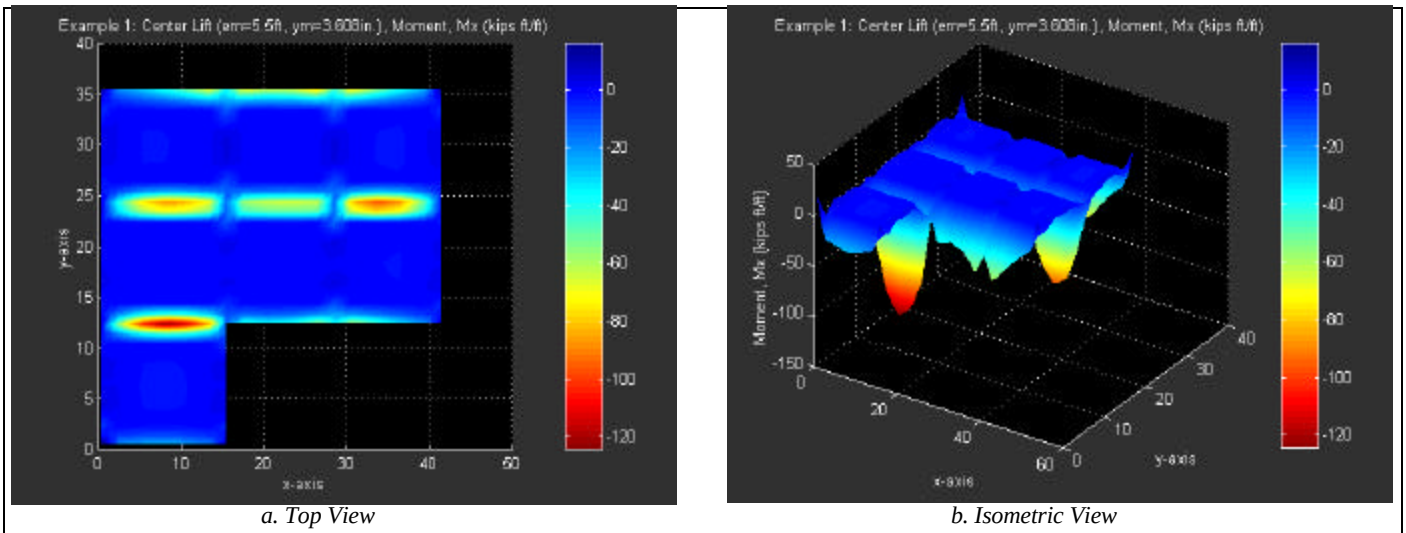

a. Top View *b. Isometric View*

Fig. D3. Example One Center Lift Case, Ribbed Slab, Moment in x-Direction.

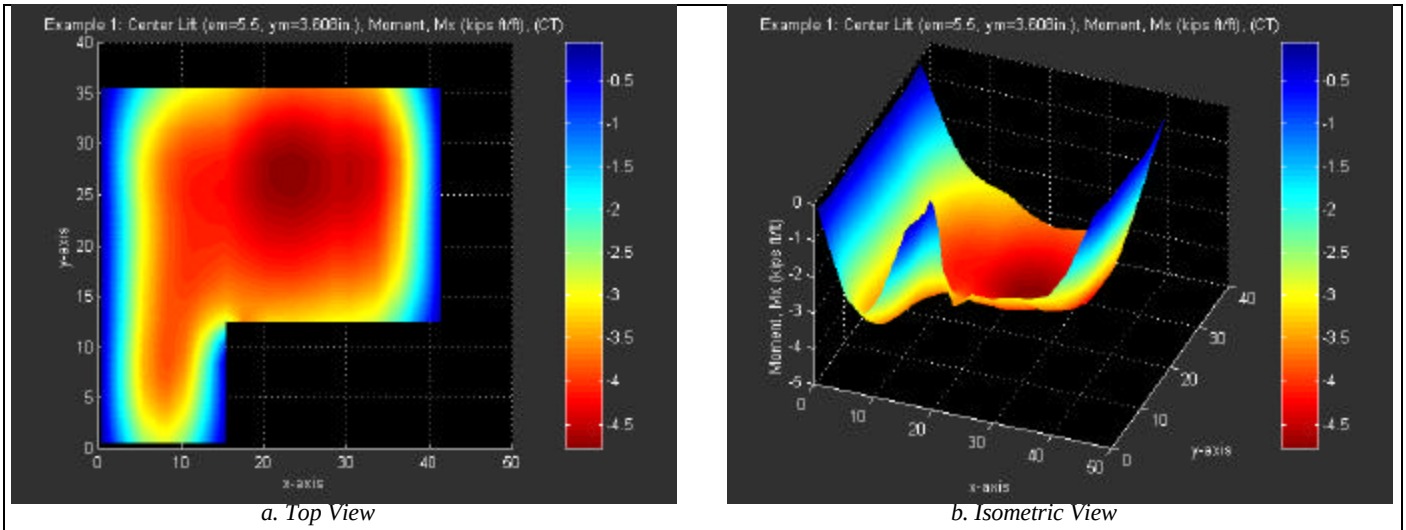

a. Top View *b. Isometric View*

Fig. D4. Example One Center Lift Case, Flat Slab, Moment in x-Direction.

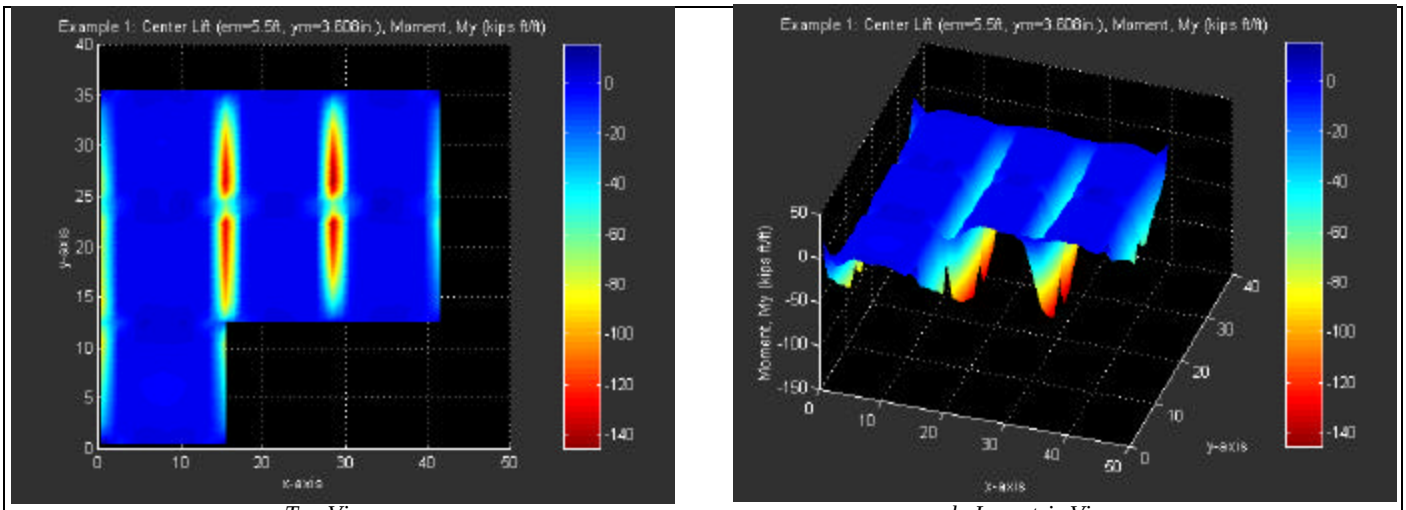

a. Top View *b. Isometric View*

Fig. D5. Example One Center Lift Case, Ribbed Slab, Moment in y-Direction.

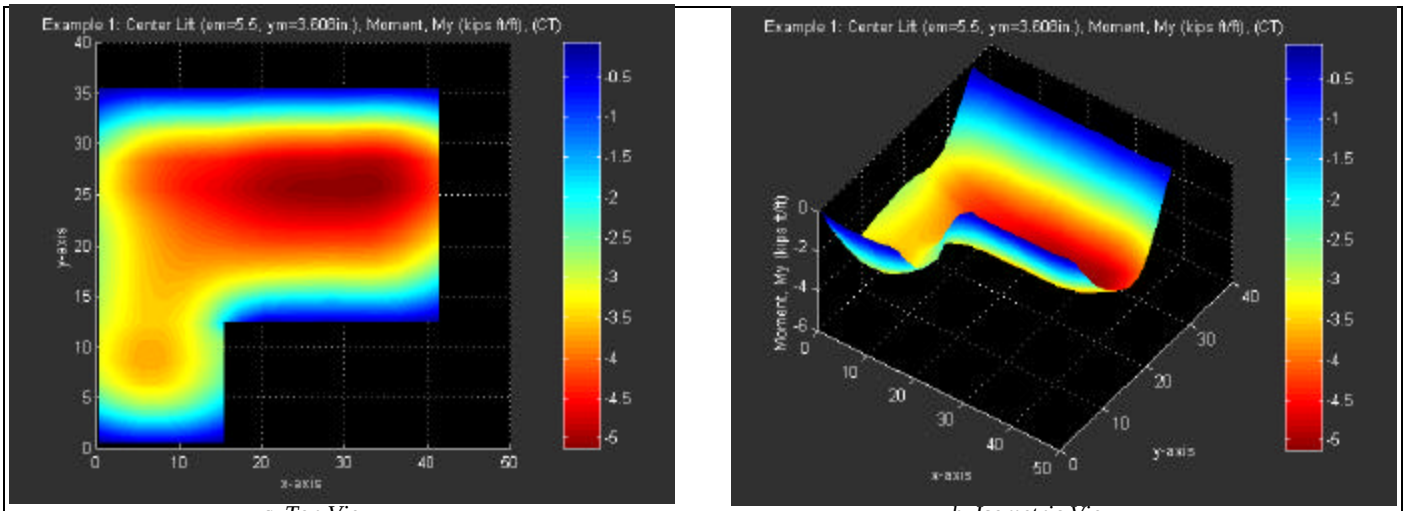

a. Top View *b. Isometric View*

Fig. D6. Example One Center Lift Case, Flat Slab, Moment in y-Direction.

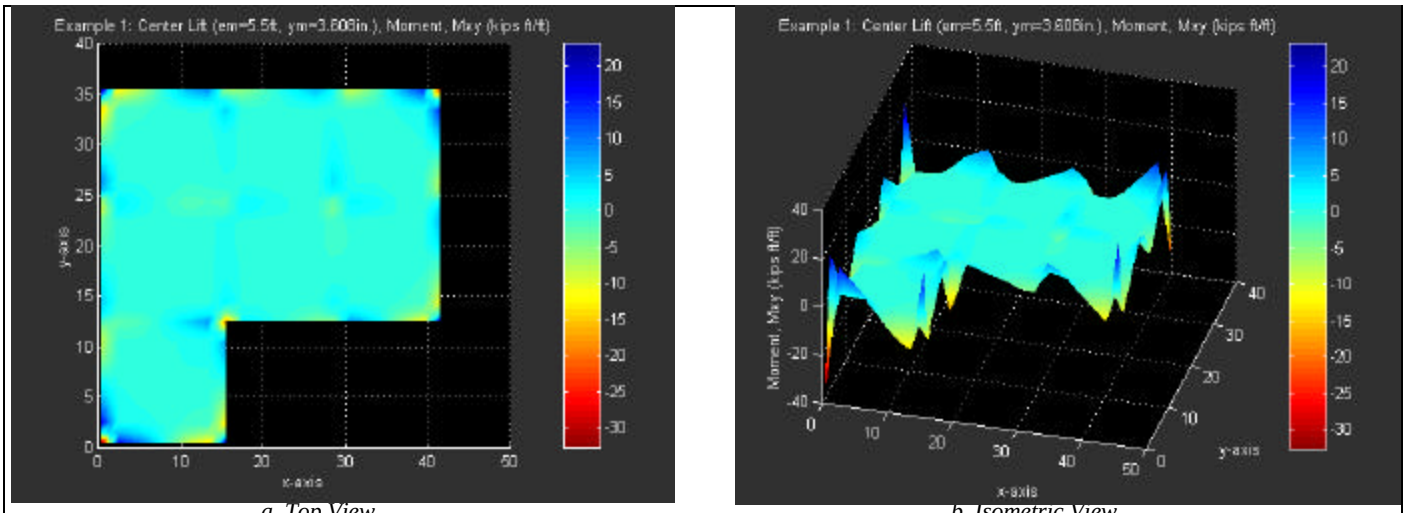

a. Top View *b. Isometric View*

Fig. D7. Example One Center Lift Case, Ribbed Slab, Twisting Moment.

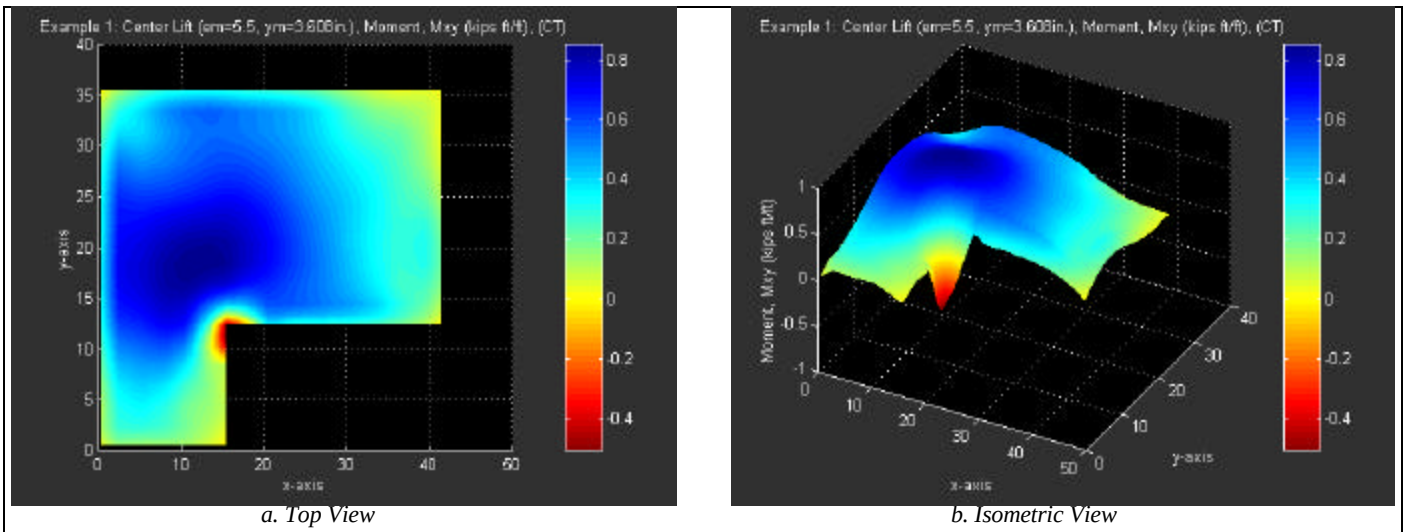

a. Top View *b. Isometric View*

Fig. D8. Example One Center Lift Case, Flat Slab, Twisting Moment.

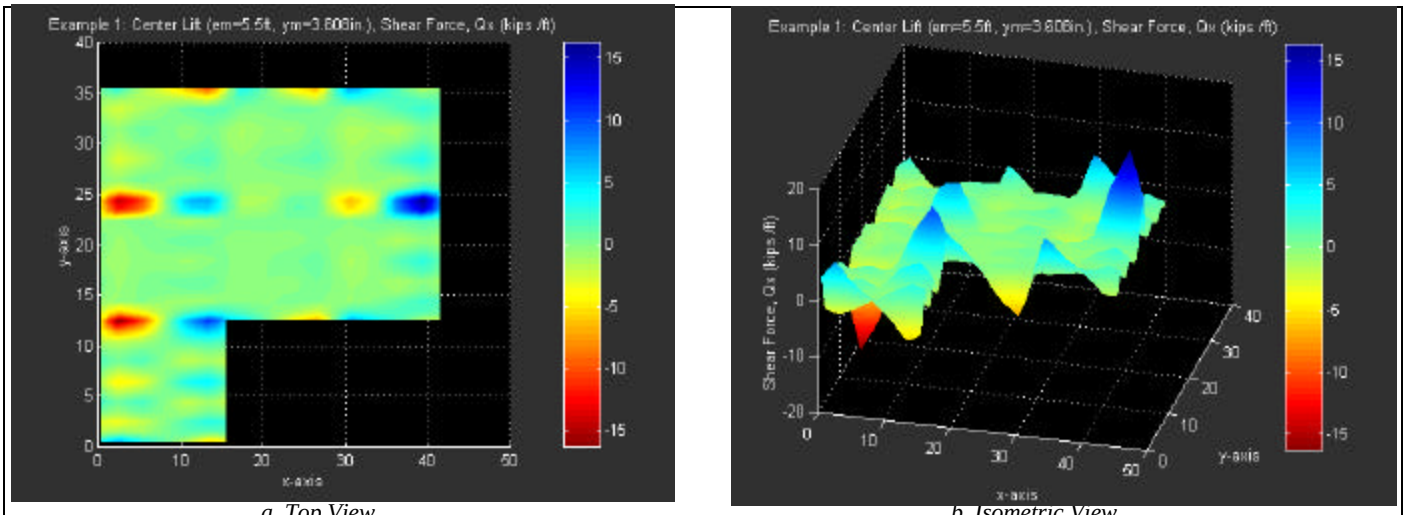

a. Top View *b. Isometric View*

Fig. D9. Example One Center Lift Case, Ribbed Slab, Shear in x-Direction.

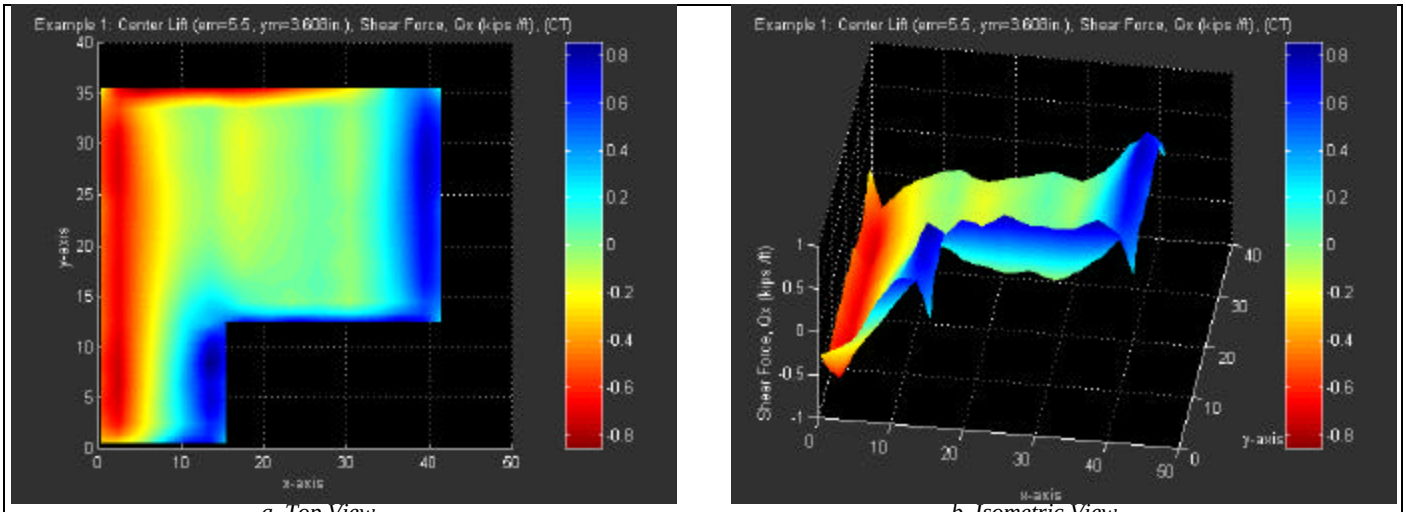

a. Top View *b. Isometric View*

Fig. D10. Example One Center Lift Case, Flat Slab, Shear in x-Direction.

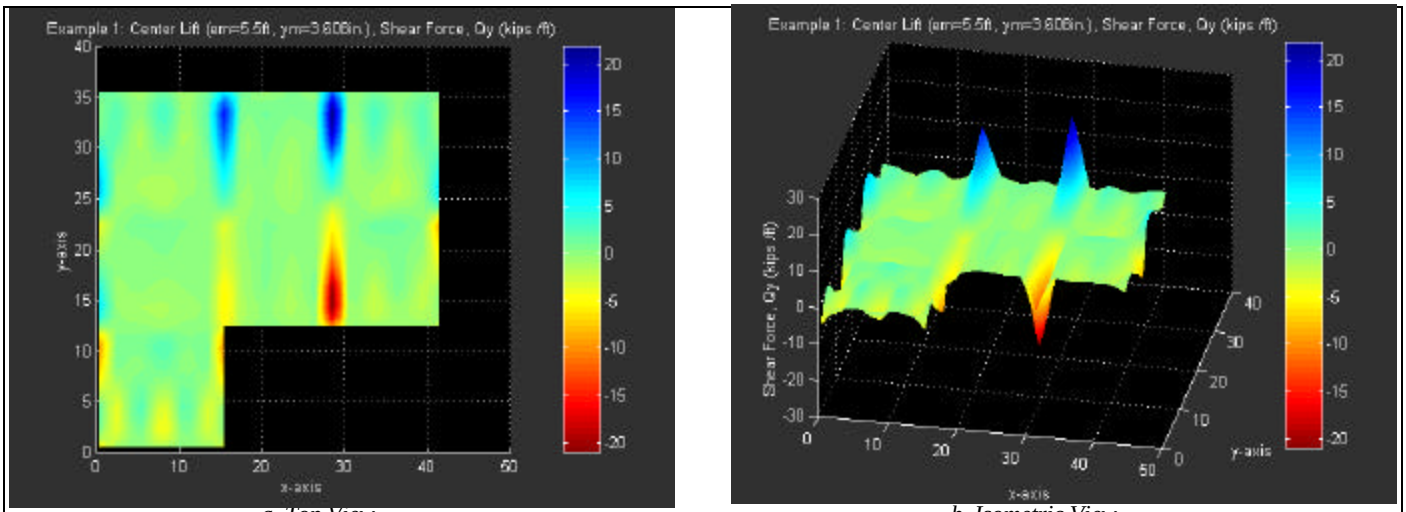

a. Top View *b. Isometric View*

Fig. D11. Example One Center Lift Case, Ribbed Slab, Shear in y-Direction.

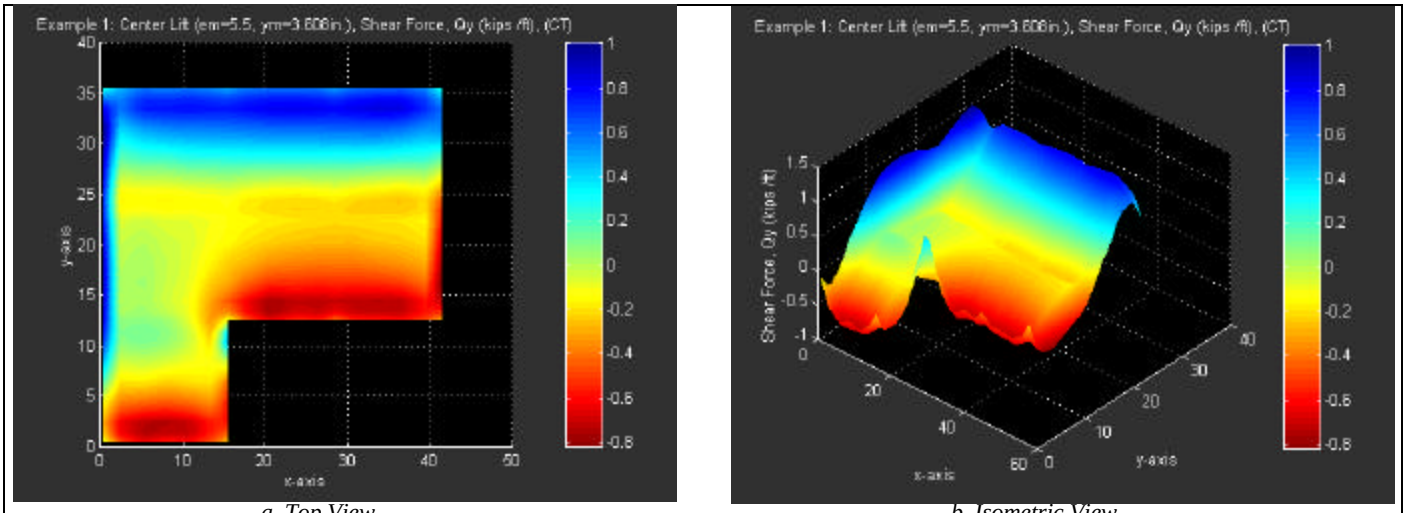

a. Top View *b. Isometric View*

Fig. D12. Example One Center Lift Case, Flat Slab, Shear in y-Direction.

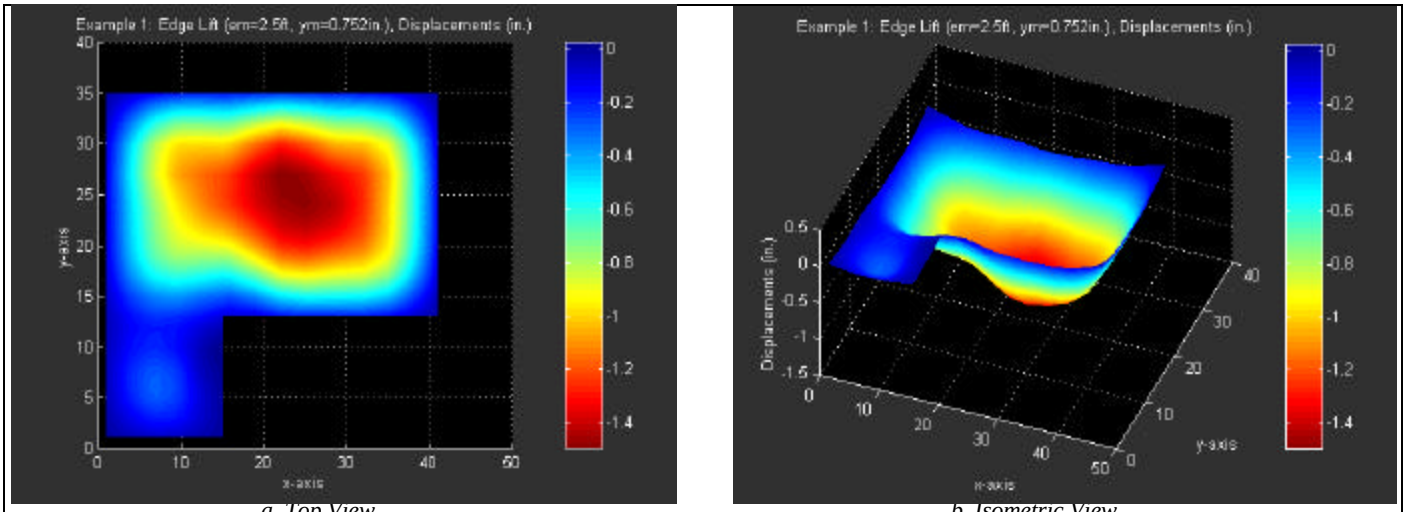

a. Top View *b. Isometric View*

Fig. D13. Example One Edge Lift Case, Ribbed Slab, Displacements.

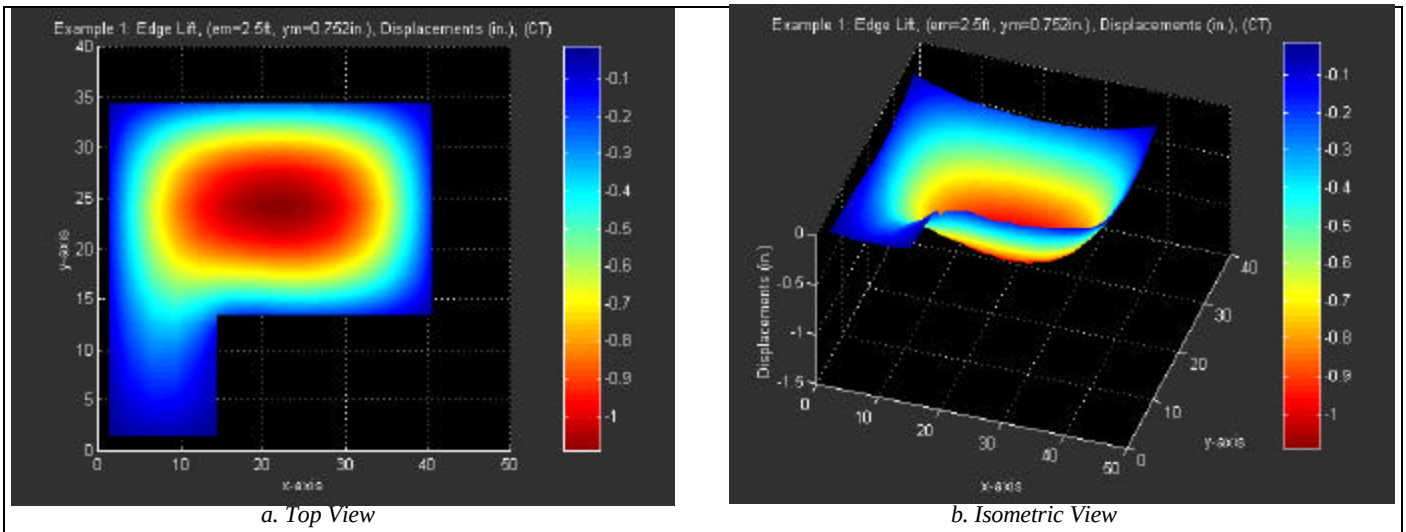

a. Top View *b. Isometric View*

Fig. D14. Example One Edge Lift Case, Flat Slab, Displacements.

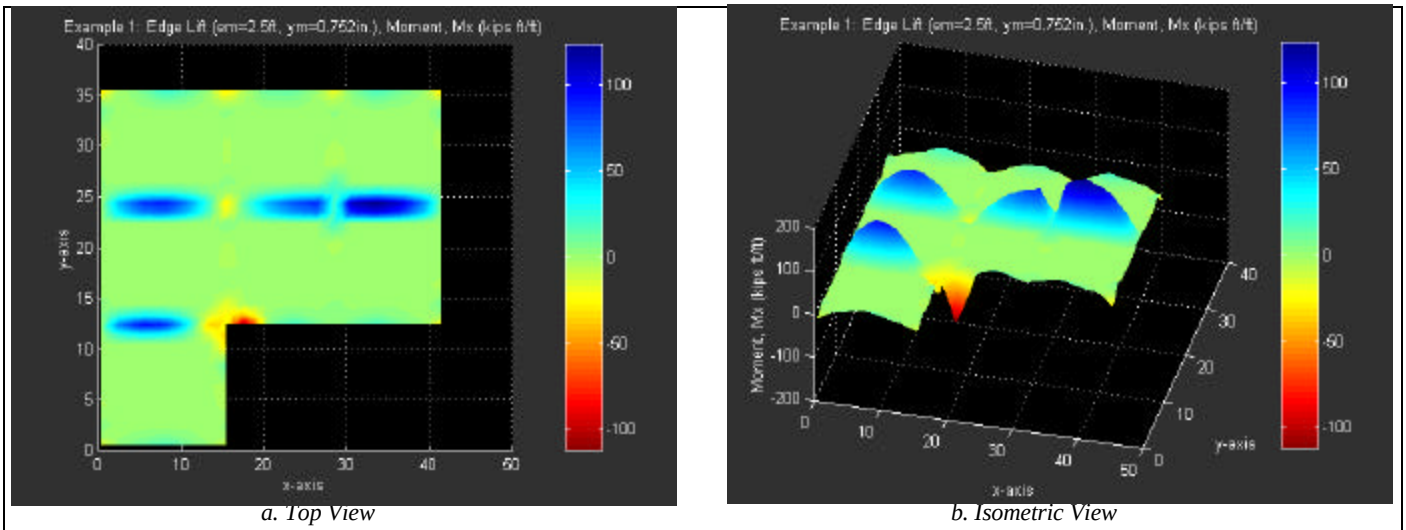

a. Top View *b. Isometric View*

Fig. D15. Example One Edge Lift Case, Ribbed Slab, Moment in x-Direction.

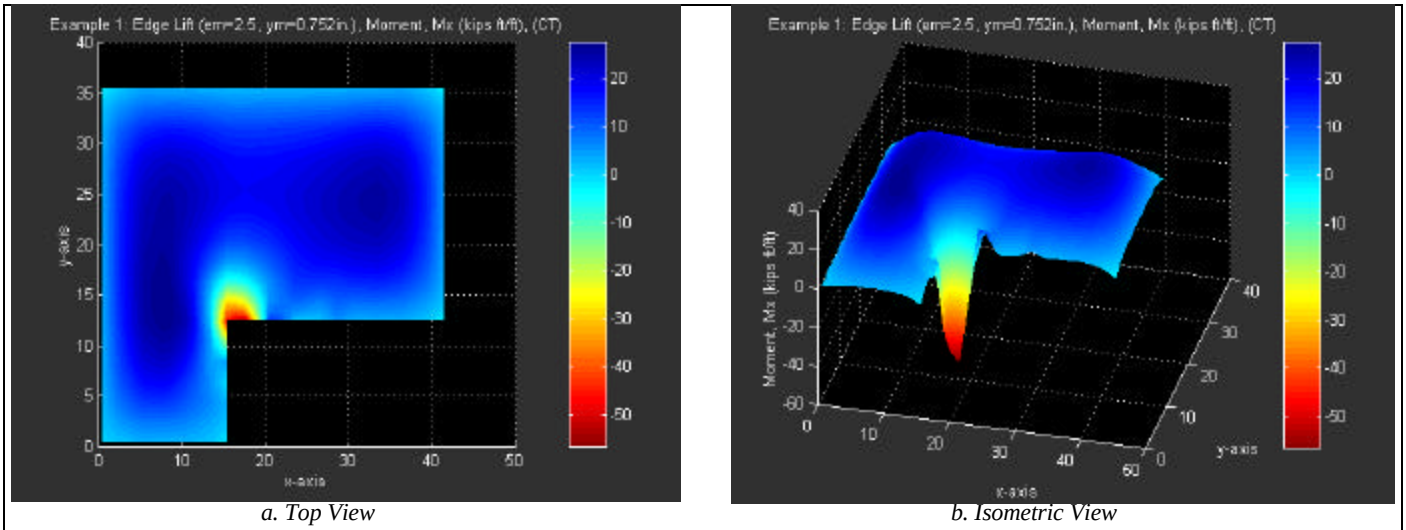

a. Top View *b. Isometric View*

Fig. D16. Example One Edge Lift Case, Flat Slab, Moment in x-Direction.

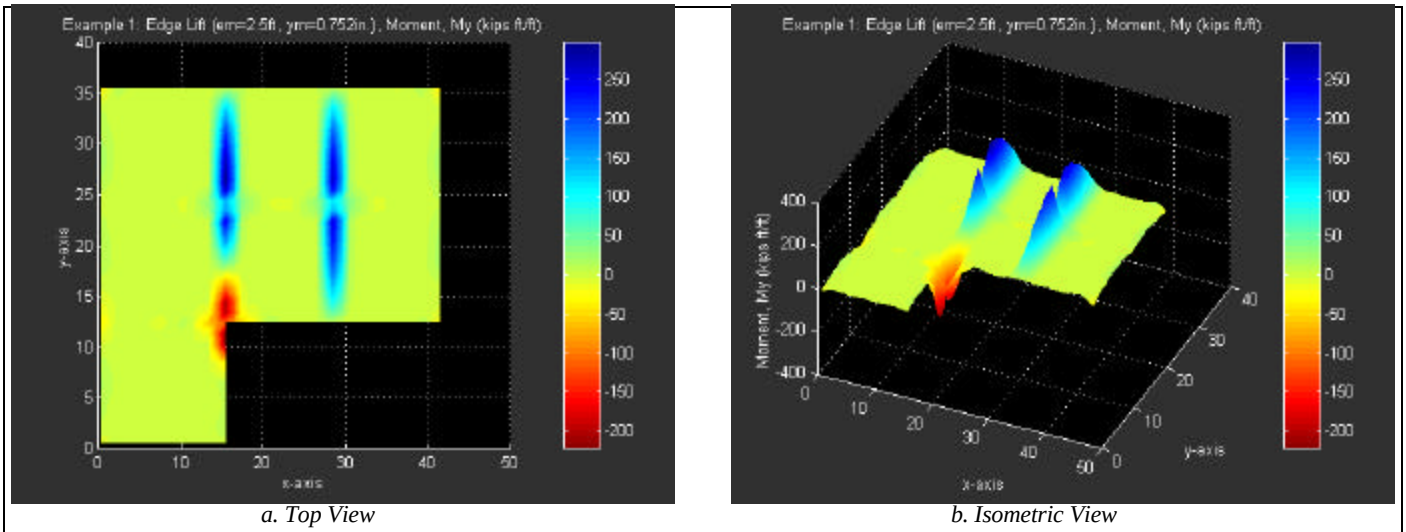

a. Top View *b. Isometric View*

Fig. D17. Example One Edge Lift Case, Ribbed Slab, Moment in y-Direction.

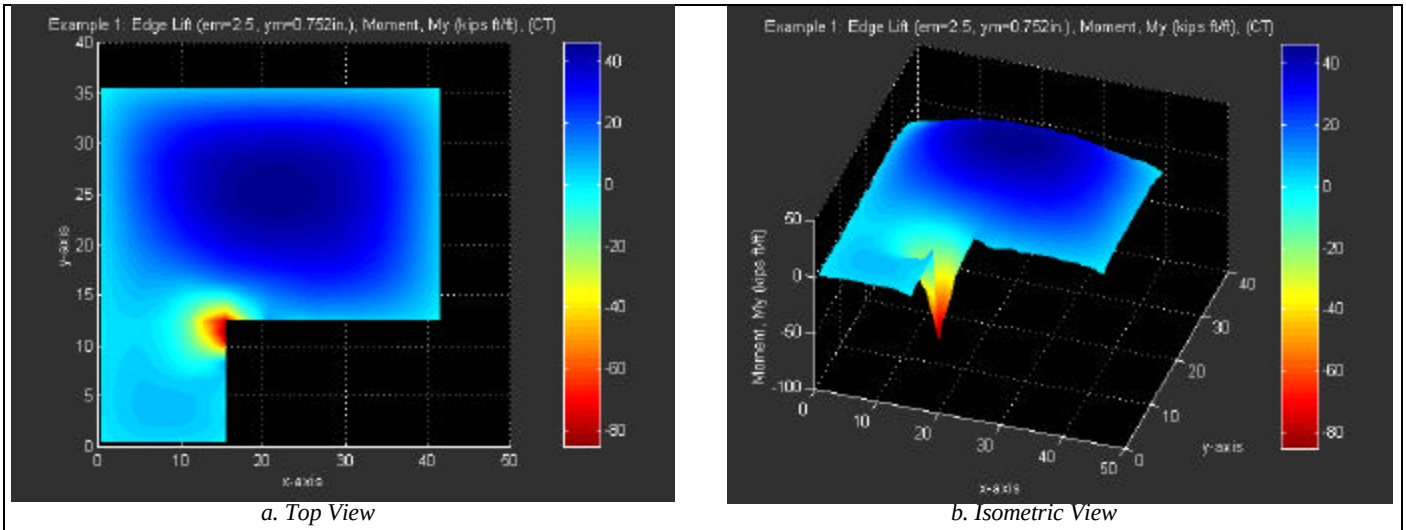

a. Top View *b. Isometric View*

Fig. D18. Example One Edge Lift Case, Flat Slab, Moment in y-Direction.

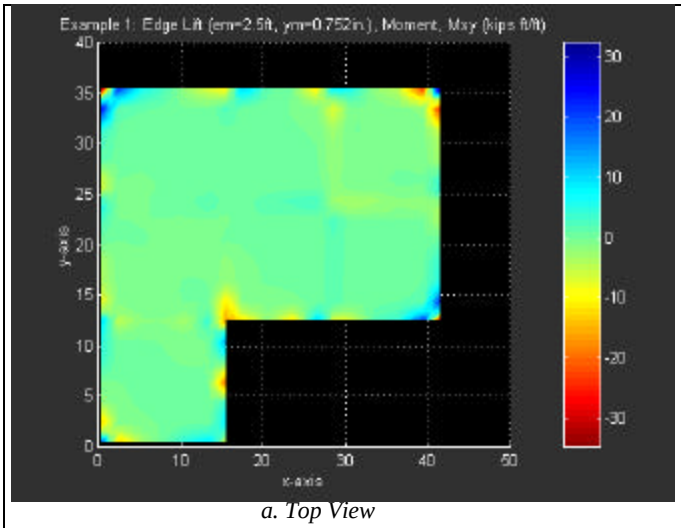

a. Top View

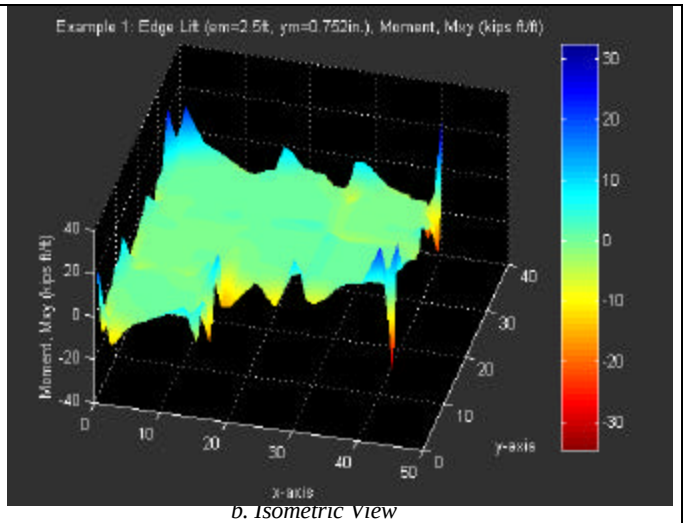

b. Isometric View

Fig. D19. Example One Edge Lift Case, Ribbed Slab, Twisting Moment.

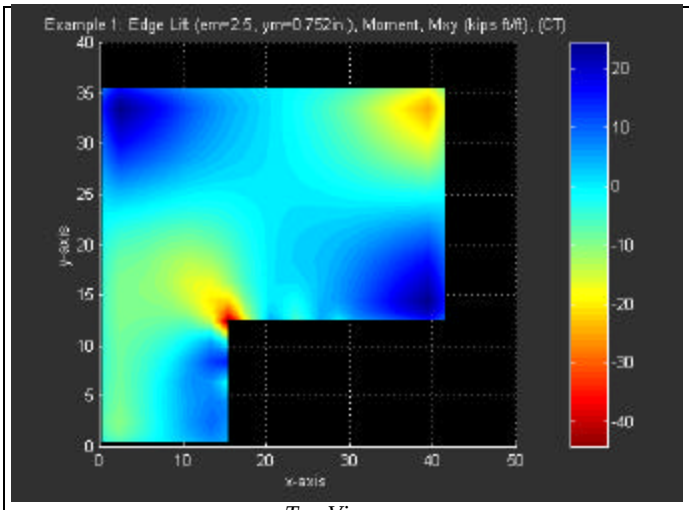

a. Top View

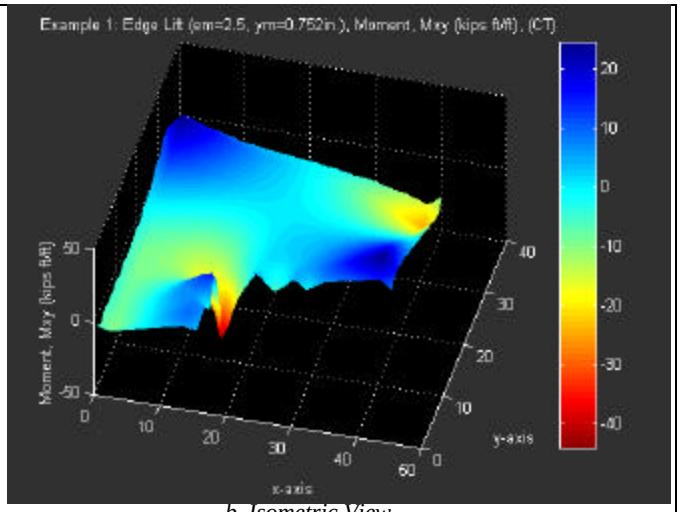

b. Isometric View

Fig. D20. Example One Edge Lift Case, Flat Slab, Twisting Moment.

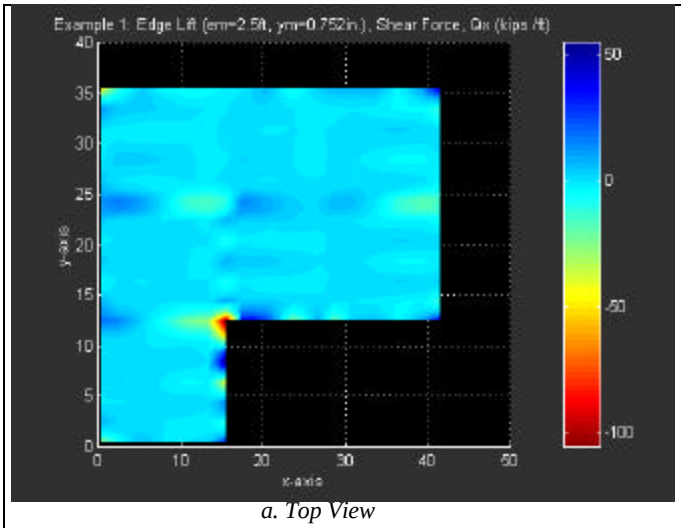

a. Top View

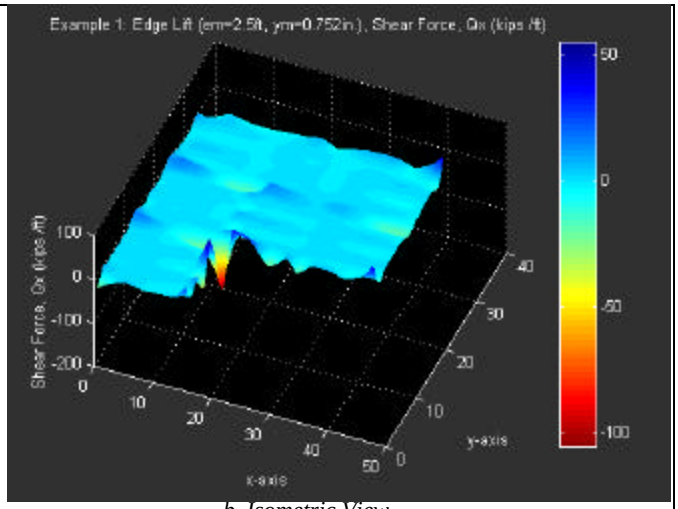

b. Isometric View

Fig. D21. Example One Edge Lift Case, Ribbed Slab, Shear in x-Direction.

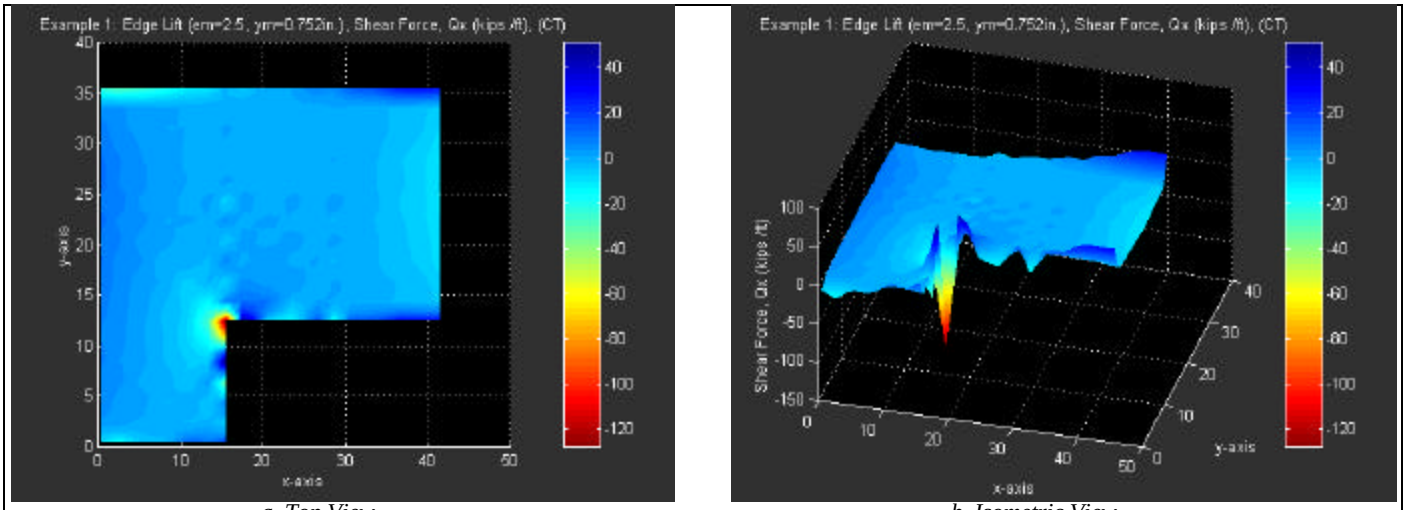

a. Top View *b. Isometric View*

Fig. D22. Example One Edge Lift Case, Flat Slab, Shear in x-Direction.

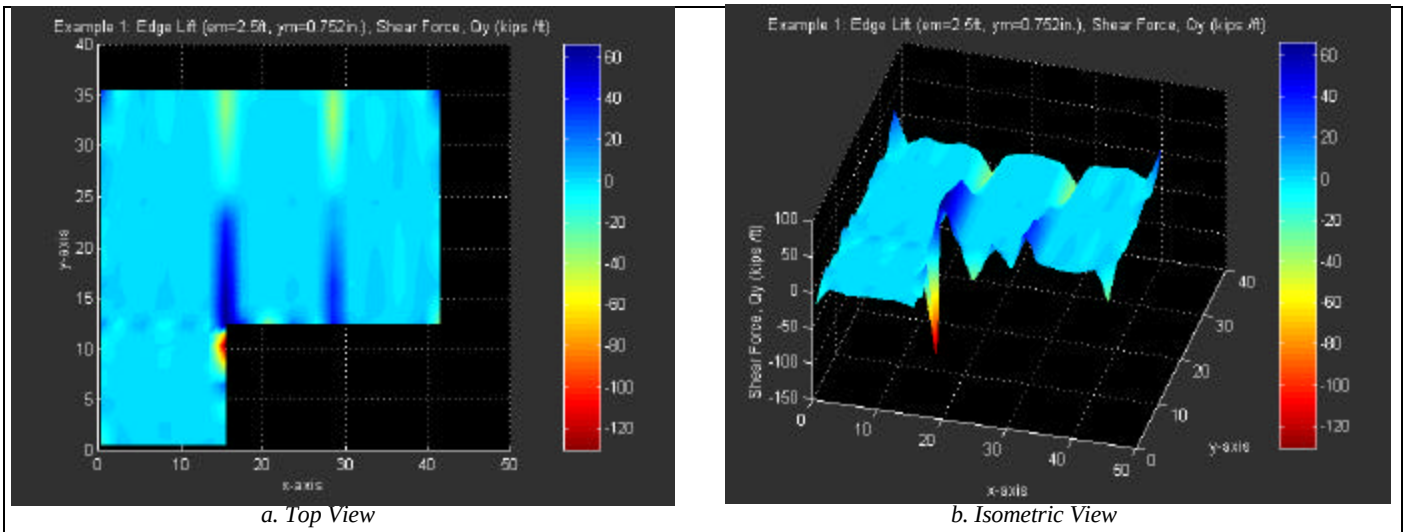

a. Top View *b. Isometric View*

Fig. D23. Example One Edge Lift Case, Ribbed Slab, Shear in y-Direction.

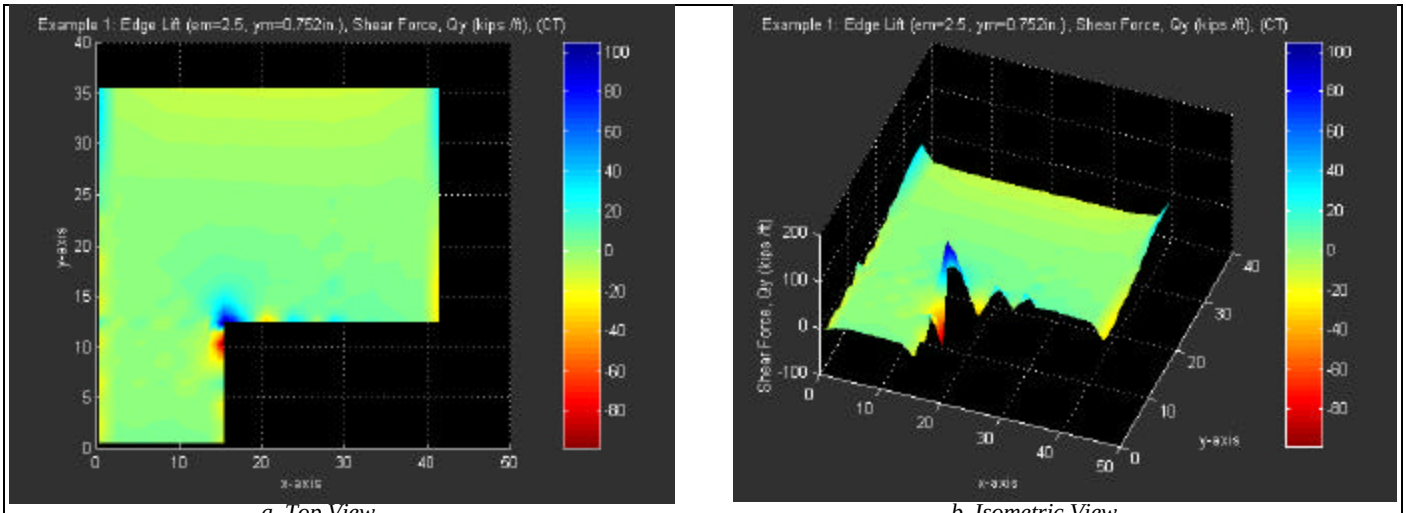

a. Top View *b. Isometric View*

Fig. D24. Example One Edge Lift Case, Flat Slab, Shear in y-Direction.

APPENDIX E
EXAMPLE TWO DISPLACEMENT AND STRESS PLOTS

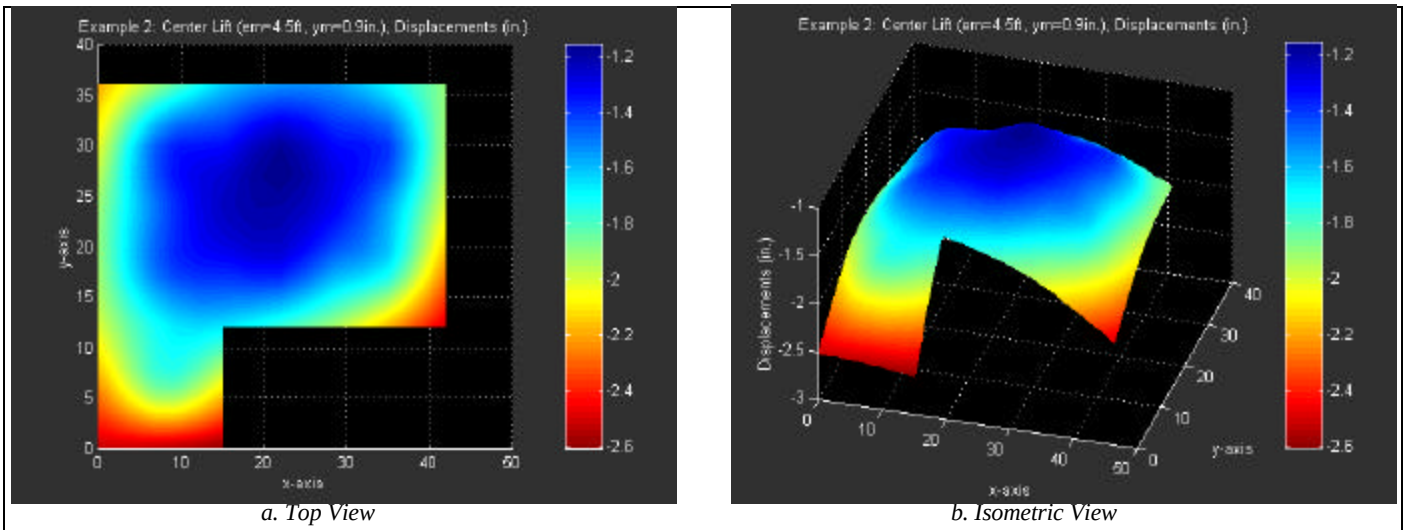

a. Top View *b. Isometric View*

Fig. E1. Example Two Center Lift Case, Ribbed Slab, Displacements.

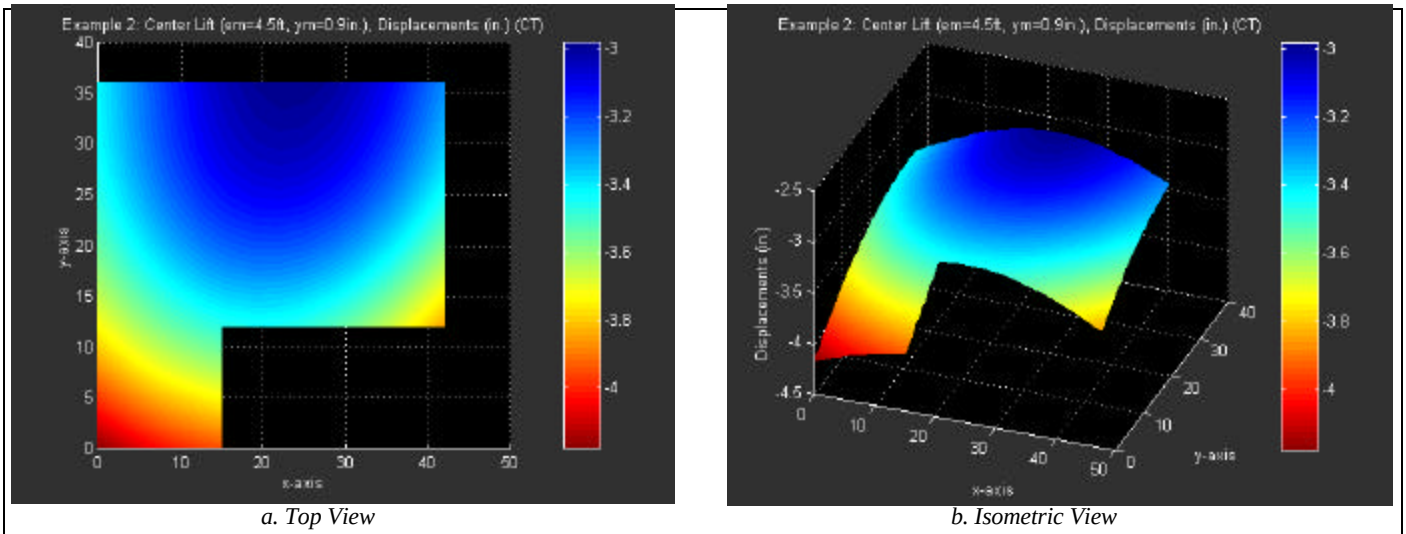

a. Top View *b. Isometric View*

Fig. E2. Example Two Center Lift Case, Flat Slab, Displacements.

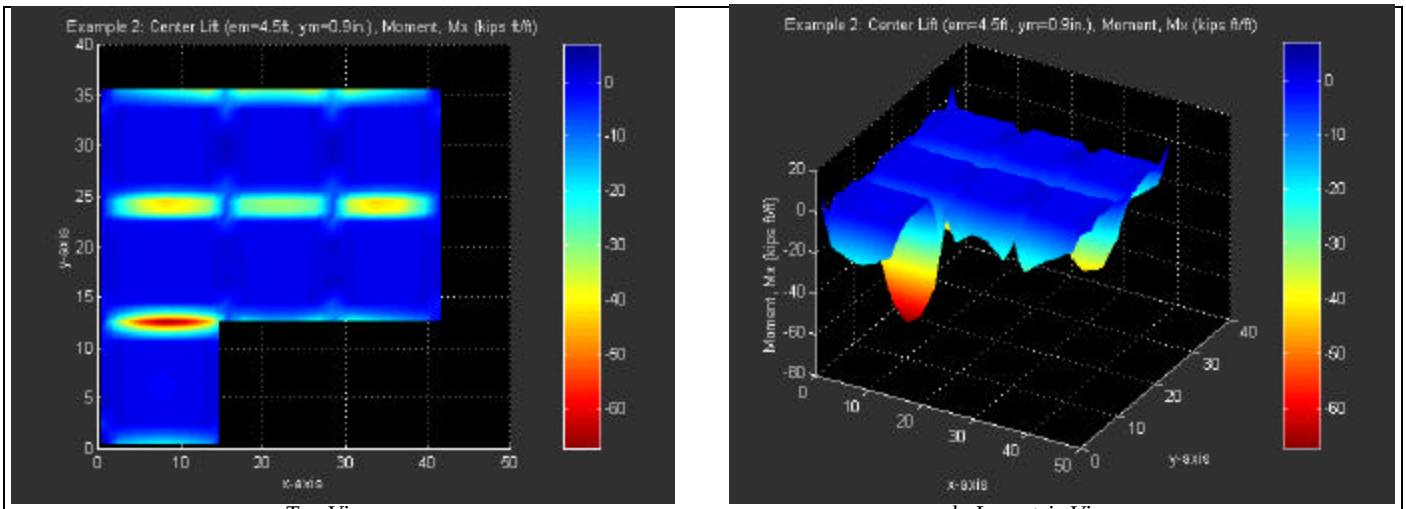

a. Top View *b. Isometric View*

Fig. E3. Example Two Center Lift Case, Ribbed Slab, Moment in x-Direction.

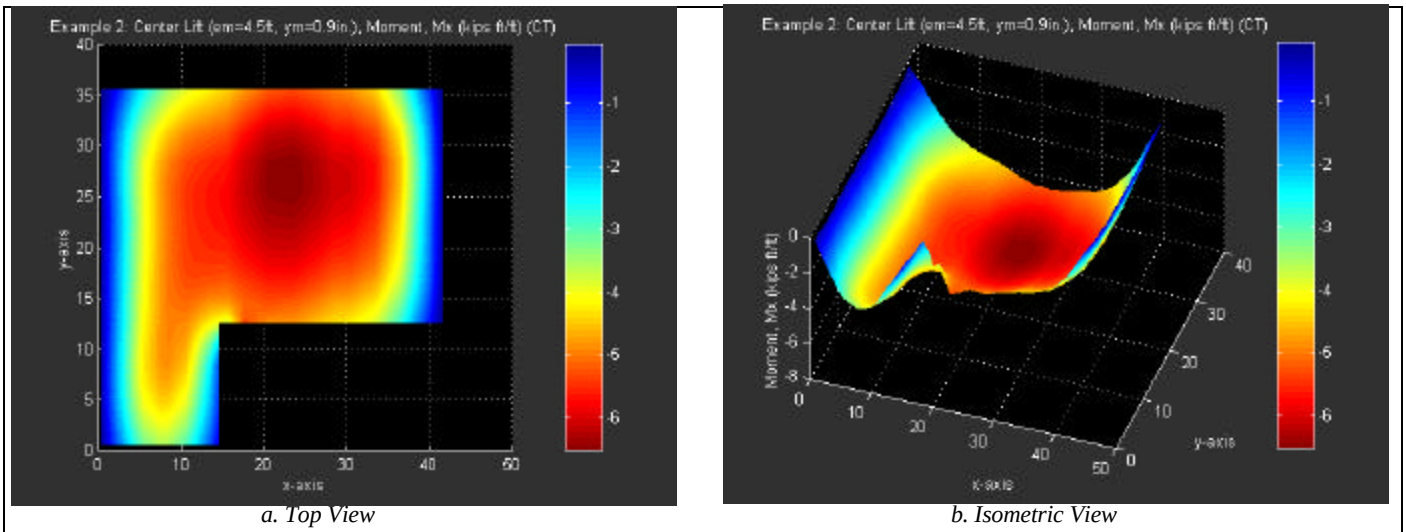

a. Top View *b. Isometric View*

Fig. E4. Example Two Center Lift Case, Flat Slab, Moment in x-Direction.

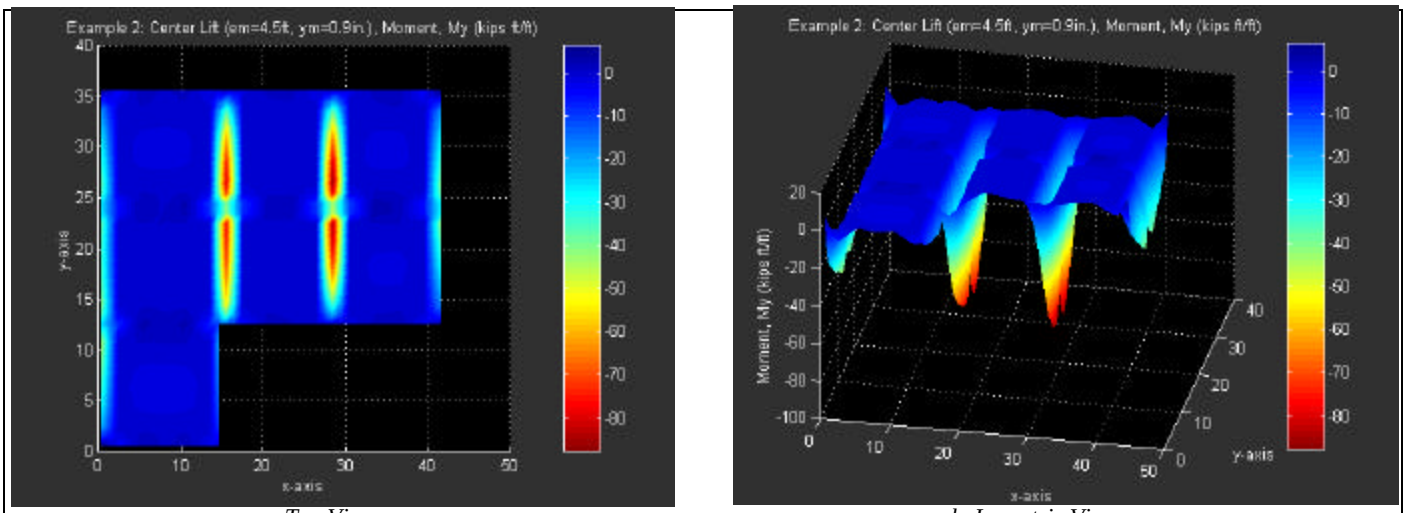

a. Top View *b. Isometric View*

Fig. E5. Example Two Center Lift Case, Ribbed Slab, Moment in y-Direction.

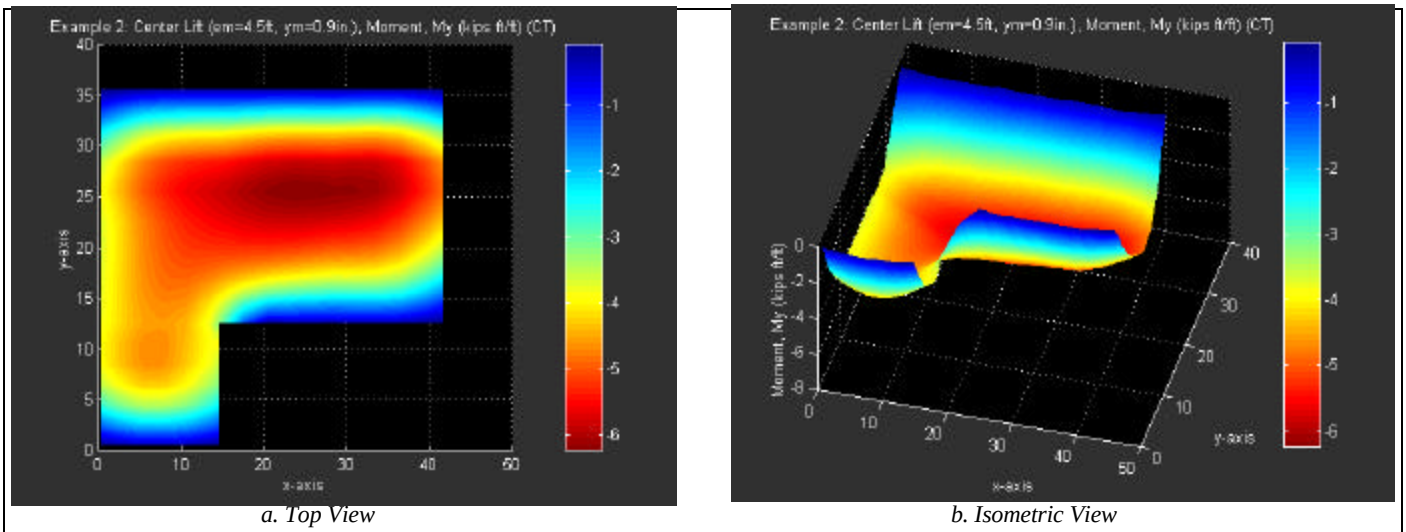

a. Top View *b. Isometric View*

Fig. E6. Example Two Center Lift Case, Flat Slab, Moment in y-Direction.

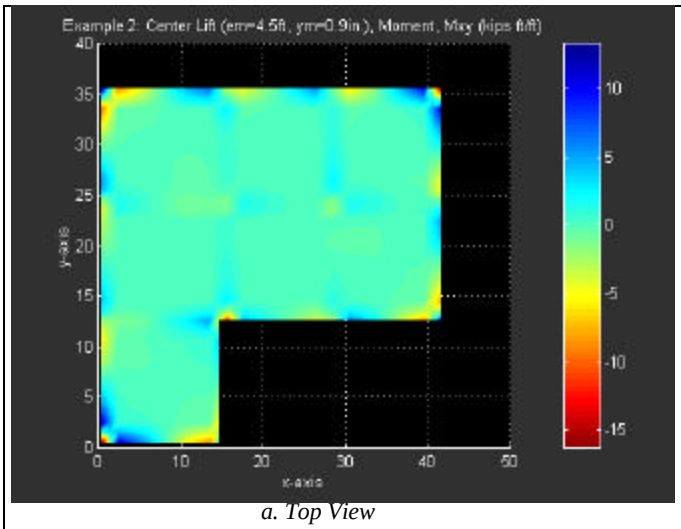

a. Top View

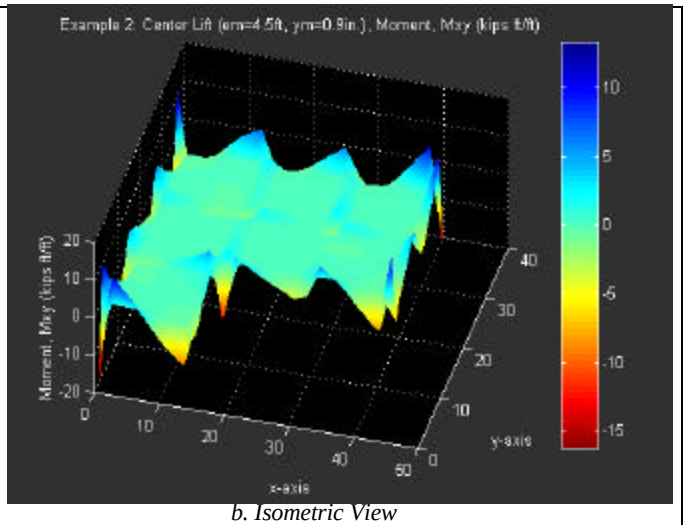

b. Isometric View

Fig. E7. Example Two Center Lift Case, Ribbed Slab, Twisting Moment.

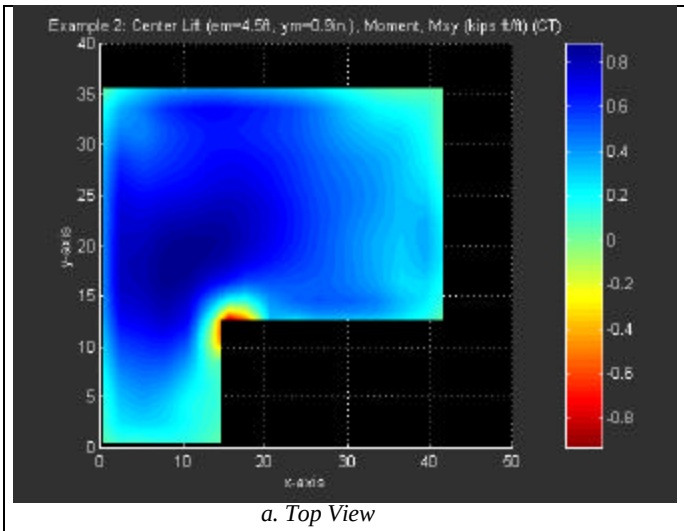

a. Top View

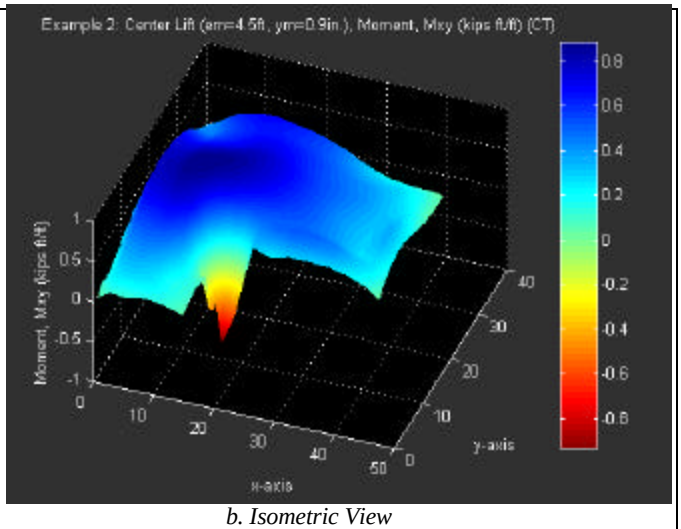

b. Isometric View

Fig. E8. Example Two Center Lift Case, Flat Slab, Twisting Moment.

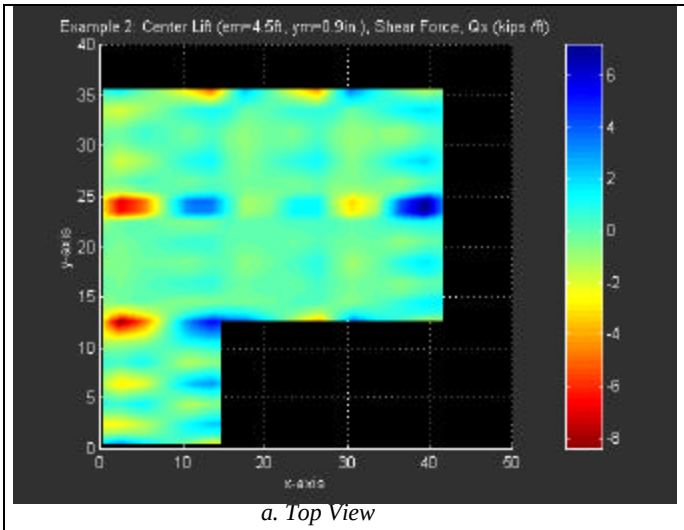

a. Top View

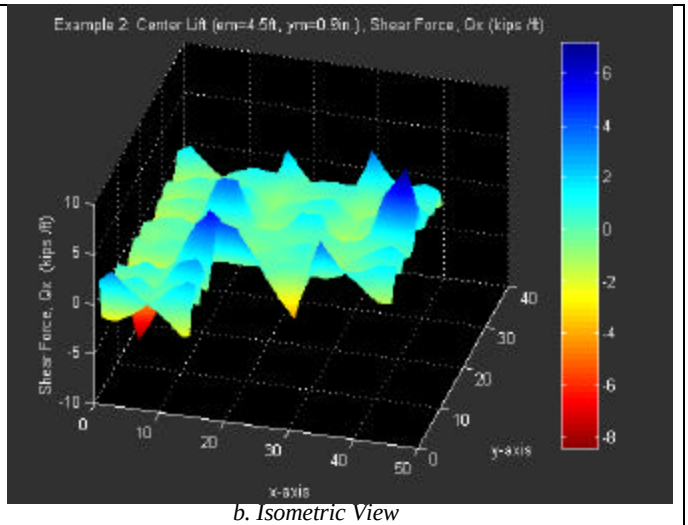

b. Isometric View

Fig. E9. Example Two Center Lift Case, Ribbed Slab, Shear in x-Direction.

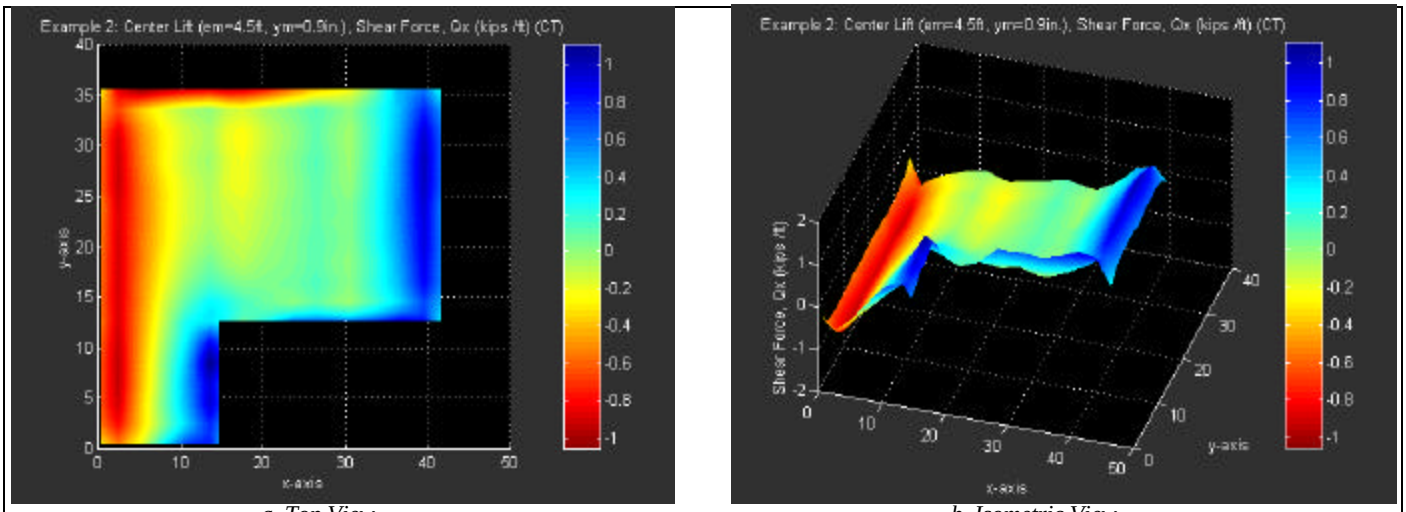

a. Top View *b. Isometric View*

Fig. E10. Example Two Center Lift Case, Flat Slab, Shear in x-Direction.

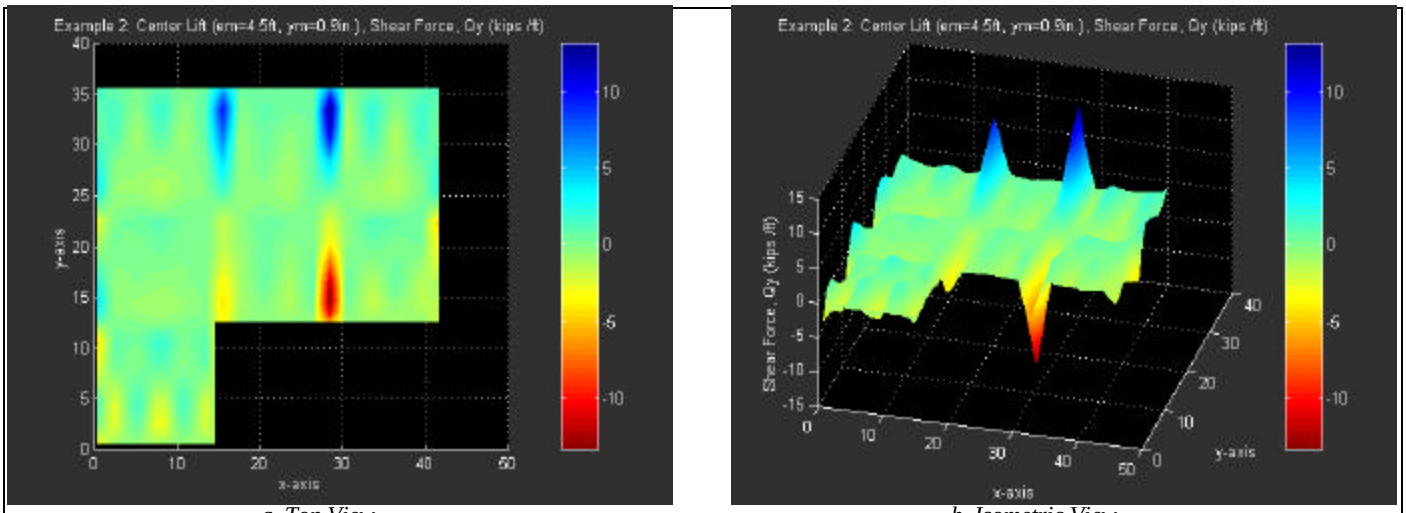

a. Top View *b. Isometric View*

Fig. E11. Example Two Center Lift Case, Ribbed Slab, Shear in y-Direction.

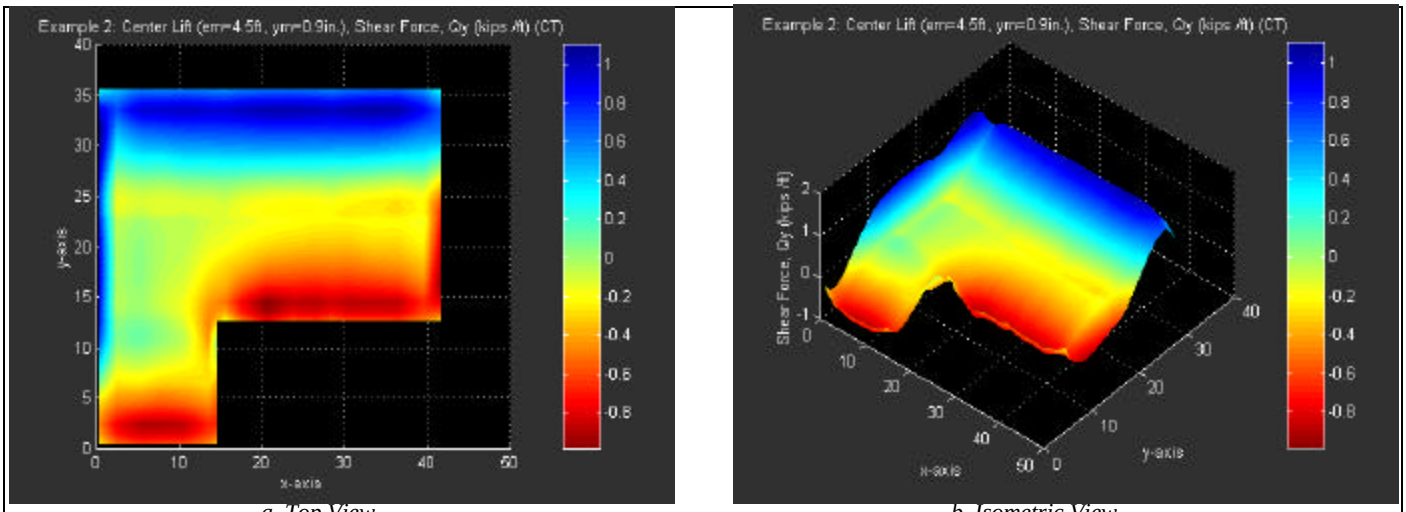

a. Top View *b. Isometric View*

Fig. E12. Example Two Center Lift Case, Flat Slab, Shear in y-Direction.

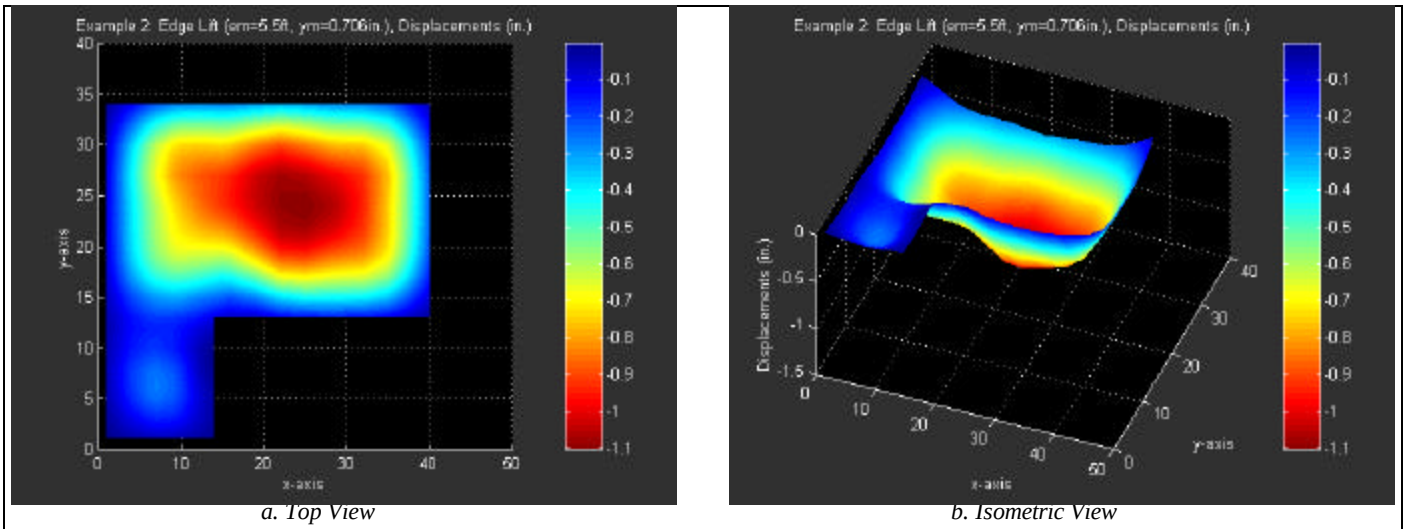

a. Top View *b. Isometric View*

Fig. E13. Example Two Edge Lift Case, Ribbed Slab, Displacements.

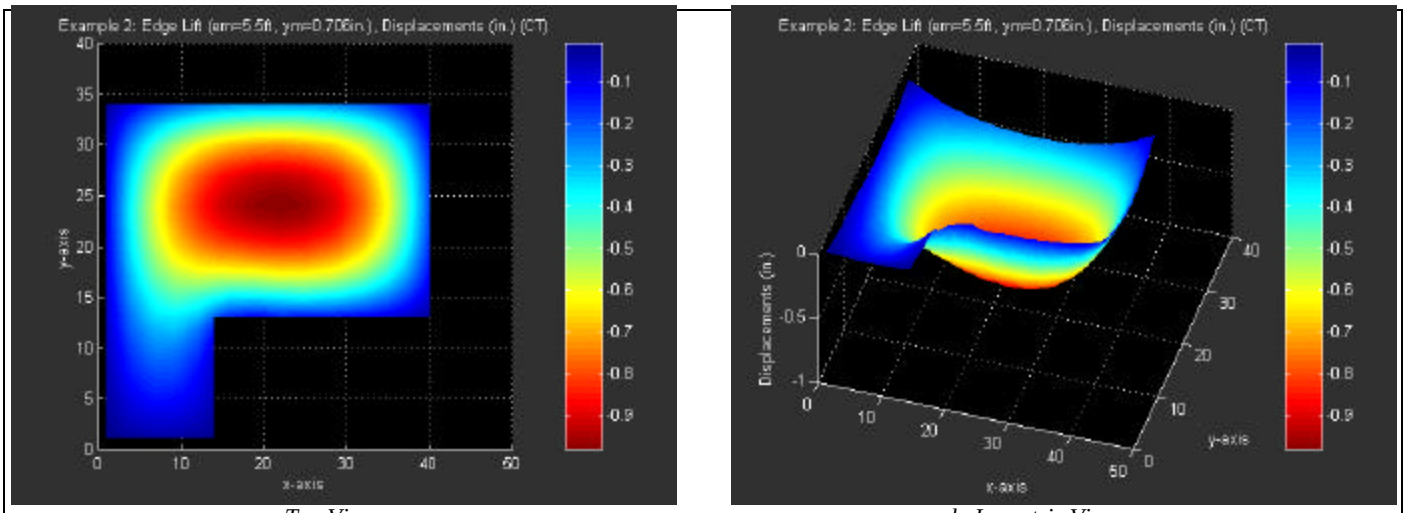

a. Top View *b. Isometric View*

Fig. E14. Example Two Edge Lift Case, Flat Slab, Displacements.

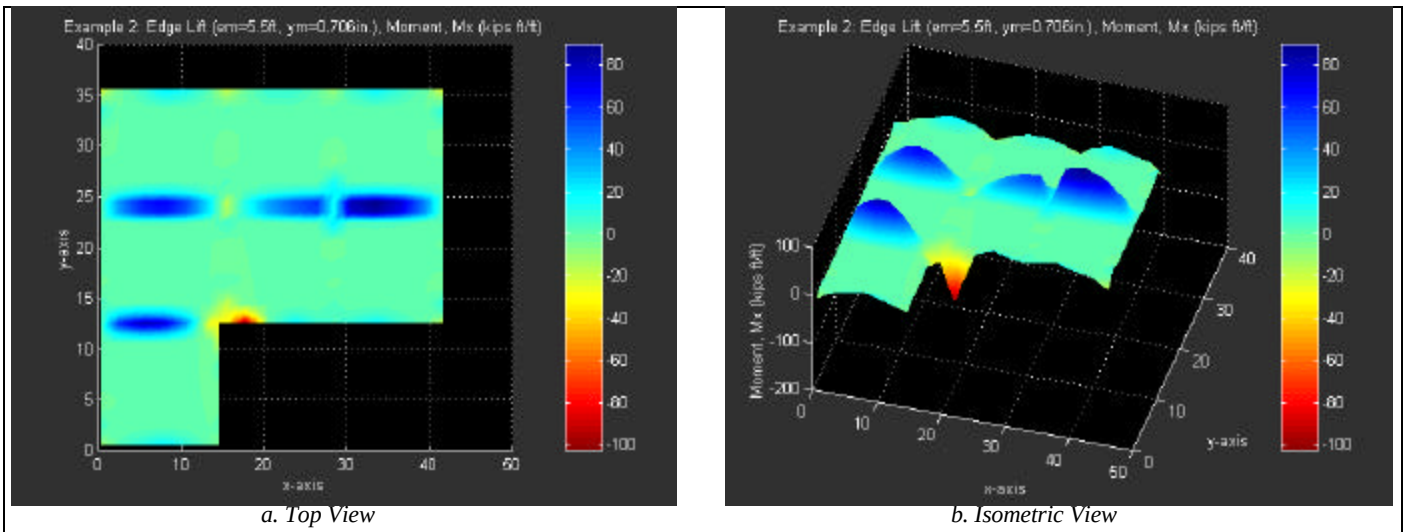

a. Top View *b. Isometric View*

Fig. E15. Example Two Edge Lift Case, Ribbed Slab, Moment in x-Direction.

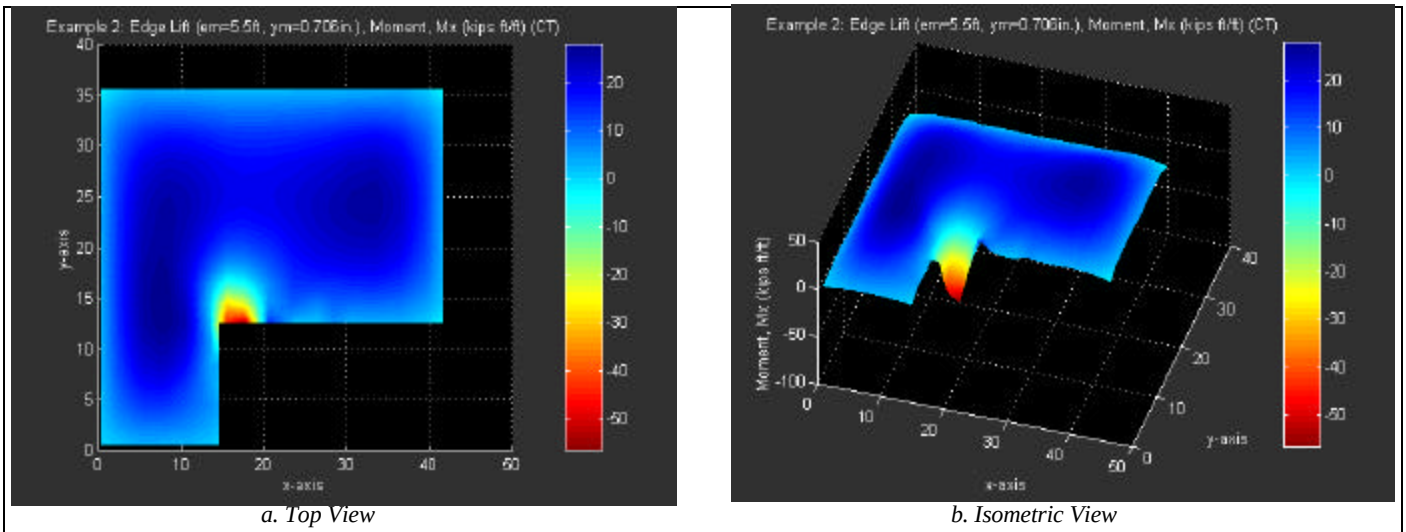

a. Top View *b. Isometric View*

Fig. E16. Example Two Edge Lift Case, Flat Slab, Moment in x-Direction.

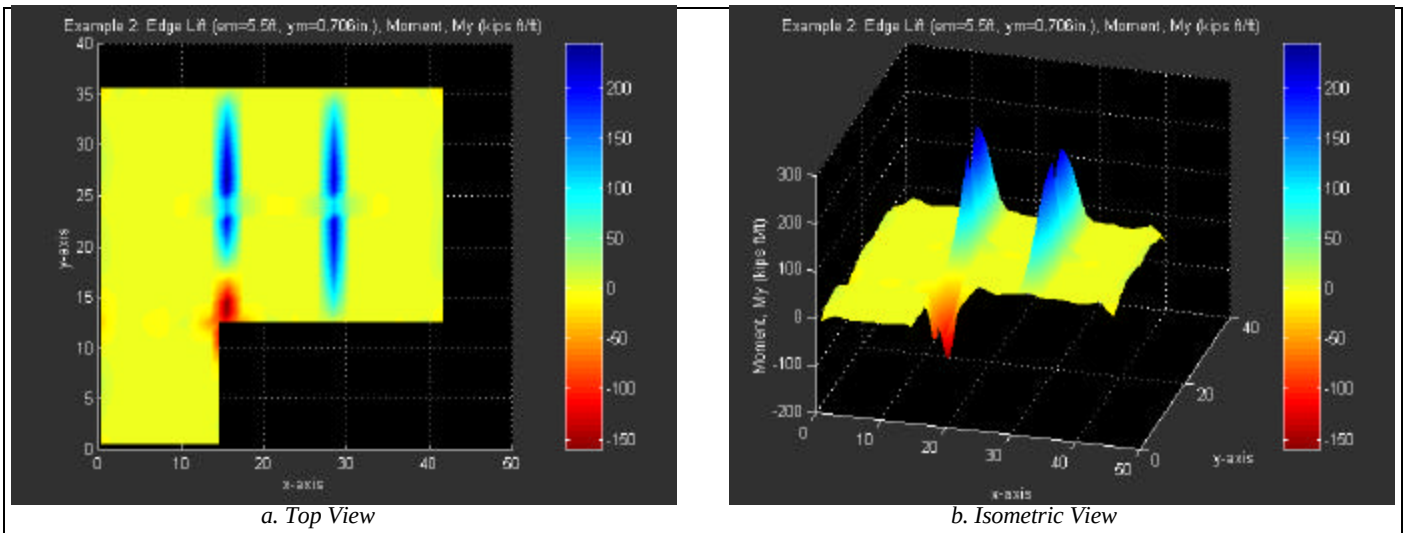

a. Top View *b. Isometric View*

Fig. E17. Example Two Edge Lift Case, Ribbed Slab, Moment in y-Direction.

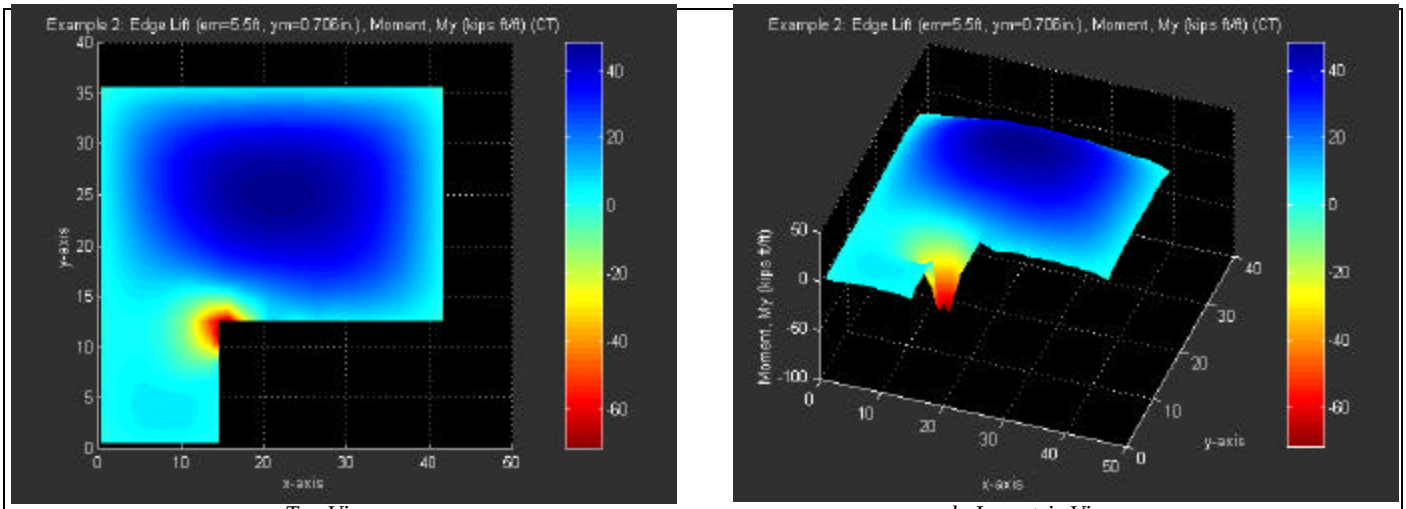

a. Top View *b. Isometric View*

Fig. E18. Example Two Edge Lift Case, Flat Slab, Moment in y-Direction.

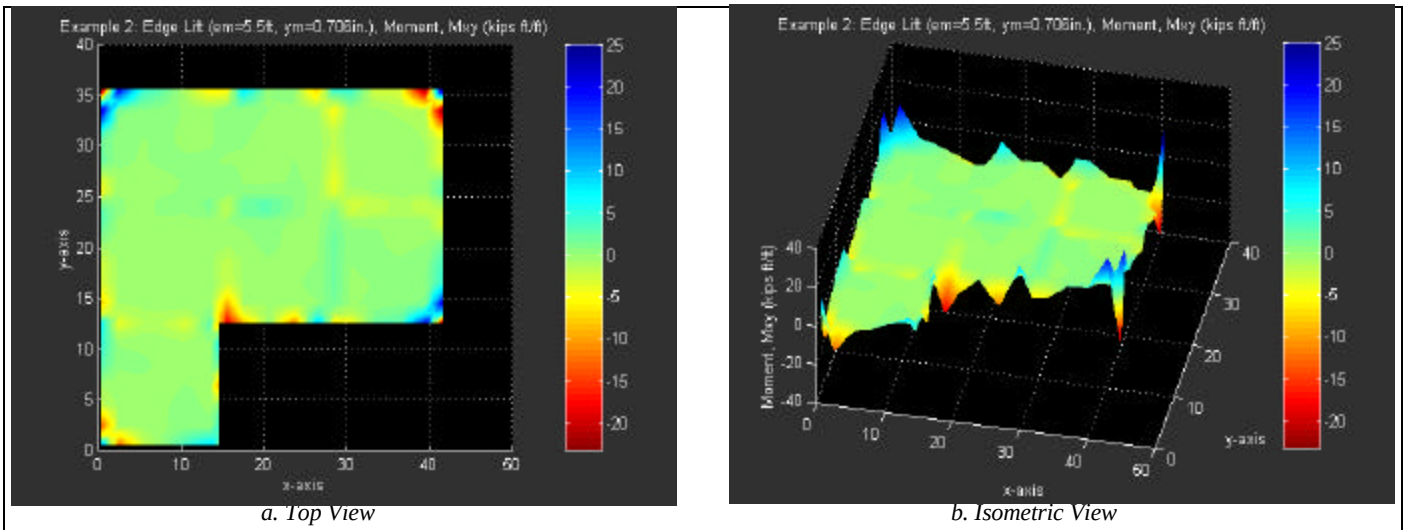

a. Top View *b. Isometric View*

Fig. E19. Example Two Edge Lift Case, Ribbed Slab, Twisting Moment.

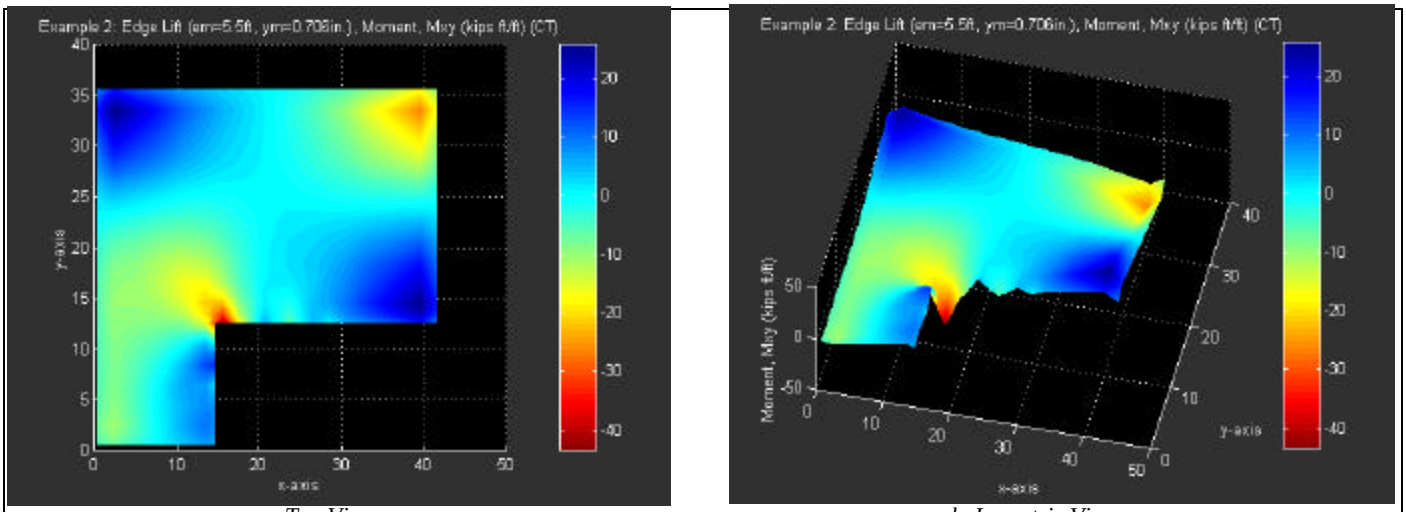

a. Top View *b. Isometric View*

Fig. E20. Example Two Edge Lift Case, Flat Slab, Twisting Moment.

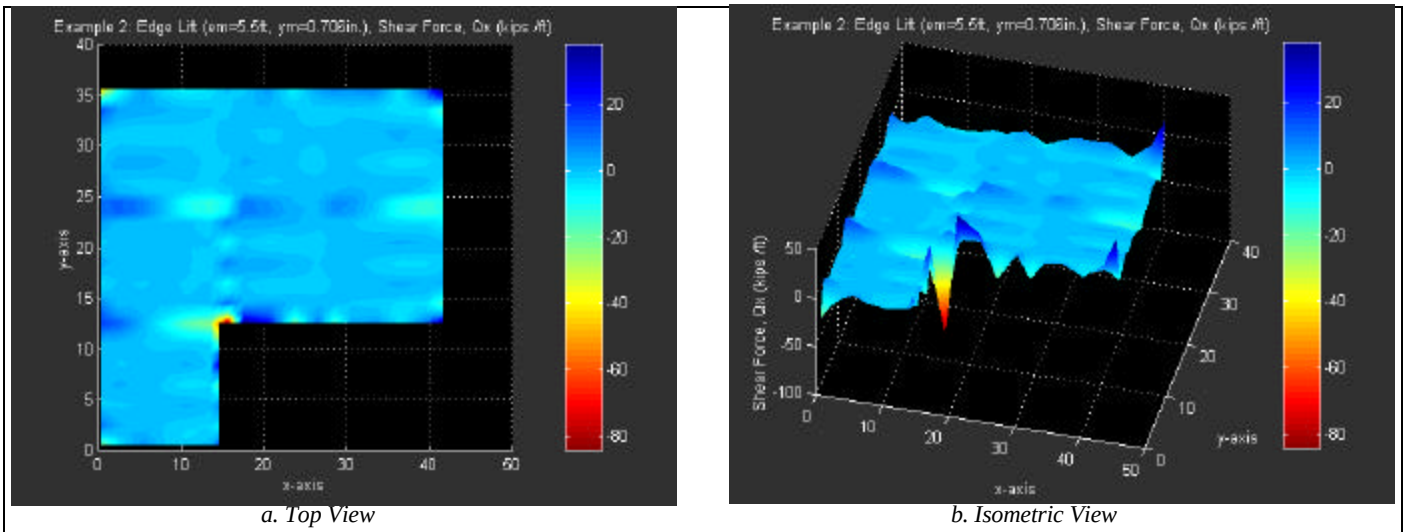

a. Top View *b. Isometric View*

Fig. E21. Example Two Edge Lift Case, Ribbed Slab, Shear in x-Direction.

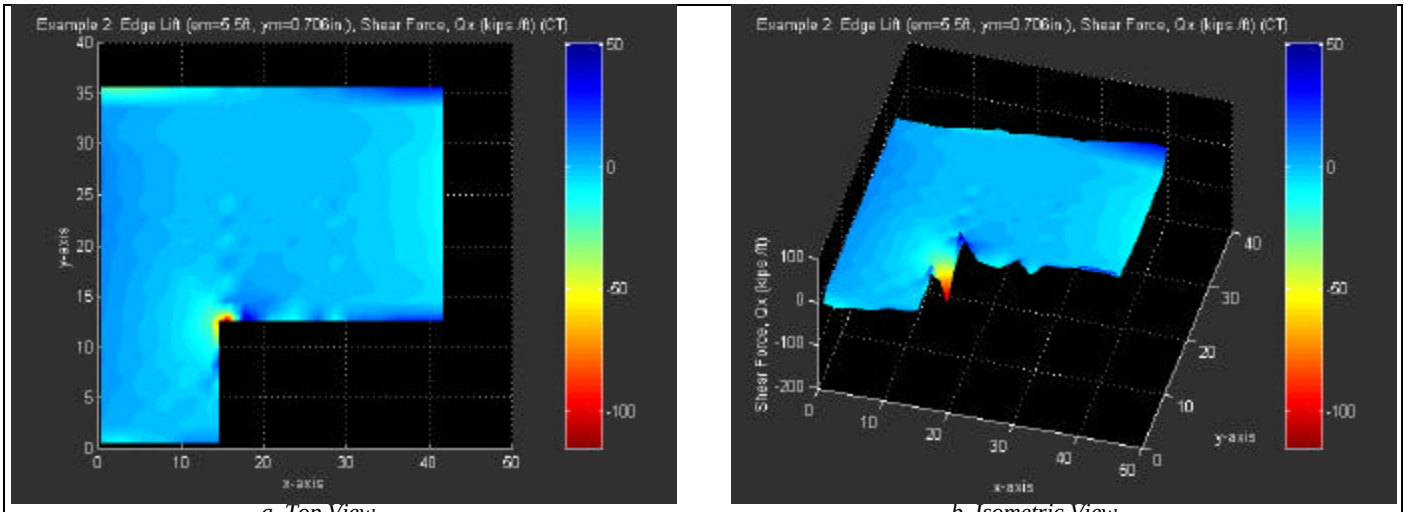

a. Top View *b. Isometric View*

Fig. E22. Example Two Edge Lift Case, Flat Slab, Shear in x-Direction.

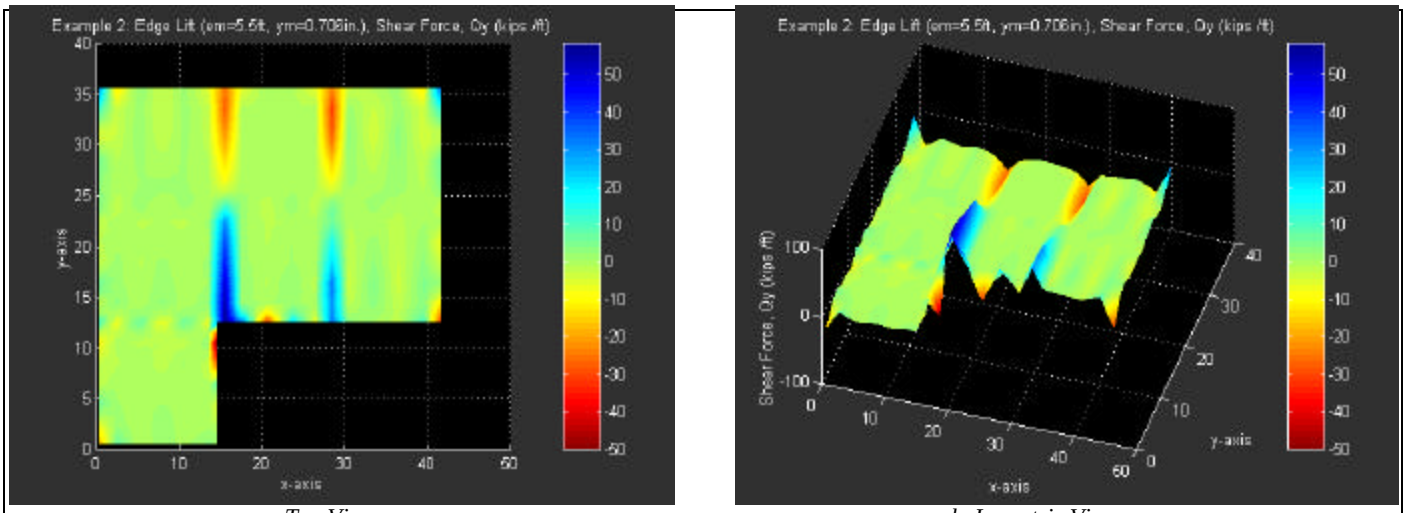

a. Top View *b. Isometric View*

Fig. E23. Example Two Edge Lift Case, Ribbed Slab, Shear in y-Direction.

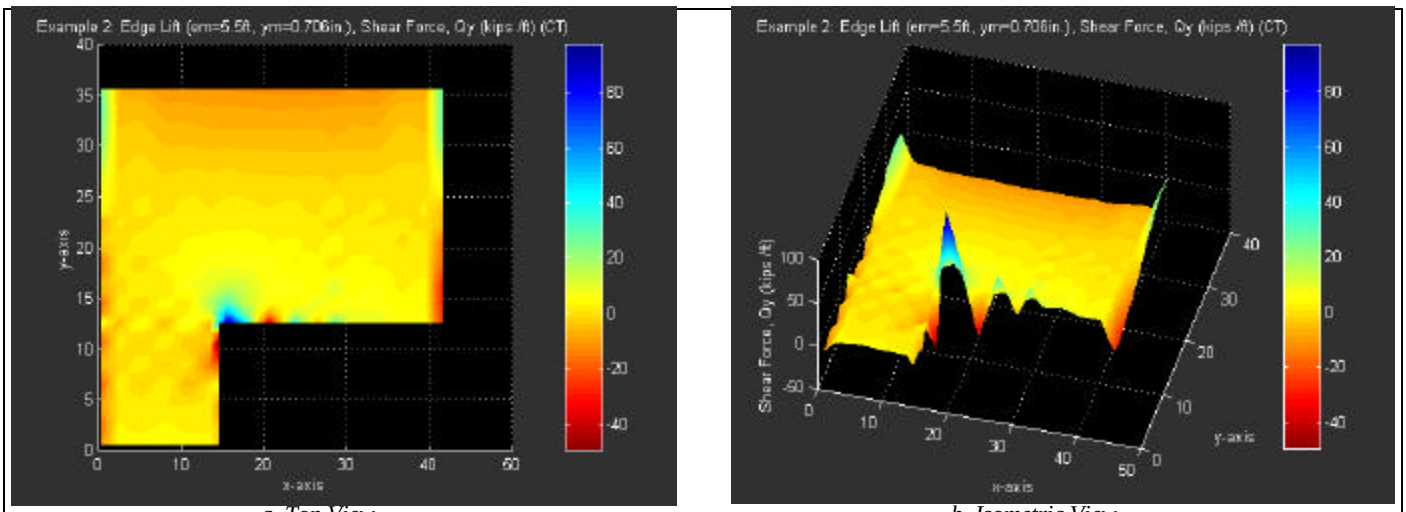

a. Top View *b. Isometric View*

Fig. E24. Example Two Edge Lift Case, Flat Slab, Shear in y-Direction.

APPENDIX F
EXAMPLE THREE DISPLACEMENT AND STRESS PLOTS

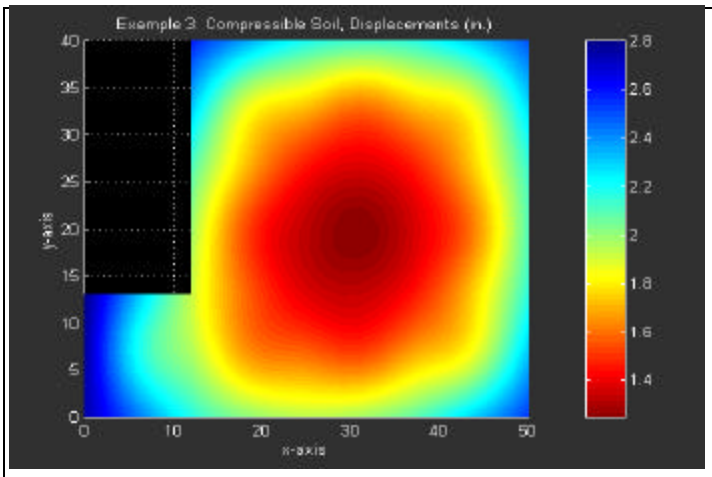

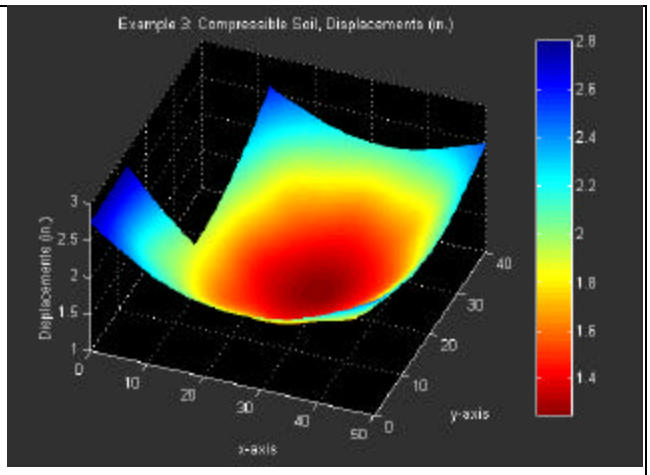

a. Top View *b. Isometric View*

Fig. F1. Example Three Compressible Soil, Ribbed Slab, Displacements.

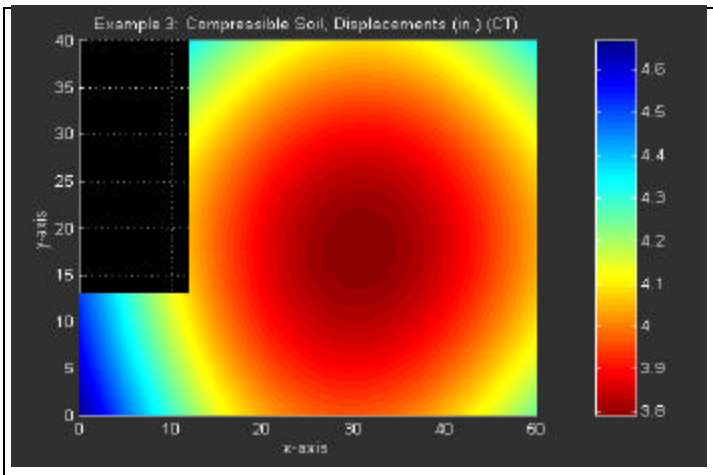

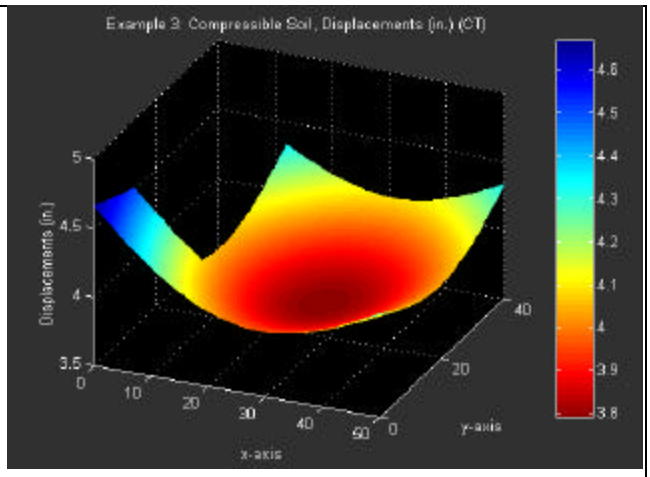

a. Top View *b. Isometric View*

Fig. F2. Example Three Compressible Soil, Flat Slab, Displacements.

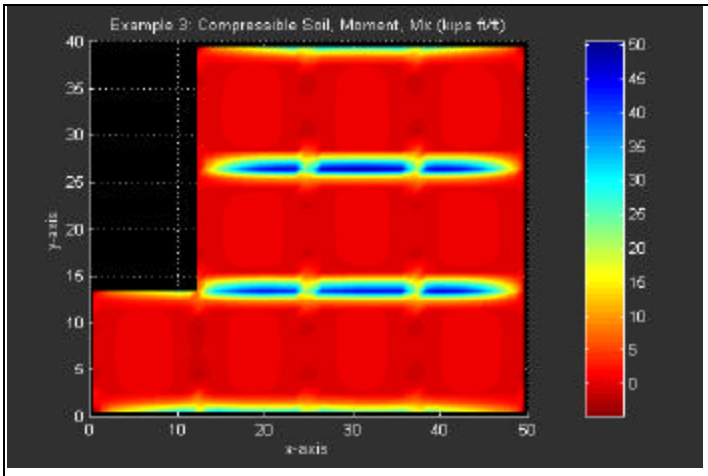

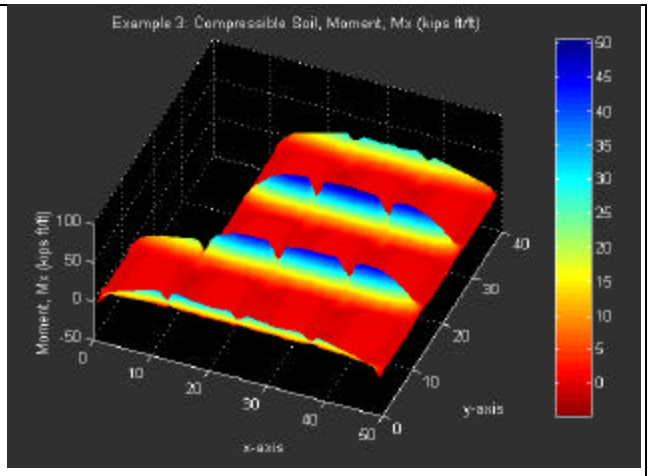

a. Top View *b. Isometric View*

Fig. F3. Example Three Compressible Soil, Ribbed Slab, Moment in x-Direction.

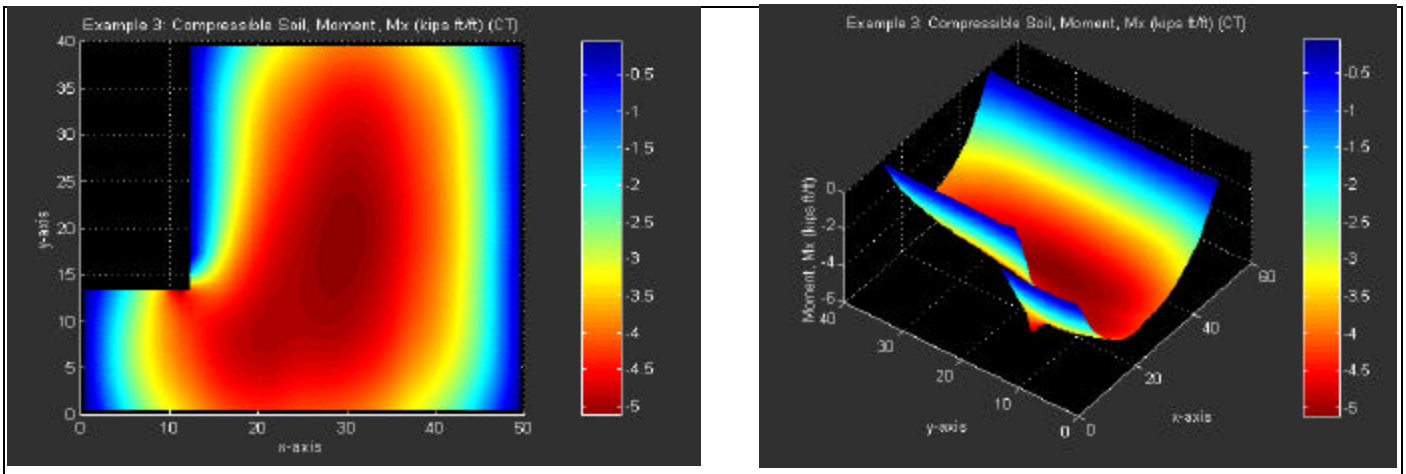

a. Top View *b. Isometric View*

Fig. F4. Example Three Compressible Soil, Flat Slab, Moment in x-Direction.

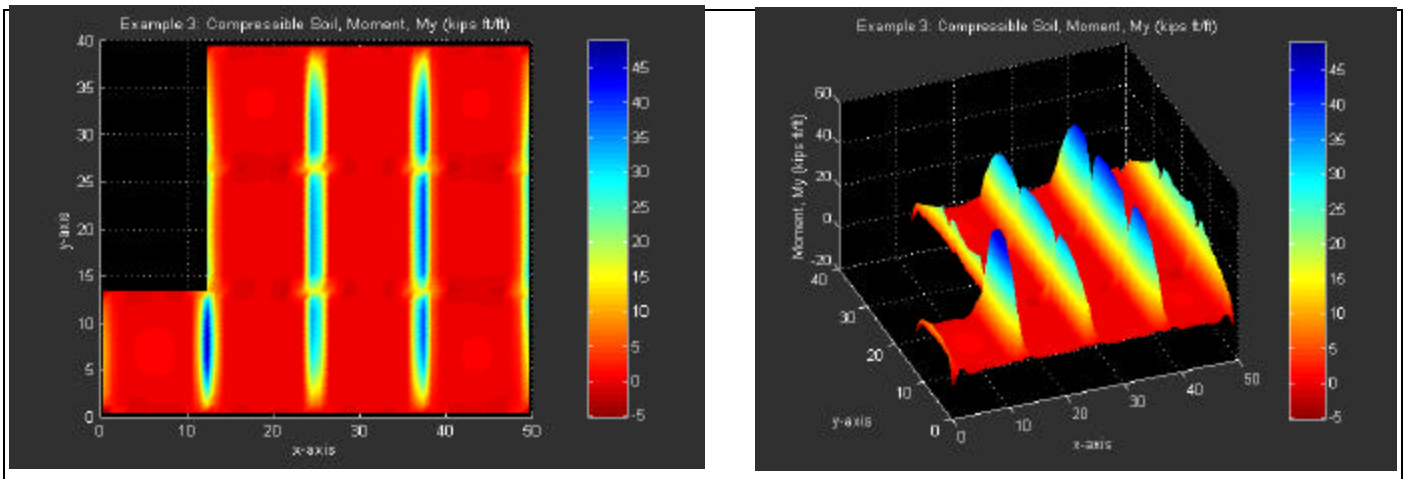

a. Top View *b. Isometric View*

Fig. F5. Example Three Compressible Soil, Ribbed Slab, Moment in y-Direction.

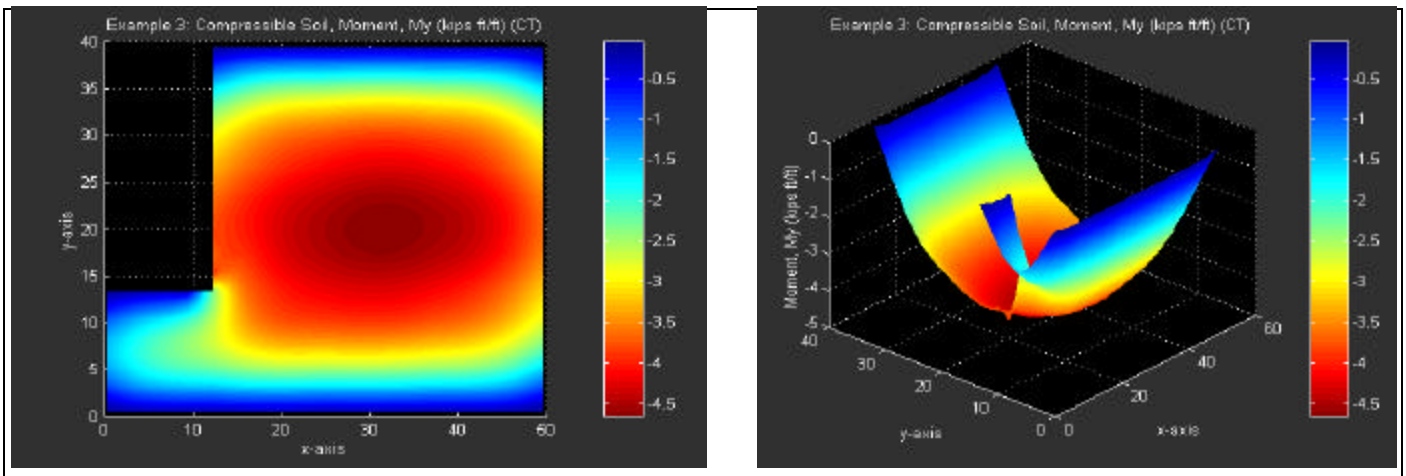

a. Top View *b. Isometric View*

Fig. F6. Example Three Compressible Soil, Flat Slab, Moment in y-Direction.

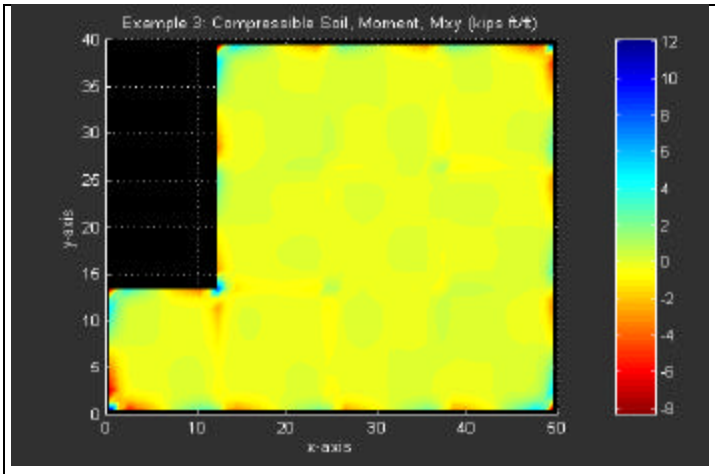

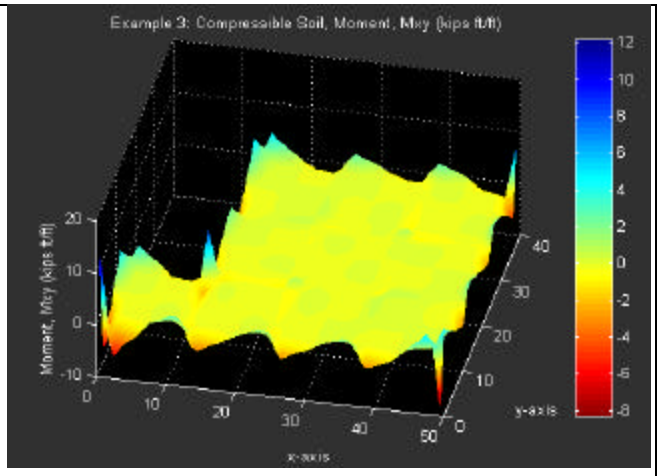

a. Top View *b. Isometric View*

Fig. F7. Example Three Compressible Soil, Ribbed Slab, Twisting Moment.

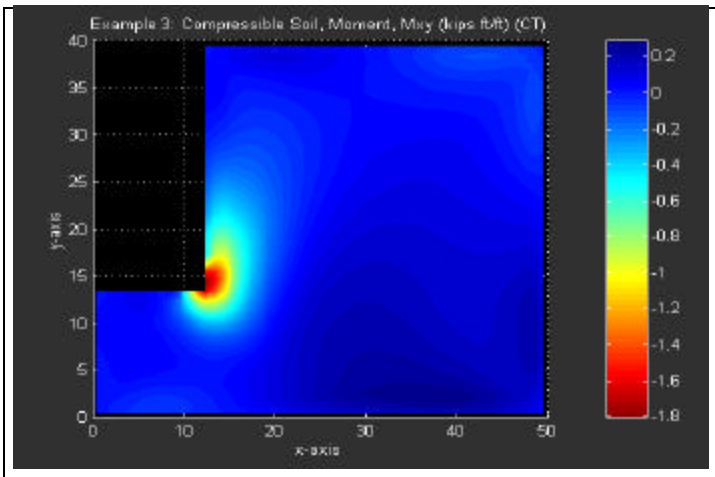

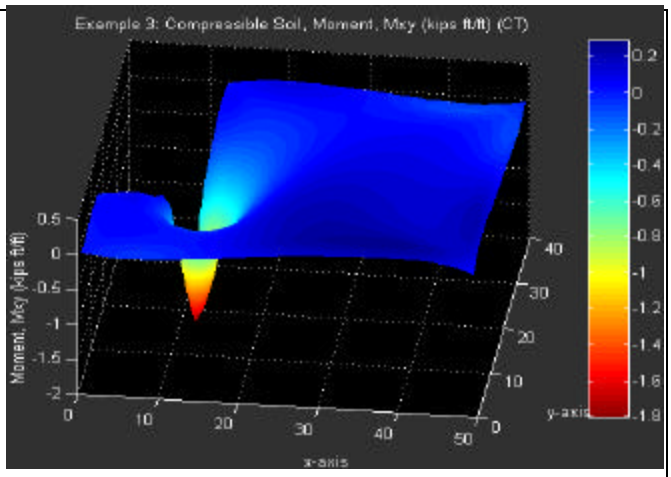

a. Top View *b. Isometric View*

Fig. F8. Example Three Compressible Soil, Flat Slab, Twisting Moment.

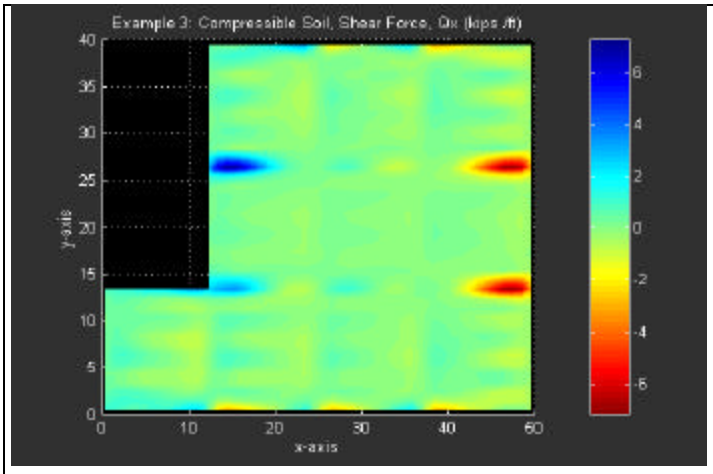

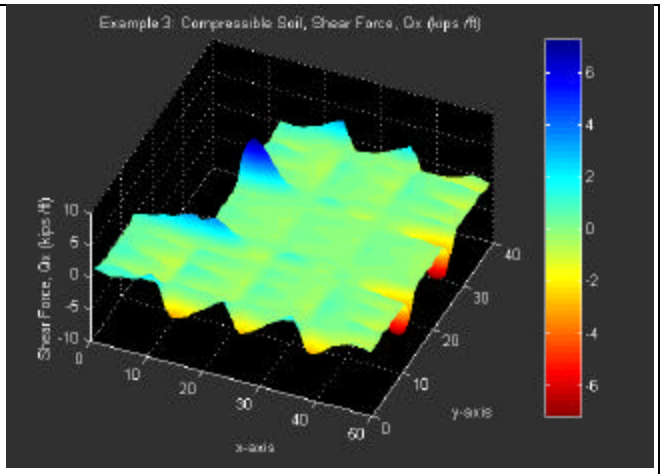

a. Top View *b. Isometric View*

Fig. F9. Example Three Compressible Soil, Ribbed Slab, Shear in x-Direction.

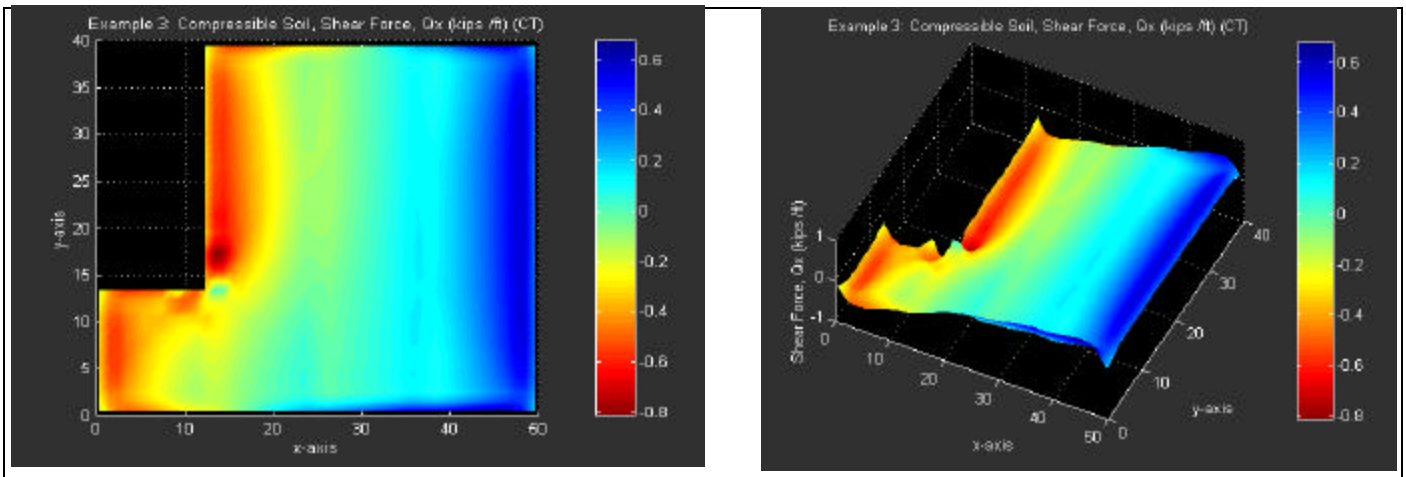

a. Top View *b. Isometric View*

Fig. F10. Example Three Compressible Soil, Flat Slab, Shear in x-Direction.

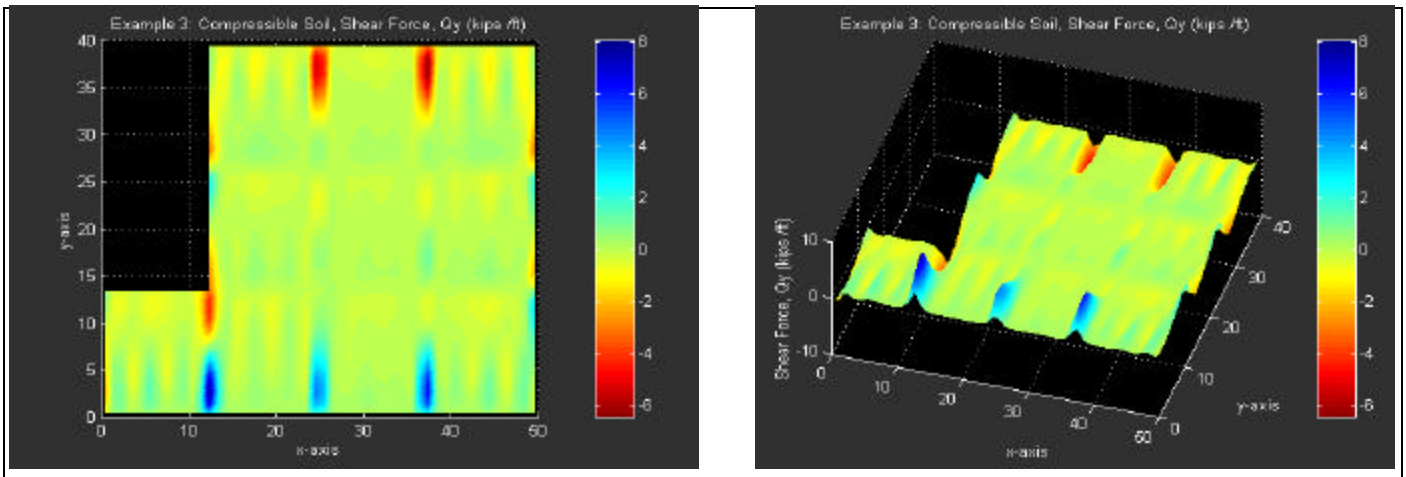

a. Top View *b. Isometric View*

Fig. F11. Example Three Compressible Soil, Ribbed Slab, Shear in y-Direction.

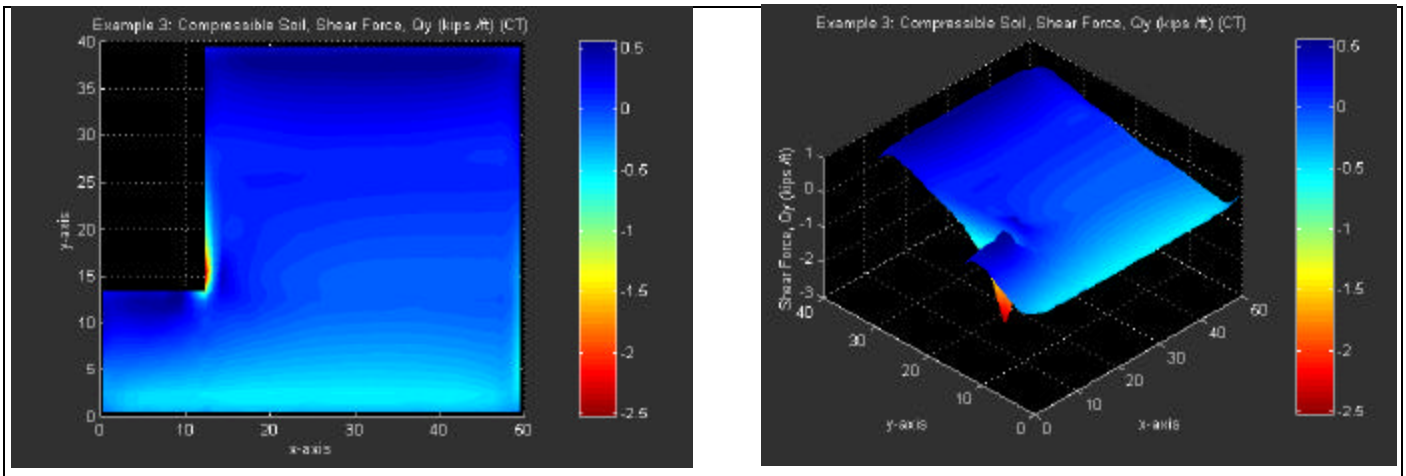

a. Top View *b. Isometric View*

Fig. F12. Example Three Compressible Soil, Flat Slab, Shear in y-Direction.

APPENDIX G
A TYPICAL OUTPUT FROM RSLAB^N PROGRAM

```
KASE 2, Center Lift, Example A.6 from PTI Manual
 ____________________________________________________________________
          OUTPUT  FROM  PROGRAM RSLAB^N
 ____________________________________________________________________
              A  SLAB-ON-GRADE  PROBLEM  IS  ANALYZED
               (USING THE SHEAR DEFORMATION THEORY)

    MATERIAL PROPERTIES OF THE SLAB ANALYZED:
       Modulus of elasticity, E1 ..............=  0.2160E+09
       Modulus of elasticity, E2 ..............=  0.2160E+09
       Poissons ratio, ANU12 ..................=  0.2500E+00
       Shear modulus, G12 .....................=  0.8640E+08
       Shear modulus, G13 .....................=  0.8640E+08
       Shear modulus, G23 .....................=  0.8640E+08

    MATERIAL PROPERTIES OF THE FOUNDATION SOIL:
       Modulus of Elasticity, YMS .............=  0.1440E+06
       Poissons ratio, PRS ....................=  0.4000E+00

    SLAB WEIGHT, THICKNESS, AND LOAD:
       Unit weight of reinforced concrete, UWRC.=  0.1500E+03
       Uniform slab thickness, STHIC ..........=  0.4000E+02
       Uniform distributed load, DSLOAD ........=  0.3300E+00

       *** A General Domain Mesh Consisting of ***
         *** Rectangular Elements is Used ***

    FINITE ELEMENT MESH INFORMATION:
       Number of nodes per element, NPE ........=   4
       No. of primary deg. of freedom/node, NDF =   3
       Number of elements in the mesh, NEM .....= 246
       Number of nodes in the mesh, NNM ........= 282
       Number of equations to be solved, NEQ ...= 846
       Half bandwidth of the matrix GLK, NHBW ..=  60
 ____________________________________________________________________
    Kase 2 Iteration Data:
       Iteration No., KTW ....................... =   1
       Number of zero coefficients at
       current iteration, KTWO .................. = 384
       Number of zero coefficients at
       previous iteration, KTWOP ................ =   0

    Kase 2 Iteration Data:
       Iteration No., KTW ....................... =   2
       Number of zero coefficients at
       current iteration, KTWO .................. = 212
       Number of zero coefficients at
       previous iteration, KTWOP ................ = 384

    Kase 2 Iteration Data:
       Iteration No., KTW ....................... =   3
       Number of zero coefficients at
       current iteration, KTWO .................. = 208
       Number of zero coefficients at
       previous iteration, KTWOP ................ = 212

    Kase 2 Iteration Data:
       Iteration No., KTW ....................... =   4
       Number of zero coefficients at
       current iteration, KTWO .................. = 208
       Number of zero coefficients at
       previous iteration, KTWOP ................ = 208
```

S O L U T I O N :

Node	x-coord.	y-coord.	deflec. w	x-rotation	y-rotation
1	0.00000E+00	0.00000E+00	0.28975E+00	0.16769E-02	0.84267E-02
2	0.83300E+00	0.00000E+00	0.28782E+00	0.19669E-02	0.85515E-02
3	0.36998E+01	0.00000E+00	0.28624E+00	0.20200E-02	0.13000E-01
4	0.65666E+01	0.00000E+00	0.28482E+00	0.11826E-02	0.17648E-01
5	0.94334E+01	0.00000E+00	0.28453E+00	0.36900E-04	0.18716E-01
6	0.12300E+02	0.00000E+00	0.28299E+00	-0.79860E-03	0.16063E-01
7	0.15167E+02	0.00000E+00	0.28342E+00	-0.85972E-03	0.12902E-01
8	0.16000E+02	0.00000E+00	0.28334E+00	-0.66263E-03	0.12768E-01
9	0.00000E+00	0.83300E+00	0.28202E+00	0.14816E-02	0.86761E-02
10	0.83300E+00	0.83300E+00	0.28130E+00	0.13312E-02	0.84339E-02
11	0.36998E+01	0.83300E+00	0.27482E+00	0.50555E-03	0.13076E-01
12	0.65666E+01	0.83300E+00	0.27066E+00	0.29319E-03	0.17688E-01
13	0.94334E+01	0.83300E+00	0.26835E+00	0.31942E-03	0.18757E-01
14	0.12300E+02	0.83300E+00	0.27016E+00	0.20460E-03	0.16121E-01
15	0.15167E+02	0.83300E+00	0.27213E+00	-0.38346E-03	0.12822E-01
16	0.16000E+02	0.83300E+00	0.27316E+00	-0.48746E-03	0.12930E-01
17	0.00000E+00	0.30664E+01	0.26500E+00	0.40518E-02	0.87414E-02
18	0.83300E+00	0.30664E+01	0.26107E+00	0.41629E-02	0.75173E-02
19	0.36998E+01	0.30664E+01	0.24442E+00	0.92996E-02	0.15665E-01
20	0.65666E+01	0.30664E+01	0.22773E+00	0.38883E-02	0.19451E-01

(output suppressed)

Node No.	x-ccord.	y-coord.	MAX/MIN Deflec.
1	0.00	0.00	0.2897E+00
183	19.04	24.42	0.8774E-01

F O R C E R E S U L T S:

x-coord.	y-coord.	Mx	My	Mxy	Qx	Qy
0.4165E+00	0.4165E+00	0.1591E+05	0.1537E+05	-0.3279E+05	0.4152E+04	-0.4603E+04
0.2266E+01	0.4165E+00	-0.2165E+05	-0.9000E+04	0.1699E+05	0.7320E+04	-0.3759E+03
0.5133E+01	0.4165E+00	-0.2545E+05	0.3670E+04	0.9910E+04	0.3642E+04	0.1207E+03
0.8000E+01	0.4165E+00	-0.2810E+05	0.4783E+02	0.4806E+03	0.9179E+03	-0.6532E+03
0.1087E+02	0.4165E+00	-0.2315E+05	0.2867E+04	-0.8686E+04	-0.1867E+04	0.1385E+03
0.1373E+02	0.4165E+00	-0.1789E+05	-0.6350E+04	-0.1375E+05	-0.6038E+04	-0.2507E+03
0.1558E+02	0.4165E+00	0.1047E+05	0.9680E+04	0.2164E+05	-0.3727E+04	-0.4177E+04
0.4165E+00	0.1950E+01	-0.1095E+05	-0.3018E+05	0.1897E+05	-0.4204E+04	0.4675E+03
0.2266E+01	0.1950E+01	0.5834E+03	0.3880E+03	0.1251E+04	-0.4958E+04	-0.3838E+04

(output suppressed)

Elem. No.	x-coord.	y-coord.	Max.(+)/Min.(+) Moment (Mx)
1	0.42	0.42	0.1591E+05
89	30.52	16.06	0.3257E+01
Elem. No.	**x-coord.**	**y-coord.**	**Max.(-)/Min.(-) Moment (Mx)**
158	33.56	24.00	-0.1265E+06
186	17.52	28.45	-0.4327E+01
Elem. No.	**x-coord.**	**y-coord.**	**Max.(+)/Min.(+) Moment (My)**
246	41.58	35.58	0.1587E+05
216	8.00	33.82	0.9741E+01
Elem. No.	**x-coord.**	**y-coord.**	**Max.(-)/Min.(-) Moment (My)**
173	28.58	25.76	-0.1630E+06
177	39.65	25.76	-0.5493E+00
Elem. No.	**x-ccord.**	**y-coord.**	**Max.(+)/Min.(+) Moment (Mxy)**
230	0.42	35.58	0.2727E+05
199	8.00	31.14	0.3026E+01
Elem. No.	**x-ccord.**	**y-coord.**	**Max.(-)/Min.(-) Moment (Mxy)**
1	0.42	0.42	-0.3279E+05
209	33.56	31.14	-0.1072E+02
Elem. No.	**x-coord.**	**y-coord.**	**Max.(+)/Min.(+) Shear (Qx)**
160	39.65	24.00	0.2224E+05
102	20.56	18.21	0.2165E+01
Elem. No.	**x-coord.**	**y-coord.**	**Max.(-)/Min.(-) Shear (Qx)**
146	2.27	24.00	-0.1959E+05
165	8.00	25.76	-0.2880E+01
Elem. No.	**x-coord.**	**y-coord.**	**Max.(+)/Min.(+) Shear (Qy)**
224	28.58	33.82	0.2441E+05
70	26.65	13.91	0.3127E+01
Elem. No.	**x-coord.**	**y-coord.**	**Max.(-)/Min.(-) Shear (Qy)**
71	28.58	13.91	-0.2307E+05
160	39.65	24.00	-0.3946E+00

APPENDIX H
SOIL MOVEMENT TABLES

Table H1. Soil Movement Guide Numbers: Lawn Irrigation (from Lytton 2001).

Measured Suction pF at Depth, z_m, m	y_m Guide Numbers: Controlling Surface Suction Due to Lawn Watering, pF – units				y_m Guide Numbers: With 4 ft. Deep Moisture Barrier, pF -- units			
	2.5	**2.7**	**3.0**	**3.5**	**2.5**	**2.7**	**3.0**	**3.5**
2.7	3.2	0	0	0	0.1	0	0	0
3.0	9.6	5.1	0	0	0.1	0.1	0	0
3.3	17.7	12.1	5.1	0	0.1	0.1	0.1	0
3.6	27.1	20.7	12.1	1.6	1.3	0.5	0.1	0.1
3.9	38.1	30.8	20.7	7.3	3.8	1.9	0.5	0.1
4.2	50.4	42.1	30.8	14.8	7.7	4.9	1.9	0.1
4.5	63.6	54.7	42.1	23.9	12.4	9.1	4.9	0.8

Table H2. Soil Movement Guide Numbers: Flower Bed Case (from Lytton 2001).

Measured Suction pF at Depth, z_m, m	y_m Guide Numbers: Controlling Surface Suction Due to Flower Bed Watering, pF – units			y_m Guide Numbers: With 4 ft. Deep Moisture Barrier, pF – units			
	2.5	**3.0**	**3.5**	**2.5**	**2.7**	**3.0**	**3.5**
2.7	3.2	0	0	0	0	0	0
3.0	13.1	0	0	0	0	0	0
3.3	27.3	7.0	0	3.7	1.0	0	0
3.6	48.7	14.2	1.6	11.6	6.2	1.1	0
3.9	69.5	35.1	10.2	22.5	15.2	6.4	0
4.2	90.3	56.0	21.5	35.1	26.6	15.3	2.4
4.5	111.0	76.7	42.3	49.0	39.7	26.6	9.1

Table H3. Soil Movement Guide Numbers: Tree Drying Case without Moisture Barrier (from Lytton 2001).

Depth of Tree Root Zone, ft	y_m Guide Numbers: Measured Equilibrium Suction at Depth, z_m, pF -- units						
	2.7	**3.0**	**3.3**	**3.6**	**3.9**	**4.2**	**4.5**
4	-79.1	-60.1	-43.2	-28.4	-15.6	-0.1	0.0
10	-169.6	-146.3	-124.9	-82.8	-42.6♦	-9.7▲	0.0
15	-244.7	-213.6	-182.5	-108.1♥	-42.6♦	-9.7▲	0.0
20	-333.4	-292.9	-252.5	-108.1♥	-42.6♦	-9.7▲	0.0

♥Movement active zone, z_A = 11.5 ft.
♦Movement active zone, z_A = 7.5 ft.
▲Movement active zone, z_A = 3.5 ft.

Table H4. Soil Movement Guide Numbers: Tree Drying Case with Moisture Barrier (from Lytton 2001).

Depth of Tree Root Zone, ft	y_m Guide Numbers: Measured Equilibrium Suction at Depth, z_m (With 4 ft Deep Moisture Barrier), pF -- units						
	2.7	**3.0**	**3.3**	**3.6**	**3.9**	**4.2**	**4.5**
4	-36.5	-25.2	-15.8	-8.1	-2.6	0.0	0.0
10	-116.3	-102.4	-88.4	-53.1	-21.5♦	0.0	0.0
15	-193.5	-170.5	-147.5	-78.5♥	-21.5♦	0.0	0.0
20	-278.2	-246.1	-214.2	-78.5♥	-21.5♦	0.0	0.0

♥Movement active zone, z_A = 11.5 ft.
♦Movement active zone, z_A = 7.5 ft.

APPENDIX I
EXPANSIVE SOIL VOLUME CHANGE GUIDE NUMBER

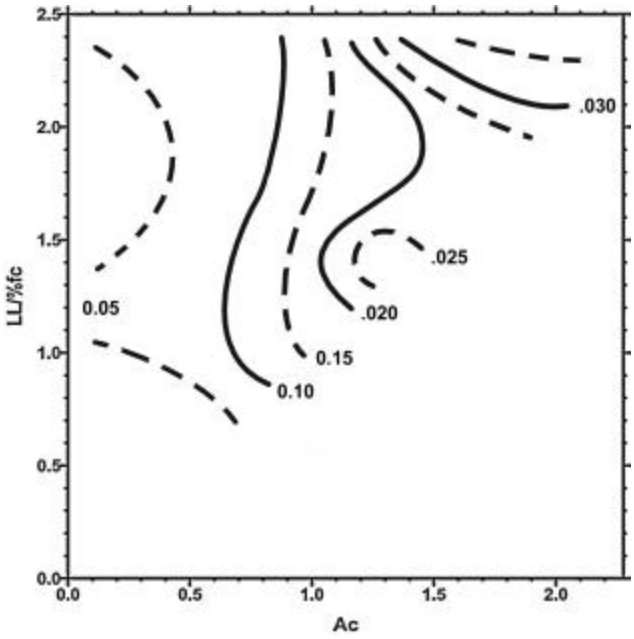

Fig. I1. Expansive Soil Volume Change Guide Number, Zone 2 (from Covar 2001).

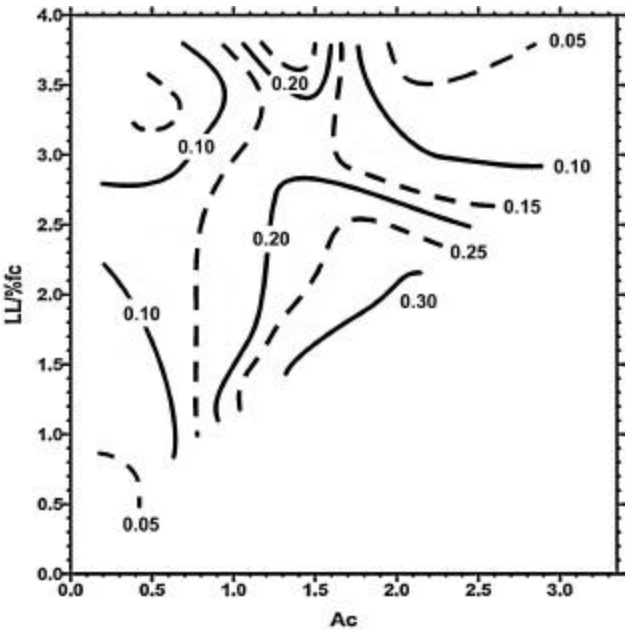

Fig. I2. Expansive Soil Volume Change Guide Number, Zone 3 (from Covar 2001).

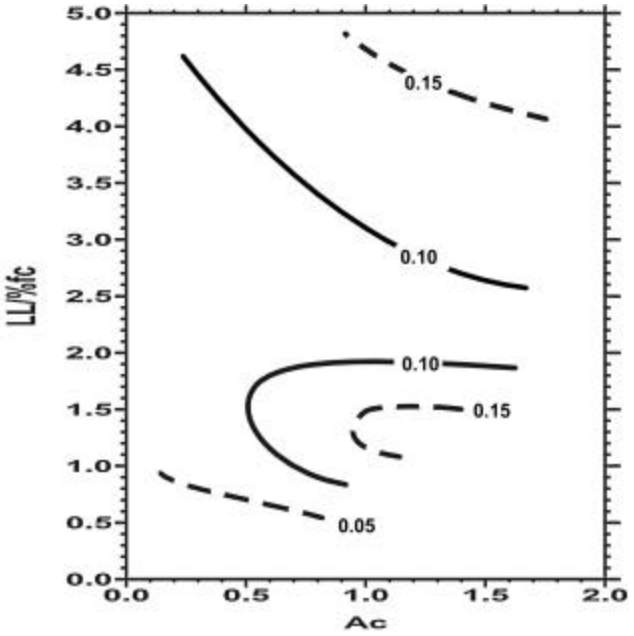

Fig. I3. Expansive Soil Volume Change Guide Number, Zone 4 (from Covar 2001).

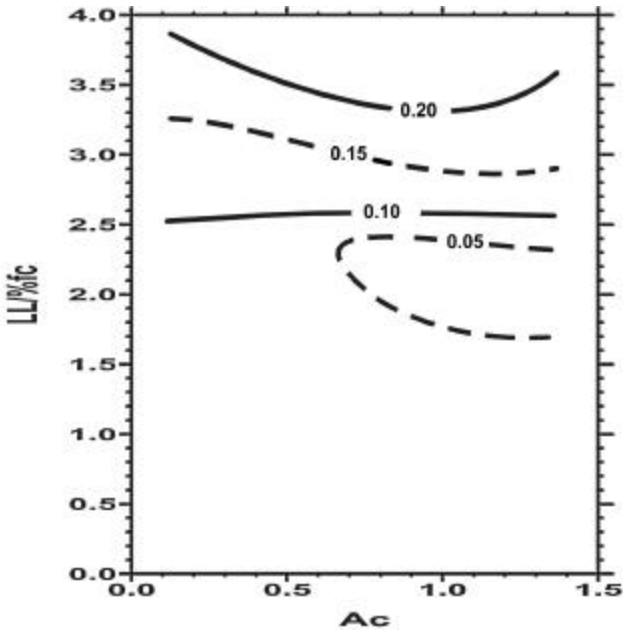

Fig. I4. Expansive Soil Volume Change Guide Number, Zone 5 (from Covar 2001).

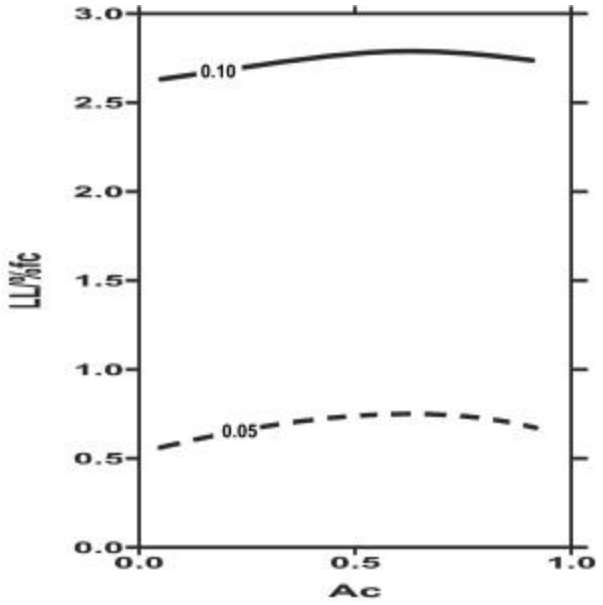

Fig. I5. Expansive Soil Volume Change Guide Number, Zone 6 (from Covar 2001).

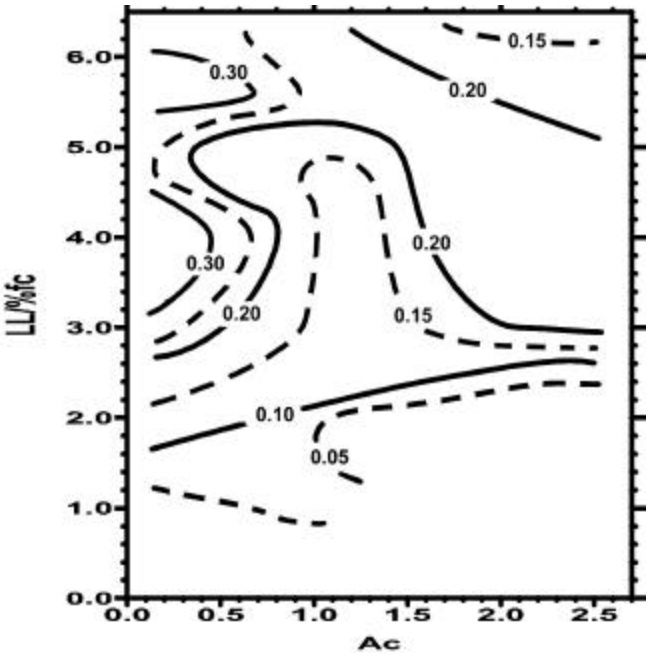

Fig. I7. Expansive Soil Volume Change Guide Number, Zone 8 (from Covar 2001).

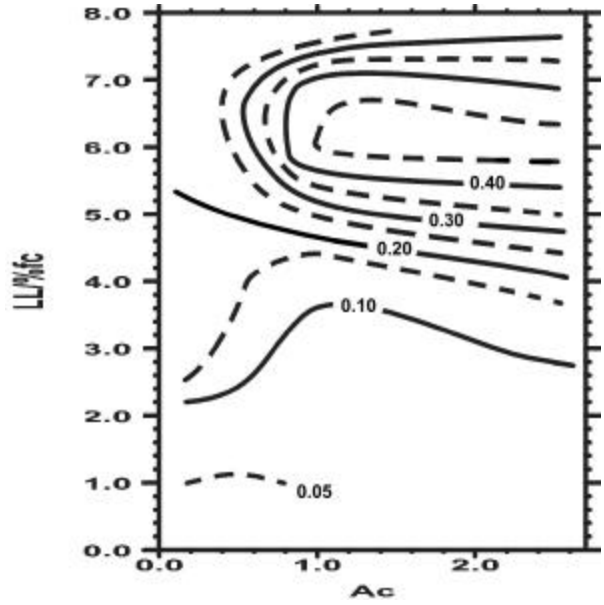

Fig. I6. Expansive Soil Volume Change Guide Number, Zone 7 (from Covar 2001).

VITA

Rifat Bulut is a citizen of Turkey; his permanent mailing address is:

Ugur Mumcu Mahellesi
195. Sok. No. 152
06370 Batikent, Ankara, Turkey

He obtained his Bachelor of Science degree in Civil Engineering from Middle East Technical University, Ankara, Turkey in 1993. After graduation, he worked for a construction company in Turkey as a site engineer for a few months.

In the spring of 1994 he was accepted at Texas Tech University to pursue studies toward the degree of M.S. within the Geotechnical division of Civil Engineering Department. He worked under the supervision of Dr. Warren K. Wray and obtained his degree in 1996.

In 1996, he started his Ph.D. studies at Texas A&M University under the supervision of Dr. Robert L. Lytton. He worked as a research and teaching assistant in Civil Engineering Department. He has been involved with modeling of slab foundations on expansive soils using finite element method for his Ph.D.
